Novel Patterning Technology for the LTCC Based Packaging of an Optical Encoder

Yves Lacrotte

A THESIS SUBMITTED FOR THE DEGREE OF DOCTOR OF ENGINEERING IN MICROSYSTEM ENGINEERING

HERIOT WATT UNIVERSITY
MICROSYSTEMS ENGINEERING CENTRE
SCHOOL OF ENGINEERING & PHYSICAL SCIENCES
SEPTEMBER 2013

Abstract

Powder blasting technology is proposed in this thesis as a new structuring tool for Low Temperature Co-fired Ceramic (LTCC). The process, consisting of mechanical abrasion through high speed particles, is mostly used on brittle material but was successfully adapted for the patterning of microstructures onto the fragile green tape substrate, through the manufacturing of novel stencil masks. These masks are based on high resolution patterned nickel sheet produced using UV-LIGA process or laser cutting coated with a thin layer of photopolymer which prevents efficiently the metal sheet deformations under particles bombardment. The magnetic properties of the metal allowed magnetic clamping to be used to maintain the mask down onto the substrate. The etching rate of the metal was shown to be low enough at a pressure of 50 psi (344kPa) at a distance nozzle-substrate (N-S) of 20mm and 50mm so that the mask could be re-used several times and ensured good pattern transfer quality from the mask to the substrate. The process was systematically characterised on DuPont 951 P2 (~165µm thick) green tapes.

The erosion of the green tape ceramic was then characterised with the micro-patterned electroplated masks. It showed that the powder blasted structures had U shape walls and verticality of the walls closed to 90° can be obtained with increasing the number of passes. The structures have smooth edges and do not have any melting parts. Smoother structures were obtained with distance nozzle-substrate of 50mm favouring lower under etching of about 15-20µm at the expense of a three times increase in process duration. Vias as small as 62µm in entry diameter and 20µm exit diameter were produced along with beams 25µm top width and 54µm bottom width were produced.

Following the green tape characterisation, a LTCC package for an optical encoder featuring 16 layers with the glass cavity was manufactured. 45x45mm nickel masks coated with LF55gn flexopolymer were produced featuring stacking pins, fiducials, cavities and circular apertures ranging from 100µm to 400µm diameters for interconnections. Each mask was powder blasted at 50 psi for a flow rate of about 0.1g/s, a distance N-S of 20mm and a speed of 5mm/s. The optical encoder was successfully attached on the package and tested.

ACADEMIC REGISTRY
Research Thesis Submission

Name*:*	YVES LACROTTE		
School/PGI:	EPS/ISSS		
Version: *(i.e. First, Resubmission, Final)*	Final	Degree Sought (Award Subject area)	EngD

Declaration

In accordance with the appropriate regulations I hereby submit my thesis and I declare that:

1) the thesis embodies the results of my own work and has been composed by myself
2) where appropriate, I have made acknowledgement of the work of others and have made reference to work carried out in collaboration with other persons
3) the thesis is the correct version of the thesis for submission and is the same version as any electronic versions submitted*.
4) my thesis for the award referred to, deposited in the Heriot-Watt University Library, should be made available for loan or photocopying and be available via the Institutional Repository, subject to such conditions as the Librarian may require
5) I understand that as a student of the University I am required to abide by the Regulations of the University and to conform to its discipline.

* *Please note that it is the responsibility of the candidate to ensure that the correct version of the thesis is submitted.*

Signature of Candidate*:*		Date:	

Submission

Submitted By *(name in capitals):*	YVES LACROTTE
Signature of Individual Submitting:	
Date Submitted:	

For Completion in the Student Service Centre (SSC)

Received in the SSC by *(name in capitals):*			
Method of Submission (*Handed in to SSC; posted through internal/external mail*)*:*			
E-thesis Submitted (mandatory for final theses)			
Signature:		Date:	

Acknowledgments

I would like to thank Professor Marc Desmulliez and Professor Nick Weston for giving me the chance to undertake this work under both Heriot-Watt University and Renishaw sponsorship. I am grateful to have been able to work under their supervision, for the guidance, support and help they provided me throughout my research.
I would like to thank John Carr, who was involved in the project and work with me on the design and manufacturing. His knowledge and his friendship were priceless. I would also like to thank Marc Leonard for his involvement and assistance and also Farid Amalou for his help. I would also like to thank all the staff at Heriot-Watt University.

Of course, I would like to show my gratitude to all my colleagues at the MISEC group who were present during this time. I won’t forget those useful discussions, laughs and nights out spent together which made this work a lot easier. I would like to thank especially Dave, Suzanne, Jack, Iqy, Brian, Deirdre, Jean-Baptiste, Shilong, Jia Ni, Norbert, Elisabeth, Alex, Curro, Xin, Robert, Sumanth, Soni, Ross, Raul, Maria, Jens... Of course I have to mention my morning teammate Gordon. His friendly and energetic welcomes were a blessing every single day. I am sad to say that, despite all my effort and our enthusiastic discussions, his love for football still remains a mystery for me. I won't forget either Stefan Wilhelm without whom I would probably still be doing experiments for this thesis. His contribution through software implementations and original ideas made huge improvements to this work. His friendship was also invaluable.

Most importantly, I would like to thank my girlfriend Amelie for her assistance and her patience, for pushing me and believing in me and my work. I know it hasn't been an easy time for us and I know I will never be able to make it up to her. I will like to thank my parents, my family and my friends for their unconditional support.

Last, but not least, I would like to give special thanks to RedBull and Nescafe for the high content of caffeine they put in their products. These fantastic drinks helped a lot, especially during the writing period of this thesis. Big up to you guys.

Table of contents

List of Figures

List of Tables

Academic Publications

Journal articles

- Y. Lacrotte, J. P. Carr, R. W. Kay and M. P.Y. Desmulliez, “Fabrication of a Low Temperature Co-fired Ceramic Package Using Powder Blasting Technology”, Microsystem Technologies, 2012, 1-9 DOI: 10.1007/s00542-013-1801-4

- S. P. Wilhelm, R. W. Kay, M. I. Mohammed, Y. Lacrotte and M. P.Y. Desmulliez, “Lamination based embossing technique for LTCC", Microsystem Technologies, December 2012, 1-7

Conference proceedings articles

- Y. Lacrotte, J.P. Carr, R.W. Kay and M.P.Y. Desmulliez, “LTCC Package Manufacturing Using Powder Blasting Technology”, Design, Test, Integration and Packaging of MEMS/MOEMS (DTIP) April 2012, Brighton, UK, pp.186 -191

- S.P. Wilhelm, R.W. Kay, M.I. Mohammed, Y. Lacrotte and M.P.Y. Desmulliez, “Surface embossing of LTCC during the lamination process”, Design, Test, Integration and Packaging of MEMS/MOEMS (DTIP) April 2012, Brighton, UK, pp.181 -184

- Y. Lacrotte, R.W. Kay, and Marc P.Y. Desmulliez, “Manufacture of a 3-D Package Using Low Temperature Co-fired Ceramic Technology”, 18th European Microelectronics and Packaging Conference (EMPC) 2011, Brighton, UK, pp.56-62

- Y. Lacrotte, F. Amalou, W. Yu and M.P.Y. Desmulliez, “Micro-patterning of green tape ceramics using powder-blasting for LTCC manufacturing”, IMAPS-ACerS CICMT 2009, Denver, Colorado, USA, pp.71-78.

Poster presentation

- Y. Lacrotte, S. Wilhelm, M.P.Y. Desmulliez, “Reliability improvement of a powder blasting process for micro-machining applications”, Electronic System-Integration Technology Conference (ESTC) 2010, Berlin, Germany, pp.1 -4

Trade press article

- S. Wilhelm, Y. Lacrotte, R.W. Kay and Marc P.Y. Desmulliez, “Novel Patterning Technologies for Ceramic MEMS”, Advancing Microelectronics, IMAPS- International Microelectronics And Packaging Society, Vol. 39, Issue 2, 2012

Chapter 1 Introduction and thesis layout

1.1 Introduction and motivation

Low Temperature Co-fired Ceramic, LTCC, is commonly used today in microsystems packaging. The fabrication process of LTCC is modular and requires low capital equipment, features which have attracted industrial interest. Layers of sheets of ceramic in a green state are machined independently, stacked and fired together resulting in a solid body. This material is therefore highly suitable for the fabrication of embedded channels and cavities, paving the way to applications ranging from micro-fluidics and optics to biology. In addition, prior to stacking, each layer can be printed with conductive tracks. This enables the embedding of passive components, such as inductors and capacitors, and of interconnects inside the package, reducing size and easing interconnect routing. The LTCC ceramic material has also become over the years a very attractive alternative to major substrates such as PCB or High Temperature Co-fired Ceramic (HTCC) due to its properties alone [1]. It is extensively used in Radio Frequency (RF) and high frequency applications due to its high dielectric constant and low electrical losses, its Coefficient of Thermal Expansion (CTE) similar to silicon and a good thermal conductivity. LTCC is a cost effective and competitive substrate for low to medium volume production.

As the microsystems industry restlessly reduces the chip footprint and volume, packages have to accommodate smaller and higher density interconnects. Up to now, conventional machining techniques such as laser and mechanical punching offer great performances for vias fabrication. They are fast, precise and versatile techniques. However, the capital costs for these equipments and their maintenance are high and can be an obstacle. In addition, the fabrication of smaller vias highlights the limitation of those machines and needs to be tackled. The need is high for a new precision tool able to avoid these issues.

Powder blasting, also known as abrasive blasting, is an old technique extensively used for surface preparation such as deburring, inscribing, surface cleaning (paint or rust removal) and stress relief as shown in Figure 1.1a. It is similar to the shot peening process in which round particles impact the substrate to create compressive stress and increase metal fatigue resistance. Powder blasting, however, relies on the abrasion of

the substrate, whereby particles hit the substrate with very high momentum conferred by compressed gas. The abrasive media can be dispensed dry or in a liquid form. Different methods exist to mix powder and gas, some of them being documented in [2]. These processes are used for large surface treatment with particles ranging from a few hundred microns to a few millimetres.

Recently, powder blasting, in its dry form, has been adapted to micromachining. The particles' high momentum confers enough kinetic energy to crack and erode the substrate of brittle material. Particles ranging from 3µm to ~100µm are used in combination with a micro-patterned mask. The process is detailed in Figure 1.1b. Alumina, aluminium oxide, Al_2O_3, is often used as an abrasive material due to its high hardness of 9 Mohs [3]. A precise description of the erosion principle of brittle material by hard particles can be found here [4, 5]. The entire process takes place in an enclosed box. Once particles have abraded the substrate, they are sucked and disposed of in a sealed container alongside the abraded material.

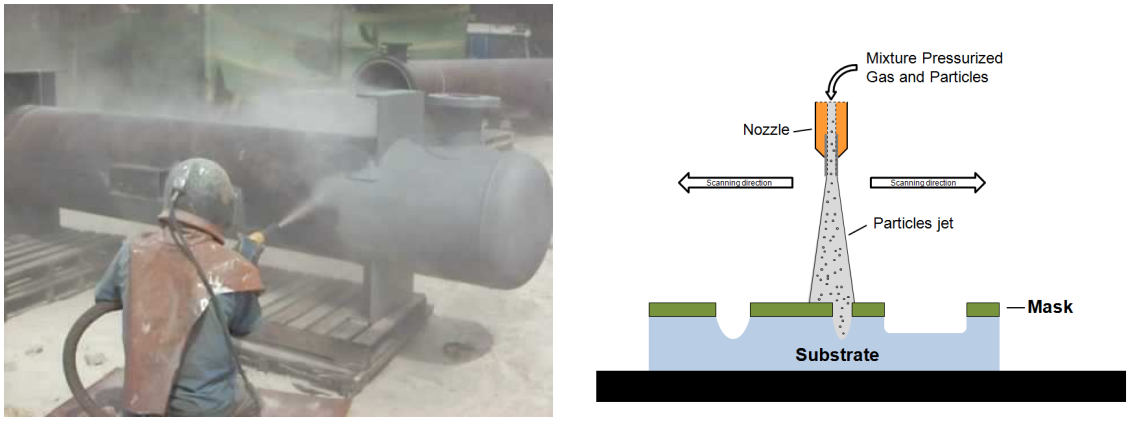

(a) (b)

Figure 1.1: (a): Example of abrasive blasting being used to quickly clean large surfaces. (b): Principle of powder blasting process applied for microstructures

As mentioned before, traditional powder blasting is not a direct writing process. The area which is under the jet of particles is several millimetres across, making the process not suitable for direct micromachining. Micro-patterned masks are applied on the substrate to enable smaller structures to be fabricated. Such masks can be made from ductile or plastic materials [6, 7], which have a lower etching rate than brittle materials. Ductile masks are plastic masks or metallic masks, which are pre-formed using laser,

photolithography or electroplating, and glued on the substrate.

Powder blasting has a certain number of advantages compared to traditional machining techniques: fast etching rate of the order of hundreds of micrometers per minute, low capital and operating costs, fabrication of fine micro-structures in glass and silicon such as interconnects [8] and channels [9], tilted structures, and creation of 3D structures such as free standing cantilever [10, 11]. This process has been used for products such as flat screens for Philips [12] (Zeus display), gyroscopes lids for BAE systems (Figure 1.2) and by glass manufacturer and foundries such as SCHOTT, PlanOptik, Micronit Microfluidics and Elume Inc.

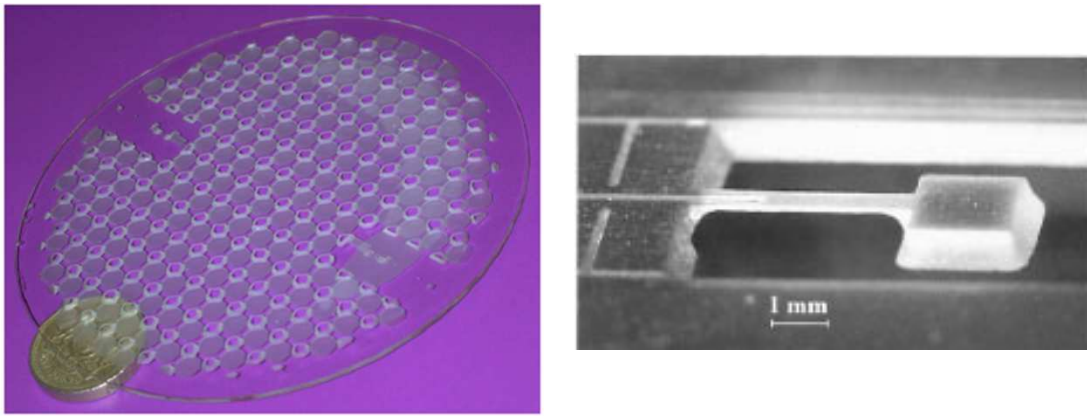

Figure 1.2: BAE gyroscopes lids and free standing inertial sensor [11]

1.2 Objectives and challenges of this thesis

The main objective of this thesis is to adapt the powder blasting technology for machining green tape ceramic at the micro-scale and characterise the process. The main objectives can be broken down as follows:

- Identify and understand the issues present with the conventional way of patterning LTCC.
- Develop and characterise a mask, which could be adapted for LTCC machining.
- Fabricate fine microstructures with such a mask.
- Characterise the erosion process on green tape ceramic, which includes the definition of the erosion process, the limits of the feasible structures

dimensions and the 3D blasting.

- Fabricate a package for an optical encoder using the technology created.

Following this list of objectives, numerous challenges appeared. First, the flow rate fluctuation of the particles had to be improved. Powder blasting machining is known for having poor flow rate repeatability [13] and is influenced by several parameters [14]. The machine owned by Heriot-Watt University is an industrial machine and is also subject to those issues. Additional challenges included the use of lower pressure than recommended by the manufacturer and low frequency usage of the machine which tended to increase powder clogging. Modifications were made to the machine with respect to the reservoir size and process temperature of 50°C to keep the moisture out between experiments. Despite these modifications, process fluctuations were not entirely suppressed.

The main challenge of this thesis was to find a material that can be applied on the LTCC without being glued on it. Unlike brittle materials on which the mask can be easily fixed on the substrate, the green tape ceramic deteriorates in contact to glue compounds. Firstly the material is very sensitive to solvent. The binder, which holds alumina and glass particles together, dissolves in contact with the solvent. Glued mask would be therefore impossible to remove. Secondly, the tape is fragile and soft to the extent that mechanical stripping the mask off would tear and ultimately destroy the tape. However, this glue is an important factor in the success of the substrate micro-structuring as perfect contact between the mask and substrate enables high transfer pattern resolution. To accurately pattern green tape ceramic and benefit from a good contact, magnetically clamped metal masks such as electroplated nickel masks were used.

The fabrication of the metal mask was the second challenge. The manufacturing cost of the mask was to be kept low as powder blasting machines are cheap. Expensive masks would significantly reduce the cost advantage of this technology with respect to others. One process was first envisaged: electroforming of nickel which can produce high aspect ratio structures. SU-8 on glass wafer is usually used as sacrificial material in nickel electroforming. However, changes in the process were made and dry film resist laminated onto larger stainless steel plate were used to ease the mask production and increase throughput. A second method of fabrication was also used involving laser

cutting of nickel masks. This solution proved to be relatively cheap for less complex patterns.

The next challenge was to prevent the high residual stresses to build up on the bare metallic surface by the particles. These stresses, defined as the peening effect, deform the thin metallic sheet, creating gaps with the substrate and lowering the resolution of the transfer of the pattern transfer. These deformations are unfortunately not compensated by the strength of the magnetic force. Materials need to resist the powder blasting process but also be easily applicable onto the metal mask and replaceable before it wears off completely. The protective coating proposed were photo patternable coating. They were spin coated or laminated on the mask.

Finally, the last challenge was to engineer and assemble the LTCC package with the powder blasted layers and to attach the opto-electronic chip onto it. In this part, large masks 45x45mm were blasted to manufacture seven different layers (some of them printed with conductive paste), stacked together, laminated and fired. The package had to be designed to house a 6.5x6mm glass window on one side and a flexible connector on the other attached using reflow solder and ICA silver epoxy paste.

1.3 Thesis layout

Chapter 1 is the introduction of this thesis. After detailing the LTCC principle and the problems occurring during the structuring of the tape with conventional techniques, powder blasting is explained to highlight the benefits that such a system could bring to the machining of green tape ceramic. The challenges encountered are also described and finally the thesis layout is given.

In Chapter 2, the LTCC technology used today in the microsystem industry is described. A comprehensive overview of the material history and composition of the green tape is given. The fabrication steps needed to produce LTCC packages is explained in details. In addition, an in-depth analysis of the different ways of structuring the ceramic tape is highlighted. The structures' shape and the minimum dimensions are detailed for each method with its advantages and drawbacks.

Chapter 3 examines the powder blasting setup custom-made at Heriot-Watt University.

The description of the device includes the details of work undertaken on the machine to improve the particles flow repeatability with the use of 9µm alumina particles. The etching rate of the green tape was then characterised as a function of pressure, flow rate, distance nozzle-substrate and angle of incidence.

Chapter 4 focuses on the development of the mask. The first part of this chapter presents the search for a material resistant enough to the particles and providing a good contact on the substrate without requiring glue. Both ductile and plastic materials were investigated. The second part describes the mask fabrication combining UV-LIGA techniques and polymer coating.

Chapter 5 covers the fabrication of microstructures on green tape ceramic with metallic mask coated with polymers. Rectangular and circular apertures with dimensions ranging from 40µm to few hundred of microns were used. The resulting beams and vias were measured, providing a range of possible apertures. Under-etching and effect of the distance nozzle-substrate were investigated.

In Chapter 6, the LTCC package for an optical encoder is fabricated using only the powder blasting as the patterning machine. A thorough description of the package design consisting of seven different layers (sixteen in total) is given. The fabrication process of such a package is detailed as well as the bonding technique used to attach the optical encoder. The encoder is electronically tested in the last part of this Chapter.

Chapter 7 draws conclusions of this thesis and future work is given.

Chapter 2 Overview of LTCC processing

2.1 Introduction

This chapter aims at reviewing progress made in Low Temperature Co-fired Ceramic (LTCC) material processing. First, a historical background on LTCC is presented, enlightening the needs for this material. Then, the material itself is described with a clear understanding of its unique properties. The different steps involved in the fabrication process are then detailed, and include tape structuring, printing, stacking and lamination, firing and post processing. Finally, and most importantly, the different techniques in use to machine the green tapes are presented with their advantages and disadvantages.

2.2 LTCC background

In the microelectronic packaging industry, LTCC is a relatively new material dating from the 1990s. However, LTCC processing originates from an older and more mature technology. The investigation of ceramic material as a substrate for electronic packages started back in the late 1950s when the basic steps for processing the ceramic material were laid down [15, 16]: green sheet fabrication, vias formation, sheets stacking and lamination. The rising interests in the ceramic substrate came from their electrical, thermal, mechanical and dimensional stability properties [17], and in 1964, IBM introduced its Solid Logic Technology (STL) [18] using this material. Integrated silicon transistors (or diodes) and resistor were mounted onto a single 12.5x12.5mm layer of sintered ceramic composed of 95% of alumina. Ink containing noble metals (mixture of gold and platinum) were screen printed and fired at 800°C to form the conductive tracks. The adhesion was promoted by the melted glass frit present in the ink. Due to firing temperature difference between metal and ceramic (around 1500°C), the tracks were printed after the ceramic sintering. The embedding of metallic tracks inside the ceramic was thus impossible and STL modules were made up of a single layer. Multilayer stack could only be created by attaching the modules together with soldered pins as shown in Figure 2.1.

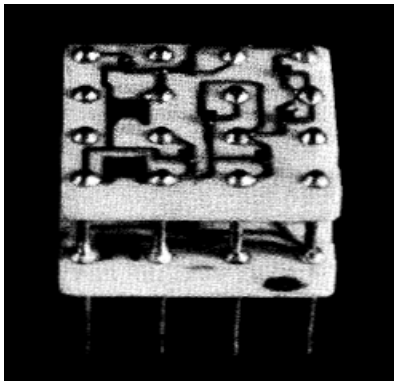

Figure 2.1: Photograph of two ceramic layers featuring silicon transistors and resistor attached together thanks to interconnecting pins [18]

The technology evolved with the arrival of Dual In-line Package (DIP) in the late 1960s. One of these new packages, Ceramic Dual In-line Package (CDIP), was composed of a ceramic carrier wire bonded to electrical connecting pins. The green tape used for this carrier was sintered after the printing of the metal tracks, requiring metal pastes with higher melting point such as tungsten which has a melting point of 3422°C [19].
In the early 1970s, the demand for higher I/O connections density grew, encouraged by new mounting techniques such as Controlled Collapse Chip Contact (C4, IBM 1969). By the end of the 1970s, the industry witnessed the appearance of Multilayer Ceramic (MCL) carriers used for Multichip Modules (MCM). IBM introduced such modules in their 4300 series computer [20] in 1979. The module was a 50x50mm carrier with 23 laminated and metalized alumina layers. The technique involved laminating metalized layers (tungsten, molybdenum or molybdenum – manganese) with via interconnects punched and filled with conductive paste, alignment and stacking, and firing at around 1400-1600°C [21]. Layers were composed of 90 to 95% of alumina powder mixed with glass frit and binder to allow flexibility in the tape: High Temperature Co-fired Ceramic (HTCC) was born. In 1983, IBM released, using this principle, their first commercialised Large Scale Integration (LSI) package for the IBM 3081 Processor Unit. The 33 laminated layers carrier could house up to 133 chips. The device is illustrated with its thermal conduction module in Figure 2.2.

The technology improved throughout the 1980s in terms of chip size reduction and increased I/O number on single packages. Ultimately, however, the limitations of the material itself were the issue: thinner wiring meant higher resistivity of the conductor,

and thus higher power consumption and increased heat dissipation.

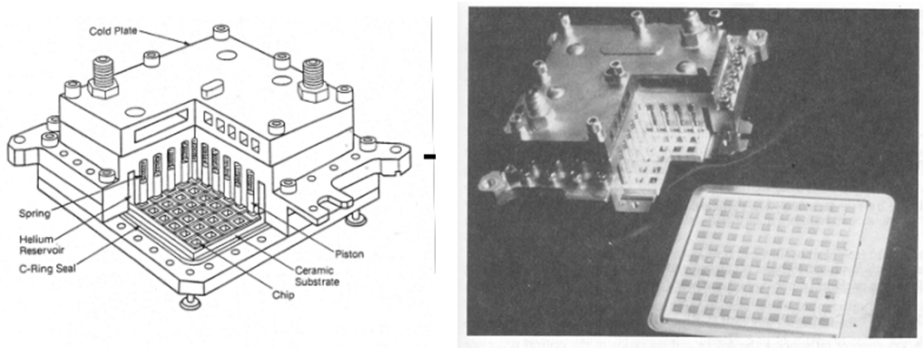

Figure 2.2: The 1800-pin TCM IBM 3081 processor (150 x 150 x 60 mm) houses up to 133 chip sites arrayed on a 90 by 90 mm ceramic substrate (courtesy of IBM)

LTCC was developed in the early 1990s to overcome these shortcomings. This new material has a higher composition in glass frit enabling the sintering temperature to be lowered to about 850°C, hence its name. It has a lower dielectric constant and a coefficient of thermal expansion (CTE), closer to the silicon CTE than HTCC. The processing costs are also reduced due to the lower temperature needed. But most importantly, metal with lower resistivity such as Cu, Au and Ag, of melting point of 1085, 1064 and 961°C respectively, could be used as conductors. The first successful industrial LTCC packages with copper wiring material were fabricated by IBM and Fujitsu in the early 1990 for their main frame computers (Figure 2.3). From large packages, the need for the LTCC technology has since then shifted to smaller packages for wireless, high frequency mobile communication devices, helped by the low transmission loss of the material.

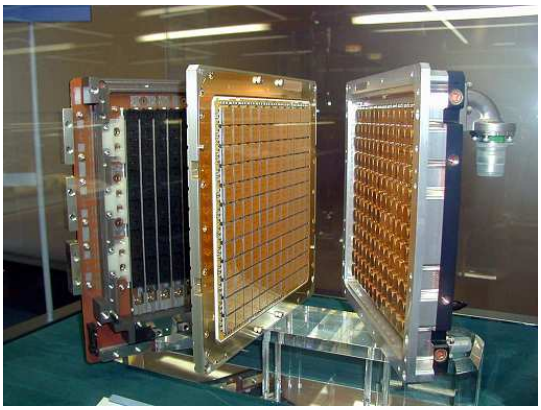

Figure 2.3: One board CPU with a maximum of 144 LSIs on both sides. The substrate (centre) is formed by 61 layers of LTCC and has a dimension of 245x245mm. Its cooling system can be seen on each side of the LTCC carrier (courtesy of Fujitsu)

2.3 LTCC composition and characteristics

As explained in section 2.2, the LTCC basic material consists of layers of green ceramic tape. The thickness of each layer varies generally between 50 to 350µm depending on the manufacturer and can be found rolled (Heraeus for example) or pre-cut into square sheets (DuPont). Samples of such layers can be seen in Figure 2.4. The material is fabricated from a slurry and is doctor bladed to the desired thickness onto a PET foil that serves the only purpose of supporting the tape during handling. The final material is soft, highly flexible and easy to handle.

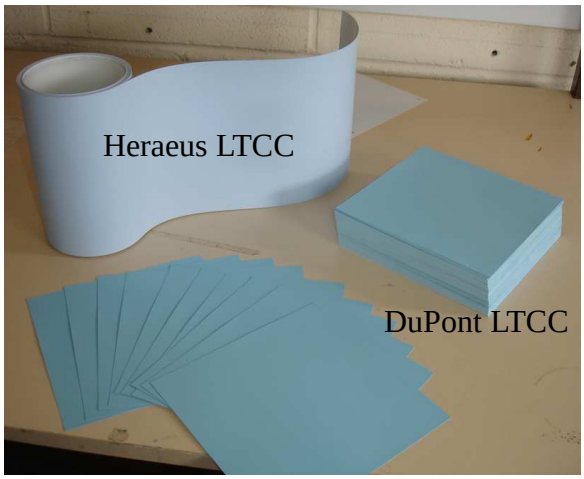

Figure 2.4: Samples of green tape ceramic bought from Heraeus and DuPont

The green tape is composed of inorganic (alumina Al_2O_3 and glass frit SiO_2-B_2O_3 of about 20 to 40% each) and organic material (binder, plasticizer...), whose sole purposes are to hold the inorganics together and give the tape its flexibility. The tape composition can be modified to a certain extend to match specific needs. The glass type, binder composition and material proportion can be varied to modify the dielectric constant, permittivity and Coefficient of Thermal Expansion (CTE) as shown in Table 2.1 where tapes with different characteristics are listed. The difference of proportion between the inorganics and organics confers the tape a certain porosity that can reach up to 40% in volume for certain materials [22]. During the sintering process, the organic binder evaporates, the glass melts encapsulating the alumina particles, resulting in loss of porosity and a densification of the material.

One of the particularities of LTCC is the shrinkage that the layers undergo during

sintering. The melting of the glass eliminates the space between particles, leading to the re-dimensioning of the layers in the x,y and z-directions. The reduction in size is significant and varies depending on the tape composition as shown in Table 2.1. This shrinkage is well controlled with tolerances within 0.2 to 0.5% provided that process parameters given by the manufacturer are followed. Customizing these parameters however modifies the shrinkage as reported in [23, 24]. Shrinkage can nevertheless be prevented by constraining the tape between porous ceramic release tape [25, 26]. Certain tapes, such as the HerausHL series, do have zero shrinkage in the x and y-directions [27], at the expense of a higher shrinkage in the z-direction.

Table 2.1: Non exhaustive list of ceramic green tapes and of their properties from different manufacturers

Tape Name	Shrinkage after sintering		Thickness [μm]	Permittivity ε_r	Tan δ	TCE [ppm/K]
Ferro A6S/A6M	x/y	~15 %	127, 254	5. 9 (100 GHz)	0.001 (10 GHz)	>8 / 7
	z	~26 %				
DuPont 951	x/y	~12.7 %	50, 114, 165, 254	7.8 (3 GHz)	0.006 (3 GHz)	5.8
	z	~15 %				
DuPont 9K7	x/y	~9.1 %	127, 254	7.1 (10 GHz)	0.001 (10 GHz)	4.4
	z	~11.8 %				
Heraeus CT2000	x/y	~10.6 %	50, 99, 133	9.1 (2.5 GHz)	0.002 (2.5GHz)	9.1
	z	~16 %				
Heraeus HL2000	x/y	~0.2 %	66, 92, 133	7.3 (2.5 GHz)	0.003 (2.5GHz)	6.1
	z	~39 %				
Heraeus CT765	x/y	~19.3%	90, 150	68.7 (2.5 GHz)	0.2 (2.5 GHz)	9.1
	z	~28.9 %				
Ceramtape GC	x/y	~21 %	310	7.9 (1 MHz)	0.002 (1 MHz)	5.3
	z	~18%				
Electro-SL 41010	x/y	~13%	100-130	7-8 (1 MHz)	0.5 (1 MHz)	7
	z	~17%				
Electro-SL 41050	x/y	~9.5%	100-130	13-14 (1 MHz)	0.2 (1 MHz)	7.15
	z	~15 %				

2.4 Fabrication process of an LTCC package

The fabrication of an LTCC package follows a series of steps that are detailed in Figure 2.5. There are seven steps, not all of them necessary: blanking, vias and cavity forming, printing, stacking, lamination, sintering and post processing.

1- Blanking and preconditioning

Tapes are pre-cut into pieces of requested dimensions and are preconditioned at around 100ºC for 10 minutes. This step relieves stresses due to backing PET foil removal. If the foil is left on (mostly to reduce dimensional changes during the tape handling), this step is not necessary.

2- Vias and cavity forming

Interconnecting vias, fiducials, stacking pins and cavity are formed on each individual layer using different techniques that will be detailed later in this chapter.

3- Via filling and conductor printing

Screen printing technology is used to print metal tacks and fill vias. It consists of depositing a conductive paste through a mask featuring aperture openings. Squeegees are used to squeeze the paste onto the substrate. Alignment with the substrate is done by fiducial markings present on both the mask and the substrate. In LTCC, two technologies are used:

- Stencil screen printing using an electroplated nickel, laser cut nickel or stainless steel foil, to fill vias.
- Emulsion screen printing, which uses an exposed photo-imageable emulsion laid on a fine metallic wire mesh, to print tracks. Unlike stencils, meshes enable complex shapes such as standalone structures, for example concentric circles, to be printed.

Due to the different screen used, each printing technique requires its own metallic paste. The paste used for the emulsion screen has always a lower viscosity than the one used for the stencil printing which enables it to be squeezed through the mesh of the emulsion mask.

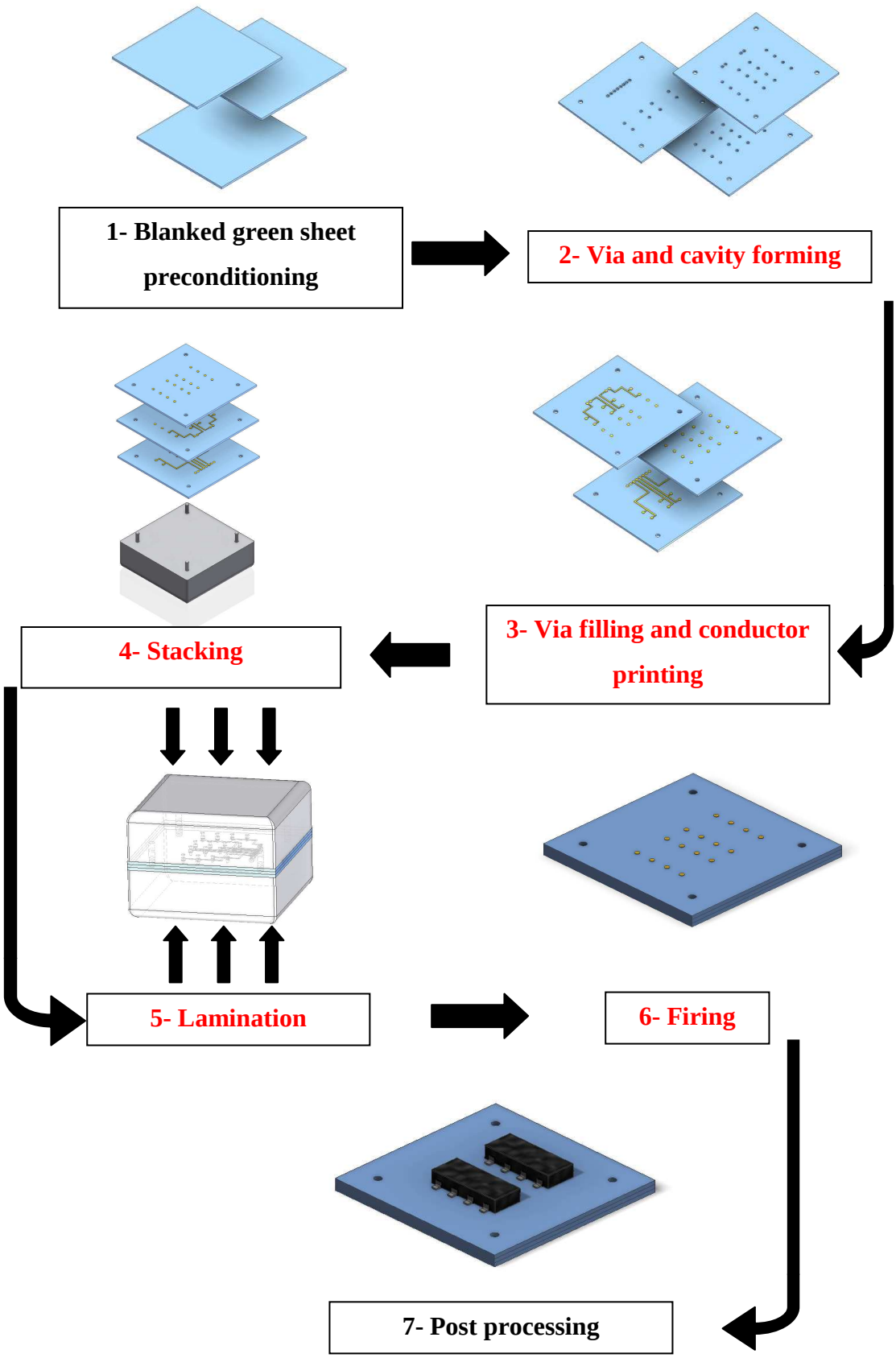

Figure 2.5: Schematic diagram of the LTCC fabrication process. The steps highlighted in red are compulsory

4- Stacking

The PET foil is removed and each layer is aligned one by one on a thick metal plate using stacking pins. This step can be done automatically with automated stackers or manually. Extra care has to be taken to avoid the tape from stretching during this step. If present in the design, cavities must be filled prior to the lamination to avoid being crushed. Solid filling, such as rubber [28], can be used for opened cavity. Sacrificial material, which evaporates during the firing process at around 600-700ºC through the green ceramic pores, can be used for inner and open cavities [29].

5- Lamination

The stacked layers are then laminated at about 70ºC for 10 minutes at a pressure between 10 to 20MPa. The lamination process creates a bonding thanks to material interpenetration at the boundary between each layer. Two lamination processes can be used:

- Uniaxial pressing: the stack is laminated heated up on a hot plate. The stack needs to be rotated by 180º half way through the process in the z direction.
- Isostatic pressing: the stack is placed in a vacuum-sealed bag and pressed in water brought to a temperature of 70ºC. No rotation is needed.

6- Sintering

The stack is then fired following a precise temperature profile. A typical firing profile can be described as follows: a first dwell is done at about 350-400ºC to drive off the organic binder, a slow ramp up and a second dwell at 850ºC to achieve glass densification. Additional dwell can be done at around 600ºC if there is presence of sacrificial material to allow the material enough time to be burnt off before the LTCC pores close.

7- Post processing

After firing, active components can be attached to the fired stack by wire bonding, flip chip bonding or thermocompression. Additional printing can also be done to enable brazing of metallic seals. Packages can then be singulated using laser machining or diamond sawing.

2.5 Advantages

The LTCC has a certain number of advantages:

- Very good dielectric properties with high relative permittivity and low tangent loss
- Integration in its core of passive components such as resistors, capacitors and inductors
- CTE close to silicon (3 ppm/°C)
- High-density 3-D package
- Resistance against high temperature
- Suitable for mass production and cost effective manufacturing process

LTCC has become a good alternative to PCB for certain applications, notably in RF where low loss and high relative permittivity are important as well as applications in harsh environments such as in the automotive industry. Table 2.2 shows a quick comparison between FR4, the mainstream PCB, PTFE and LTCC. LTCC has a better thermal conductivity, closer CTE to silicon, higher relative permittivity and lower dielectric loss. Furthermore, it is well suited for 3-D packages. However, it is not as well established in the electronics environment as the PCB and is still more expensive.

Table 2.2: Typical properties of DURAVER®-E-Cu quality 104 KF FR4 from Isola [30], TLX-9 PTFE from Taconic[31] and DuPont 9k7 LTCC [32]

Material	Relative Permittivity ε_r	Thermal conductivity (W/mK)	CTE (ppm/°C)	Tan δ
FR4	4.6	0.3	13	0.02
PTFE	2.5	0.19	9-12	0.0019
LTCC	~ 7.1	4.6	~4.4	0.001

A similar comparison can be drawn with HTCC (Table 2.3). The relative permittivity, loss tan δ and thermal conductivity values are better for HTTC but the CTE of LTCC is closer to the one of silicon. However, the higher sintering temperature of HTCC prevents the use of conductor paste material such as silver and gold. Less conductive materials such as tungsten and molybdenum have to be utilised.

Table 2.3: Properties of HTCC from Via electronic [33] and DuPont 951 P2 LTCC [34]

Material	Sintering Temperature	Relative Permittivity ε_r	Tan δ	CTE (ppm/K)	Thermal Conductivity (W/mK)
HTCC (>92% Al_2O_3)	1600°C	9.4	0.001	6.8	17 - 35
LTCC (20-40% Al_2O_3)	850°C	7.8	0.006	5.8	3.3

2.6 Structuring LTCC

Structuring the green tape ceramic is an essential part in the LTCC package fabrication. Great control on the structure quality and critical small dimensions go hand in hand with reducing the footprint of the package. Different techniques can be employed to produce the required patterns, the most conventional ones being punching and laser machining. Embossing is a technique less utilised as piercing apertures in the substrate are not possible, but the quality of the patterns is very good. These techniques are described in this section alongside their advantages and drawbacks.

2.6.1 *Mechanical punching*

Introduction

Mechanical punching is one of the conventional techniques for structuring LTCC. Its principle is based on creating a hole in a material through shear force thanks to a punch and a die. The punch, aligned with the die with matching aperture, is pushed through the substrate until the material is shredded and the punch passes through to the die (Figure 2.6). The resulting aperture has an identical shape to both punch and die and the ejected slug is discarded.

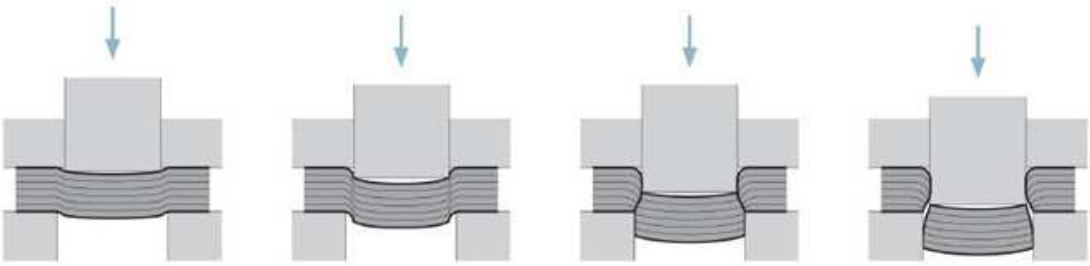

Figure 2.6: Mechanical punching principle (courtesy of Trumpf)

Punching is widely used in the manufacturing industry because of its versatility: holes can be punched in any type of ductile material: metal, plastic etc. Coarse punching of thick material featuring meso-scale patterns requires heavy-duty puncher while punching of microstructures requires higher accuracy and precise tooling. Two fully automated punchers are represented in Figure 2.7.

It is a fast and efficient tool that can punch tens (single punch) or hundreds (multiple punches) of vias per second. The speed of the punching will depend on the tool size. A wide range of shape (square, circular, triangular) and dimensions for the tooling exists to fit the desired designs. On certain machines, the tooling can be changed quickly thanks to fully rotating heads and die. Punching process cannot fabricate half way through apertures.

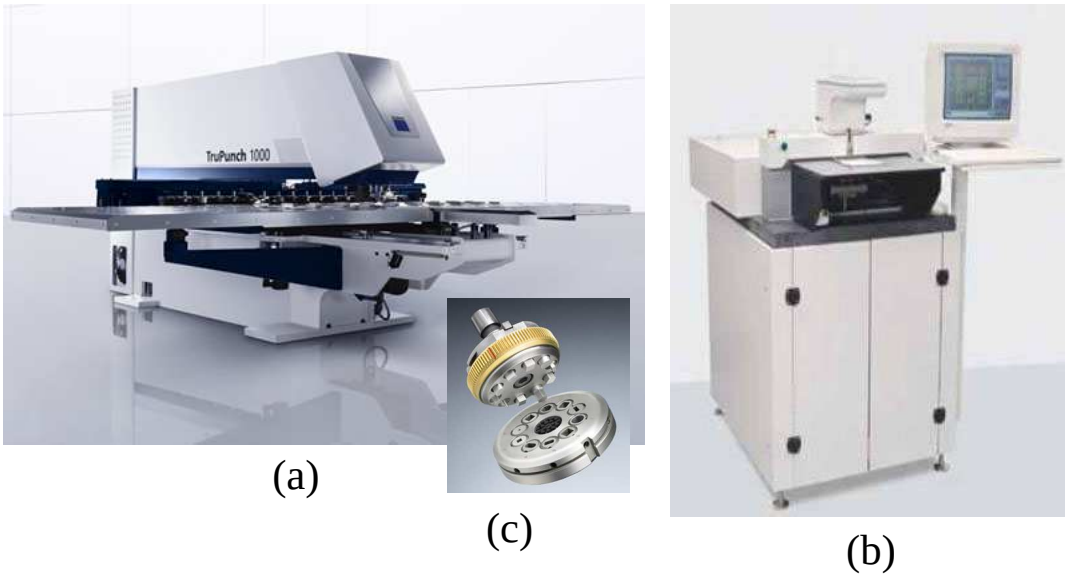

Figure 2.7: Fully automated punching machines for (a) meso-scale work 10 punch/s and its multiple punch head and die (courtesy of Trumpf) and (b) micro-scale work capable of up to 24 punch/s with tools dimension ranging from 75 to 4,760µm (courtesy of ptchips). (c) Multi-pins tooling

Clearance for micro-scale punching is a very important parameter. It is the key to production quality and enhanced tools service life [35]. Clearance length is defined as the space between the punch pin and the die as shown in Figure 2.8. If such a length is too small, the punch and die will wear quickly but the apertures will accurately match the tools' dimensions. Conversely, if it is too large, the material will not be shredded

properly with the formation of burrs. Alignment between the punch and the die is also critical as any misalignment can result in punch and die colliding with each other, wearing or breaking the former. Furthermore, if the punch is not centred, the larger clearance of one side of the punch can enhance slugs. To minimize these, punch and die must be precisely machined with low wear material and frequent inspections of the tooling are required. A more detail explanation on the punch and die fabrication and clearance can be found in [36].

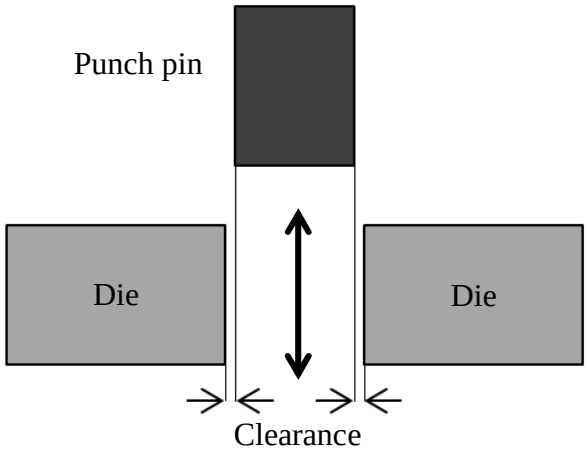

Figure 2.8: Diagram of a punch and die clearance

Typical punched apertures for microstructures are shown in Figure 2.9a with 50µm and 100µm apertures pierced with tungsten carbide tools inside a stainless steel sheet. The entry side has dimensions similar to the punch pin dimensions. Edges are sharp and clean. However, due to clearance, the exit side has dimensions closer to the die dimensions rather than the punch dimensions. The resulting apertures have an entrance smaller than the exit with the exit having less sharp edges with potential burrs [37, 38]. This is illustrated in Figure 2.9b. Despite the clearance problem, circular apertures down to 15µm in diameter in brass and stainless steel were pierced with only 2µm clearance [36]. The punch tip and the die were made in tungsten carbide.

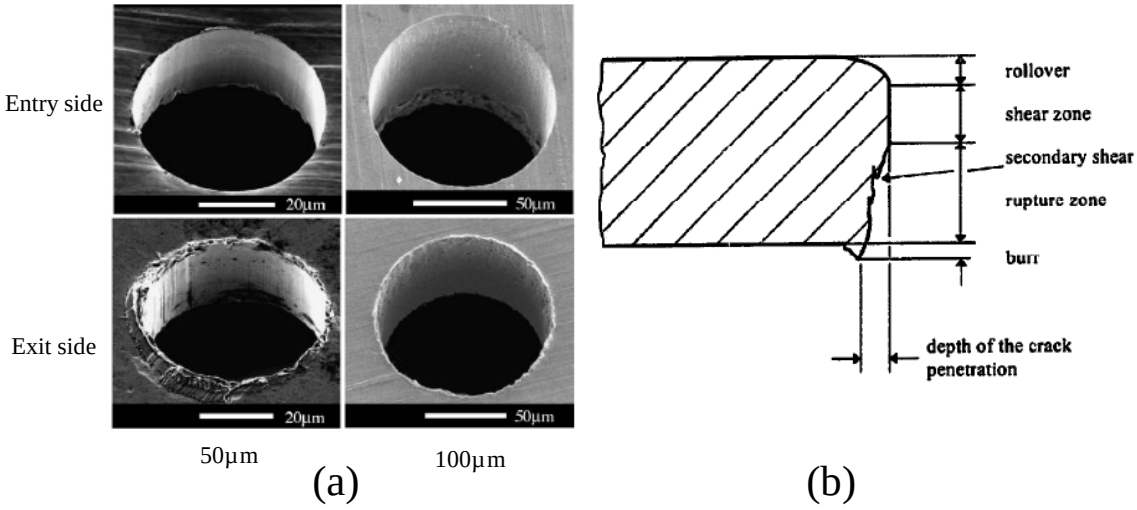

Figure 2.9: (a) SEM picture of 50µm and 100µm diameter hole (entry and exit side) in stainless steel [39]. (b) Schematic cross-section of punched part showing the different fracture zones created [37]

Micro machining in LTCC

Punching machining has been used very early on for green tape ceramic [17, 18], and is still today one of the two major machining processes [40-43]. The punching of LTCC sheets is addressed with similar tools described in the previous section. Vias are the most commonly machined structures, as this process is quick and simple. To produce channels, straight lines and cavities, successive circular punches with close steps are executed. Punched cavity and channels examples can be seen in Figures 2.10a&b. Due to the successive punching method, the channel walls flatness is directly dependent on the pitch between each punch and the punch dimensions. Channels fabricated with a pitch too large show "ripples" on their wall as illustrated in Figure 2.10b. However, for meso-scale punching, tools shape can be changed to square or rectangle to fit the designs. A detailed description on producing large channels and circular apertures using a single size circular punch can be found in [44].

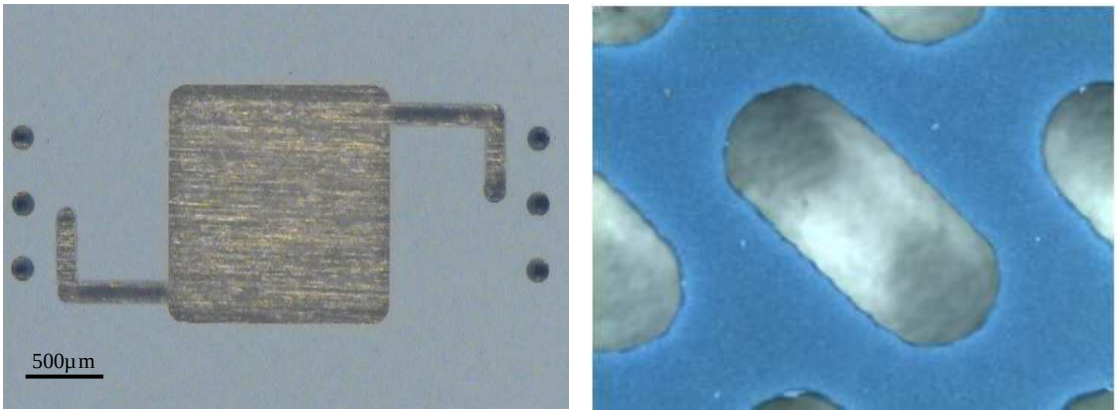

(a) (b)

Figure 2.10: Example of punched structures in green ceramic: (a) 150µm channels and cavity (courtesy of VTT) and (b) oval openings used for fuel cells [45]

Punching machining is mostly praised for the resolution of the vias and the produced uniformity. The fabrication of large vias or cavities in LTCC is not very well documented as such structures are usually manufactured with small punches of a few hundred microns dimensions, used in the fabrication of small vias. However, the size of those structures completely offsets the defects that can be produced with small punches. The tool wear is limited due to the size of the tooling and a clearance that can be large compared with the size of the features. However, a lot of research has been done to fabricate sub-100µm vias.

Mechanical punching has been demonstrated to be very reliable for small vias of 50, 75 and 100µm diameter and for tape thicknesses up to 360µm, including the PET foil [46]. Such vias display very sharp edge and high uniformity as shown in Figure 2.11. Indeed, for certain applications, uniformity is critical, for example in the manufacturing of a 94 GHz antenna array where 10,000 identical vias needed to be created [47]. The inverted tapered shape present in the metallic substrate (larger exit side than entry side) is less present with LTCC. For example, despite a clearance set at 12µm, the difference entry-exit was similar for every vias dimensions and less than 2.5µm, taking into consideration the tools wear for the 100µm vias [46].

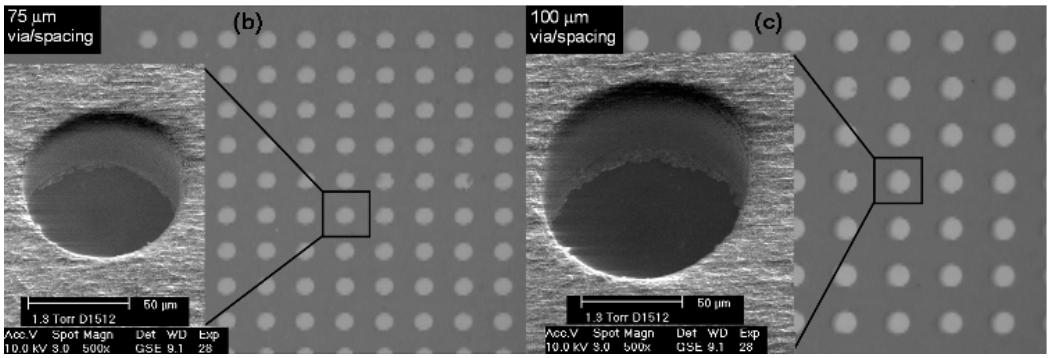

Figure 2.11: Punched 75µm and 100µm vias in 163µm thick green tape [46]

However, similarly to the metallic sheets, the exit side reveals approximate circular shape with burrs or slugs, as shown in Figure 2.12, compared to the entry side. Burrs and slugs increase the smaller the punch [46], but were found to be independent of the tape thickness.

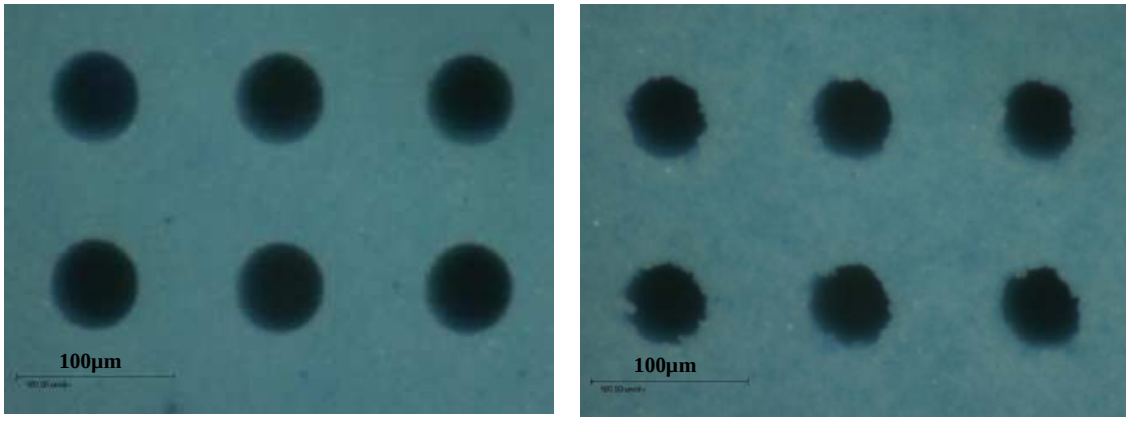

(a) (b)

Figure 2.12: Punched 55µm entry (a) and exit (b) side [48]

As stated before, mechanical punching system can pierce at the same time both green ceramic and PET sheet. However, for sub-100µm vias, it adds complications to the process as it increases the formations of burrs [49]. During the process, the compressed green ceramic under the punch tends to behave as an extension of the punch, pushing the uncompressed ceramic underneath. The force distribution on the PET foil before piercing changes the shear pattern and increases burrs. Moreover, the more the material is compressed, the more the burrs formation occurs. Placing the tape upside down with the foil facing the punch pin does reduce this effect. With this method, 30µm vias were even reported [50]. However, the pressure exerted on the PET foil by the punch tends to imprint the green ceramic, creating caved-in edges [48, 51] as showed in Figure 2.13.

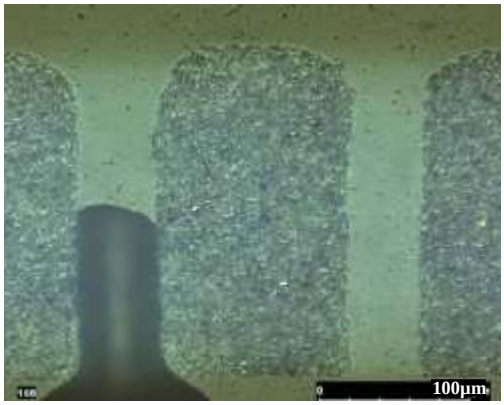

Figure 2.13: 55µm via with rounded edges imprinted by the PET foil [48]

Sacrificial materials such as carbon paste are also one of the materials that can be punched through [52], proving the versatility of the process. Unlike lasers, which evaporate the carbon paste and create large trenches, punching does not modify the carbon paste composition. Accurate and precise cuts were demonstrated in tape thickness ranging from 36 to 200µm. One such example is displayed in Figure 2.14.

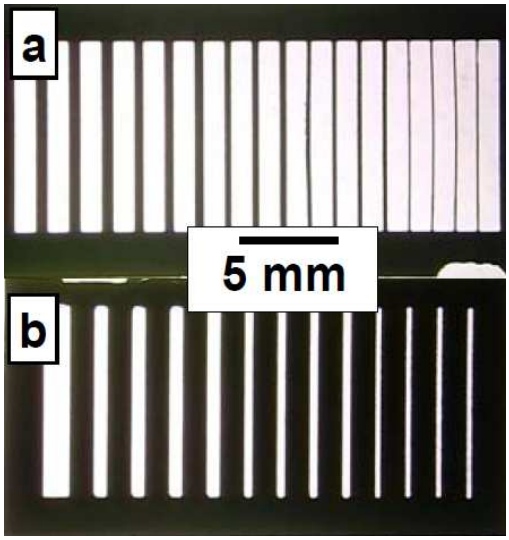

Figure 2.14: Example of precise cut in a carbon based sacrificial material with a puncher. The structures have beam width ranging from 110 to 625µm (top row) and channels ranging from 227 to 645µm (bottom row) [52]

Green tape contains alumina particles which are extremely hard. These particles are able to wear off the punch and die to the point where the clearance increases as the cost of more burrs and slugs. Wear of the tools can also cause structure failure such as partial

vias formation, rough wall shape or PET foil not completely punched. This is even more relevant for micro-tools which are more sensitive to wear. Frequent inspection of the tools is required to avoid throughput loss.

After the punching process, the tape is cleaned by blowing dry air onto its surface to remove slugs [51] stuck inside the vias and fallen off the punch tip onto the tape surface. Such debris can be blamed for printing short cuts and track bridging [53]. Greater amount of debris occurs with rough or worn punches.

2.6.2 *Laser machining*

Introduction

Laser machining is the other conventional technique employed to structure green tape ceramic. Lasers are used by the manufacturing industry as a cutting, engraving, scribing, and trimming tools on a wide range of material from metals to plastics, woods and ceramics. Their principle is based on the absorption by the substrate of a large quantity of energy in a very short period of time (pulses) that results in the substrate ablation through evaporation or sublimation as shown in Figure 2.15. The process replicates the same principle described during the punching machining: each pulse acts as a puncher and ablates the substrate, although no dies here are necessary.

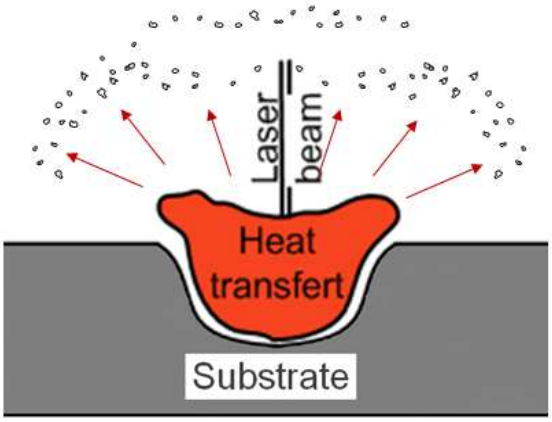

Figure 2.15: Schematic of the laser ablation process

Micromachining is possible thanks to the narrow dimensions of the beam profile hitting the substrate. Lenses are used to focus the laser beam into a focal spot, which enables higher resolution but also higher energy density. The focal spot can be calculated by

equation 2.1:

$$d_f = \frac{4\lambda}{\pi} * \frac{f}{D} * M^2 \qquad 2.1$$

with d_f the focal spot, λ the beam wavelength, D the diameter of the unfocused beam at the lens, f the focal length of the lens and M^2 the beam mode. The conversion of the photon energy to thermal energy relies on the capacity of the material to absorb the photons: if the material has low laser beam absorption, the energy transfer will be low, and so will be the laser ablation. This makes the process very dependent on the laser wavelength.

Laser machining is mostly carried out in two-dimensions. The substrate has to be perfectly perpendicular to the incoming beam as the focal spot of the laser is small and change in height of the part to be etched would decrease the beam efficiency drastically. In recent laser development, lasers have been mounted onto state-of-the-art workstation featuring 5-axis stages. The machines are able to calculate the position of the substrate and move the beam accordingly to focus the focal spot on the substrate. This enables machining of 3-D surfaces and thus increases greatly their laser flexibility. However, these stages are very expensive.

Laser machining on LTCC

Lasers are frequently used in LTCC because of their cutting speed and accuracy. Also, despite the low absorption of the laser beam at certain wavelengths, the tape can easily be pierced. Indeed, as described in the section 2.4.6, the binder contained in the tape decomposes at around 300 to 400ºC. This temperature is easily reached with the laser, and the binder vaporizes with resulting gases carrying the freed glass and alumina particles. Lasers also do not suffer from tool wear, as there is no direct contact with the substrate. However, they do need to be serviced regularly. Unlike punching machining, lasers can partially ablate a surface: the laser does not pierce the tape but raster its surface in order to remove a thin layer of the material. Fined tuned cavity thickness can then be fabricated inside one single layer of green sheet. The flatness of the rastered surface depends on several parameters such as pitch between passes, laser power and frequency, rastering speed, etc.

A typical lasered structure exhibits a tapered shape where the entrance is larger than the exit as shown in Figure 2.16. This shape is inherent to the laser ablation process: the heat transfer is maximal at the top surface and then diffuses inside, reducing the ablation rate. Thus, more material is removed close to the top surface. This makes the structure shape and the minimum dimensions achievable very much dependent on the tape thickness [46]. This tapered shape can be, however, more finely tuned by varying the laser power, number of passes, pulse frequency. These parameters will also change depending on the tape composition. Tapered edges can also be the result of loss of focus of the focal spot [46, 54]. Defocused focal spot decreases the energy density of the beam and thus the ablation power. This can happen during low power cut requiring several passes inside a relative thick material.

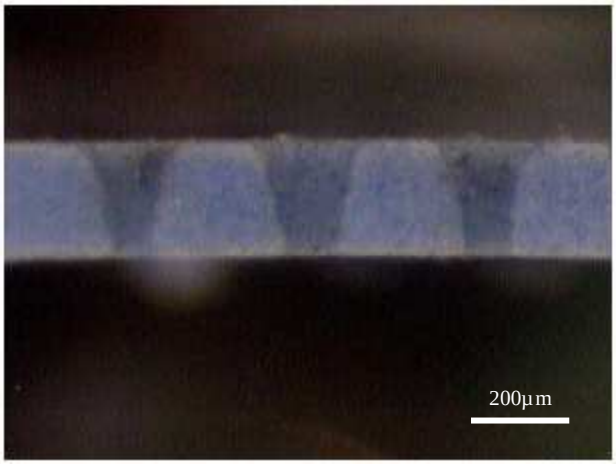

Figure 2.16: 75µm vias pierced in 163µm green tape [50] with CO_2 laser

Lasers have a good repeatability. Thousands of structures can be made rapidly. However, certain factors which are difficult to control can deteriorate the uniformity. Power fluctuations is one of them [50] and is enhanced at low power. The fluctuations translate into the structures with shape variations or having their edges melted as shown in Figures 2.17a&b. De-focussing of the focal spot, dirt present on the optics or on the tape itself are other factors. Laser machining can also suffer from uneven surface finish and coarseness in structures: the area where the laser starts and finish its cut (for a closed structure) is exposed to more energy than the rest of the geometry [55].

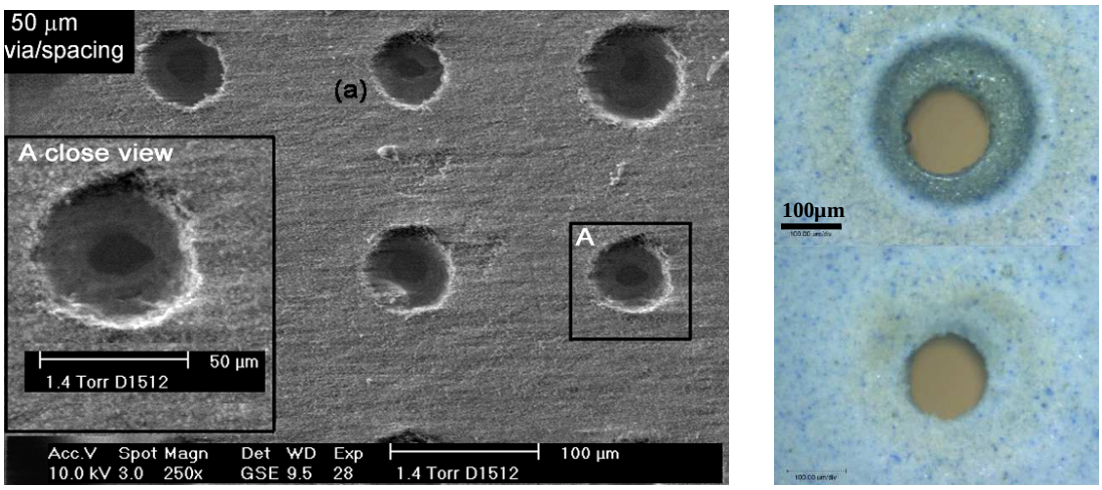

(a) (b)

Figure 2.17: Set of images showing examples of Nd:YAG laser fluctuation. (a) SEM photo of an array of 50µm vias pierced in 163µm græn tape [46] which highlights the differences in vias dimensions, (b) two vias lasered with similar process parameters, one showing glass vitrification (top), the other not [50]

Similarly to punching machining, lasers can cut the PET foil at the same time as ablating the green ceramic. PET foils are easily cut also, but the remaining structures have melted edges that can stick to the ceramic [56]. This can be troublesome during the PET foil removal with green ceramic structures being torn or stretched. Moreover, the foil is not entirely vaporized and residues can be found inside the apertures or deposited on the substrate surface [46]. These residues can impinge printing, thereby preventing proper filling of the vias, and can create delamination of the stack if left uncleaned. However the use of a 9.4µm CO_2 lasers has been shown to reduce the residues [56].

In the following part, two most commonly used laser on LTCC are presented: CO_2 lasers and solid state laser (Nd:YAG or Nd:YVO_4). The quality and characteristics of the resulting structures are described.

CO_2 lasers

These types of lasers are based on CO_2 gas active gain medium, and typically emit in the mid-infrared (wavelength around 10.6µm). The beam spot size is in the order of tens of microns. CO_2 lasers are also affordable with basic laser systems price starting at a

few tens of thousands of pounds such as Epilog systems [57]. CO_2 lasers can etch the green ceramic tape without melting the glass particles. The so-called cold ablation process was demonstrated in [58] and is based on the higher absorption of the ceramic particles than the binder as shown in Figure 2.18. The heat absorbed by ceramic particles is redistributed to the surrounding polymer, sublimating it rapidly into gases. The expending gas is ejected from the substrate, carrying away the particles with it. Due to the small Heat Affected Zone created inside the medium as the energy has less been absorbed by the binder, this process has a resolution equivalent to the beam spot size. The glass only melts inside the plume of gas through the incoming beam, not on the tape, preventing the formation of melted glass on the edges of the structure. However, thick tape above 200um might be subject to glass remelt as the molten material has more distance to travel out from the aperture and can deposit itself on the edges.

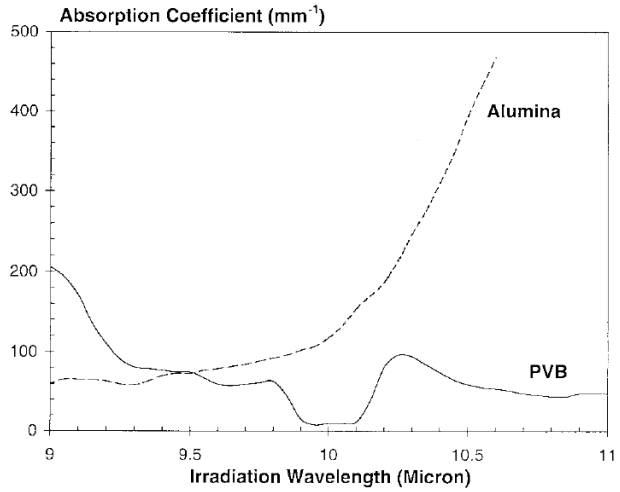

Figure 2.18: Absorption coefficient of alumina and PVB, polymer similar to the LTCC organic binder. The large absorption of alumina (factor of 10 compared to PVB) favours the absorption of energy by the particles [59]

Due to the principle of the process, the effects of the cold laser ablation are largely dependent on the composition of the green ceramic. According to [60], the resolution obtained is reduced with higher binder content. In such a tape, the heat propagates deeper in the binder and increases the etching depth inside the material. Fabrication of 50µm entry and 30µm exit diameter vias in HL2000 have been demonstrated with a single pulse of spot size of around 49µm and 100µs pulse duration [58]. Analysis of the structure edges did not show any melted glass and were virtually free of debris. The fine particles can be aspired with a dust collector during the process. Fine structures were

also fabricated as shown in Figure 2.19: the fine mesh in the bottom right corner has beams of 120µm in diameter. The structure quality will vary according to the laser frequency, writing speed, etc. The resolution achievable with such a laser being 49µm, it then behaves as a 50µm puncher. Pulses have to be shot at very close pitch in order to attain flat edges on the lasered structures. If pulses are shot with too large a pitch, cog wheel shape can appear, especially on the back of the structure as shown in the top right inset in Figure 2.19.

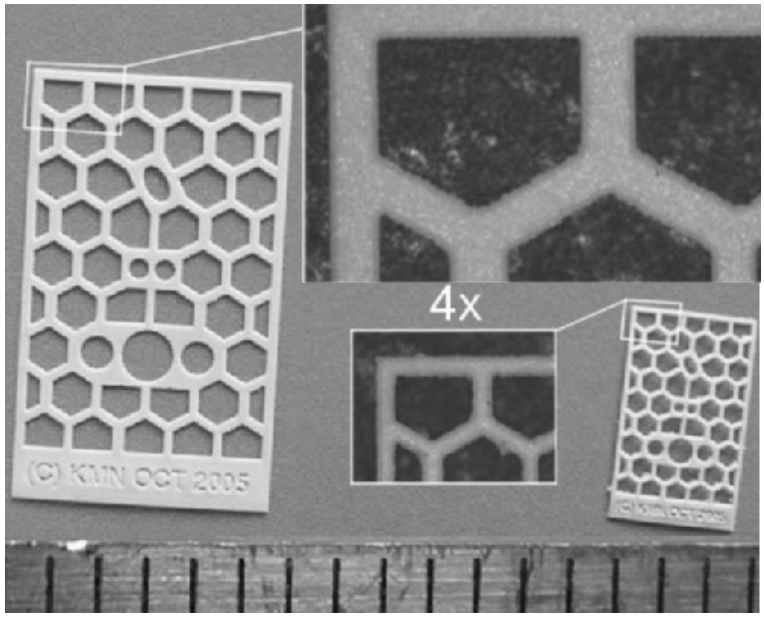

Figure 2.19: Example of LTCC mesh structure fabricated with CO_2 laser [58]. Ruler division= 1mm

Solid-state lasers

These lasers have a glass or crystalline active gain medium doped mostly with rare earth elements. The most common solid state laser is the Neodymium-doped Yttrium Aluminium Garnet (Nd:YAG) laser. The laser can be operated in Q-switch mode such that the beam can be pulsed with a duration of a few tens of nanoseconds, generating higher peak power than their average power. Most Q-switch pulse repetition rate ranges from a few Hz to 10s of kHz. Usually, Nd:YVO_4 lasers are preferred than Nd:YAG lasers because of their higher output power, better beam quality M^2 and lower threshold high [61]. Their fundamental wavelength is in the near infrared (1064nm), but can be changed using harmonic generators that double, triple or quadruple the frequency, thus lowering the wavelength to respectively 532nm (green light), 355 (near UV) and 266nm

(mid UV). However, lowering the wavelength requires additional harmonic modules and suitable optics that increase the overall laser cost.

Despite the relative poor absorption of ceramic material at these wavelengths [54], with the exception of the fourth harmonic, solid state laser are very often used in LTCC. The high energy density obtained from the combination of high peak power of a single pulse and the small dimension of focal spot - with adequate optics, the spot diameter at 355nm can be about 8µm - enable a rapid ablation of the tape. Moreover, the smaller focal spot increases the resolution compared to CO_2 lasers.

One consequence of this high energy density and the low absorption of the material is the melting of the glass particles contained inside the tape. This results in melted glass either projected onto the tape or remaining on the edges of the lasered structure. In extreme situations and small features, melted glass can solidify inside the via and totally obstruct the openings as shown in Figure 2.20a. More frequently, the structures of the edges look rough with melted glass attached on their edges as presented in Figure 2.20b. The quantity of melt is dependent on the quantity of glass content in the tape [62] but can be controlled by optimizing the laser parameters and reducing the amount of power used by the laser.

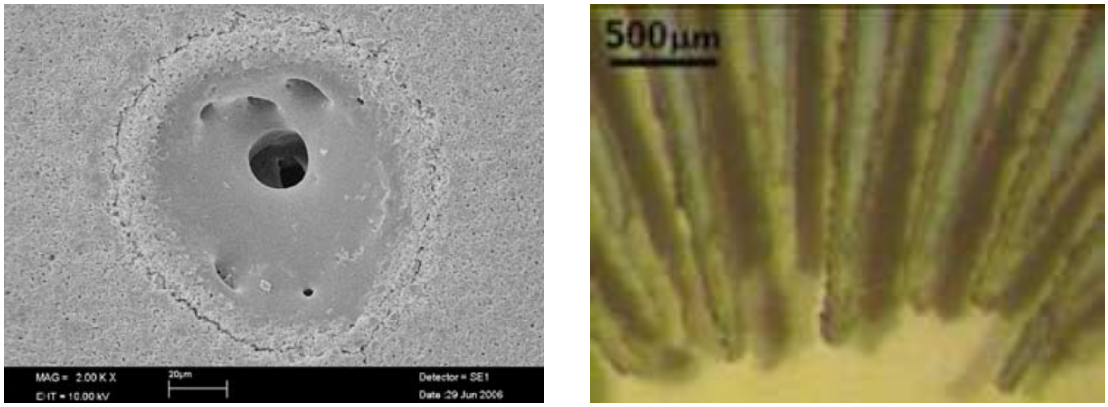

(a) (b)

Figure 2.20: Photos showing melted glass particles generated from Nd:YAG laser (a) inside a 80µm vias [63] and (b) on the edges of beams [55]

With a 15µm focal spot, solid-state lasers have been able to produce vias of 25µm in diameter [46]. However, such via diameter was only possible in 50µm thick layer. Although 50µm vias were pierced in thicker sheets, only 80% were properly pierced

through. Larger vias above 75µm in diameter were pierced for any tape thickness up to 254µm [46]. Thus 50~75um is accepted as the minimum diameter size for vias in LTCC tapes. 30 to 40µm vias were also reported in [64] in a ~100µm thick layer, but the laser was used with the fourth harmonic at 266nm wavelength. Interestingly, no thermal damage was reported. With the accuracy of such a system, very sharp structures can be fabricated as demonstrated in [55] and Figure 2.21. But, as for the vias, the line cut has a width larger than the focal spot which has to be taken into account. The line cut can be a few tens of microns large [65], which increases the structure dimensions. Reverse engineering can be implemented to compensate this.

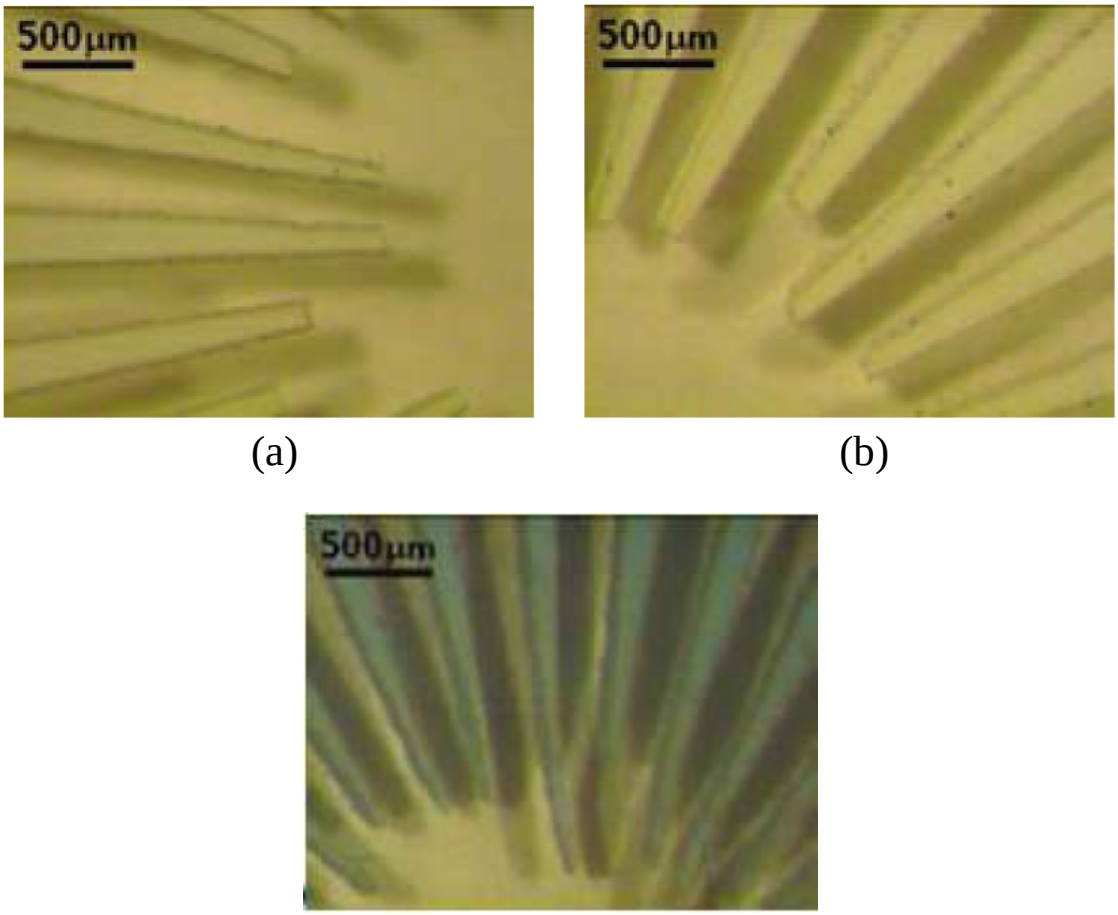

Figure 2.21: Thin beams cut in different LTCC tapes with Nd:YAG laser at wavelength of 1064nm: (a) 100µm, (b) 190µm and (c) DuPont 951P2 165µm tape [55]

2.6.3 *Hot embossing*

Embossing is a replication process in which a substrate is shaped by means of a

patterned mould with the aim of creating raised or sunken structures on its surface as shown in Figure 2.22. The material must be malleable, flexible and have low viscosity. Pressure is needed to conform the substrate to the mould while heat is applied to the entire system to increase the material ability to flow and relieve stresses [66]. The embossed pieces are then cooled down under constant pressure and are separated at ambient temperature.

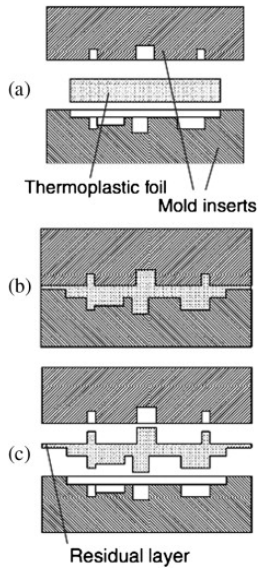

Figure 2.22: Hot embossing process [67]

The advantages of this technique include the use of a single master for the fabrication of thousands of pieces and the difficulty in designing complex patterns presents itself only during the master fabrication (not during the manufacturing of the embossed pieces). Due to the malleable properties of the organic binder and plasticizer, LTCC can easily be embossed. The mould usually consists of a simple metallic foil with raised structures. Electroformed nickel foil using LIGA process seems to be the most appropriate solution and is used in most cases [68, 69].

Embossing on LTCC

Embossing can be done on a single green tape layer or on laminated layers. However, once embossed, it is difficult to laminate additional layers on top of the structures: the structure collapses under the lamination pressure [70]. The temperature of reference for embossing ranges from 70 to 80 ºC, which is also the lamination temperature range of

LTCC. A lower temperature would result in a lower material flow making it difficult for the tape to conform to the mould. A higher temperature would increase the difficulty in removing the tape from its mould, especially for small structures, after the cool-down period [71]. An anti-sticking coating can be used to reduce this phenomenon. The holding time depends on the experiment and ranges generally from 1 to 3 minutes [68, 71], longer dwell affecting not significantly the shape of the structure [22]. Recent work has demonstrated the possibility of embossing green tape ceramic at ambient temperature [72, 73]. However, in each test, the tapes were specifically fabricated for this purpose and had a higher flexibility than commercialized tape. Embossing in itself is not capable of creating apertures. Vias and cavities fabrication has to rely on conventional machining techniques, mostly mechanical punching.

Embossed structures are only limited by the mould patterns capability and the ability of the material to flow inside the recessed structure. Because the base of the structure is attached to the layer surface, complex shapes can be easily created in the LTCC surface with stand alone patterns possible, examples of such structures are given in Figure 2.23 [68]. Sharpness and resolution of the structures will depend on the ability of the material to fill the mould.

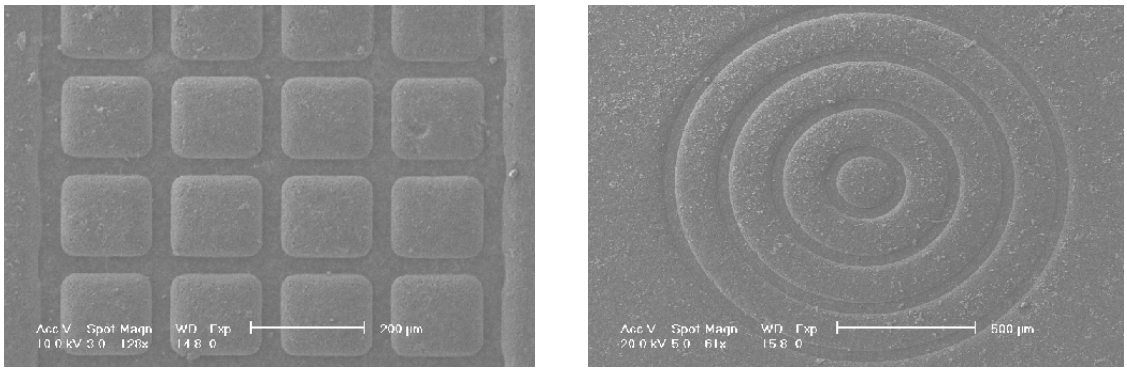

Figure 2.23: Examples of patterns embossed in LTCC [68]

Uniaxial or isostatic pressing are used to create such structures. However, roller embossing machines have been also successfully used. Such machines offer the advantage of a small contact surface between the tape and the roller and quick embossing can be realised. Although the mask is in permanent contact with the tape, the pressure is only exerted during a few seconds at the roller position. Demoulding is therefore facilitated. Fine 50µm width embossed channels were created on Heraeus

HL2000 [69]. However, the process limitation lies in the structure depth: only 20µm depth was achieved for 40µm thick patterns. The structure edges exhibit also large round corners that decrease significantly their resolution. Finer, sharper and deeper structures can be fabricated using uniaxial press. Channels with width/lines of 100µm/100µm and 50µm/100µm were successfully produced [71]. Figure 2.24a shows an embossed 40µm deep channel with an end smaller than 5µm. Incomplete filling of the mould, seen for large channels and small pitch, resulted in structures having round edges and inadequate depth. It is thus suggested that embossing works better for small channels and large pitch than large channels and small pitch [74]. Channels as small as 25µm wide were fabricated. They are shown in Figure 2.24b. Embossing can also be used to improve tracks system inside the LTCC package [75, 76]. Thin channels were embossed and filled with conductive paste in order to increase the thickness of the tracks and lower the sheet resistivity of the conductor.

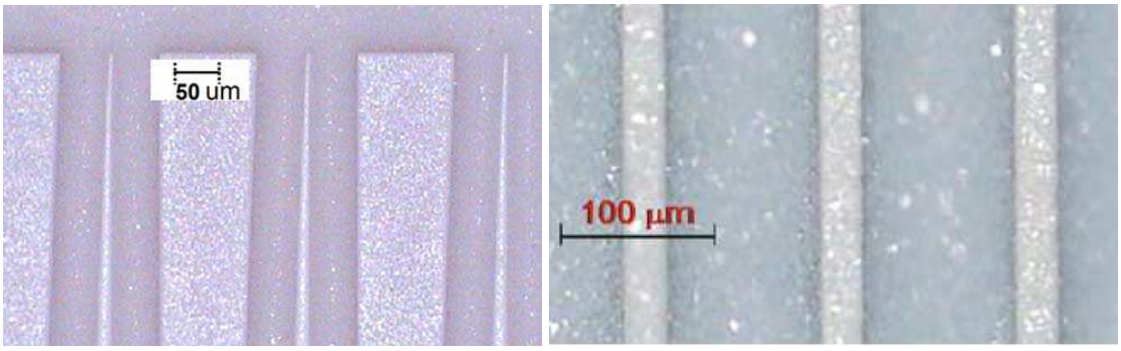

(a) (b)

Figure 2.24: Photograph of (a) tapered beam and (b) 25µm channel spaced by 100µm in HL2000 [74]

Combination of punching and embossing has also been demonstrated by [77, 78]. An embossing tool formed by a series of spikes with swollen base was used to create U shaped apertures in the LTCC green tape as illustrated in Figure2.25. This structure was realised on a stack of 8 to 12 layers that was laminated at the same time than being punched-embossed.

Figure 2.25: Combined punching-embossing technique: The LTCC is pierced and the aperture walls shaped by spikes [77, 78]

Combining lamination and embossing techniques has also been employed to pattern the ceramic tape in the hope of reducing the number of machining steps [79]. Structured metal sheet were inserted directly during the stacking process between the large stacking plates and the green tape (Heraeus HL2000) as shown in Figure 2.26. The lamination of the stack and the embossing were done simultaneously in an isostatic press at 70°C for 8-10 minutes and at a pressure of 10MPa, which are the recommended lamination parameters of the ceramic tape. The longer embossing time and higher pressure did not pose any problems with channels having similar properties than observed in [74].

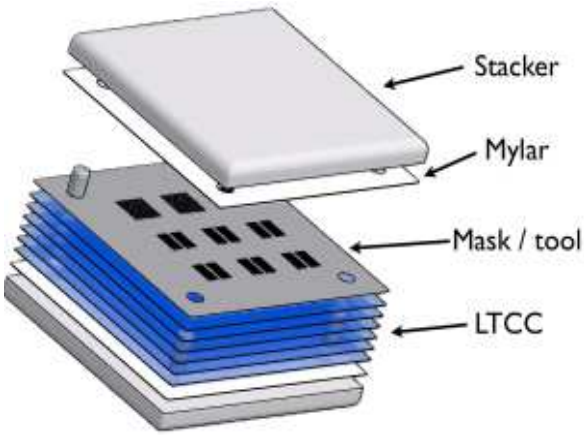

Figure 2.26: Layers setup in the stacker for combined lamination-embossing [79]

The same paper also reported the fabrication of raised structures using a mould with only recesses. Unlike traditional embossing where the material is squeezed in the substrate, the structures are “raised” by squeezing the material in the mask openings. Tests were done with 100µm and 50µm thick mask on HL2000 using the lamination parameters of the tape. Results are displayed in Figures 2.27a&b. The structures conformed to the 100µm mask thickness, even for beam only 90µm in width. 50µm thick pillars of 160µm in diameter were also created with the 50µm thick mask. However, the structure analysis revealed small cracks around the raised LTCC base. Shrinkage of the structures in the z-direction was modified for the structures with 100µm heights, not for the 50µm heights.

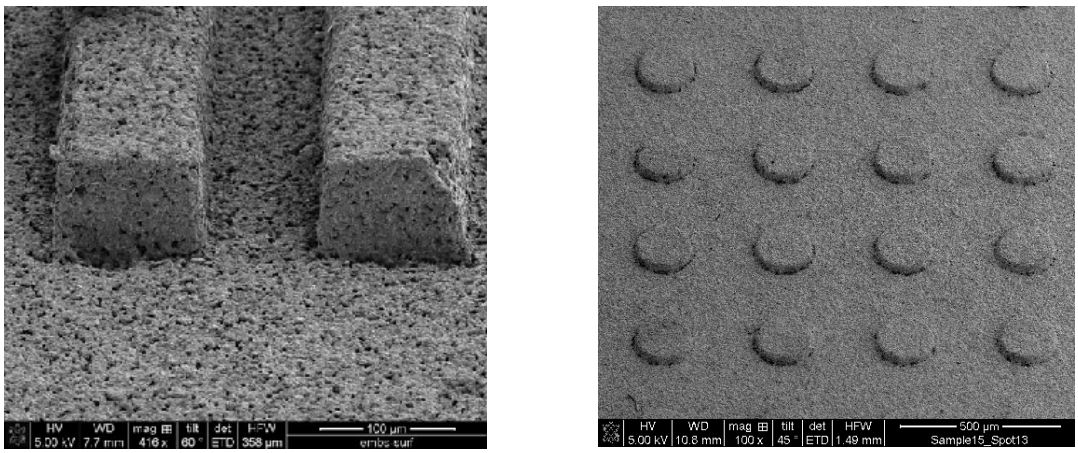

Figure 2.27: (a) 100µm height raised beam (cofired) and (b) 160µm diameter dots raised with a 50µm thick mask (cofired) [79]

2.7 Conclusion

In this chapter, an overview of the LTCC material and fabrication process has been presented. The composition of the green tape was described and its advantages compared to other substrates were identified. The different steps needed for the fabrication of an LTCC package were laid down.

Three methods of machining the green tape were described. Two of these methods, punching and lasering, were shown to be the most commonly used methods to pierce the tape and achieve sub 100µm structures. They are efficient and fast ways of cutting green tapes, but create remelts, burrs and slugs that can impede the use of the smaller

structures. Debris of PET foil can also be found on the structures edges which can have the undesired effect of delaminating the stacked layers during the sintering. The third technique, embossing, was shown to be dedicated to shape the surface of the tape rather than pierce it.

Chapter 3 Powder Blasting Apparatus and Preliminary Experiments

3.1 Introduction

An essential part of the work reported in this thesis is to characterize the equipment to distinguish controllable from uncontrollable parameters. Similarly, the understanding of the abrasion process on the ceramic material must be known to reduce the number of parameter to use.

This chapter aims to provide a first approach on the utilisation and interaction of the powder blasting process on the green tape ceramic. First, issues related to the adaptation of the powder machine setup for the machining of ceramic tape are addressed. Secondly, the behaviour of the green tape ceramic under particles bombardment without mask is investigated.

3.2 Experimental setup

3.2.1 Powder blasting apparatus

A powder blasting unit can be broken down into three central parts: the high pressure unit, the sealed enclosure box in which the abrasion process takes place and the aspiration unit. Those three units are the basics of a powder blasting setup and ensure the handling, containment and extraction of the micro particles. The setup owned by Heriot-Watt University and used in this work is shown in Figure 3.1.

The powder blasting machine has been acquired from the company Texas Airsonic [80]. Two units, shown in yellow in Figure 3.1, have been bought and are connected to a single control panel. The latter controls the pressure exerted inside the reservoirs and the intensity of the flow. The intensity can be defined as the quantity of powder expelled at the nozzle tip. In other words, the intensity controls the flow rate of the particles. It ranges from 0 to 9, from no flow to maximum flow rate possible. These numbers are, however, not present in the original setup and have been added arbitrarily. The optimal operating pressure range of the system is comprised between 85psi (586kPa) and 195psi (1344kPa). Compressed air or nitrogen gas can be used, but the maximum pressure available for both gases is around 100psi (689kPa). The reservoirs have a 3 litres capacity and can handle particles size ranging from 5µm to 350µm. The nozzle tips are

made from titanium/tungsten carbide. The nozzle tip has a cylindrical aperture with a diameter of 0.8mm.

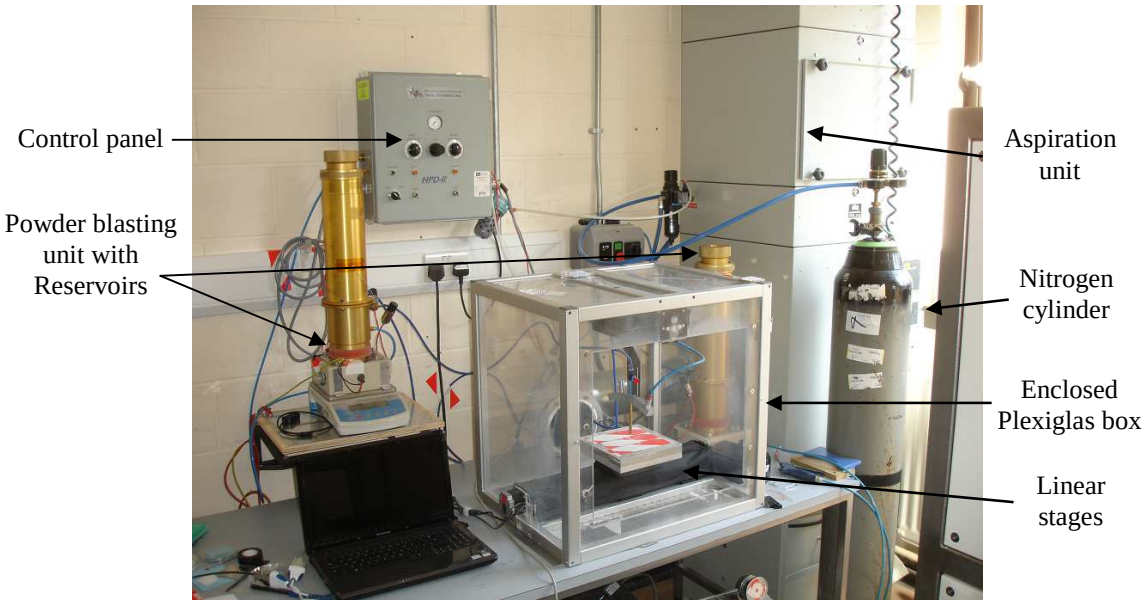

Figure 3.1: Powder blasting setup with the powder reservoir, the enclosed box and the extractor

Each unit can be broken down into two elements: a reservoir on the upper part and the feeding chamber in the bottom part. A detailed schematic of the unit can be seen in Figure 3.2. The reservoir contains the powder. The powder gradually passes through to the feeding chamber at the same rate as the powder in the feeding chamber is emptied; there are no mechanical movements involved in this process. Once in the feeding chamber, the particles are transported to the nozzle thanks to a vibrating mechanism [81].

The feeding chamber consists of a vibratory system and a spiral chamber containing the powder from the reservoir. The vibrations generated by the system create a rotational movement that drags the particles along a spiralling ramp placed on the wall of the feeding spiral chamber. This ramp has a 5º angle of inclination and ends at the top of the chamber with a tube leading the particles to the nozzle. This process allows the particles to be skimmed from the agglomerated particles at the chamber bed and creates a steady stream of powder ready to be expelled at the exit tube. By varying the intensity of the vibrations, the quantity of particles reaching the exit tube, and thus the flow rate at the nozzle, can be changed.

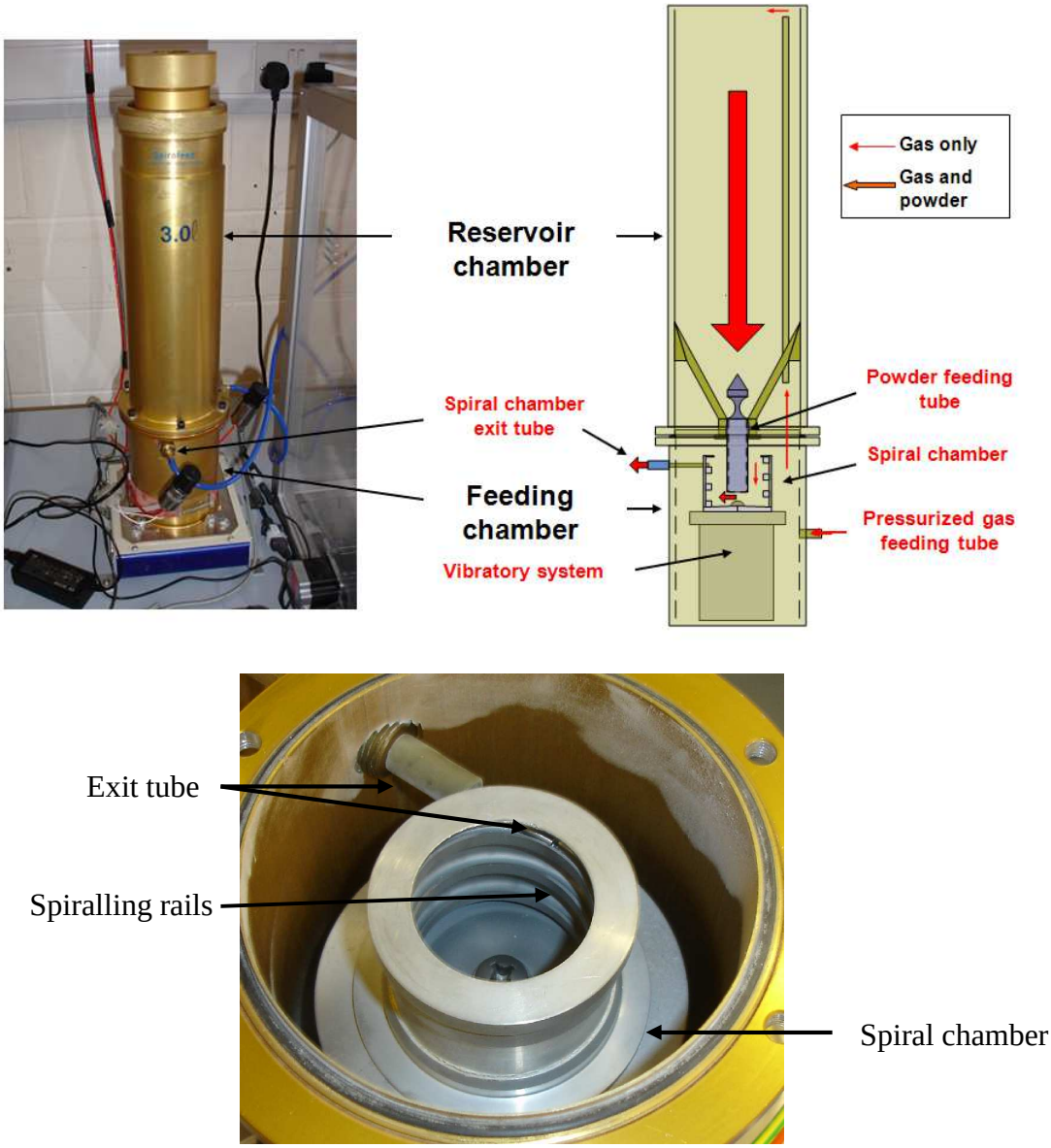

Figure 3.2: Schematic of a powder blasting unit and photo of the spiral chamber

The enclosed box has been fabricated at Heriot-Watt University from Plexiglas sheet 6mm thick with an aluminium framework. A removable front panel is used as a door and allows easy access to the samples. In the back, a large opening connects the enclosed box to the extractor unit. The latter is constantly recycling the air inside the box during the powder blasting process, removing at the same time the particles and chipped substrate. Small apertures in the Plexiglas wall allow fresh air to be injected in. After the powder blasting process, an air dust blow gun is used to force the static powder left in the box out to the recycling unit.

The nozzles are placed onto an arc holder attached on a motorized axis (y axis) fixed on the ceiling of the enclosed box. The arc holder can also be orientated to vary the angle of the nozzle compared to the normal. The stage on which samples sit is fixed onto another motorized axis (x axis) placed at the bottom of the box (Figure 3.3). Both axis are at 90ºC to each other, enabling scanning in x and y. A VXM Stepping Motor Controller (Velmex.inc) operated from a computer controls the two independent linear stages. The maximum speed for the stages is 152mm/s, the default speed set at 40mm/s. The minimum increment that the motors can produce is theoretically 2.54µm. The dimension of the working area is 200x200mm.

The controller cannot operate both stages at the same time. This particularity only allows the nozzle to scan the samples in x, then y or inversely, one axis at the time. It is then impossible to follow circular geometries. Furthermore, as the controller changes endlessly from one axis to the other, it introduces pauses between each swap lasting around 0.1 of a second and leading to overexposure of certain parts of the substrate.

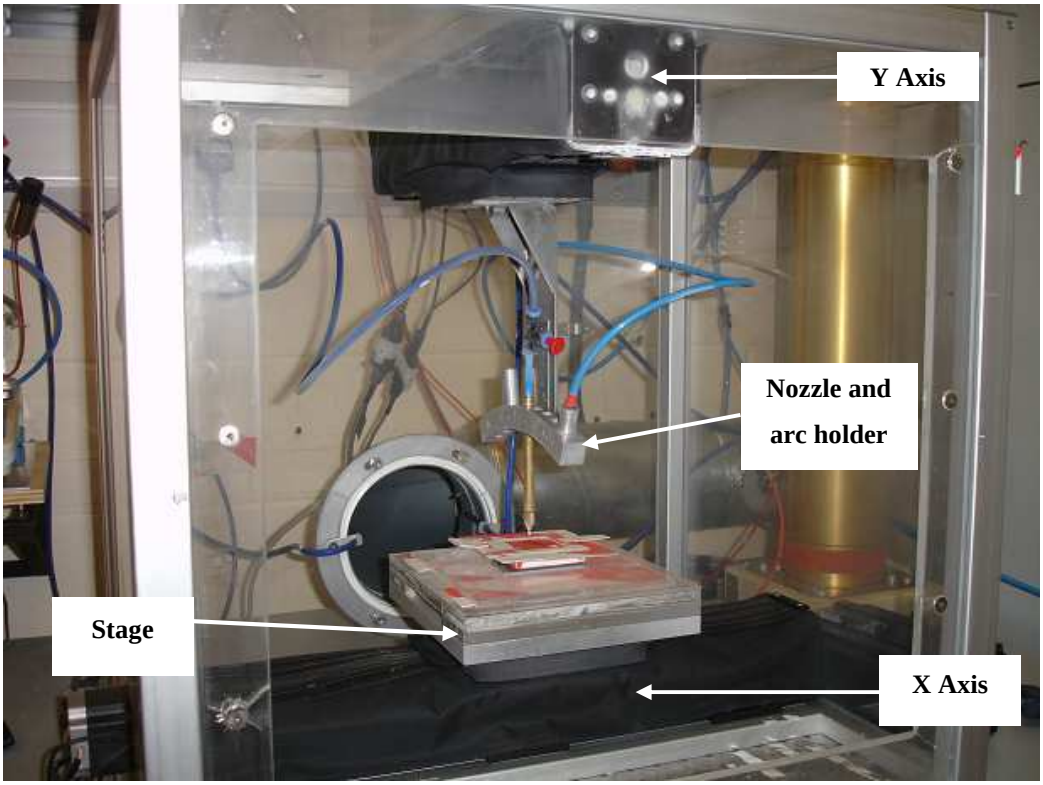

Figure 3.3: Enclosed box with the 2 stages

The variation of the mass of powder during the experiment is recorded by measuring the

mass of the entire system. The balance is placed under the powder blasting unit and measures the mass of the powder blasting machine and the powder inside the reservoir. Fully charged, the total mass of the system is about 8.5kg. Thus the scale must be able to measure such a high mass. To achieve this, a balance from Radwag (model WLC 10/A2) was employed. The disadvantage of such setup is the low accuracy of the balance (~0.2g) and 3 seconds stability required for each measurement. However, this prevents powder being lost during potential transfer from the reservoir to a more accurate balance. Furthermore, the balance is able to feed a computer with live measurements every 0.5 of a second thanks to a proprietary program which records the data and compiles them into an .xls files. From it, the flow rate can be calculated.

This method provides a more accurate measurement than the calculation of the mass loss obtained by subtracting the mass of powder at the start of the experiment to the mass of powder at the end. Plotting the time dependent curve of the lost mass allows indeed the detection and correction of any abnormal deviations that would change the total mass of powder used during the test. The slope is also computed automatically from the trend line of the plot, thus providing an average of the flow rate which takes into account the variations of the flow during the test. It is, however, not possible with this program, to see the live flow rate during the experiment.

The computer interface which is used to control the linear stages is presented in Figure 3.4. It is a custom made program based on C-sharp language. It was written by Stefan Wilhelm, a PhD student also studying at Heriot-Watt University. This interface is based on a graphical user interface which allows simple shapes such as squares and rectangles to be drawn to define the surface to be scanned (1). Parameters such as speed, rastering pitch and number of passes can be set for each one of these areas in the process sequence (2). Up to 10 surfaces can be set. The scanning sequence is controlled with the “play”, “pause” and “stop” buttons (3). In addition, the software provides real time feedback positioning of the nozzle in both working area and machine position (4).

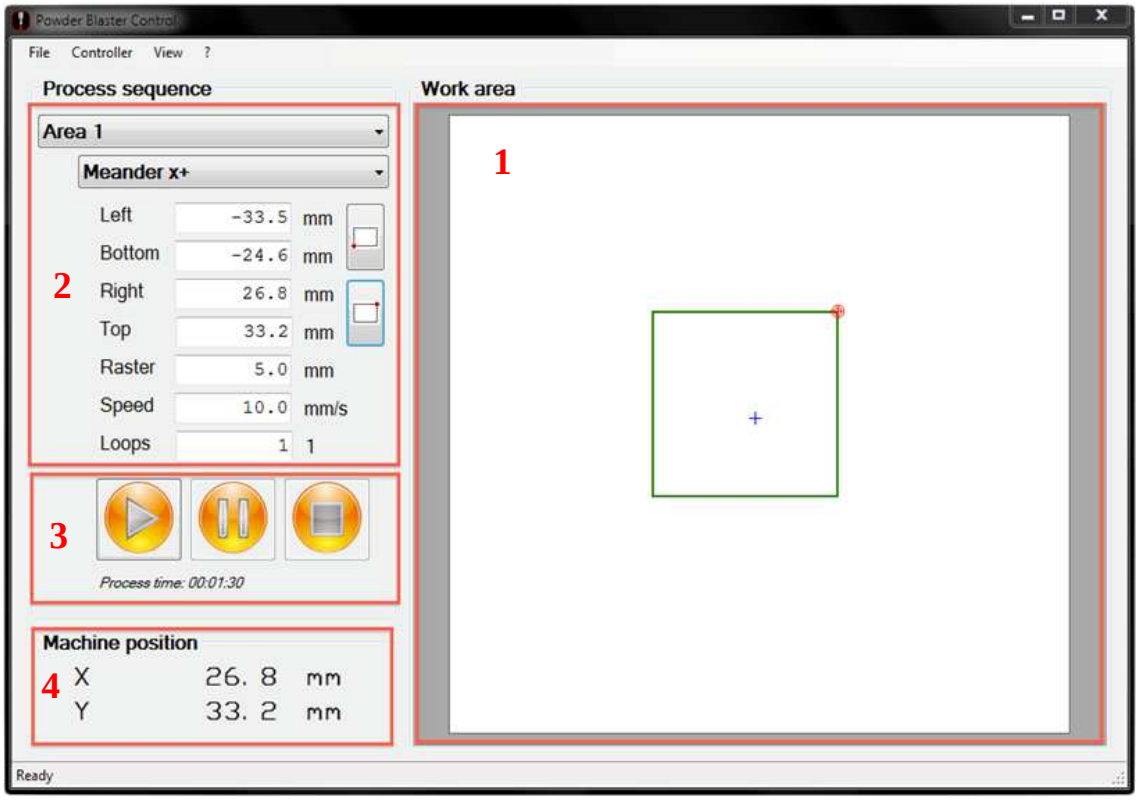

Figure 3.4: Diagram showing the graphical user interface controlling the linear stages

3.2.2 Powder characteristics

The powder used with the powder blaster is composed of sharp 99.5% aluminium oxide (alumina) particles. Heriot-Watt possesses particles in two average sizes: 9 and 30µm. The latter size will not be used in this thesis due to the particles' higher erosion rate which will abrade the ceramic, but also the mask rapidly. In addition, smaller particles have other benefits that can be used to an advantage in this thesis. Firstly, 30µm size particles will reduce the resolution of the patterning compared to 9µm particles as demonstrated by Anne-Gabrielle Pawlowski in her thesis [82]. And secondly, 9µm have been shown to reduce blast lag (eroded depth lag) which occurs between cavities with different widths [83, 84]. This means that the eroded depth is less dependent on the mask aperture dimensions with smaller particles and the same particles will produce more consistent results with different aperture widths.

The alumina particles were supplied by Guyson International Ltd (through ETC limited). This type of powder belongs to the low hand range with a bag of 25kg costing about £185. The drawback of such powder is the particles size distribution: the

deviation can be large as evidenced in Figure 3.5a. With an average size of 9µm, particles as large as 35µm and sub micron can be found (the same can be said for the 30µm particles). This increases the erratic behaviour of the particles during the process. In comparison with a top of the range 9µm alumina powder from Comco, the variation of the particles diameter is smaller (Figure 3.5b). The particles are however expensive with a bag of similar size (25kg) being priced at around £1589. As the focus of this thesis is to benchmark this process to the laser and punching processes, cost is here an important factor. Thus the powder selected to accomplish the experiment work of this thesis will be the powder bought from ETC limited.

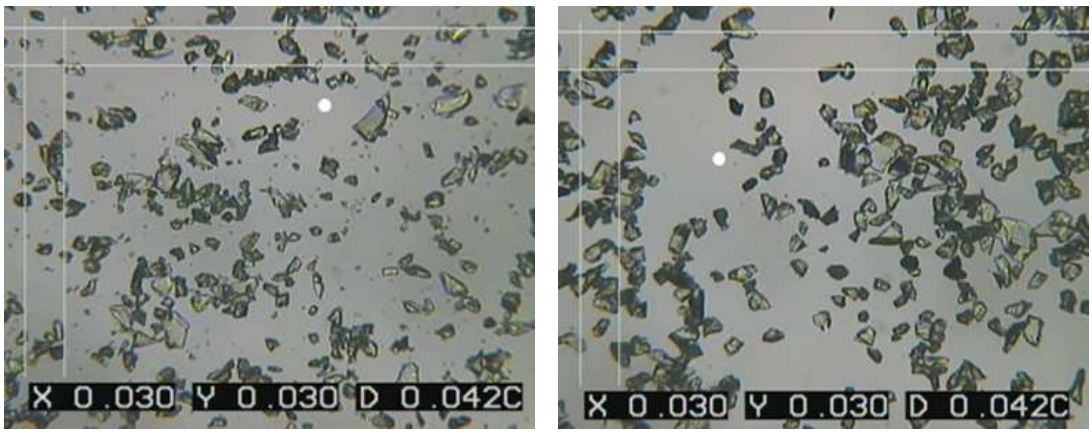

(a) (b)

Figure 3.5: Photograph taken with an optical microscope of (a) ETC powder and (b) Comco powder. The white round circle represents a particle with a diameter of 9µm

3.2.3 LTCC material

The materials used in this thesis are the DuPont 951 green ceramic manufactured by DuPont.

These tapes were selected because they are widely praised for their global properties i.e. low x&y shrinkage (12.7%), relatively good dielectric constant (7.8), low loss tangent (at 3GHz: 0.006). They are readily available in large quantity and at different thicknesses: 50µm (C2), 114µm (PT), 165µm (P2) and 254µm (A2) in 152x152mm square sheets. Furthermore, the industry extensively uses DuPont ceramic tape for package fabrication, especially in electronics and Microfluidics. Only the 165µm P2 layers will be however used as they fit both the process characterisation and the package

fabrication.

Furthermore, the shrinkage of the tape can also be used as an advantage. It is very well controlled within a given set of parameters (as explained in Chapter 2). This allows the fabrication of larger structures in the green tape, structures which will shrunk by ~12% after firing. However, this does not fit all applications (free standing single layers for example) as shrinkage also induce warpage which can be detrimental to package.

3.3 Setup adaptation

The powder blasting unit used in this thesis is a commercial unit designed to undertake heavy duties such as deburring, paint and rust removal on metal, glass and ceramic cutting. The high kinetic energy of the particles is an important parameter and is obtained through high pressure applied in the reservoir. This explains why the Texas Airsonic unit was built to sustain a minimum pressure of 80psi (586kPa). However, as it will be explained later in this chapter (and in Chapter 4), the machine needs to be used at lower pressure.

3.3.1 Original setup flow rate characterisation

Flow rate

The tests were conducted at the pressure of 50 psi (344kPa), with 9µm particles size, for different intensities ranging from 5 (I5) to 9 (I9). This series was repeated 5 times, no powder being added between each one. Two different initial quantities of powder were tested: 2300g of powder which corresponds to the maximum capacity of the reservoir and 800g of powder (reservoir 2/3 empty). The flow rate is then recorded over a period of 60 seconds. The flow is calculated at the end of each experiment once the excel file that has been created can be opened.

This experimental procedure was selected to simulate a practical use of the machine with changing intensities and decreasing powder mass. The results are shown in Figure 3.6. Each point on this graph is the average value of the 5 measurements recorded with the same parameters. Six measurements were initially done to calculate the mean and standard deviation. But the flow rates obtained during the first series were so different from the rest that it was decided not to take them into account. This is detailed later.

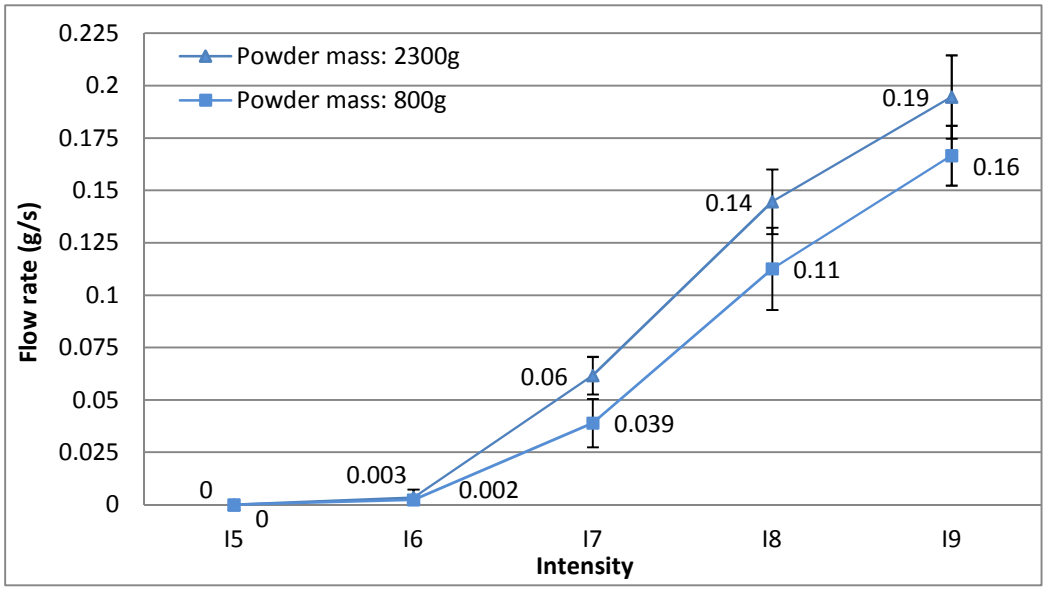

Figure 3.6: Variation of the particles flow rate at 50 psi as a function of measurement series and intensity

The results in Figure 3.6 highlight some of the machine characteristics such as the flow rate values for each intensity which will be used as benchmark for future experiments. There is no flow at I5 and intensities below. This is despite a jet of powder being visible. The flow at these intensities is too weak to be measured by the balance over the length of a minute. Erosion still occurs but is, with no mass change recorded, unusable for the experiment. The flow is very weak at I6. Moreover, Figure 3.6 also clearly shows that the mass of powder contained in the reservoir has an impact on the flow rate: at all intensities, the flow rate is higher when the mass of powder contained in the reservoir is large. The pressure exerted by the particle's own weight feeds more powder to the spiral chamber than when the powder mass is low.

However, the impact of the powder mass on the flows decreases when the flow rate increases (intensity): the difference between the two flows drops from around 35 % for I7 to 14% for I9. In addition, when sampled over a small quantity of powder loss, the impact of the powder mass on the flow is very limited as evidenced in Figure 3.7. The data shown are from the flow rate recorded in Figure 3.6 for each intensity before the 5 series of tests were averaged. As mentioned before, each series were composed by the measurement on the flow rate at intensity I5 to I9 for 60 seconds, and the 5 series were recorded in a row. The flow shows no real dependence over the mass change during

each series as the curves are fairly flat, despite the mass varying between the start of the series and the end of the series of about 120g for the full reservoir and 96g for the 2/3 empty reservoir powder mass.

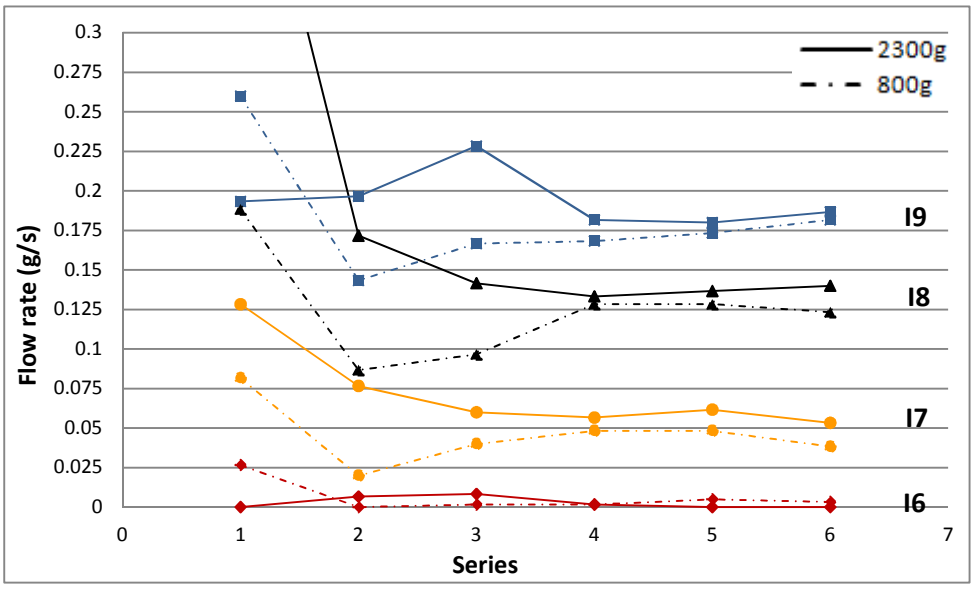

Figure 3.7: Evolution of the particles flow rate at 50 psi as a function of the intensity

Flow variations

From the average flow recorded in Figure 3.6, the standard deviation was calculated and represented by the vertical black lines at each point on the graph. However, to interpret correctly the variations of the flow, the coefficient of variation (CV) is used. It is defined as the standard deviation σ divided by the mean A, and multiplied by 100 (equation 3.1).

$$CV = \frac{\sigma}{A} * 100 \qquad 3.1$$

The coefficient of variation is a useful tool to express the variation. Standard deviation (SD) alone is only relevant in the context of the mean it is calculated from and cannot be compared with another mean. For example, two results of a population average, let say 10 and 100, can have the same standard deviation, 2. However, the amplitude of the variations is extremely different as it represents a 1/5 of the value of the former and a 1/98 of the value of the second. On the other hand, CV compares the ratio of the standard deviation and the mean. Thus it offers the possibility to compare different sets of SD and their means. In this example with a population average of 10 and 100, the variation is 20% and 2% respectively.

The coefficient of variation of Figure 3.6 is shown in Table 3.1 for each intensity. It shows a clear increase in the repeatability of the flow when the latter increases. The variations at I6 are very high, but can be partly due to the low accuracy of the balance as the flow rate measured oscillates between 0 and 0.5g/s. Overall, without taking I6 into account, the repeatability is better when the reservoir is fully loaded with powder.

Table 3.1: Evolution of the coefficient of variation calculated from data obtained in Figure 3.6

Intensity	I6	I7	I8	I9
CV (800g)	81%	29%	17%	8%
CV (2330g)	117%	14%	10%	10%

As mentioned before, the series 1 was not taken into account in Figure 3.6 and Table 3.1 but was left voluntarily in the graph in Figure 3.7. As it can be seen, there is a large discrepancy between the flow rate of the series 1 and the rest of the series. This can be explained by the powder organisation inside the reservoir after refilling. Before both tests (at different powder masses), the reservoir was emptied to remove moisture contaminated powder and refilled with freshly dried powder. The powder, poured from the top of the reservoir, falls all the way down the 30cm height reservoir, filling the latter and the spiral chamber at the same time. This chaotic powder organisation, hardly reproducible, introduces huge variations in the flow rate which continue until the powder settles in both the spiral chamber and the reservoir. As a proof, taking the coefficient of variations of series 3 to 6 (Table 3.2) shows that the repeatability increases even further (except at I6 for the fully loaded reservoir where the flow rate of series 5&6 was 0).

Table 3.2: Coefficient of variation calculated with series 3 to 6 from data obtained in Figure 3.6

Intensity	I6	I7	I8	I9
CV (800g)	54%	12%	13%	3
CV (2330g)	158%	6	3	12%

Clearly the repeatability of the machine is poor at I6 and this intensity should not be used. For a good repeatability, it was considered the variations should not exceed 10%. To some extent, I7 can be used, but only I8 and I9 achieve this target. Moreover, the random organisation of the particles after filling the reservoir pushes the user to wait for a settling period for the powder to increase the repeatability of the flow.

Clogging

Another typical problem with powder blasting machines is the "clogging" of particles inside the reservoir. The term clogging is used here to designate a discontinuation of the flow of particles at the nozzle. It originates mostly from a lack of powder inside the spiral chamber due to cavities formed inside the reservoir (Figure 3.8). These cavities forms naturally due to the particles cohesive strength [14]. They are solid structures that prevent the powder from flowing from the reservoir to the particle feeding system. The phenomenon is accentuated by the presence of moisture inside the powder and affects mostly small particles. Larger particles, such as the 30µm alumina used mostly for glass and silicon cutting at Heriot Watt University, hardly clog: the mass of each particle is large enough to overcome forces applied to each individual particle and prevents the cavity formation.

With the 9µm powder, clogging happens frequently, despite powder being dried at 150°C for a few hours before each test. Collapsing the cavity by shaking the reservoir is then the only alternative to restart the flow, but this has the effect of filling the chamber erratically, changing the flow rate to the same effect but to a lesser extent as in series 1&2 shown in Figure 3.7.

Figure 3.8: Typical example of a cavity formed inside the powder in the reservoir

Flow fluctuations are then increased by factors such as a forming cavity collapsing before the stop of the flow or decrease in the powder when the powder is about to run out in the spiral chamber (when cavity is formed). It is however important to note that clogging occurs more frequently when high intensity, thus high flow rate, is used (I8 or I9) and the cavity has less time to collapse.

In its current state, and due to the low pressure used for these tests, the variations of the flow render the process difficult to use in a repeatable manner. Although the structuring characterisation of the green tape would not be impacted, it is important to have a repeatable and uniform process to define process timing according to certain parameters. This prevents uneven piercing of the layers and reduces (if any) clogging occurrences frequency and ensures durability of the etching process over extended machining time. The impossibility to correct the flow during the experiment increases the risks of high structure erosion variations. In order to overcome those difficulties, modifications of the setup had to be implemented.

3.3.2 Improvements

Flow issues are a well known phenomenon in the powder blasting industry. Flow fluctuations come from a large number of factors such as moisture content inside the powder, storage time, compaction of the particles inside the reservoir [13, 14], but also on the particles' properties such as size, texture, shape etc. All these factors are difficult to control and variation of the flow is at best only reduced, but never suppressed. To improve the operation of a powder blasting machine, Ghobeity et al. [13] successfully introduced a vibrating tool or mixer in the reservoir to limit powder stagnation and reduce clogging. On the other hand, work has been done on the nozzle shape to improve the uniformity of the erosion line shaped (line shape Laval nozzle, Karpuschewski et al. [85, 86]). In regards to the system used in this thesis, such modifications would require a considerable amount of time and involve a lot of resources which cannot be spared. Thus the improvements had to be kept simple and as less destructive as possible.

Reservoir re-dimensioning

A simple modification proposed in this thesis is based on the modifications of the reservoir dimensions. A plastic tube with a diameter of 52mm was introduced inside the

original reservoir as shown in Figure 3.9a. The new reservoir has a diameter half the size of the original reservoir (102mm). With equal length, the maximum powder capacity has then been reduced by a third to about 800g. The smaller reservoir allows the same pressure to apply on the powder as if the reservoir was filled with about 2300g of powder. And the large space available between the two reservoirs can be used to house desiccant stones on a rack design specifically for this new reservoir as illustrated in Figure 3.9b. The stones prevent moisture from entering the reservoir when the system is not pressurised. It allows the powder to be reused as the experiments realised for this work do not use the entire reservoir. Moreover, the reservoir should at least have a certain amount of powder so variation between large quantities of powder is minimised.

(a) (b)

Figure 3.9: (a) The new reservoir; (b) placed inside the original reservoir with desiccant porous stones

The new reservoir has been tested following the same experimental procedure described earlier. The tests started with the reservoir at its full capacity (800g) and no powder was added between tests. The results are compared with the original setup and are displayed in Figure 3.10. The first series was not included in this graph.

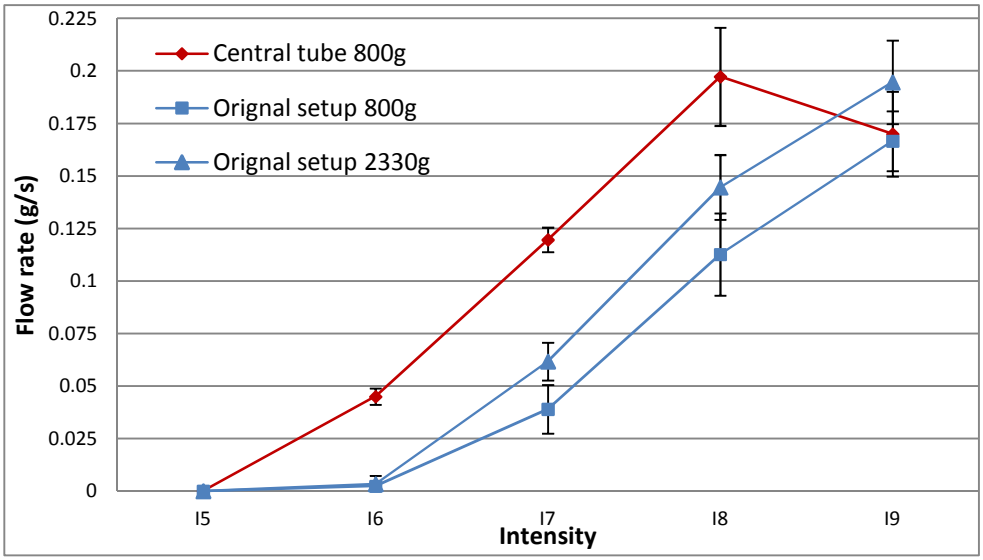

Figure 3.10: Comparison between the original setup flow rate and the modified setup

The graph clearly shows an increase in the flow rate at each intensity, except at I9. The curve obtained with the new reservoir has a similar slope to the original reservoir, but shifted to the lower intensity. The flow rate is then higher at lower intensity: I6 can then be used, and has roughly the same flow than I7 of the original reservoir, I7 of the new reservoir has the same flow rate than the original reservoir at I8, etc...

Although the use of intensity 6 is an advantage for the new reservoir, the limitation at the intensity I9 to a value of 0.175±0.02g/s does not enable the use of higher flow rate as it could be suggested by the shift of the curves. However, with the new reservoir, the variations of the flow rate have substantially been reduced, as shown in the updated coefficient of variation Table 3.3. The variations are now well below 10% of the mean value for intensity 6 and 7 and match the variations recorded with the original setup for I8 and I9.

Table 3.3: Coefficient of variation calculated from the Figure 3.10

Intensity	I6	I7	I8	I9
CV (2330g)	117%	14%	10%	10%
CV (800g)	81%	29%	17%	8%
CV new setup (800g)	8%	5%	11%	11%

In addition to the flow rate improvement, the powder can be left overnight and be used

the next day thanks to the desiccant stones. Tests have actually shown that powder left for one month inside the tube was usable although the repeatability was then not as good as with fresh powder. The clogging of the particles has also been reduced. It has not been entirely eliminated, but significantly been reduced as cavities are less likely to form, or their formation and their collapse happen more often, reducing the flow stop and particles flooding.

Reservoir temperature at 50ºC

A flexible heater was also added to the outside of the reservoir. This heater was installed to maintain a temperature of around 50°C inside the reservoir to prevent overnight moisture contamination. However, in addition to keeping moisture out, it appeared that the higher temperature also increased the flow rate. To assess the improvement, tests were done with the original reservoir setup filled with 2,300g of powder and the new modified reservoir, both with and without the flexible heater at 50°C. The results are displayed in the Figure 3.11.

It shows that the heat increases the flow rate for a given intensity. The original reservoir flow is even higher than the flow of the modified reservoir without heater. But the flow with the new reservoir combined with the heater is even higher. Again, a limit after intensity 8 can be seen where the flow rate decreases at I9. Flow rate at I5, albeit very small, could be recorded with both reservoirs with the heater, but with large variation amplitude ranging from 30 to 60%. Except at I5, the variations shown in Table 3.4 have similar amplitude than the test of the new reservoir without the heater. Clogging was slightly improved, although this is difficult to measure due to the only slight improvement of the results with the heater.

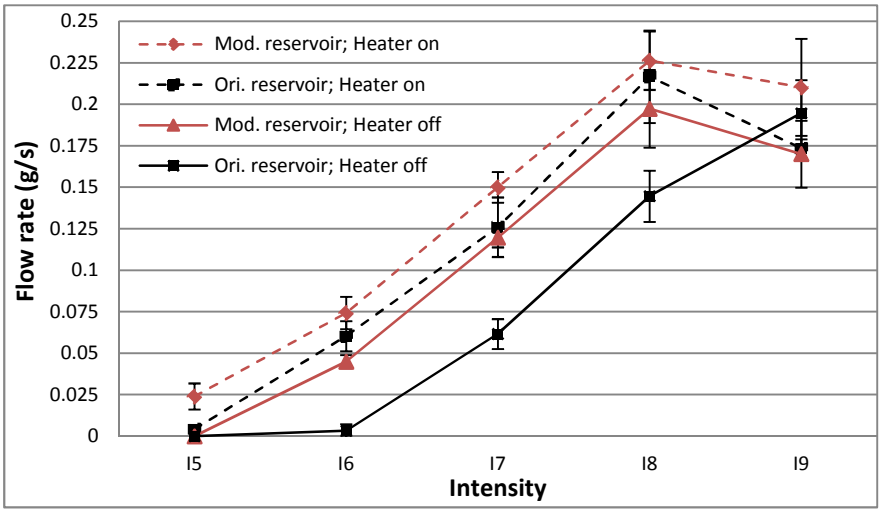

Figure 3.11: Flow rate of the original and new reservoirs with and without the heater

Table 3.4: Coefficient of variation expressed in percentage of the mean for the 4 different setups

Intensity	I5	I6	I7	I8	I9
Ori. reservoir, heater off		117%	14%	10%	10%
Ori. reservoir, heater on	58%	14%	14%	12%	3%
Mod. reservoir, heater off		8.6%	4%	11%	11%
Mod. reservoir, heater on	32%	13%	6%	7%	13%

One noticeable improvement with the heating resistance concerns the consistency of the jet. At ambient temperature, it is frequent to see the powder being pulsed from the nozzle i.e. the powder seems to be delivered in small packets instead of a continuous flow. In fact, the jet is always pulsing, but at such a high frequency that a continuous flow of particles seems to be exiting the nozzle. But, for reasons which have not been fully identified (this is in relation with the powder feeding mechanism), the frequency of pulses does sometimes slow down to a level where bursts of powder can clearly be seen. With the temperature at about 50°C, the jet seems to be more continuous and uniform. Although the heater does not remove entirely the pulsing, it reduces the chances of seeing the jet pulsing with a low frequency.

Reducing flow spikes and flow control during the experiment

There are external factors in the lab that can contribute to sudden and brief spikes in the recorded mass during the process. The blasting unit and the balance were first placed onto the same table which host the powder blasting enclosed box and the cyclone unit. The latter releases every five minutes a short and powerful burst of pressured air which can temper the mass loss records. In addition, there are shocks coming from the linear stages which can potentially also disrupt the measurements, not to mention unintentional shocks coming from the operator. In order to suppress such factors and reduce measurement "noise", the balance was isolated on a shelf attached to a wall as shown in Figure 3.12. The hanging hoses feeding the pressure gas to the reservoir and the powder to the nozzle were tidied and fixed to the wall to prevent any movements. Nitrogen gas is also used instead of pressurized air to prevent any moisture coming in the reservoir.

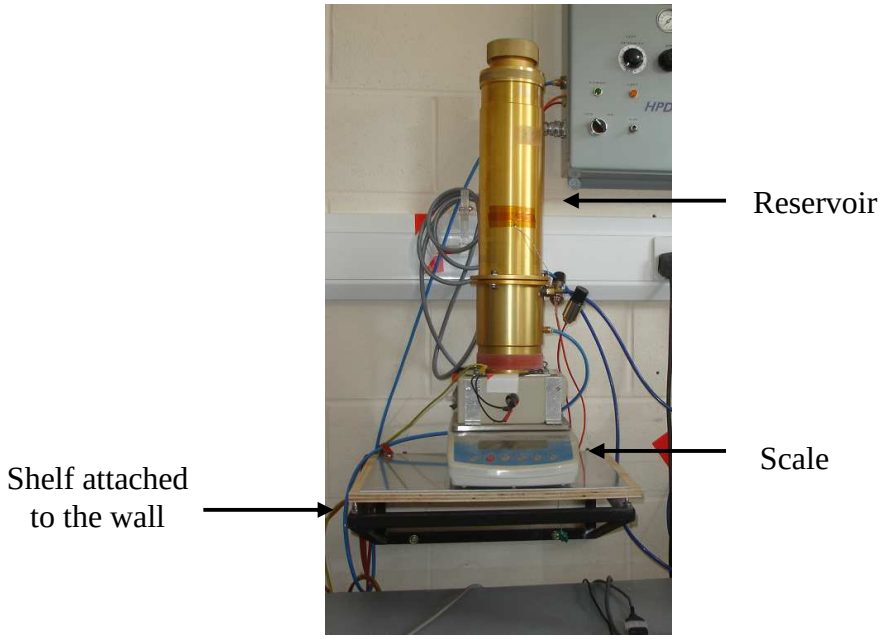

Figure 3.12: Powder blasting unit isolated from the rest of the setup on the shelf

To further reduce the impact of the variations of the flow during an experiment, a program was written (Stefan Wilhelm's work) to take advantage of the feed of the balance and calculate the live flow rate (an option which is not available with the proprietary program). To do so, the program takes ten measurements of the mass of the system (over a period of five seconds) and calculates the flow. The flow can only be known after the first five seconds following the start of the recording, but is then

repeated every second using the last ten measurements. Due to the three seconds stability required by the balance, this calculation is not very precise but gives a good indication of the flow value. Moreover, large changes in the flow can be spotted and controlled by modifying the flow during the experiment.

3.3.3 Conclusion

Thanks to the reduction of the size of the reservoir, the variations of the flow rate and the clogging frequency have been significantly reduced. The repeatability of the machine has been improved without the use of a complex re-engineering of the machine. Thanks to the desiccant stones and the heater, the new reservoir keeps the moisture out for longer and enables the re-use of the powder. Furthermore, the addition of a flexible heater reduces pulses occurring on the particles jet. These improvements do not, however, totally suppress the problem. This powder blasting machine can then be used more efficiently at pressure as low as 50psi with a maximum flow rate is about 0.2g/s.

3.4 Powder blasting green tape ceramic

The erosion of the green tape is investigated in this chapter in order to understand the behaviour of the tape under the bombardment of the particles. The results will help to narrow down the usable range of each modifiable parameter to the best efficiency value.

3.4.1 Experimental approach

The experiments are kept simple and consist of moving the nozzle over the ceramic surface in the absence of a mask. The tests are defined as “dynamic mode” tests in opposition to “static mode” for which the nozzle does not move. The dynamic mode is a more realistic approach to study the erosion rate: in the static mode, the thin green tape is pierced quickly and no substantial data between the flow rate and the mass loss of the green tape can be extracted.

Erosion rate

The erosion rate is defined as the amount of material removed per unit of mass of impinging particles and is expressed in equation 3.2:

$$Erosion\ rate\ E = \frac{m_{gt}}{m_p} \qquad 3.2$$

where m_{gt} is simply the mass lost by the green tape layer during the powder blasting and m_p the mass of powder used. The mass of powder lost, m_p, during the test is calculated from the flow rate μ of the powder, obtained in g/s, and the length of time of the erosion of the green tape as equation 3.3 shows:

$$m_p = t * \mu \qquad 3.3$$

The mass of green tape loss is measured with a high precision scale manufactured from Denver Instrument. It has an accuracy of 0.1mg. Due the a large difference (in the order of 1000) between the mass loss of green tape and powder mass loss, the erosion rate will be expressed in milligrams of green tape per grams of powder (mg/g). The erosion rate is a good indicator of the efficiency of the particles etching the substrate.

Scanning definition

The powder blasting of the samples is done by rastering the surface. The rastering is done as follows: the nozzle moves along the x axis over the sample in one direction, performing what is defined as a "pass". The nozzle position is then incremented along the y axis so that the nozzle performs another pass along the x axis in the opposite direction. The increment prevents the nozzles carrying out the pass from eroding the same part of the samples. A scan is defined as the set of passes needed to cover the entire sample (Figure 3.13). Depending on certain parameters, several scans might be needed to pierce the layer of green ceramic. The pitch of the scan is the space between the passes which make up the scan.

In this work, the erosion was measured for a duration of 60 seconds. However, the pauses of the nozzle after each axis swap (during increments) are equivalent to the static mode in which the tape can be pierced quickly. This would impede with the measurement of the mass of the tape. To prevent this, the axis swaps are carried out over a metallic frame (protected with sticky tape) placed beforehand on the green tape. The frame leaves an area of 50x30mm of green tape exposed to the particles. The frame

is clamped magnetically and the protected green tape setup can be seen in Figure 3.13.

To ensure the tape is only exposed to 60 seconds of blasting material, the passes are carried out along the width of the frame (30mm) at a speed of 5mm/s. Then one single pass erodes the sample for a total duration of 6 seconds. Ten passes are necessary to erode the green tape for a timing of 60 seconds and these 10 passes make up for one scan. However, one scan lasts about 90 seconds as 30 seconds is the necessary time to have the axis swapped 10 times.

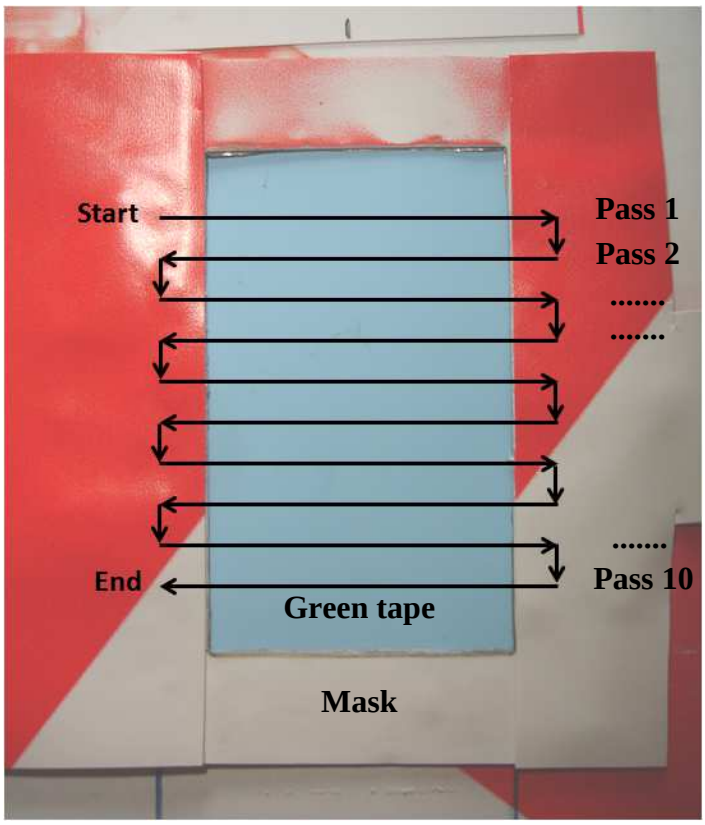

Figure 3.13: Nozzle path over the scanning area. The green tape (light blue) is maintained clamped down by the surrounding frame cover in red and white sticky tape

The pitch between passes is selected according to the width of the blasted channel and must be as large as possible to avoid passes overlapping. This ensures the consistency of the measurements and that the particles only erode the substrate at "normal" incidence. With a pitch smaller than the channel width, the passes would overlap the slope of the channels blasted with the previous pass and particles would not erode the substrate at normal incidence. However, the width of the blasted channel can become too large

compared with the metallic frame that the latter becomes too small. In that case, the pitch would be set at its maximum to fit the area.

3.4.2 Erosion behaviour

In this section, the erosion behaviour of the LTCC material under powder blasting process is characterised. The erosion profile is studied as well as its dependence to parameters such as flow rate, distance between the nozzle and the substrate, pressure and angle of impact of the particles.

Erosion profile of the jet

With ten microns particles and a nozzle opening of around 0.8mm, the distribution of the particles in the jet has been shown to follow a Weibull distribution [87]: particles are highly concentrated in the centre of the jet with a slow decrease in the particles density the further away from its centre. Particles on the edge of the jet have a lower velocity which reduces the erosive power [4]. This Jet's shape is directly reproduced in the erosion profile of the green tape once powder blasted. The typical profile of a powder blasted channel in green tape ceramic is displayed in Figure 3.14. The erosion profile was measured with a Zygo Viewmeter 6020 phase shifting white light interferometer. This profile was obtained at 50 psi and a distance N-S of 20mm. One single pass was done on the green tape with a flow rate of 0.1g/s. The total depth measured was 56µm for a total width of 4.2mm.

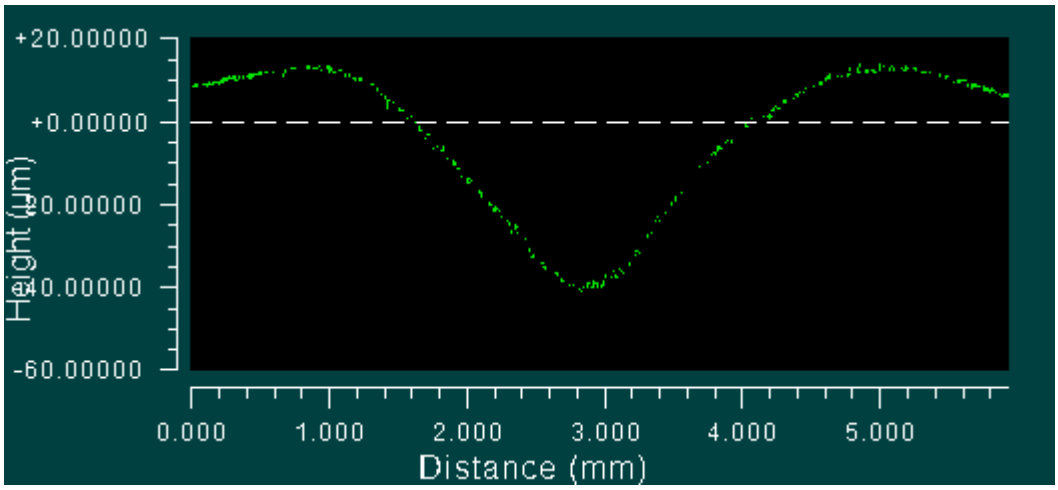

Figure 3.14: Surface profile of green tape channel at N-S=20mm

At 20mm, the width of the channel blasted was given for 4.1±0.05mm. It is, however, difficult to assess correctly the eroded area diameter, especially at distances N-S above 30mm. The smooth edges blur the boundaries between none eroded and eroded surface. Precise measurements of the area diameter cannot be done. To remedy to this problem, some literature have defined the core of the jet as the impacted area which depth is within 90% of the main depth [85]. This enables the removal of the smooth edges on the top of the channel which impact are negligible on the etching rate. The width becomes 3.1±0.05mm.

In addition, phenomenon such as interactions between particles inside the nozzle and turbulences outside the nozzle created by the medium (air) scatters the particles and give the jet a conic shape [88] which changes in diameter depending on the distance N-S. The calculation of the eroded area with a round nozzle can be done following equation 3.4 to 3.7:

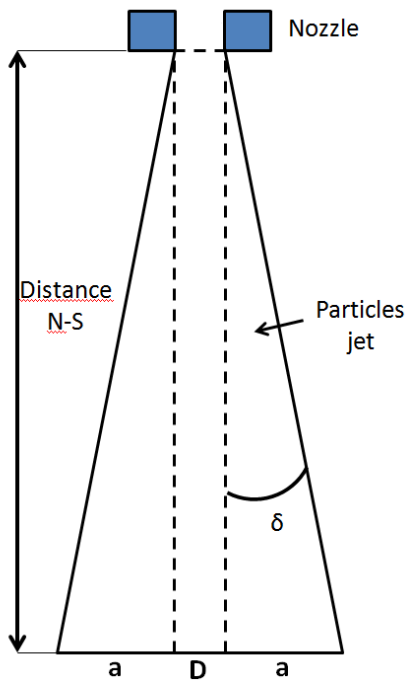

Diagram of the jet of particles

$$A_{blasted} = \pi * r^2 \quad 3.4$$

$$r = \frac{D}{2} + a \quad 3.5$$

$$a = \tan\delta\,(N - S) \quad 3.6$$

$$A_{blasted} = \pi * (\frac{D}{2} + \tan\delta\,(N - S))^2 \quad 3.7$$

$$\delta = \tan^{-1}\frac{a}{(N - S)} \quad 3.8$$

with N-S the distance Nozzle-Substrate, δ the angle and D the diameter of the nozzle (0.8mm). The area profile was mapped on a glass substrate (static mode) at 50 psi with a flow rate of 0.1g/s. The distance N-S was varied between 5mm to 50mm. Although the erosion rate obtained on this substrate will be different than on green tape ceramic, the erosion profiles will be similar. The main interest in using glass is that it is easier for

the white light interferometer to detect the light patterns than on green tape ceramic. The Zygo was used in Stitching mode in which a series of pictures are taken and assemble together. This enables large area to be mapped.

Table 3.5: Dimensions of the eroded area on glass depending on the distance nozzle-substrate

Distance N-S (mm)	5	10	15	20	30	40	50
Eroded surface diameter (mm)	1.95	2.53	3.85	4.35	5.88	8.5	10
Eroded surface area (mm^2)	2.98	5	11.7	14.85	27.14	56.72	78.50
Calculated jet angle δ (º)	6.56	4.94	5.82	5	4.84	5.5	5.26

Table 3.5 shows the increase of the eroded surface from 2.98mm^2 at a distance of 5mm to 78.5mm^2 at a distance of 50mm. It also shows that the angle of the particles at the edges of the jet is relatively constant ranging from 5 to 6.5º. Thus particles have the same angle at either a distance of 5mm or 50mm.

Planarity

It is important for the powder blasting process to uniformly etch the substrate. In doing so, it ensures that the erosion rate is constant and therefore that the piercing of the tape occur simultaneously over a random surface area. It also helps to create flat etched surface. The difficulty of uniformly exposing the surface to the same particle erosion power comes from the shape of the jet, which erodes the substrate with a similar erosion profile: the erosion is the stronger in the centre and lower on the edges. In other words, the planarity of the surface depends on the distribution of particles in the jet combined with the pitch set between each passes.

To remedy to the issue, Ghobeity et al.[89] have succesfully implemented a target oscillating mechanism perpendicular to the direction of the nozzle. By rapidly oscillating the target with a very high speed ratio oscillation, the energy distribution of the particles on the substrate becomes uniform. Their results also showed that reducing the distance between two passes increases the surface planarity. And that the oscillation frequency and scan speed must be selected accordingly to the erosion rate. In this thesis,

this system will not be used but instead a careful set of pitch depending on the erosion profile will be used.

To select the right pitch for these experiments, the channel shown in Figure 3.14 was analysed and its depth recorded in a graph in Figure 3.15 every 0.25mm.

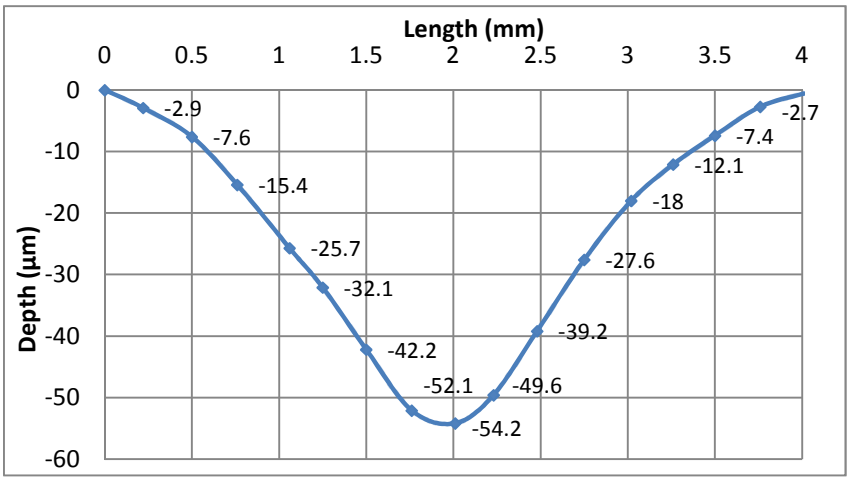

Figure 3.15: Depth profile of a channel blasted at N-S=20mm after 1 scan in green tape

To study the planarity that such profile would create with a set of different pitch, the erosion profiles data of the single pass was added according to the pitch selected. The pitches selected were 0.5, 1, 1.5, 2, 2.5 and 3mm and the results displayed in Figure 3.16. This is of course a simplified model which does not take into account the flow fluctuations and the different erosion rate that occurs between a flat surface and an angled wall (slopes).

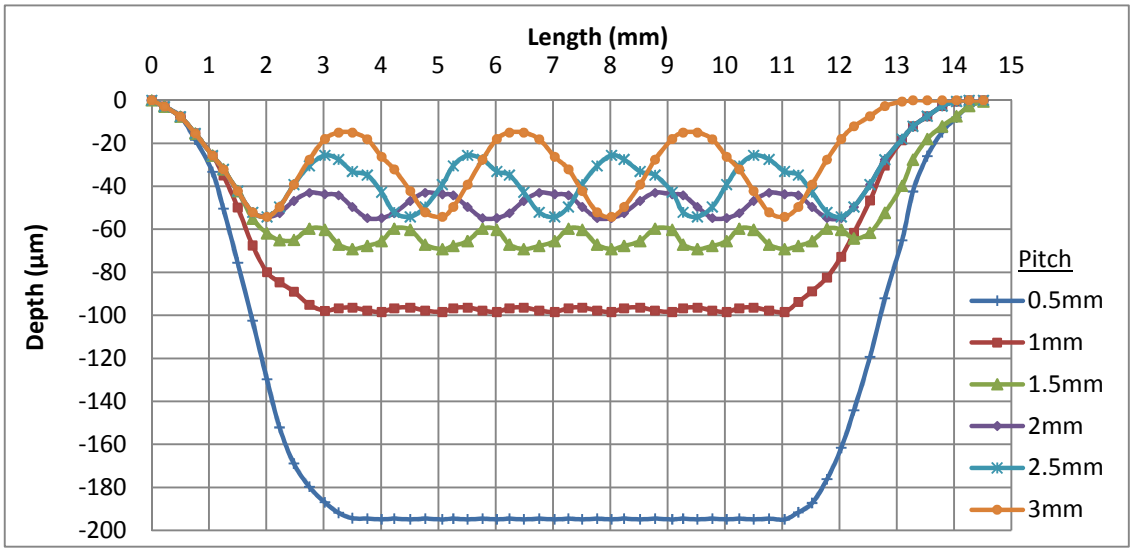

Figure 3.16: Theoretical surface profile of multiple passes set with different pitch

As it could be expected, lower pitch length increases the flatness of the eroded surface. A very flat surface is obtained with pitch of 0.5mm. When the pitch doubles to 1mm, there is a slight wavy pattern with amplitude of 2µm but the surface can still be considered flat. However, at larger pitches above 1mm, the amplitude of the waves are too large and the surface cannot be considered flat anymore. From this theoretical profile, it also seems that a single scan at a pitch of 0.5mm would pierce the 165µm thick tape.

Similarly, the experiment was conducted at N-S=50mm. The weak erosion and the larger eroded area showed that pitches smaller than 1.5 to 2mm produced an erosion profile equivalent to the one recorded at N-S=20mm with a pitch of 0.5 and 1mm, but with a lower etched depth.

Erosion rate vs. flow rate

This study was carried out for a flow rate ranging from 0.03g/s to 0.16g/s (intensity I5 to I9). The pressure was set at 50 psi, the distance N-S set at 20mm. The pitch between 2 passes was set to 3mm and the heater temperature to 50ºC. The results are displayed in Figure 3.17.

At first glance, it can be seen that the mass of green tape etched increases as the quantity of particles expelled increases (Figure 3.17a). At a flow of around 0.03g/s, the mass eroded is about 19mg. When the flow increases to 0.16g/s, the mass eroded becomes around 27.5mg. This increase was expected as more particles hit the substrate when the flow increases. This relation is however not linear and the erosion clearly diminishing with increasing powder flow. This behaviour is confirmed by comparing the erosion rate with the different flow rate (Figure 3.17b). There is a large decline where the erosion rate drops from 9.38mg/g to 4.4mg/g when the flow increases from 0.035 g/s to 0.085g/s, and then a slower decrease from 4.4mg/g to 2.8mg/g as the flow increases from 0.085g/s to 0.16g/s.

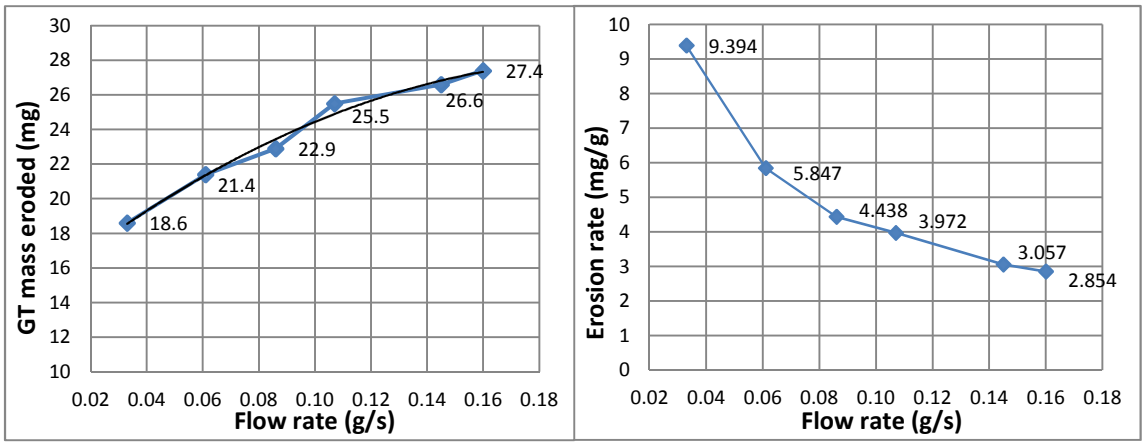

(a) (b)

Figure 3.17: (a) Mass of green tape eroded in 60 seconds in function of the powder flow; (b) Graph of erosion rate obtained in function of the flow rate

The drop in the erosion rate with increasing powder flow underlines a clear decrease in the particles erosion efficiency when the quantity of powder increases. This is a well know phenomenon studied in the literature. The lower efficiency is not due to a decrease in number of particles striking the substrate, but rather due to the loss of their kinetic energy as the particles collide with the rebounding particles from the substrate [7, 90-93]. Experimental study have shown that the erosion rate increases when the distance between particles increases: the particles are less likely to interact with each other and lose their kinetic energy [94]. At a distance between particles 17 times the particle diameter, the interaction is considered negligible and the erosion becomes independent of the flow. In addition, the increase of the number of particles in the gas reduces the gas flow speed thus reducing the kinetic energy that is given to the particles [95].

From the literature and the present tests, it emerges that a low flow rate would then be preferred to a have the highest particles efficiency. But there are a few reasons why a higher flow rate is preferable. First, despite a better efficiency, a low flow increases the machining time necessary to perforate the tape: there is a 50% increase in the tape mass removal with a flow rate set at around 0.016g/s instead of 0.035g/s. Secondly, the repeatability of the flow is better at flow ranging from around 0.07 to 0.16g/s (Figure 3.11 and Table 3.3). Thus the flow rate of choice for powder blasting green tape ceramic

lies around 0.1g/s.

Pulsing jet: It is not rare, despite improvements conducted on the powder machine, to see the jet pulsing particles with a relatively high frequency, but clearly visible. As mentioned before, the reason for this is not clearly known. This behaviour has been shown to affect the erosion rate. The experiment conducted with a pulsed flow was compared with another experiment with constant flow and similar parameters (Pressure=50 psi, distance N-S=10mm, pitch=3mm). The flow rate ranged from 0.012g/s to 0.0168g/s. Results are displayed in Figure 3.18 which shows the erosion rate of green tape ceramic in function of the flow of the particles

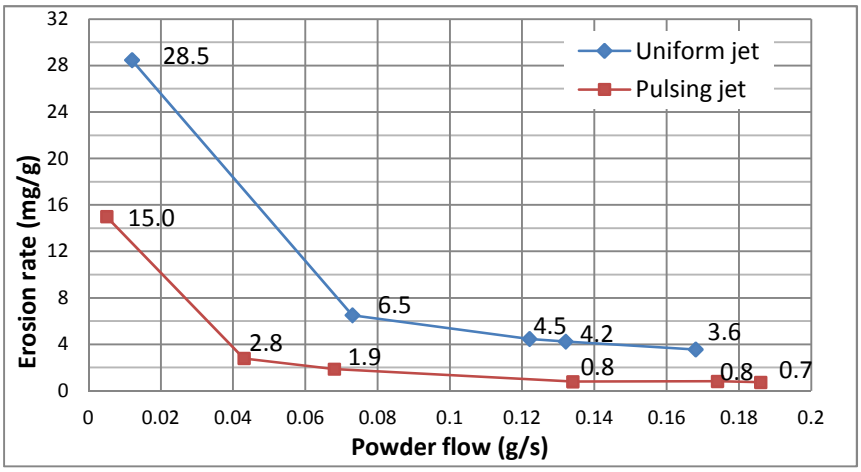

Figure 3.18: Comparison of the erosion rate between a uniform and a pulsed jet

This experiment highlight the lower erosion rate obtained with a pulsed jet. For equivalent flow rate, the erosion rate was around four times lower than the one obtained with a constant flow, except with a very low flow rate. This phenomenon can be explained with the particle distribution affecting the erosion rate: during the entire test, it was shown that the powder quantities are equivalent between a pulsed and a constant flow. It thus implies that, for the pulsed flow, large burst of powder expelled which contains more particles which interact with each other, collide, lose their kinetic energy and finally reduce the erosion power.

Pulsed jet at low frequency should not be used as it changes the erosion rate and render the comparison difficult with other experiments. It should only be used when its uniformity and consistency is satisfactory i.e. when the frequency of the pulse is high

enough and the jet looks continuous. As the jet undergoes very frequent change in the pulsing frequency from one experiment to another, selecting only constant flow from use in experiments would imply discarding most of the tests. Fortunately, the example used in Figure 3.18 was easily identifiable from the start.

Erosion rate vs. distance nozzle-substrate

The erosion rate has been investigated at different distances N-S. The variations of this distance will, as mentioned earlier, affect the powder blasted area and the speed of the particles which will change the erosion rate. The erosion rate was studied at 50psi and a flow rate of about 0.11g/s. The pitch between the passes was set to 3mm for the distance N-S of 5 to 15mm, and then set at 4.5mm for 20 to 50mm N-S. The results are displayed in Figure 3.19.

An increase in the erosion rate can clearly be seen from 5mm to 10-15mm N-S, then a decrease the further away the nozzle is from the substrate (from 15mm to 50mm). The distance 10 and 15mm distance offer the highest etching rate with a flow of 0.11g/s and the distances at 5 and 20mm have almost the same erosion rate.

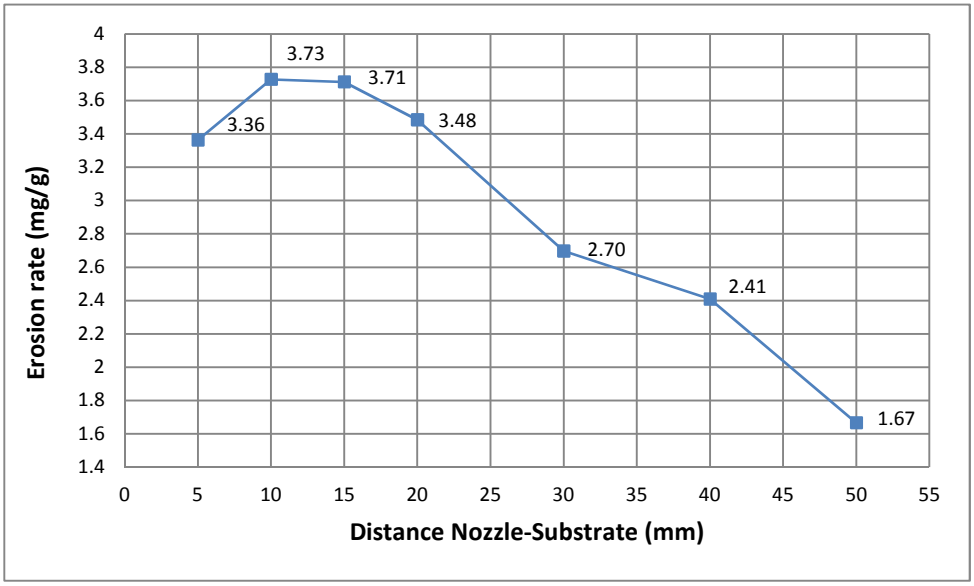

Figure 3.19: Erosion rate depending on the distance nozzle-substrate

This can be seen at first as a surprising result as it would be expected that the closer to the substrate to the nozzle the highest erosion rate. However, this result is well explained in the literature. The speed of the particles varies along the distance nozzle-

substrate (N-S). In the vicinity of the nozzle tip, the flow of air has a higher speed than the particles. As a consequence, particles are still accelerated outside the nozzle by the flow of air over a distance that can varied to about 10 times the dimensions of the nozzle aperture [84, 88]. After this point, the particles start to slow down due to the interactions with the medium (air). The kinetic energy, and thus the erosion power, of the particles increases first over a short distance after their exit and then decreases gradually due to aerodynamic forces. This is exactly what the graph in Figure 3.19 shows.

Erosion rate vs. pressure

In this section, the erosion rate of the green tape is studied as a function of the pressure applied in the reservoir, thus as a function of the kinetic energy of the particles. On other material such as glass, the erosion rate is found to be linear after a 100kPa (14Psi) [82]. To conduct this test, four pressures were used: 20, 40, 60 and 80psi. The intensity was fixed at 7 (about 0.15g/s). The distance nozzle-substrate was fixed at 10mm. The results are displayed in Figure 3.20.

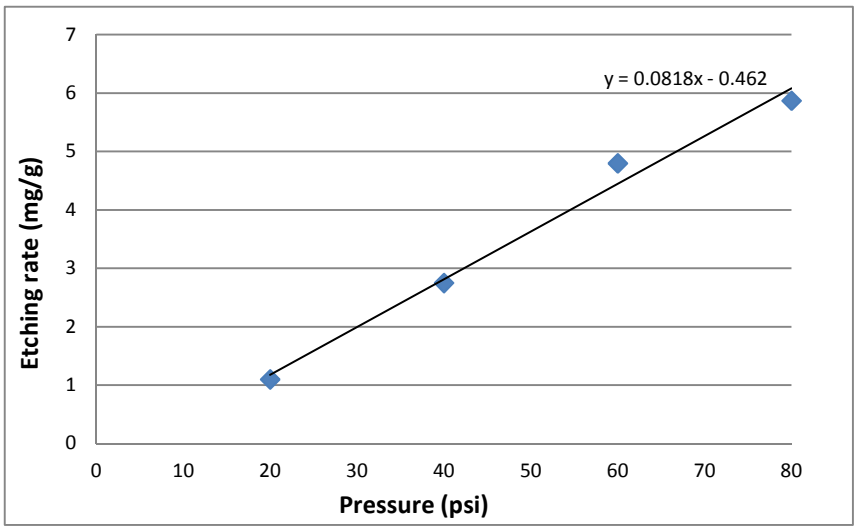

Figure 3.20: (a) Flow rate dependence on pressure; (b) Erosion rate vs. flow rate at different pressures

The graph in 3.20 shows the erosion rate of the green tape ceramic is also linearly proportional to the pressure applied: the highest the pressure, the highest the erosion rate. A trend curve can be drawn with a slope coefficient of 0.08: the erosion of the

green tape increases by 0.08mg per gram of powder when the pressure increases by 10psi. However, it was noticed that the flow rate fluctuations increases the lower the pressure, with 20psi being not really reliable. At 80 psi, the flow rate was very good. However, the high pressure exerted too much force on the mask holding the tape down and clear lift off could be seen. Additional clamping tool such as metallic bars could be added to prevent such phenomenon. However, the magnetic field prevented to do so as the bars were pushed in the centre of the field, which meant that re-engineering of the holder was required.

Erosion rate vs. particles impact angle

One of the interesting particularities of the powder blasting technique is that the angle of impact of the particles can be easily changed by tilting the nozzle. Unlike other machining techniques, the particles do not require to be positioned accurately at the focus point or to use specific tools such as an inclined die, which would be required for punching machining. Using this process property, suspended structures have been made in brittle material [10, 96] very easily. In this section, the tests will highlight the behaviour of the green tape ceramic depending on the angle of impact of the particles. For example, the erosion behaviour of ductile and brittle material will vary with the angle of impact of the particles [97, 98]. Ductile materials have their highest erosion rate at around 15° from the normal while brittle materials have theirs at normal impact 90° (Figure 3.21).

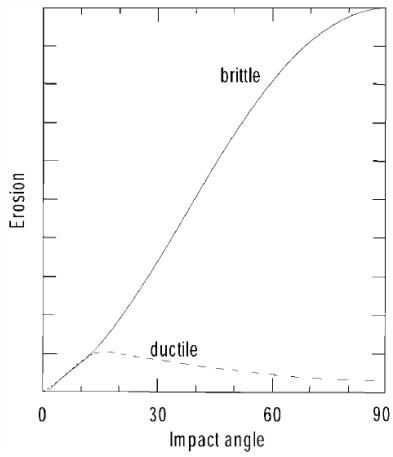

Figure 3.21: Dependence of the erosion rate of ductile and brittle material on the impact angle of the particles

The angle of impact was varied from the normal incidence (90°) to the lowest angle possible with this setup, 30°. The pressure used was set at 50psi, flow rate of 0.16g/s and a nozzle-substrate distance of 10mm. The pitch between passes is set at 3mm for angles ranging from 90° to 60°, 3.5mm between 50° and 40° and 4mm for 30° angle. The change of pitch is changed to compensate the increase in size of the machined area when the impact angle is increases. The results are displayed in Figure 3.22.

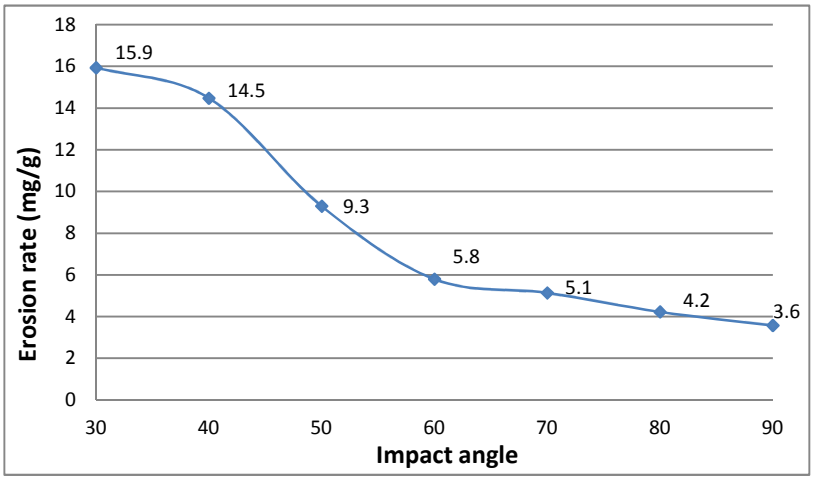

Figure 3.22: Effect of the angle of impact of the particles on the erosion rate

It clearly shows the dependence of the erosion rate to the angle of impact of the particles. The green tape exhibit a ductile behaviour. This curve can be separated into two parts: a first part from normal incidence to 60° where the erosion rate increases slowly from 3.6mg/g to 5.8mg/g respectively and a second part from 60° to 30° where the erosion rate increases strongly from 5.8mg/g to 15.9mg/g respectively. It is interesting to note that 15.9mg/g at 0.16g/s is about the same erosion rate obtained at normal incidence at a flow rate of around 0.04g/s.

This is clearly following a ductile behaviour with higher erosion rate at low angle. Unlike brittle materials which are cracked by the particles with high energy (obtained at normal incidence), ductile materials are eroded thanks to frictional wear better obtained at low angle. In addition, the particles at low angle are less submitted to collisions than at incident angle. First, the area eroded is larger as shown in [94] which increases space between particles. Secondly, the particles do not bounce back into the jet but are blown away instead. This can definitely play a role on the high erosion rate recorded at lower angle.

3.5 Conclusion

This chapter gives a description of the setup used at Heriot-Watt University during this thesis. It also enlightened the problems encountered such as flow variations and clogging. To improve the machine, a detailed characterisation of the flow was done with the original setup and a modified system. The modification consisted in the addition of a central tube to reduce the dimension of the reservoir. Furthermore, a flexible heater was added to keep the temperature to around 50C^{o}. The investigation demonstrated that they reduced the variations of the flow rate and the clogging.

The characterisation of the erosion of the green tape without mask was achieved based on the erosion dependence on the flow rate, distance nozzle-substrate, pressure and angle of impact. It was found that the optimum flow rate should be around 0.1g/s, and that the pressure should be between 40 to 60psi to avoid poor repeatability at low pressure but also avoid mask lift off at higher pressure. And the distance N-S should be set around 15 to 20mm for best erosion rate at a flow of 0.11g/s.

Chapter 4 Powder blasting micromachining adapted to LTCC

4.1 Introduction

Chapter 3 demonstrated that powder blasting could be used to erode the green tape ceramic. This chapter will now detail the investigations carried on in order to adapt the process for LTCC. The first section provides an understanding on the type of material and methods, which are used conventionally to mask the substrates in powder blasting. Following this short review, this chapter then highlights the constraints present and the solution envisaged to adapt the process. The third section characterises the mask for the green tape while the last section focuses on the mask fabrication.

4.2 Masking LTCC

4.2.1 Masks in powder blasting

Powder blasting is used widely on brittle material such as glass, ceramic or silicon. It has indeed a higher etching rate than conventional etching processes. With it, very fine features in the order of tens of microns can be fabricated. However, direct patterning of microstructures is not possible with powder blasting, as the area eroded by the particles is very large. This technique requires the use of masks to protect the substrate from undesired erosion leading to the fabrication of specific structures. The main features required for a mask are low erosion rate compared to the substrate it is protecting and high patterning resolution of the mask.

Material used

There are two types of material for these masks: ductile (metals) and elastomer/polymers materials [6]. These materials have a low erosion rate with a minimum at around 90º impact angle [83, 99]. Metal masks are frequently used and can be patterned using laser cut, drilling or electroforming process. The latter confers to the mask better aperture resolution and smoother walls [100] but is more complex. Metals such as laser cut stainless steel [12, 101, 102] and electroplated copper are the most used. Copper is softer than stainless steel, and thus will resist better the blasting [5]. Metallic masks are subjected to the peening effect. The particles bombardment builds up tensile stresses on the top surface, which, in turn, bends the mask upwards. This process is shown diagrammatically in Figure 4.1. The peening effect results in a loss of

contact which allows the particles to penetrate between the mask and the substrate. This deformation, if not controlled, results in loss of machining accuracy. This effect can be compensated by increasing the thickness of the mask, at the expense of the mask quality.

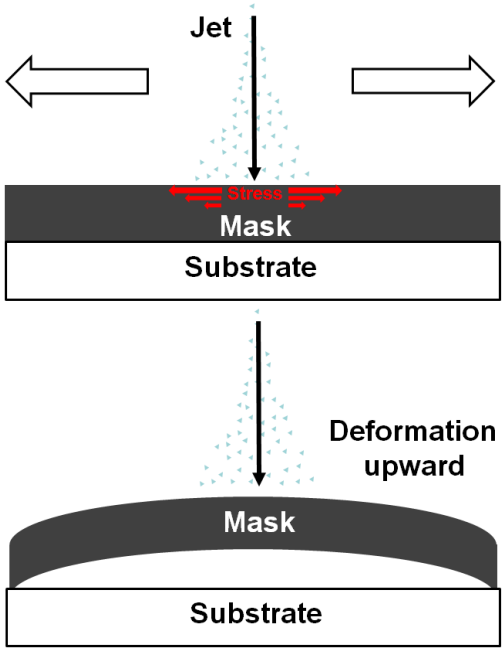

Figure 4.1: Schematic of the peening effect on a metallic mask

Polymers mask used for powder blasting mostly regroup photolithographic material such as photoresists (dry film [103-105], SU-8 [106]) or flexopolymer LF55gn [107]. But polydimethylsiloxane (PDMS) which is patterned using a moulding technique is also used [108, 109]. For the latter, an additional step is required in which a photoimageable sacrificial material is patterned on the substrate on which the PDMS is knife coated. Photoresists are easier to use than rubber like polymers (LF55gn, PDMS) but have a higher erosion rate: particles are absorbed more readily due to their rubber like properties [99].

Metallic masks have the advantage of being more robust than plastic masks. It has been shown for example that particles can hit the substrate through the 30µm thick polymer layer without piercing it [82]. Similar metal sheet thickness would not let the substrate be damaged by the particles, but will undergo high deformations after a short exposure to the particles. Compared with dry film resist, the edge of the apertures in a metallic mask and rubber like polymers are less vulnerable to side etching. This results in an increase of the inner diameter and loss accuracy of the pattern transfer [6, 99].

Under etching

A very good pattern transfer accuracy between the mask and the substrate is guaranteed by the perfect adhesion of the mask to the latter. It reduces under etching and also prevents particles from travelling under the mask and grinding the substrate surface. Under etching is a common phenomenon in powder blasting. It arises through particles impacting the walls of the substrate underneath the mask at various angles due to the non planarity of the surface or collision between particles. The resulting structures are larger than the original pattern featured in the mask. Two types of under etching can be distinguished:

- Wall under etching (Figure 4.2, marker a). Particles erode the inside of the wall, slowly increasing the width of the structure. It is a necessary step to pierce the material to the desired dimensions. However, as the process continues, the width of the structures can exceed the width of the aperture with which they have been created.
- Edge under etching (Figure 4.2, marker b). This type of under etching occurs at the boundary between the mask and the substrate. The particles bounce back from the back side of the mask and etch the substrate underneath. This results in the smooth rounded edge of the structures. This only happens at the top surface and is enhanced by poor mask adhesion.

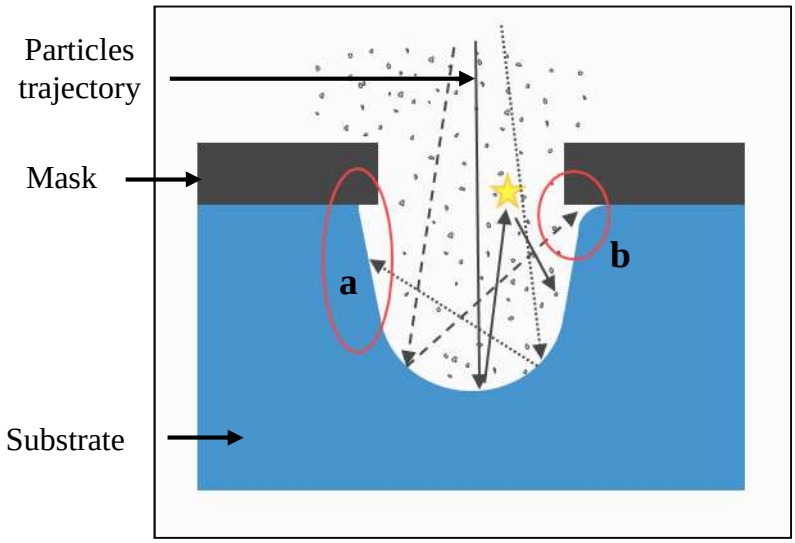

Figure 4.2: Schematic of trajectory of particles responsible for the under etching underneath the mask

Mask attachment

As powder blasting has been developed for brittle materials, techniques to attach the masks and reduce the under etching have been developed accordingly and depend on the mask material. Wax is frequently used to fix pre-patterned masks. Wax is rendered viscous by heating it to about 100°C to 150°C. The wax is then applied to the substrate and the mask placed on top. The substrate is then left to solidify to form the bond. To release the mask, the wax has to be reheated. Wax can be abraded quickly by the particles. This is an advantage as the particles have to pierce through the wax that has inevitably clogged the apertures during the application of the mask onto the substrate. The wax creates a strong bond and is easy to use. Glue will provide the same contact characteristics than the wax, but is less sensitive to the powder blasting and is more difficult to remove. Metal masks are preferentially chosen with such an attaching method [6, 11, 110].

Polymer masks create a strong bond through lamination for dry films or spin coating for photoimaging (LF55gn). They are laid down, exposed and developed directly onto the substrate. PDMS, on the other hand, is moulded on the substrates. This method requires a sacrificial material such as SU-8 to be first patterned onto the substrate.
Metal masks can be also directly electroplated onto the substrate following the LIGA process developed in the late 1970 [6, 108]. The substrate is patterned with a sacrificial layer and plunged into the electrolyte solution to grow the metallic layer. As the substrate needs to be conductive, a conductive layer has to be deposited on the brittle substrate prior to the electroplating. The contact of the mask with the substrate is very good and its alignment with the substrate potential features is excellent. The bonding strength is good, but needs to be weak enough to enable the peeling of the mask after powder blasting. Deformations occurring on the top of the mask can delaminate the metal sheet.

Finally a clamping method can be used in combination with metal masks fabricated using LIGA process. The mask is then placed on the substrate and is either side clamped or magnetically clamped. The former applies the force on the edges of the mask. Although efficient, side clamping introduces voids in the centre of the mask due to the lack of clamping force in. This allows the particles to penetrate underneath the mask as shown in Figure 4.3. Magnetic clamping, on the other hand, applies a more uniform

pressure over the entire surface of the mask. Fewer voids are created preventing the erosion of the substrate underneath the mask. The clamping force is however dependent on the characteristics of the magnetic field and the mask dimensions and patterns. Indeed, the mask is not submitted to the same force of the field throughout its entire surface. This can create in certain points a lifting force instead of clamping force. Thin masks or masks with large apertures would not produce the same clamping force than a plain thick mask. Furthermore, it requires the material with which the mask is made to be magnetic. This then excludes a large number of potentially interesting material. Alternatively, extra magnetic tools can be placed on the mask to either create (for non-magnetic) or increase the clamping force.

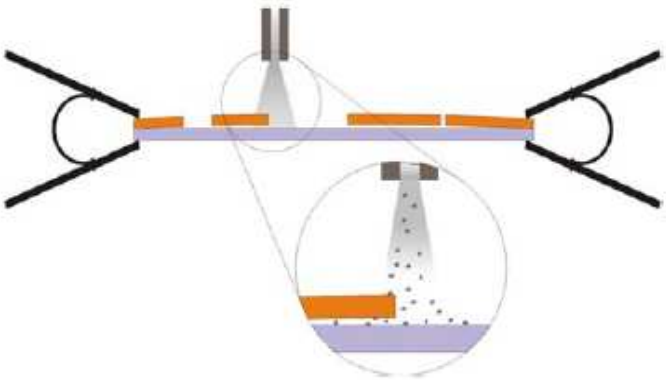

Figure 4.3: Schematic of a mask clamped on its edges introducing voids underneath [6]

4.2.2 Masking adaptation for LTCC substrate

As mentioned in Chapter 2, the green tape ceramic is composed of two inorganic materials: aluminium oxide Al_2O_3 and glass, usually SiO_2-B_2O_3. These two components are present in a form of powder at a level of 20 to 40% each depending on the tape manufacturer. Organic materials are also present in the slurry and include a binder for good mechanical strength, a plasticizer, dispersing agent, solvent and wetting agent. These organic materials confer to the tape its flexibility and its softness for easy machining by conventional tools (laser, mechanical puncher), as well as printing and lamination with other layers.

Selecting the attaching method and the mask material

Due to the properties of the green tape, the common methods employed to attach the masks onto the substrate are not suitable on LTCC. Growing a metal mask on the green

tape ceramic is not possible. The deposited conductive layer (titanium) would be impossible to remove and would prevent interlayer penetration during lamination. The tape would also have to undergo the development of the sacrificial material and the plunge into the electrolyte solution. The whole process would destroy the green tape.

Glue or wax are neither usable. Upon mask removal, the wax remaining on the substrate needs to be cleaned using chloroform. Similarly, isopropanol or acetone are used to remove glue. Solvents not only destroy the gluing agent but also destroy the organics inside the tape. In fact, a small amount of solvent has been used to melt the green tape material during cold lamination [111, 112]. Stripping of glued masks using other means is also not possible: the tape is too thin and fragile. Small structures would be torn or broken, and dimensional changes would be induced during the tape stretching. In addition, tests carried out with this technique and a glued mask with a low bonding strength showed that, in addition to the tape deformation after mask removal, glue was left on the tape surface as evidenced in Figure 4.4. This would result in delamination, had the layer been fired.

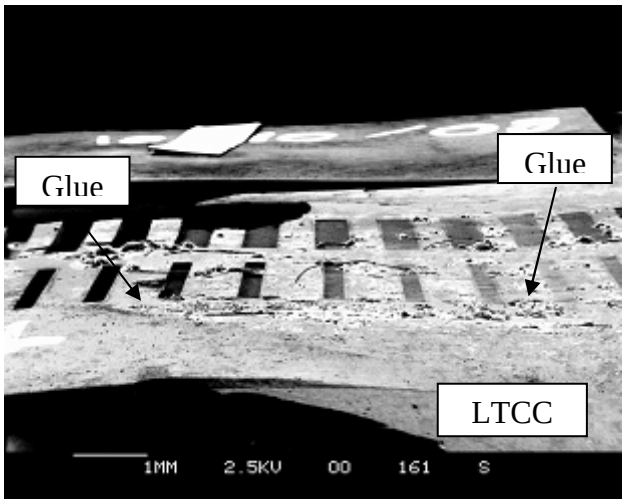

Figure 4.4: Green tape ceramic powder blasted with a glued copper mask. After mask removal, remains of glue could be observed on the green tape surface

Polymer masks are also impossible to apply conventionally. As the patterning occurs onto the substrate itself, the green tape would not resist the development process and mask stripping steps of the solutions employed (KOH for dry film, toluene for photoimageable PDMS or water for (LF55gn). Similarly, the use of sacrificial material for the moulding process of PDMS is not compatible with the green tape.

Laminated dry film onto LTCC was demonstrated by J. J. Santiago-Aviles et al. [113,

114]. Their process involved the use of HF ($HF:H_2O$ 1:4) to machine DuPont 951 green tape ceramic layers. The issues of developing the resist onto the tape were bypassed by semi-firing the individual layers just above the glass transition temperature (810ºC) at 850ºC for only 2 minutes. The glass flows for a period of time short enough for the grains of ceramic to be loosely attached together. After cooling down, the dry film resist (Riston) can be laminated onto the semi-fired layers and exposed to UV light (365nm). They reported with this method a very strong bond and the process offers a reasonable resolution as Figure 4.5a demonstrates. However, the issues appeared during the stacking of the layers. The layers are semi-fired, so organics are missing from the tape composition and the lamination step cannot properly join the ceramic layers together. A low temperature glaze layer, DuPont QQ550, has to be inserted between each one to provide the bonding. According to their results, the glaze layer does not fire properly and destroy the stack (Figure 4.5b).

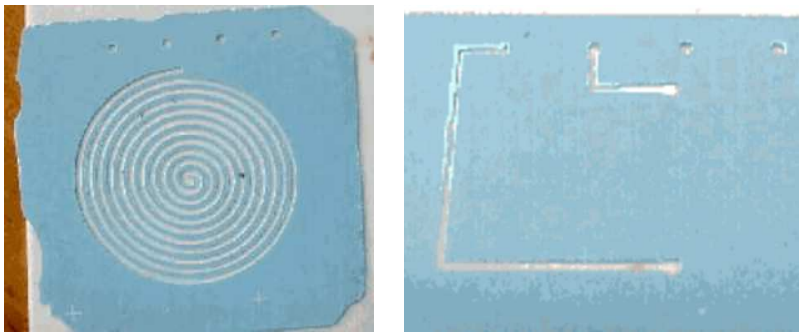

(a)

(b)

Figure 4.5: Patterned LTCC with dry film resist [113]: (a) example of structured tape in semi-fired state with HF, and (b) destroyed stack after firing

Currently, there is no gluing material that can be washed off without chemical compound. Thus the only option which is viable is to pattern the mask off the green tape and use clamping method which does not require any gluing agent. Theoretically, it can

be used either with polymer film or metallic mask. For the former, however, this involves fabricating the mask on a dummy substrate, removing the mask and applying it onto the green tape. With rubber like material, the stripping and handling steps induce too much stresses and stretching which greatly undermine the pattern dimensional integrity. Dry films, on the other hand, are more rigid (they come with two protective foils, one of them can stay on during the blasting process) and can be transported after patterning. Unfortunately, they must not be laminated onto a support which makes the development step difficult as the film is not attached on a hard surface. Tests have nevertheless been conducted to verify the usability of such a technique. The resist is a Quickmask 75µm thick from Mega Electronics and was exposed (UV light at 200mJ) and developed in water with a simple brush. The resulting sheet can be seen in Figure 4.6a. The supporting foil can be seen inside the patterns, except for the bottom right patterns, which were already powder blasted. The film was then clamped onto an LTCC layer with stainless steel plate protected with sticky tape. To prevent the foil from lifting off, clamps were placed very closely to the patterns (Figure 4.6b).

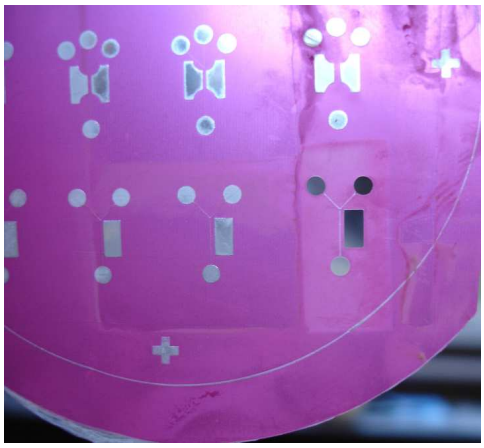

(a)

(b)

Figure 4.6: (a): Quickmask resist film after development; (b): the resist is tightly clamped on the substrate

After powder blasting at 80psi, a distance nozzle-substrate of 50mm and 7 scans, the green tape was pierced and the film resisted the process. However, the resist suffered lateral erosion mentioned earlier, which increased significantly the dimensions of the apertures by about 200µm (Figure 4.7). These lateral changes are gradual and were transferred to the LTCC structures. Furthermore, despite the proximity of the clamps, the jet of particles was able to lift the foil off the green tape, lowering the pattern

transfer accuracy.

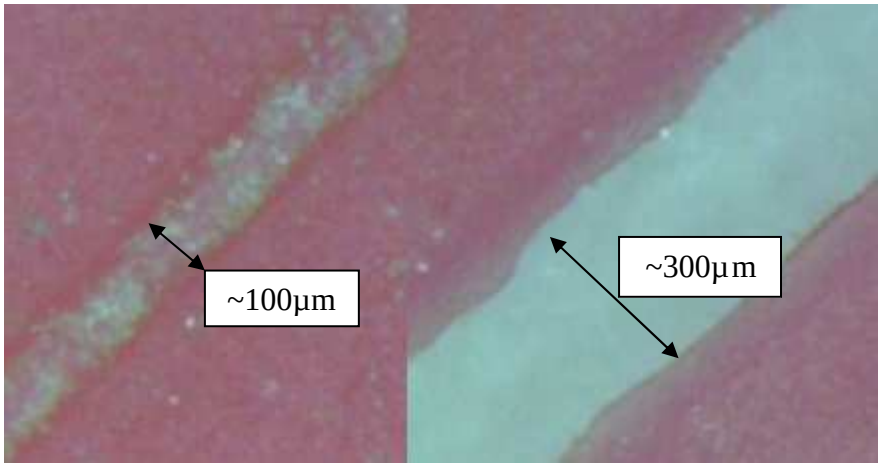

(a) (b)

Figure 4.7: Picture of a 100µm channel patterned in the Quickmask photoresist (a) before powder blasting and (b) after powder blasting

From these results, it is clear that dry film resist is not appropriate as a mask for powder blasting green tape ceramic. It is etched too quickly and the extra clamping tool necessary to maintain a good contact is difficult to setup or impossible depending on the complexity of the patterns. Metallic masks, which are more rigid and robust, are thus more adapted with clamping method. However, care has to be taken with the peening effect. To compensate this effect, thick masks can be used [115] but this restricts the quality and minimal dimensions of the apertures. To achieve high quality sub 100µm aperture, thinner masks have to be used. To keep such a mask in contact with the substrate during the process, magnetic clamping is preferred to side clamping as the entire metallic sheet is hold down and reduces the voids between the substrate and the mask.

Nickel was selected as the material of choice for such purpose. Unlike copper, it is magnetic and produces a stronger magnetic force than stainless steel for similar sheet thickness (experimentally, a 30µm thick nickel foil produced a clamping force stronger than a 100µm thick stainless steel sheet). Furthermore, it can be electroformed, producing high resolution patterns [100], but it can also be laser cut with resonable high resolution features (sub-100µm).

Protective coating

As mentioned earlier, unprotected metal sheet will sustain deformations attributed to the peening effect. Powder blasting of a 60µm thick nickel mask was done at 50 psi, a distance N-S of 20mm, a speed of 5mm/s and a number of scans equal to 4. The result is illustrated in Figure 4.8a. It clearly shows the amplitude of the deformations. The mask was only clamped magnetically. The latter is not able to prevent the deformations resulting in a lift off of the mask from the substrate (Figure 4.8a&b)

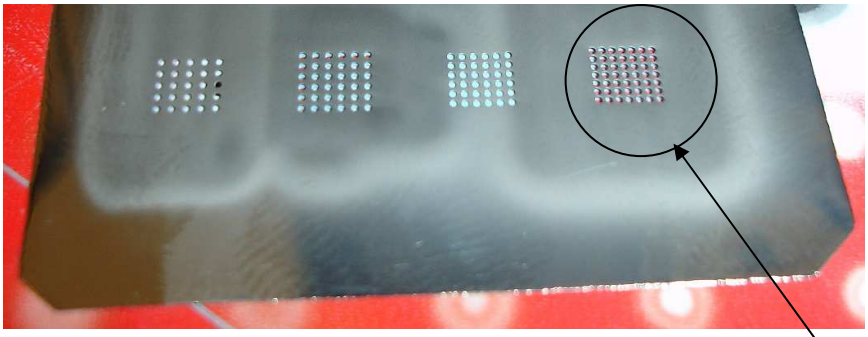

(a)

Mask lift off

(b)

Figure 4.8: Powder blasted 60µm thick nickel mask: (a) clear lift off around the apertures can be seen (circled in black) despite the magnet underneath, and (b) without the magnet

To prevent deformation of the metal mask, a protective foil can be used as a shield from the particles, keeping thereby the benefit of a thin mask as far as resolution of the machined patterns is concerned. Ideally, this coating would have to sustain the particles bombardment long enough for the green tape ceramic to be pierced, and then be replaced if needed by a new coating which will allow the same metal mask to be reused. In consequence, the coatings should be fairly easy to place on and remove from the mask and should have high erosion resistance. In the light of these requirements and the

specifications detailed in the first part of this chapter, polymers materials have been trialled for protecting the metal mask. Indeed, they resist well the process, do not experience the peening effect and are easily patterned directly onto the substrate enabling high alignment accuracy with the apertures of the metal mask. A good patterning resolution is preferable but not essential as the metal mask is solely responsible for the transfer of the patterns. In this thesis, two polymers where investigated: dry film resist Riston fx930 and flexopolymer LF55gn.

Setup stage and clamping force

A good pattern transfer accuracy also depends on the contact between the mask and the substrate. In this thesis, the magnetic field was generated by two permanent dipoles 50*30mm in dimensions placed side to side creating an equivalent surface of 50*60mm. A stainless steel plate 0.8mm thick is attached to the magnet to serve as a stage. The setup can be seen in Figure 4.9.

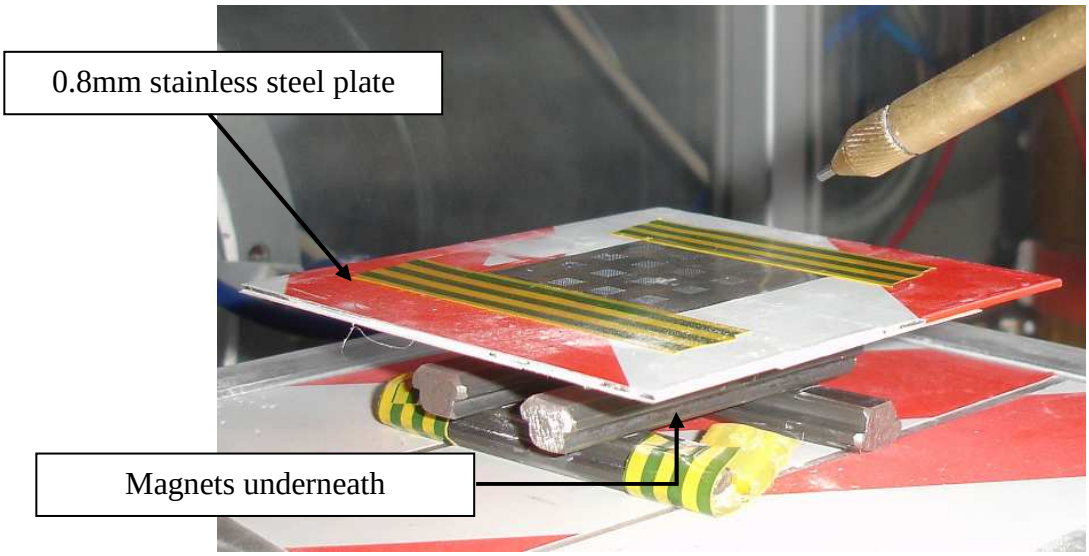

Figure 4.9: Magnetic stage setup

The clamping force exerted on the mask depends on certain parameters such as the thickness of the mask and the complexity of the pattern, but also on the pressure and the distance N-S of the nozzle. The masks are held onto the green tape ceramic thanks to sticky tapes placed on each side. Without them, once the nozzle passes the edge of the metal mask, the pressurized air can easily penetrate beneath the mask. This creates an airbed between the substrate and the mask which can displace the mask. A similar effect

can be seen over the mask: the gas high pressure can lift off the mask in locations where the clamping force is weaker. This can be generated by large or complex apertures or by a high density where little surface of the mask is left.

Tests have shown that, with a thick 100µm sheet, apertures larger than 0.5mm^2 are subject to a slight lifting at N-S=20mm and 50 psi. At N-S=50mm, no lifting was seen. Higher pressures increase the lifting process and are therefore not recommended. Thinner mask generate less clamping force and are subject to more lifting: at N-S=20mm, a 20µm thick mask lift off with apertures larger than 0.125mm^2. It thus requires the addition of clamping equipment such as small metallic tools to increase the clamping force. However, due to the magnetic field, it can be difficult to place the tools at the desired location. Their addition could then impede the blasting process as their positioning can cover the mask apertures. On the other hand, tests have shown that, if the clamping force is too strong, the green tape can stick to the mask. Removing the mask without destroying fragile structures underneath can then become difficult.

4.3 Masks behaviour under powder blasting

4.3.1 Nickel mask

Erosion rate

A nickel foil of thickness 40µm was powder blasted at 50 psi, a distance N-S of 20mm, a scanning speed of 5mm/s with a pitch of 1mm. The powder flow rate was kept at 0.110g/s. The foil was blasted over a surface of around 350mm^2. However, the foil was protected with sticky tape and only a square aperture of 100mm^2 enabled the metal foil to be eroded. This helps the calculation by providing a precise eroded surface which is impossible to have otherwise due to the distribution of the particle in the jet. The nickel foil mass was recorded before and after the process with an accuracy of 0.1mg. 19 scans of 12 passes were done for a total experiment length of 790 seconds.

The quantity of powder expelled during this experiment is calculated from the amount of time that the nozzle spent over the surface to be eroded and the flow of powder. From the parameters above, the nozzle only spent 456 seconds over the 100mm^2 area which gives a total mass of powder used of 50.16g (456s x 0.11g/s). During this time, the mass of nickel lost equal to 22.3mg. The erosion rate is given in equation 4.1:

$$E_{erosion} = \frac{m_{nickel}}{m_{powder}} = \frac{0.0223}{50.16} = 0.00044g \qquad 4.1$$

There is 0.4mg of nickel eroded per gram of powder. From the mass of nickel lost, the total thickness of material removed can be known thanks to the density equation of a material (Eq 4.2):

$$\rho = \frac{m}{V} = \frac{m}{L \times l \times h} \qquad 4.2$$

$$h = \frac{m}{L \times l \times \rho}$$

With m the mass of the material and V its volume. The density of nickel is ρ=8.908g.cm^3 and the volume area is L=10mm and l=10mm, thus the nickel thickness lost is 25µm i.e. 1.3µm per scan. Measured experimentally with a thickness gauge, the eroded thickness was 27µm, close to the calculated one.

To confirm nickel as being an appropriate material for powder blasting green tape ceramic, the selectivity between the two materials can be measured. The selectivity is a dimensionless number indicating the erosion rate difference between two materials: a selectivity of 0 means that the two materials have the same erosion rate; a selectivity of ten signify that one material has an erosion rate ten times lower than the other. The selectivity between the mask and the material should therefore be as high as possible in favour of the mask. The selectivity is expressed as the ratio of the thickness h of material etched and is shown in equation 4.3. As the thickness etched depends on the scanning speed and pitch between passes, it is therefore better to use the mass eroded and the density of the materials (Eq 4.4)

$$S = \frac{h_{green\ tape}}{h_{mask}} \qquad 4.3$$

$$S = \frac{h_{GT}}{h_{Ni}} = \frac{\frac{m_{GT}}{L \times l \times \rho_{GT}}}{\frac{m_{Ni}}{L \times l \times \rho_{Ni}}} = \frac{m_{GT} \times \rho_{Ni}}{m_{Ni} \times \rho_{GT}} \qquad 4.4$$

In Chapter 3, the green tape erosion with similar parameters was about 3.9mg/g of powder. Thus we can calculate the selectivity with one single gram of powder: the green tape has lost 3.9mg and the nickel 0.4mg. With a green tape has a density of 3.1g/cm^3 (DuPont 951), the selectivity is:

$$S = \frac{3.9 \times 8.9}{0.4 \times 3.1} = \frac{34.71}{1.24} \cong 28$$

Nickel has an erosion rate 28 times lower than the green tape. It is a confirmation that nickel can be used as a mask for green tape ceramic. Theoretically, to pierce a green tape layer of 165µm, a nickel foil of about 6µm thick is sufficient.

Edge erosion

In this section, attention will be focused on the erosion of the edges of the structures patterned in the mask. Sharp edges are eroded quicker than a plain foil, and dimensional changes in the structure shape have to be investigated. The edge deformations were studied using an array of beams of length 2mm with different beam widths varying from 100µm to 500µm. The spacing between beams also varies from 100µm to 300µm. The mask employed is a laser cut mask from Tannlin Ltd 100µm thick. The blasting parameters are similar to the one used for the erosion rate. To identify the weaknesses of the structure edges, the number of scans was varied from 1 to 30. The large space between each set of beams was covered with sticky tape to reduce the deformations. A photograph of powder blasted mask can be seen in Figure 4.10.

Figure 4.10: Photograph of a 100µm thick powder blasted mask featuring 6 sets of rectangular apertures 2mm long

Figure 4.11 presents the evolution of the mask thickness through a study of a powder blasted beam with a width of 400µm cross section as a function of the number of scans. The beam cross sections are displayed in Figure 4.11a and the beam thickness measurements shown in Figure 4.11b. Then the width of this beam and of a 100µm and 500µm wide beams were measured and shown in Figure 4.12).

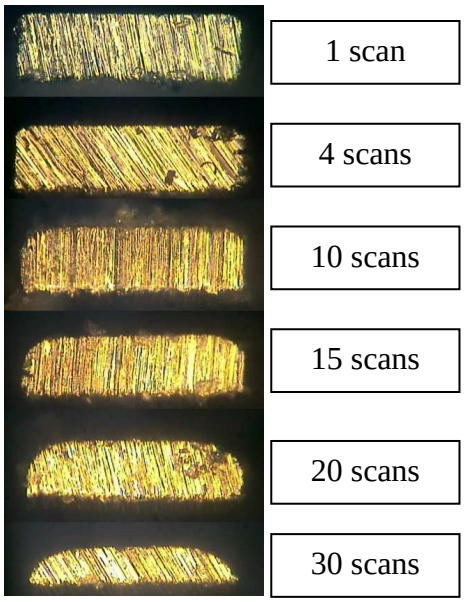

(a)

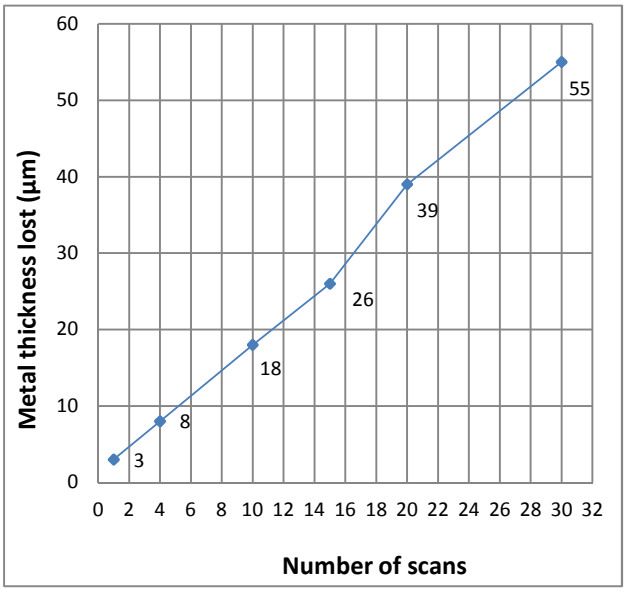

(b)

Figure 4.11: (a) Cross section of a 100µm thick nickel beam depending on the number of scans; (b) Thickness of nickel lost as a function of the number of scans

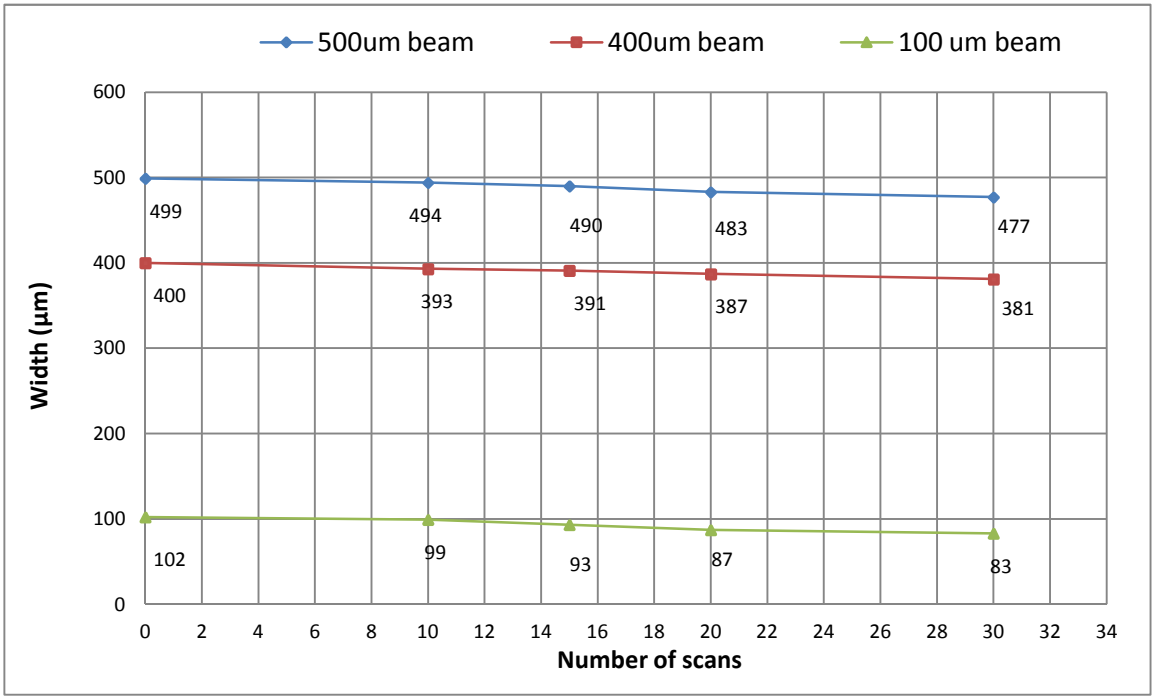

Figure 4.12: Variations of the width of the beam of the mask of 100, 400 and 500µm wide beam

From these results, nickel foil can be seen resisting very well to the particle bombardment. Despite a clear smoothing of the structure edges, the dimensional changes of the width are limited over 30 scans. Nevertheless, they are too important to be left unnoticed. Taking into account measurements error of about +-2µm, the beam width is reduced by about 7µm per 10 scans, which give about 20µm lost over 30 scans. In the same way, the material thickness lost is constant and is about 18µm for 10 scan, or 1.8µm per scan. The discrepancy with the results obtained previously (1.4µm per scan) originate for the flow fluctuations and the location of the cross section which was probably done on an area powder blasted by the centre of the jet of particles. These measurements set a limit in the re-usability of the mask and the latter will depend on the patterning accuracy needed for a given powder blasted structures.

Henk Wensink [84] noticed that, at the beginning of the powder blasting process, the apertures in their copper mask significantly reduced in size (about 60µm). He explained this phenomenon by the compression exerted by the particles on the top edges of the aperture which “cave in” over the channel. This “outgrowth” is removed gradually, but delays the machining of the substrate channel, increases the blast lag. Unlike in copper no noticeable outgrowth was found with the nickel foil.

4.3.2 Mask coating

Polymer characteristics

LF55gn is a liquid photopolymer (MacDermid Inc) used by the industry for hand stamp manufacturing. LF55gn is capable of high aspect ratio structures over 10:1 to 27:1 used in MEMS [116] and optical components [117] fabrication. Some examples are shown in Figure 4.13. It is photo-sensible to UV light with a maximum absorption peak at 366nm [116]. The polarity is negative (what is exposed stays) and the crosslinked polymer stays transparent to the visible spectrum after exposure. During the exposure, a transparent PET foil has to be laid over the polymer to isolate it from oxygen to avoid polymerisation. The high viscosity of the polymer allows fabrication of thick structures by spin coating (up to 1mm) or moulding. The flexopolymer is developed in a water based developer mixed with detergent. This is not a real developing step as the water based solution does not dissolve the uncross linked polymer, but rather only helps to push it away. Ultrasonic bath or stirred water can be used to force out the unexposed viscous polymer. However, these solutions only apply to structures with large openings. For smaller sub millimetre apertures, spay guns with pressurised water up to a few bars are more efficient. Post development exposure can be done to emphasize cross linking of the polymer left. To strip the polymer off the substrate, it is plunged into its developer and left in ultrasonic bath for one hour. Once exposed, the flexopolymer has a Shore A hardness of 55 and a Young's modulus of 0.7MPa [118]. The material is rubber like and adheres extremely well to substrates such as glass, silicon and metal. It surface is also sticky.

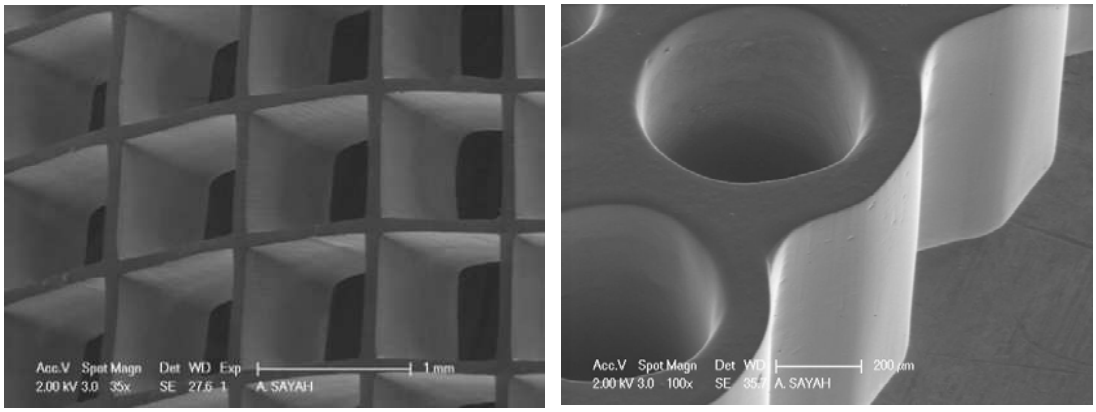

(a) (b)

Figure 4.13: Example of patterned LF55gn 1mm thick grid/mesh with 0.1mm thick walls

Dry film resist Riston fx930 is manufactured by DuPont and has a thickness of 30µm. It is a negative resist and was selected as a coating material for its ease of use and its pattern resolution, which is of about 10µm for a single layer. Unlike LF55gn which requires a protective foil, there is no additional step before exposure and the film is simply laminated onto the metal mask. After exposure with a UV light, the film is developed using MFS 1120 aqueous developer. Lamination of multiple layers is possible which can be used to increase the resistance of the protective foil. The film is easily stripped using a solution of 10% MFS 1102 diluted in water. To catalyse the reaction, the temperature is set at 50°C.

Feature resolution

Dry film resist has a higher resolution than the LF55gn and structures as small as 10th of µm can be made. This is however only possible with a single layer. With 3 to 4 laminated layers, it was very difficult to develop structures smaller than 100µm in diameters. Similarly, the LF55gn can be easily patterned and sub 100um features can be created. But the high viscosity of the LF55gn renders the polymer extremely difficult to remove inside tiny apertures. Tests have shown that sub-200µm via were extremely difficult to clean. It was also found that unexposed polymer is difficult to flush from the exposed structures and in sharp corners. As a coating for the nickel mask, this must be removed prior to the blasting to prevent clogging. This is shown in Figure 4.14 were unexposed polymer almost clog after only one scan the metallic rectangular apertures. More scans are able to remove the unexposed polymer, but the phenomenon introduces a delay in the machining of the green tape. To remedy to this problem, over exposure of the LF55gn is done to crosslink this unexposed polymer.

High resolution for coating purposes is not on the other hand very critical. Indeed, the pattern resolution is passed on by the nickel mask, Therefore the apertures of the coating have to be as good as the mask, which is made by the dry film resist Riston fx930. Furthermore, apertures of both polymers are designed to be 150µm larger than the apertures of the nickel mask. This fulfils two intended purposes: compensate for misalignment during the polymer exposure and prevent the added polymer thickness to the already thick nickel mask to play a role in the powder blasting process behaviour

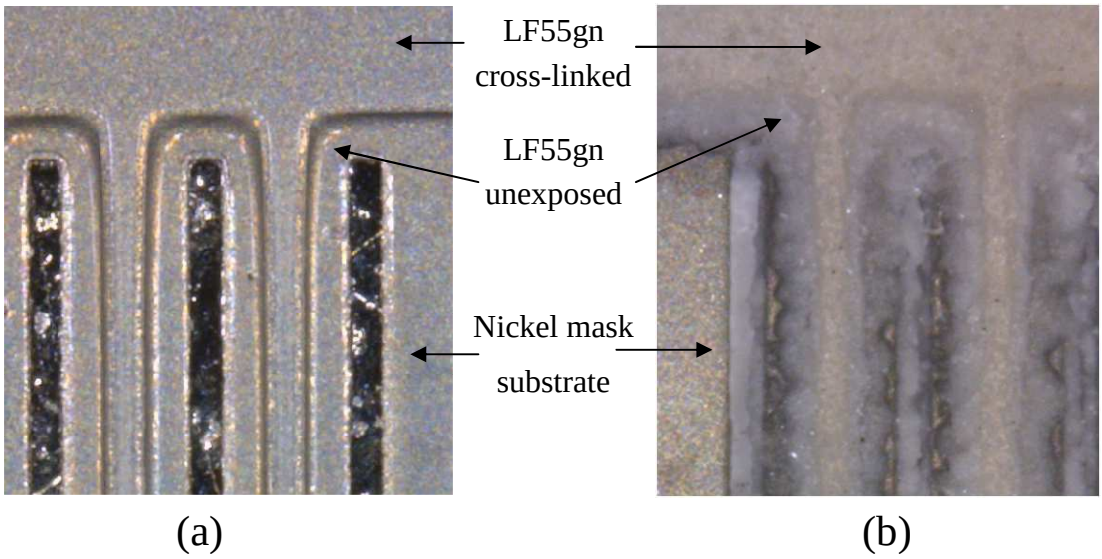

Figure 4.14: Photograph of LF55gn: (a) before powder blasting with unexposed polymer surrounding the apertures and (b) after a single powder blasting scan. The viscous unexposed polymer can be seen in blue-grey colour pushed toward the nickel apertures

Erosion behaviour

Comparison of the erosion behaviour of LF55gn and dry film resist under powder blasting has been conducted by Slikkerveer et al [119]. The dry film used is an Ordyl BF410, a film very similar to Riston fx930. The particles used have an average diameter of 23µm, which give them a higher eroding power than the 9µm particles used in this thesis. Nevertheless, it can be assumed that the difference in the erosion rate obtained between the two polymers would lay similar differences with smaller powder. Both materials were tested with a thickness of 100µm. The predicted erosion profile of the two materials was calculated analytically by the author and illustrated in Figure 4.15.

Dry film is shown to be a lot less resistant than LF55gn: the film is entirely etched after being machined with about 12g/cm^2 of powder while only 10µm were removed from the flexopolymer for a similar powder exposure. This gives a selectivity ten times higher for the LF55gn. Most importantly, the dry film is highly eroded from its side wall: this is the lateral wear seen previously in this chapter. The powder is not only decreasing the film thickness, but is also reducing the side of the structures. In

comparison, the base of the LF55gn is not changed at all.

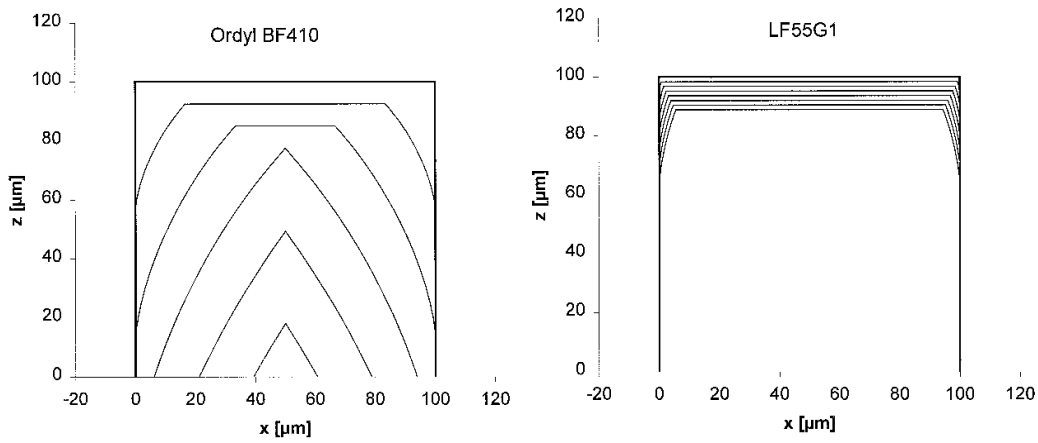

Figure 4.15: Erosion profile of a 100 thick dry film resist Ordyl 410 and 100µm thick flexopolymer LF55gn [119]. Each line represents the shape of the beam after a powder dosage of 2g/cm^2

This behaviour was confirmed in tests carried on Riston fx930. Four layers were laminated onto a glass wafer for a total thickness of 120µm. Rectangular beams were patterned with an exposure dosage of 3000mj and powder blasted at 50psi with a flow rate of 0.08g/s, a distance nozzle-substrate of 20mm, a scanning speed of 5mm/s and a pitch of 1mm. The number of scans was set to 1, 2, 4 and 6. The results shown in Figure 4.16a&b confirm the very high lateral erosion rate of the dry film. The quick erosion of the film which starts rapidly is clearly visible after only 2 scans. After 4 scans, the beam has lost about 150µm in lateral dimensions. After 6 scans, beam smaller than 300µm have totally disappeared.

Similarly, and in agreement with [119], tests on LF55gn spin coated with a thickness of ~55µm onto a nickel mask have shown the low erosion rate of the material. Similar parameters to the ones used for the dry film, with the exception of the flow rate (0.11g/s instead of 0.08g/s) and the number of scans (only 20 scans), were used. Figure 4.17 presents a photograph of the mask before and after the process. In the centre of the picture, where the powder blasting was the strongest, the polymer can be seen totally etched. There the thickness of polymer removed is about 50µm. Thus, taking the latter figure, a 120µm thick layer of flexopolymer would require 50 scans to be completely etched though. A quick approximation with the dry film (despite the lower flow rate) shows that it is eroded about eight times quicker than the flexopolymer.

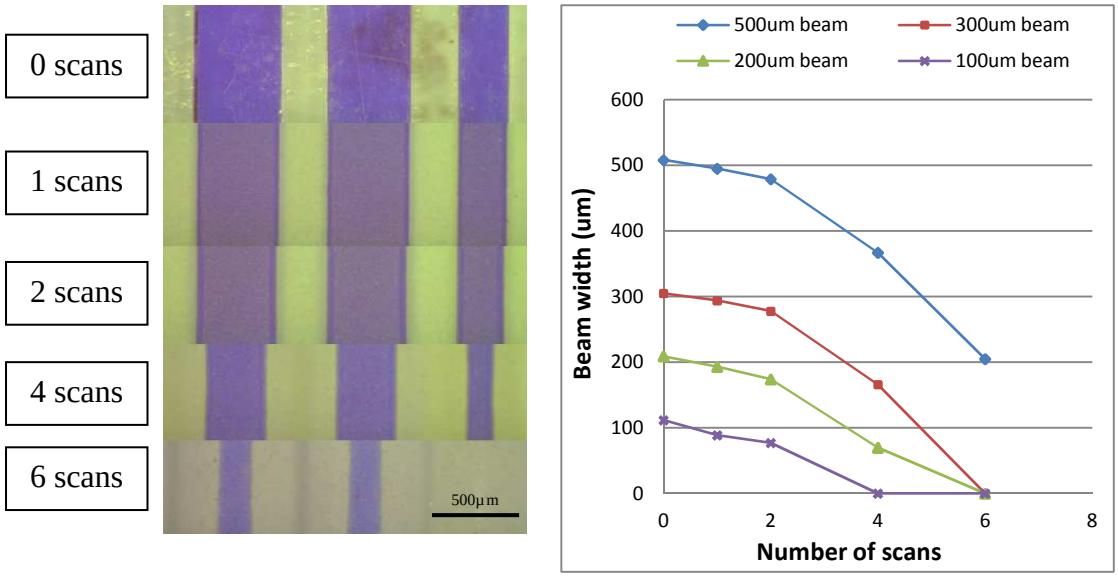

(a) (b)

Figure 4.16: Powder blasting erosion profile of dry film resist: (a) Photograph of the different erosion stage of the rectangular beams after a series of scans; (b) Graph featuring the measurement of the width of rectangular beams as a function of the number of scans

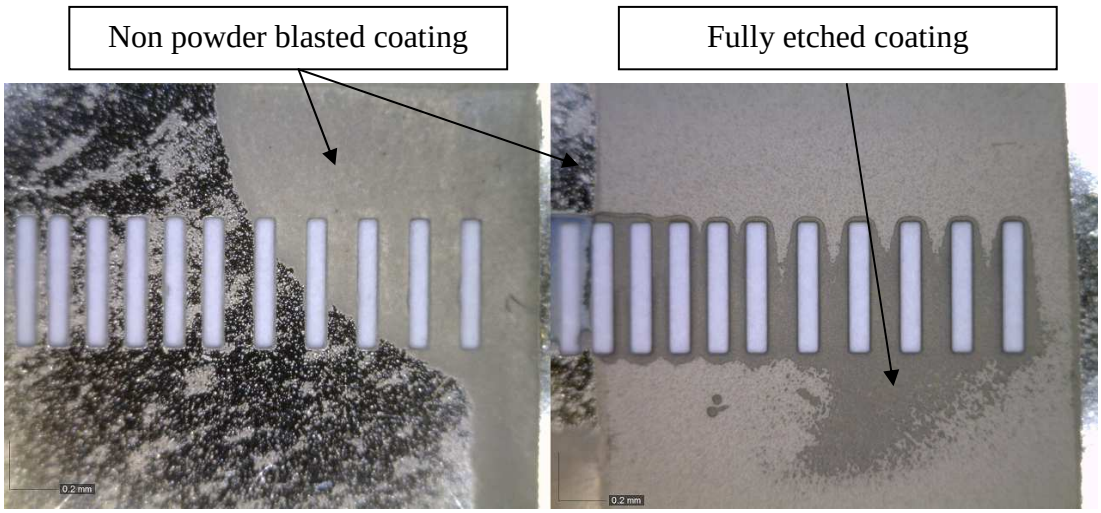

(a) (b)

Figure 4.17: Photograph of the patterned 55µm thick LF55gn onto a nickel mask (a) before and (b) after powder blasting

4.4 Mask process fabrication

4.4.1 Electroformed nickel mask

LIGA is the German acronym for LIthographie, Galvanoformung, Abformung respectively lithography, electroplating and moulding. This technology is used in the MEMS industry for the fabrication of high aspect ratio microstructures. The UV-LIGA process uses UV light source to expose a photosensitive material preliminary deposited on a conductive surface to form a pattern on the latter. UV lithography is the most common light source. It is more affordable than X-ray lithography, but creates lower aspect ratio structures. After development, electrodeposition of a metallic structure is done onto the substrate. The plated metallic layer is then stripped off the substrate once the desired thickness is achieved. A schematic of the process steps is shown in Figure 4.18.

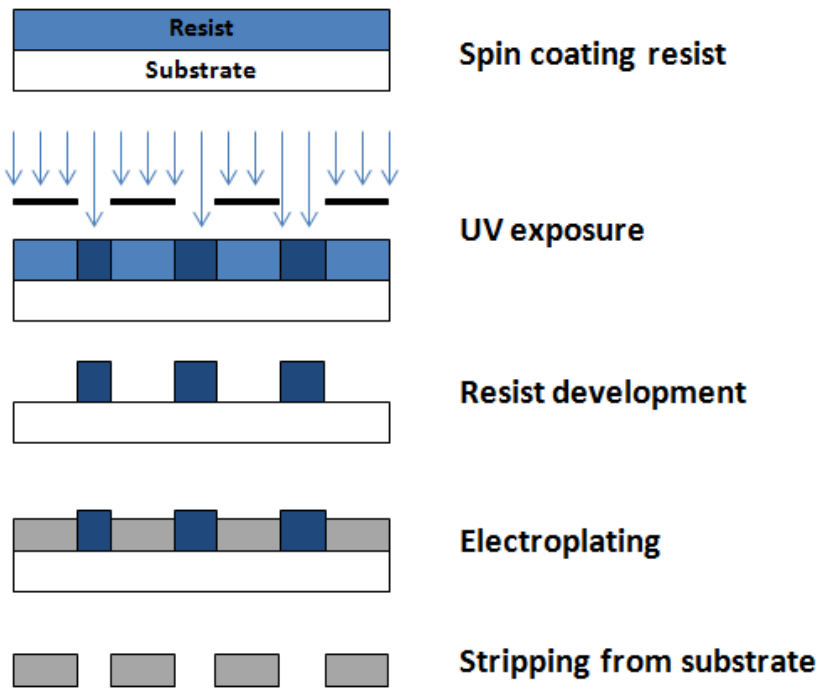

Figure 4.18: LIGA process steps used for the mask fabrication

Photo resist patterning

The photosensitive material used for the fabrication of the mask is the same negative dry film resist as described previously for the mask coating: DuPont Riston fx930. The film thickness is 30µm and is protected by two PET foils. This material is becoming increasingly popular in the industry: the resolution is lower than more traditional resist

such as SU-8, but is easier to use as there are no backing steps and the film is capable of high resolution of 10µm. Furthermore, it allows the use of only one resist, reducing the overall cost.

The film is laminated with an Excelam plus 655RM laminator machine manufactured by GMP (Figure 4.19). The film is laminated at 115ºC at about 0.6m/min and 2.5bar of pressure. The substrate is a stainless steel plate 1mm thick. This plate has a large usable area of 140*140mm^2, is conductive and bonds very well with the dry film. This substrate has many advantages compared to a more conventional glass coated wafer substrate. There is no need to use an e-beam deposition system to coat the glass wafer with a conductive layer prior to resist deposition. The plate will also not break under lamination pressure and has a larger usable space so many masks can be made at once. Unlike a coated wafer, the conductive layer does not come off the substrate and the plate can therefore be reused. Furthermore, the plate is held in the electroplating tank by two hooks that can easily be mounted/ dismounted and which also ensure the passing of the current during plating. The only drawback of this plate is a roughness of the surface, which scatters the reflected light and decreases the aspect ratio. However, the features made in the mask are large enough and such accuracy is not needed.

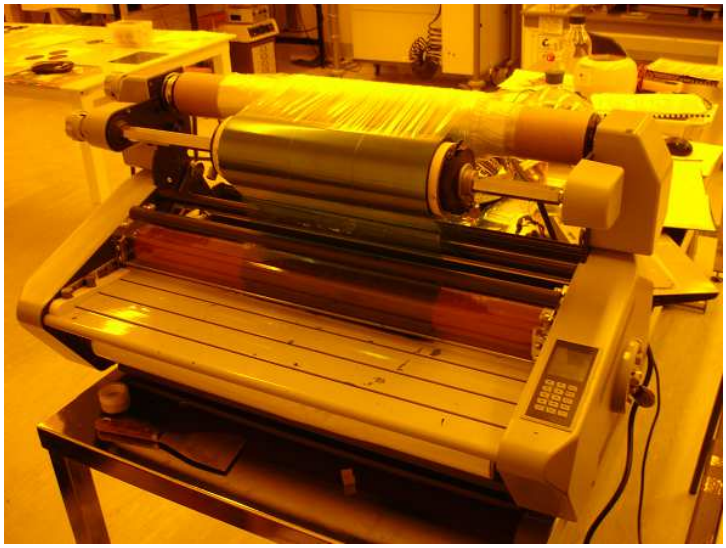

Figure 4.19: Excelam plus 655RM laminator machine

The exposure is carried out with a collimated UV exposure system from Tamarack model 152. A single mercury arc lamp provides high intensity UV light at peak intensity of 365nm. The collimation of the light ensures uniformity of the illumination over the

entire 300x300mm^2 exposure area. Dual CCD cameras can be used to precisely and manually align mask and substrate, but they are not needed here. The exposure is done in contact mode where the mask is in contact with the dry film resist as the mask is an emulsion. The photomask used is a high resolution emulsion mask from JD Photo-tools.

One to four layers of dry film are laminated onto the stainless steel plate depending on the final nickel thickness desired. The lamination of the first layer is the most critical step as the other layers laminate very well on top of each other. One single layer of film only requires 45mJ of energy to crosslink and solidify. However, with 3 to 4 layers of film, most of the energy is absorbed by the first layers, preventing the bottom layers to be fully crosslinked. Exposure tests were carried out with 2, 3 and 4 laminated layers and the results of the best paramters are presented in Figure 4.20. It was found that the relationship number of layer vs energy was not linear and that 800mJ were needed for a three layer resist and 3000mJ for 4 layers.

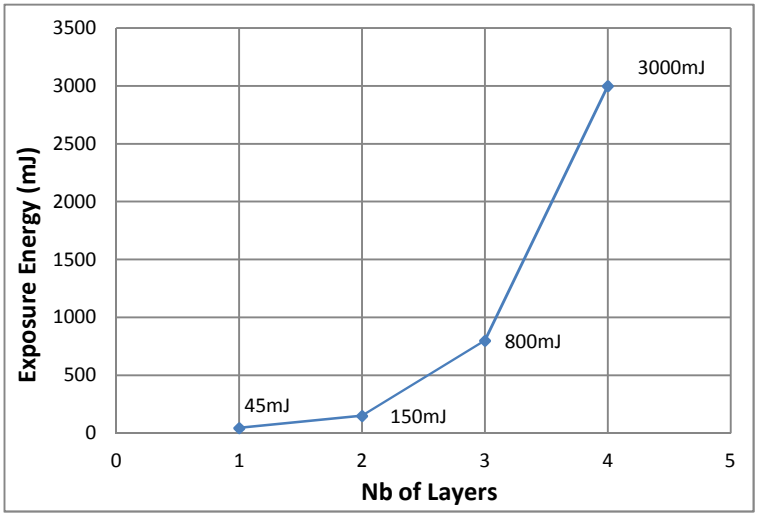

Figure 4.20: Exposure energy depending on the number of laminated layer

The resist is then developed with a spray gun using the MFS 1120 developer. The spray ensures that the non exposed resist is washed away uniformly. Furthermore, while one layer can be easily developed in a stirred beaker, such a large area and thick film would require a considerable amount of time using this technique. The unexposed film is removed after a few minutes. The developed dry film laminated onto a stainless plate is shown in Figure 4.21.

Figure 4.21: Complex pattern design created with 4 laminated dry film layers exposed at 3000mJ onto the stainless steel plate

Electrodeposition

Electroplating consist of depositing metal ions on a conductive surface. The current reduces metallic cations at the anode, passes through the ionized solution and deposit them on the cathode. The intensity of the current determines the rate of deposition of the ions. The cations move from the anode to the cathode in an electrolyte solution containing metal salt and other ions allowing the electrical current to flow.

The nickel electroplating bath at Heriot-Watt University (Figure 4.22) is a 20 litres plating bath based on nickel sulphamate process. At the anode, a basket filled with 99.99% pure nickel pallets serves as the nickel cation provider. At the cathode, the target is the stainless steel plate with dry film pattern. The agitation of the bath is done by a jet, which pulses the electrolyte though a hose toward the target. Fixation of hydrogen bubbles due to hydrogen ion gain at the cathode is therefore reduced. The electrolyte is also filtered upstream from the hose to remove any particles in the bath. The temperature is maintained at 54ºC and the pH, controlled by the addition of sulfamic acid, is kept between 2.8 to 3.9.

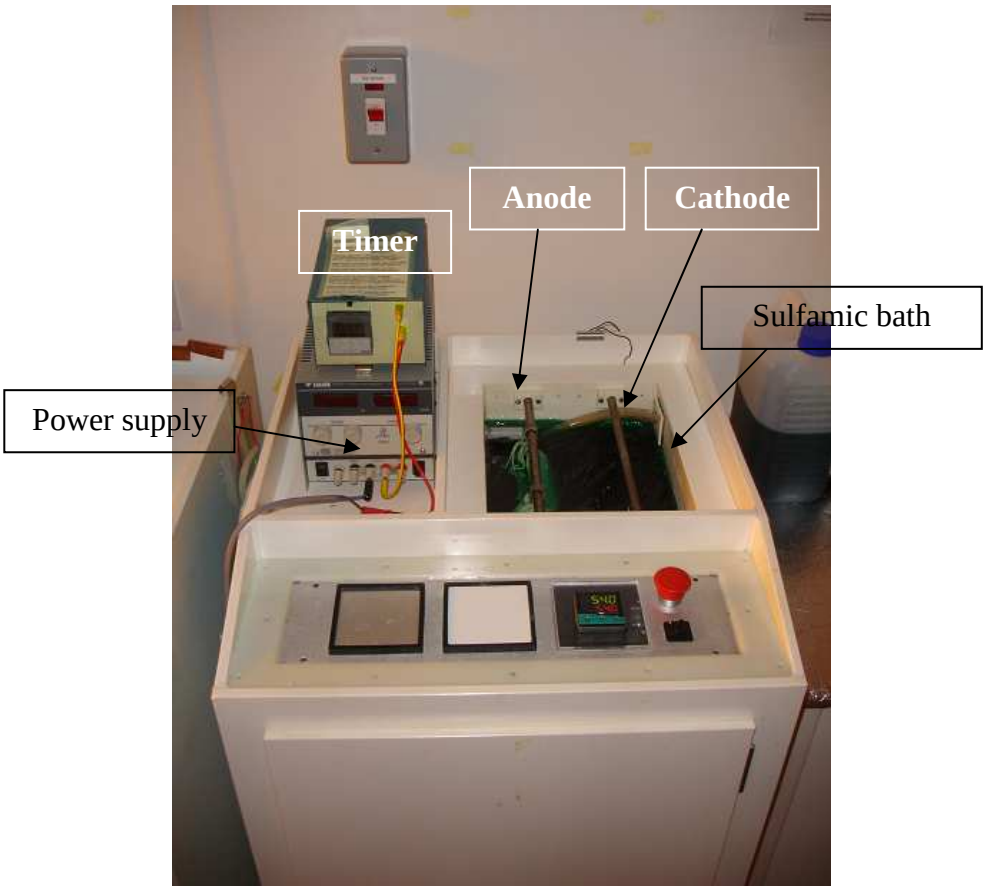

Figure 4.22: Picture of the DC plating bath with cover opened

Nickel deposition is done with at a current density ranging from 10 to 15mA/cm^2, giving a plating rate of around 10-15µm per hour. This current density is a good compromise between time vs residual stresses. Higher current density will plate quicker, but will generate too much stress on the deposited layer at the cathode, which will lift the metal foil off from its substrate. Once plated, the nickel mask is released from the plate by plunging it into the dry film stripper. The exposed film reacts very well to the stripper and is removed after a few minutes. To accelerate the process, the temperature of the bath is set at 50ºC. This step avoids stretching the mask when stripping it off from the plate.

Setup issues and laser cut masks

Certain issues encountered during the metal mask fabrication could not be fixed before the end of this work. Non-uniformity of the plated layer is a recurrent problem in electroplating. Current density is determined by the shapes of the structures. The more

complex shape with sharp edges will draw more current, resulting in a faster deposition rate. This effect is especially present on the edges of the substrate. To reduce this effect, current thief zone areas are created on the sides of the main structure. Those lines are 2mm wide and will draw the most current. They can be seen in Figure 4.21. Despite this, plating thickness uniformity is still a problem with metal foil thickness varying greatly. Figure 4.23 shows a photograph of a mask plated at 12mA/cm^2 for 250mins. The metal thickness was measured and marked in black: variation can be as high as 30µm between the centre and the mask edges. Thus, while metal in the centre can be plated to the right thickness, metal close to the edges can exceed the thickness of the sacrificial material and grow over it, destroying the designs.

With this setup and this material, it was also extremely difficult to fabricate sub-100um features within the 2, 3 or 4 laminated layers. Most of the 80 or 100µm pillars and thin beams collapsed during the development step.

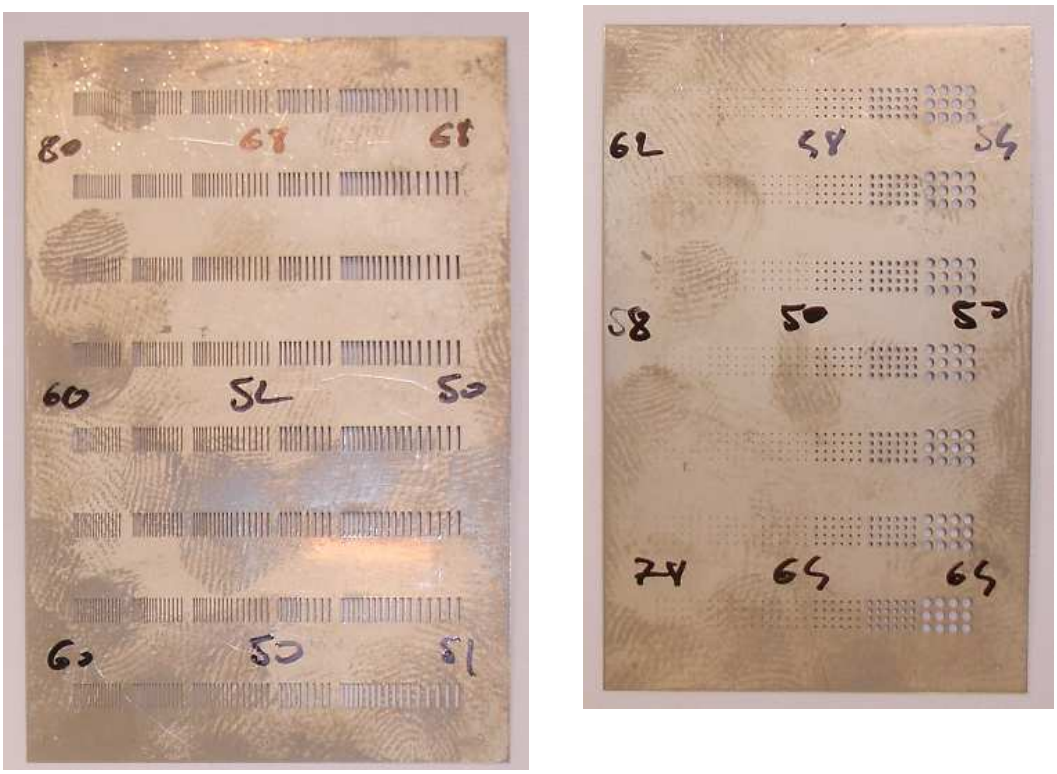

Figure 4.23: Electroplated Nickel mask featuring beams and circular apertures

In the light of these problems, it was decided that for the time being, some masks would be produced by Tannlin Ltd. This company is specialised in laser cutting of metal sheets for stencil printing and can produce highly accurate patterns into thin metal sheets. They

will supply nickel masks 100µm patterned with apertures as small as 80µm. Those masks have a better aperture dimensional uniformity which will enable a good characterisation of the green tape ceramic. However, such requirement is not essential for the LTCC package and electroplated masks will be used.

4.4.2 Coating preparation:

This step was carried out on both electroplated nickel mask and laser cut masks. Two coatings were used for protecting the mask: dry film resist Riston fx930 and the flexopolymer LF55gn. The technique employed is very simple, but will vary depending on the polymer used. It consists of first coating the resist onto the nickel mask and then exposing it to the UV light to reveal the apertures of the mask underneath. As both resist are negative, the photomask used is the same emulsion, which has the opposite polarity to the one used for the nickel electroplating.

Riston fx930 procedure: The procedure is similar to the one described earlier for the metal electroplating. Lamination is done onto the metal mask at 115ºC at a speed of 0.6m/min and 2.5bar. Three to 4 layers of dry film are laminated to ensure the protective coating can resist for 2 to 4 scans. The film is then developed with a spray gun with MFS 1120 developer. As the film is coated onto the apertures of the nickel mask, it can be developed from both sides, increasing the development speed.

LF55gn procedure: The flexopolymer can either be spin coated onto the mask or placed in a mould and knife coated using a roller. In this thesis, spin coating was the preferred method. The masks are taped down on a glass wafer and spin coated at 2500 rpm, 200rpm per second for 40 secondes. The thickness obtained is around 60 to 70µm. The protective transparent film is then carefully laid down manually. This foil, manufactured by HiFi Industrial Film Ltd, has a siliconized face which prevents it from sticking to the polymer. It thickness is 23µm. Knife coating was however also used as the roller enables the polymer and the PET foil to be rolled over at the same time. This eliminates bubble formation that quite often occurs during manual lay down of the foil over the glass wafer. Bubbles trapped under the foil are powder blasted through very quickly, failing to protect the metal. The exposure of the polymer is done with an emulsion mask and exposed at 250mJ. After exposure, the PET foil is removed and the

polymer is developed in a water base solution mixed with 4% detergent. A spray gun is used to force the viscous liquid out. Similarly to dry film resist, the development can be done from both sides, which helps in clearing the smallest apertures.

Two samples of the mask coated with dry film resist and LF55gn can be seen in Figure 4.24.

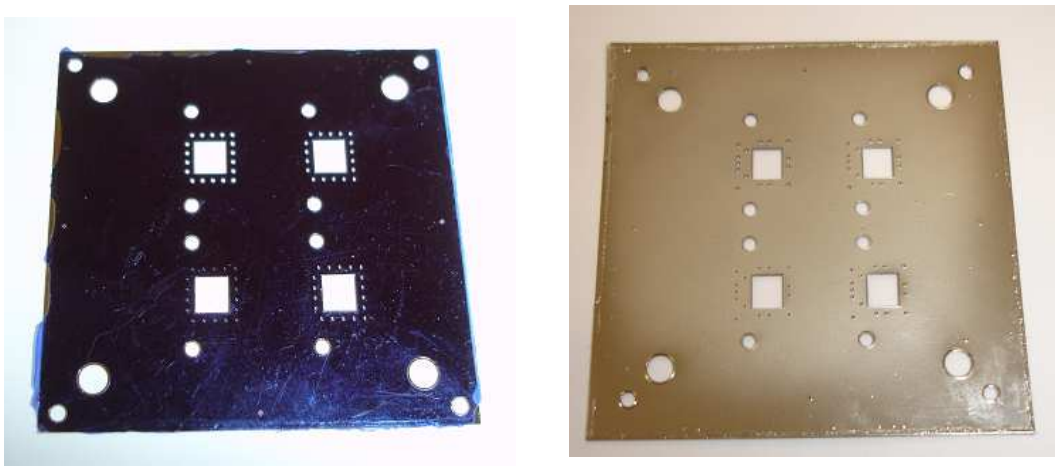

(a) (b)

Figure 4.24: Finished nickel mask coated with its coating:(a) dry film resist and (b) LF55gn

4.5 Conclusion

This chapter has shown that the issues with conventional masking techniques in adapting powder blasting technique on green tape ceramic can be solved using a magnetically clamped nickel mask coated with a polymer such as dry film or LF55gn.
Nickel is the material of choice as a mask for powder blasting green tape ceramic. It combines excellent feature resolutions through electroplating or laser cutting and a great clamping strength compared to stainless steel. A thickness of about 100µm with the setup presented here is sufficient to keep the mask in place for a distance N-S minimal of 20mm and a pressure of 50psi. However, it does not prevent localised lift off around the mask apertures. Additional clamping tools are therefore required if thinner mask is to be used. Lift off is prevented at N-S=50mm.

The protective coatings will protect the mask enough so deformations on the metal are limited. With dry film resist, thicker coating could be investigated at the expense of

resolution. With 4 layers, the coating will have to be changed after every 4 scans. The LF55gn, on the other hand, will protect the nickel mask for a longer period, and a layer of 70 to100µm thick would ensure that the polymer protects the mask until it has worn off. But the development step and the use of a PET foil are problematic.

In this thesis, LF55gn will be preferred as a coating. Despite a more delicate development step, it offers a stronger protection to the particles than the dry film resists. Furthermore, it is a transparent coating that enables precise alignment with the nickel mask features during the photoimaging of the polymer.

Chapter 5 Fabrication and characterisation of microstructures

5.1 Introduction

Chapter 4 looked at different solutions to adapt the powder blasting technique to LTCC. A viable alternative to using glued mask on the ceramic was to pattern a sheet of nickel which can then be magnetically clamped. In order to prevent the bare mask from deforming during the constant particle bombardment, a coated polymer was applied on its top surface. This solution offers both a very good resistance to the particle erosion power while providing high patterning transfer resolution.

In this chapter, this type of mask will be used to pattern microstructures. The characteristics of the process such as erosion profile, under etching and structure dimensions are detailed and correlated to the mask aperture size and distances between the nozzle and the substrate (distance N-S). The possibility of 3D erosion technique to create angled walls is also investigated.

Most of the experiments have been carried out at a pressure of 50psi and the flow rate fixed at 0.1g/s unless otherwise indicated. Two values for the distance nozzle-substrate have been selected: 20mm and 50mm. The scanning speed was set at 5mm/s as it does not influence the erosion rate [82]. The 100µm thick nickel masks used for this characterisation have been laser cut and bought from Tannlin Ltd, Scotland. Thinner mask of a thickness of 35µm were electroplated and either fabricated at Heriot-Watt or bought from Microstencil Ltd. The masks are coated with LF55gn polymer, unless specified otherwise. As mentioned in Chapter 3, the experiments will be done on DuPont P2 165µm thick green tape ceramic.

5.2 General erosion behaviour

A general characterisation of the micro structuring of the green tape sheets with powder blasting is investigated in this section. The jet pressure used for this first analysis is set at 50psi for a distance N-S of 50mm. As a reminder, a scan is composed by an ensemble of passes set with a defined constant pitch to process a certain area. Passes do not powder blast the same area during the scan, but several scans do.

Typical profile

The typical erosion profile of the powder blasted structures is simply shown in Figure 5.1a. Rectangular channels of about a 100µm wide can be seen from a cross sectioned angle. The powder blasting was stopped before the etching particles pierced the tape. Firstly, a clear rounded circular shape was formed at the bottom of the aperture. This U shape is typical of the powder blasting erosion process also obtained in brittle material [120] and depends on parameters such as blasting time, width of the mask aperture and the depth of the pattern to be implemented [120, 121]. With larger structures such as the 1mm^2 square shown in Figure 5.1b powder blasted in the same conditions, only the intersections between the wall and the bottom are round (circled in red) while the rest of the bottom surface is flat.

The walls of the channels are inclined inwards. This is also typical of powder blasting as the process cannot produce highly vertical wall (unlike Dry Reactive Ion Etching for example). However, for deep structures, this angle will be closer to the normal incidence in the upper part of the structure than in the bottom part which is round. Moreover, shallow structures will have highly sloped walls as the rounded bottom is close to the surface of the tape.

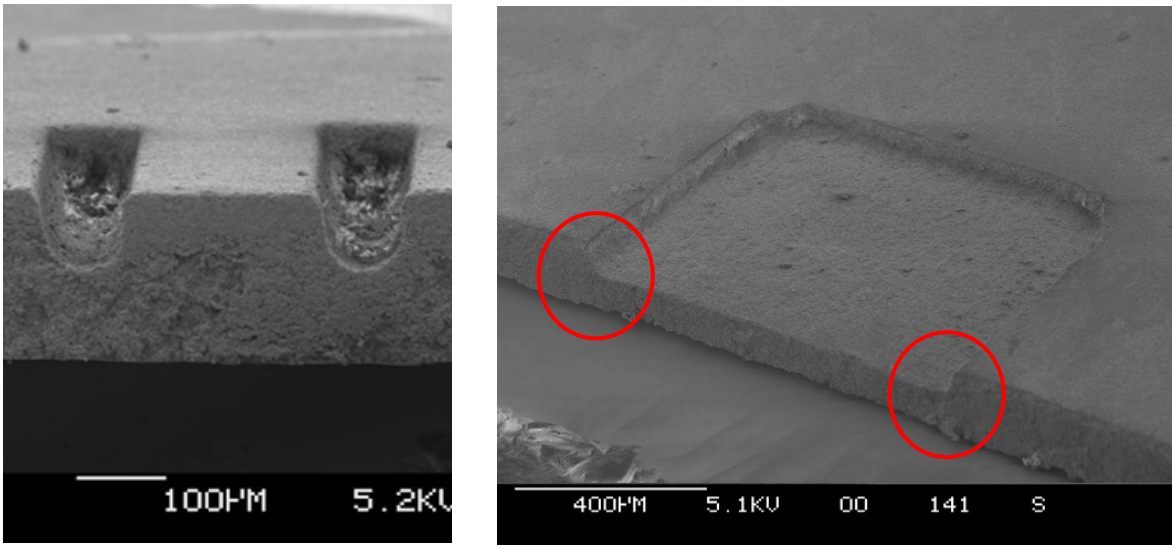

(a) (b)

Figure 5.1: 100µm channels (a) and 1mm^2 square (b) powder blasted in DuPont P2 tape

The time evolution of the erosion can be seen in Figure 5.2a where the cross section of a given section of ceramic green tape is powder blasted after 3, 6, 9 and 12 scans

(pressure 80psi, N-s = 50mm). The mask used for these structures had circular apertures of 180µm in diameter. The results show the gradual erosion of the tape. The tape is only just pierced after 6 scans, and a clear U shape profile can be seen after both 3 and 6 scans. After only 6 scans, the U shape creates a “conic” via which has an exit side diameter about two fifth smaller than the entry side diameter (190µm entry/75µm exit). The gap between the entry and the exit side is about 115µm. However, this conic shape can be reduced by increasing the scanning and thus the erosion time: after 9 scans, this gap is reduced to about 50µm. The exit opening becomes 140µm in diameter while the entry diameter remains at around 190µm. The verticality of the via walls has thus been increased. As suggested by the Figure 5.2b, both sides will eventually approach a similar diameter.

Walls slope angles that can be calculated from the dimensions of the openings are not really relevant for the structures powder blasted after 3 and 6 scans due to their U shape. But for 9 and 12 scan, the angle of the slopes can be calculated as the walls are more or less straight. After 9 scans, the slope angle is around 82º and after 12 scans, the slope angle is 85º.

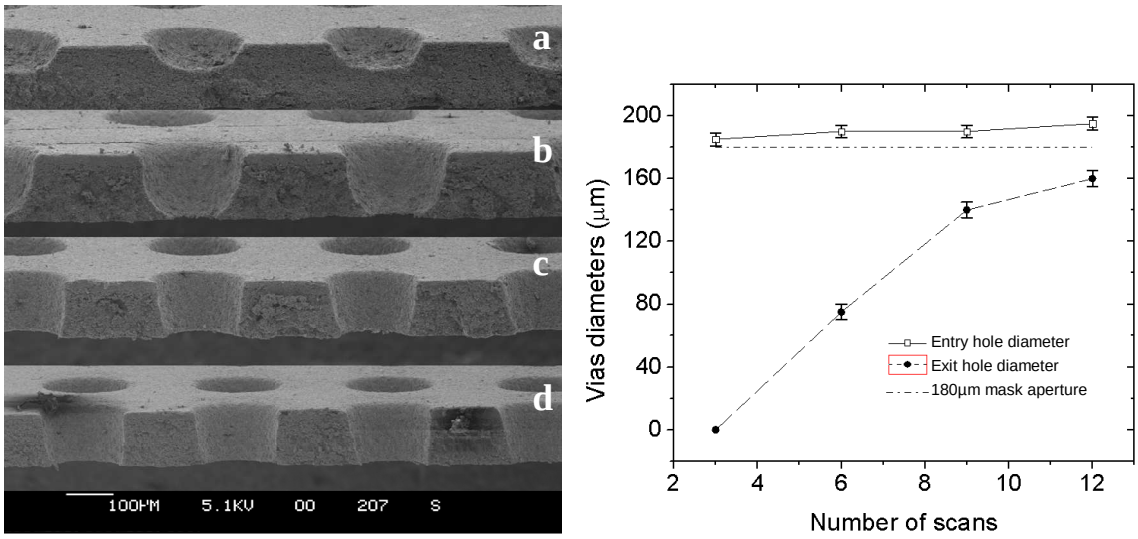

(a) (b)

Figure 5.2: (a) SEM picture of cross-sectioned vias powder blasted at different lengths of time with a= 3 scans, b= 6 scans, c= 9 scans and d= 12 scans. The graph in (b) represents the variation of the via diameter entry and exit as a function of the number of scans

The fabricated structures do not exhibit any heat affected zone commonly found in the laser ablation process and described in Chapter 2. The structures do not have remelt glass on their edges as evidenced by Figure 5.3 showing a close up cross section of a via. A clear rounder smooth edge can be seen on the entry side, indicating that the powder is being able to etch underneath the mask. Conversely the edges of the exit via are sharp. Inside the vias, the walls are very smooth, almost polished. The material is not visibly shredded despite the presence of large particles in the powder, one of them visible in the figure below.

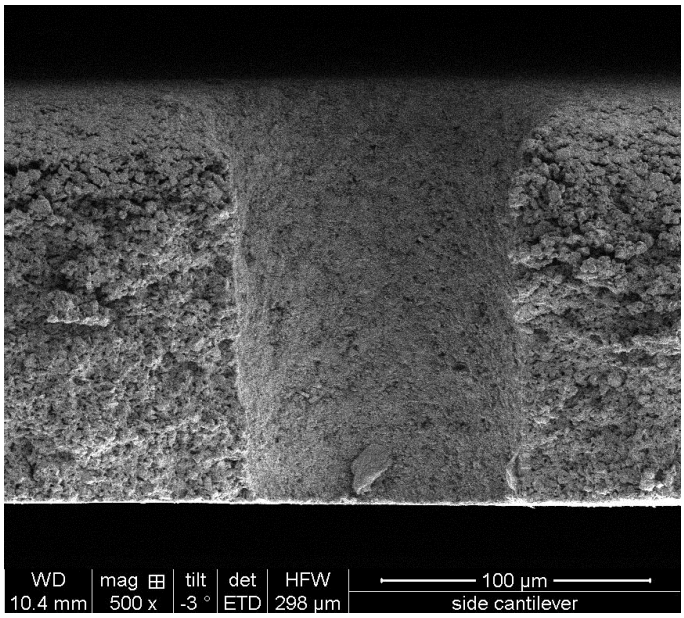

Figure 5.3: Surface profile of a 120µm powder blasted via. A 20 x10µm alumina particle can be seen at the vias bottom. The shredded surface surrounding the vias is due to the cross-section which was carried out using a scalpel

Surface roughness

The surface roughness of the green tape powder blasted surface was measured by using the Zygo. A single pass was done at a distance N-S of 20mm and 50mm with 9µm particles. The reflectivity of the ceramic green tape was enhanced by sputtering a few tens of nanometres of gold. The Zygo imaged the centre of the pass over a surface of 0.35x0.26mm. The roughness number is obtained by averaging the roughness value of 10 sample lines taken from the imaged area. To limit the effect of the particles erosion pattern, in addition to the small dimensions of the sampled area, the lines are taken along the direction of the pass. Three sampled LTCC surfaces were studied: one surface

before the process and one after the powder blasting at N-S=20mm and one at N-S=50mm (Figure 5.4)

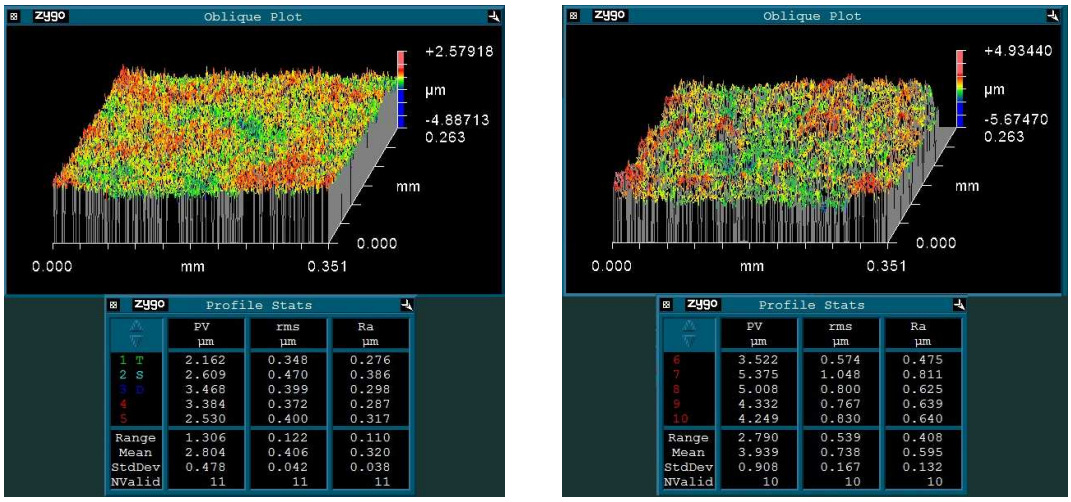

(a) (b)

Figure 5.4: (a) Surface roughness of the non machined green tape (b) Powder blasted with 9µm at N-S=20mm

The virgin LTCC tape has a surface roughness Ra of about 0.320µm. After powder blasting with 9µm alumina powder, the Ra is around 0.595µm, almost twice as much. The increase in the distance N-S to 50mm slightly reduces this number to 0.550µm. In contrast, the tape roughness of a tape powder blasted with 30µm powder was 1.8 µm at 20mm and 1.19µm at 50mm. To compare with powder blasted glass, the roughness ranges from 0.8 to 6µm with particle average sizes from 9 to 204µm [99].

The particles do not impregnate the soft ceramic tape. Particles do not stick on the surface. However, a very thin layer of powder can be seen on the tape surface. Despite the masks strong clamping, thin particles can spread beneath the mask during the blasting process and during the cleaning process of the powder inside the enclosed box with the air gun.

The particles on the tape can easily be cleaned with a soft brush and/or with the air dust blow gun directed directly to the layer. Extreme care should however be considered with highly complex and fragile patterns. Cleaning thin structures or small vias can be problematic as a soft brush might not be able to reach the particles. Too many particles inside vias could induce open circuits during vias filling or increase the surface contact

resistance with the track underneath. Fortunately, even the smallest clogged vias have been successfully cleaned using compressed air. The impact of the few remaining particles hanging on the structure walls as illustrated in Figure 5.3 can be considered negligible.

If not cleaned, such layer of particles could reduce the adhesion of the conductive tracks during the printing step. But it would have a minimal impact in the lamination step as alumina particles are a prime component of the tape. Delamination was not observed during the firing of laminated powder blasted green tape.

5.3 Characterisation of the apertures

5.3.1 Methodology

The magnetic holder described in Chapter 4 was used for these experiments. The ceramic green sheets were pre-cut into more convenient 50*30mm pieces and placed with their original backing foils on the holder, centred over the two magnets. The nickel masks were then applied on the LTCC. The edges of the mask were duck taped and powder blasted in the direction parallel to the lines of apertures (Figure 5.5). This limits the number of stops that the nozzle performs between passes with only 6 passes necessary to scan the entire lines of apertures.

From the previous results, the pitch selected for both N-S=20 and 50mm during these experiments was set at 1mm. This produces a very flat surface for both distances and ensures that the tape is not pierced too quickly at N-S=20mm with a tighter pitch. There are not such requirements at N-S=50mm and the pitch was chosen in order to have matching scan areas between distances. The measurement repeatability with the optical microscope focused on the surface was established at ± 2µm.

5.3.2 Vias

Vias fabrication is one of the most important features in LTCC. The need for small diameter vias is increasing as electronic packages require denser wiring/routing and, therefore, smaller tracks. In 3-D circuits, badly shaped or partially clogged vias can induce open circuits due to poor filling of the paste inside the vias, provoking the discard of an entire package. Conversely, the lack of control of the vias' dimensions can create short circuits during track printing. The quality of the powder blasted vias was

assessed based on their dimensions, circularity, shape and propensity to clogging.

The masks used for this experiment (Mask A, Figure 5.5) are 55x35mm in dimension with 7 sets of circular apertures organised in blocks of similar diameter (800, 400, 300, 200, 100 and 80µm). Each block has four lines of apertures, except for the 800µm apertures which only have three.

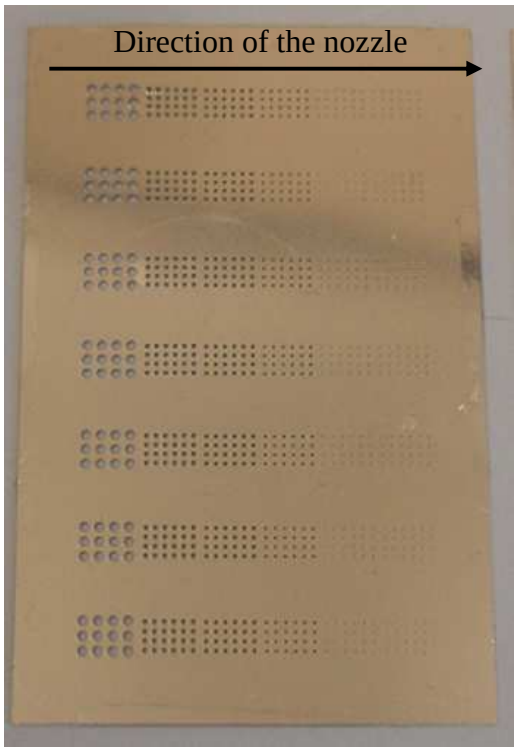

Figure 5.5: Nickel Mask A featuring circular apertures arranged in sets

Erosion at a distance of 20mm

Mask A was scanned 1, 2, 3, 4 and 6 times with a pitch of 1mm. The vias dimensions resulting from powder blasting are displayed in Table 5.1. The 165µm thick tape was pierced after only 2 scans. However, strangely, vias powder blasted with the largest apertures (800 and 400µm) were not entirely pierced. A very thin layer of green tape was left at the bottom. For the 100 and 80µm diameter apertures, the vias were barely pierced with exit diameter about half the size of the entry diameter. Three scans were necessary to pierce the tape with the 800 and 400µm apertures. Such a number of scans gave the smallest vias a better verticality of the aperture walls. The exit diameter of the vias reaches the dimensions of the mask apertures after 3 to 4 scans. At this point, the vias have an entry diameter about 20 to 40µm larger than the mask apertures. These

results also show that the increase in the entry side diameter is more contained for small apertures (around 20µm increase) than for large one (30 to 40µm).

Table 5.1: Via dimensions (entry and exit diameters expressed in microns) obtained after different scans and mask apertures. These dimensions are displayed into two graphs below representing entry and exit sides

	2 scans		3 scans		4 scans		6 scans	
Apertures	Entry	Exit	Entry	Exit	Entry	Exit	Entry	Exit
800µm	819	N/A	830	773	840	804	850	820
400µm	415	N/A	420	388	429	403	451	421
300µm	312	278	320	290	333	311	349	320
200µm	212	175	218	190	222	207	232	215
100µm	108	59	112	82	120	93	130	105
80µm	88	36	94	60	96	73	108	86

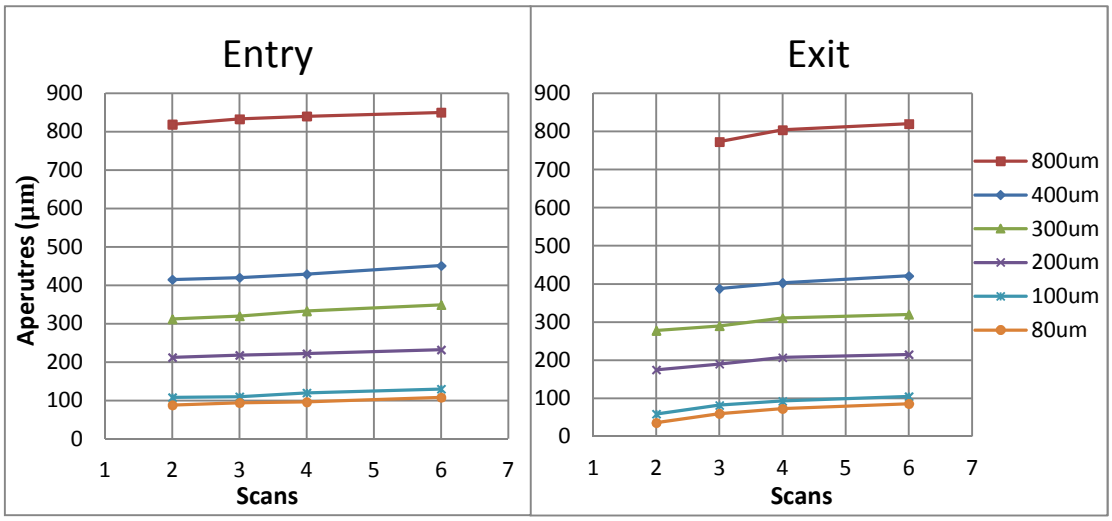

The variations in the entry and the exit side diameter of vias blasted with the same number of scans are different. Entry diameters only vary in a range of 5% and are constant with any number of scans. For the exit diameter, the variations are important after only two scans when the tape is just pierced, but they then decrease after 3 to 4 scans. This is due to the U shape of the structure and the thin layer which forms the

bottom of the via. This layer is highly affected by slight changes in powder flow. Thus, after 2 scans, the variations between exit diameters can be as much as 30%, but decrease to only 10% after 3 and 4 scans.

Erosion rate and apertures size: From the results displayed above in Table 5.1, the erosion rate is lower for the large apertures 800 and 400µm which were not pierced after 2 scans, but also for small apertures, 80 and 100µm. Those findings partially contradict the results published in the literature, especially those of Anne-Gabrielle Pawlowski [122]. It was shown that below the 100-150µm aperture diameter threshold, the erosion rate decreases with decreasing aperture diameter: the mask acts as a filter and increased collisions inside the apertures between particles reduces the erosion power [120]. Above this threshold, the erosion rate is independent of the dimensions of the aperture. However, the scanning method was different, the flow rate was twice as high, the apertures were rectangular and the mask thickness was only 50µm.

To confirm the results found in Table 5.1, additional tests were done with Mask A. One single scan was done and the measurement of the depth of the powder blasted vias were recorded using the Zygo white light interferometer (after only one scan, the tape is not pierced). Figure 5.6 illustrates the average depth obtained from a series of tests with two different flow rates. The bottom surface being reflective and not very flat, the measurements were difficult and limited to the deepest point in the vias.

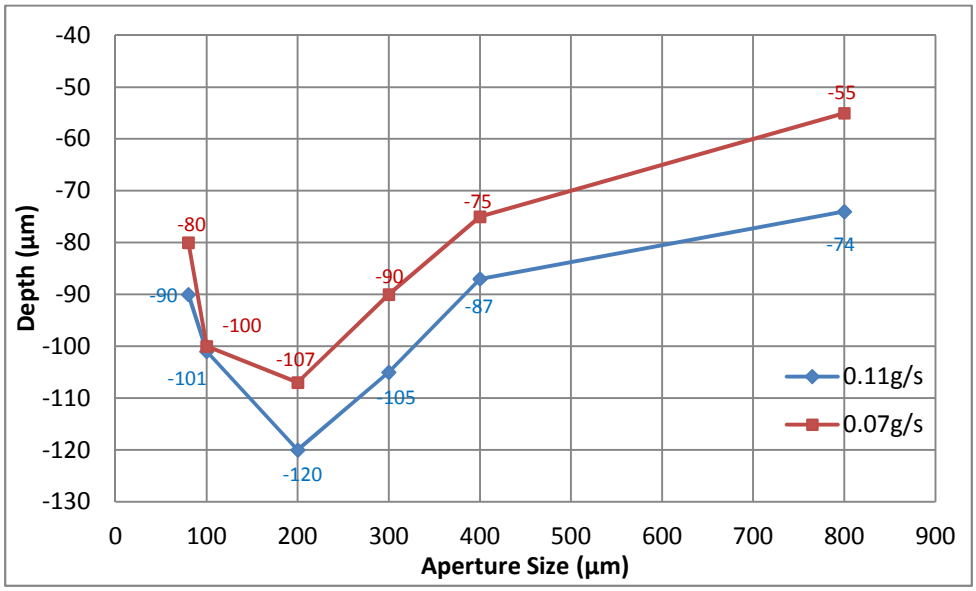

Figure 5.6: Graph of the depth of powder blasted vias with different mask aperture measured after 1 scan

The results show a similar erosion pattern to the one drawn in Table 5.1. Lower erosion rate was obtained with 80 and 100µm aperture diameters as well as with the largest 400 and 800µm diameters. In addition, a peak of erosion can be seen for apertures in the 200µm diameter region. In light of these results, the scanning process was also investigated. The pass direction was changed by 90º: the lines were powder blasted perpendicularly with a pitch of 1mm. The erosion rate pattern was similar to the one exposed in Figure 5.6.

The thickness of the mask combined with the second impact effect of the particles can partially provide an explanation for the change in behaviour compared with Anne-Gabrielle Pawlowski's findings. Particles' second impact is a well known phenomenon and is created by particles bouncing from the mask edges or the structure wall towards the substrate [123]. In the substrate itself, they contribute in giving high aspect ratio vias their typical funnel or bottleneck shape. The latter have been used to an advantage for microfluidics applications in glass substrate [8]. For larger and shallow structures, the effect is materialized by shallow trenches localized in the vicinity of the mask edge (Figure 5.7a). The width and depth of the trenches depend on the mask thickness. The thicker the mask, the more particles rebound [124] and the deeper the trenches are. These effects are clearly materialized in the largest vias that have been powder blasted before they were pierced (Figure 5.7 b)

It is therefore possible that trenches created by a circular aperture having a diameter equal to the trench width increase the erosion of the substrate as illustrated in Figure 5.8. It was however not possible to obtain an accurate measurement of the width of the trenches created in the circular apertures. There was no reliable explanation found during this thesis for the lower erosion obtained for 400 and 800µm apertures.

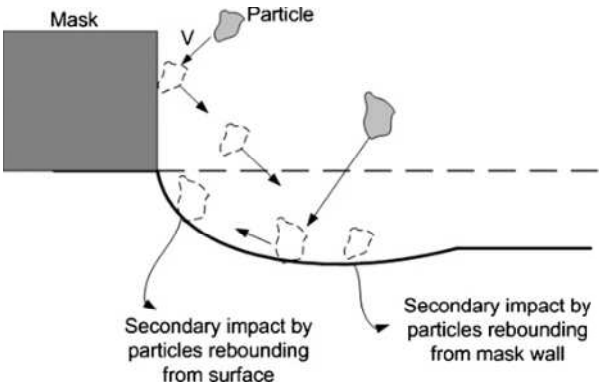

(a)

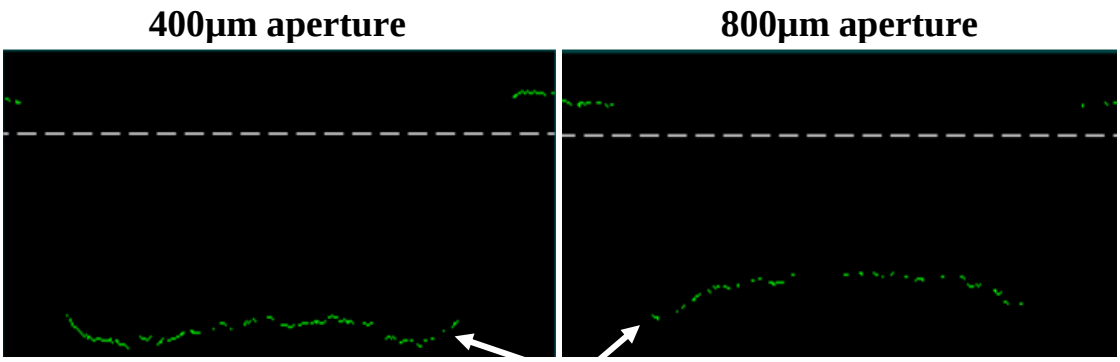

(b)

Figure 5.7: (a) Drawing of mask and substrate detailing the phenomenon responsible for the creation of trenches [124]. (b) Cross section profile of 400 and 800µm vias in green tape after a single scan showing the trenches created by the particles

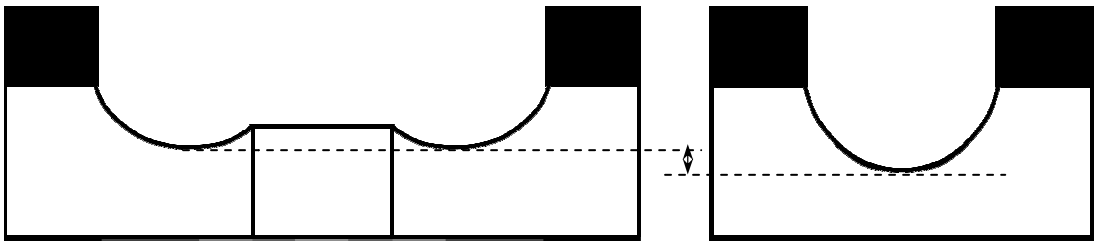

Large aperture: two distinct trenches

Small aperture: Combined erosion effect

Figure 5.8: Schematic of the trench erosion with large aperture and small apertures

Under etching: Under etching is due to particles impacting the substrate underneath the mask. As detailed in Chapter 4, under etching occurs on the wall of the substrate,

resulting in larger structures, and on the top surface which gives smooth edges to the structures. The under etching of the edges of the green tape ceramic can be seen in Figure 5.9.

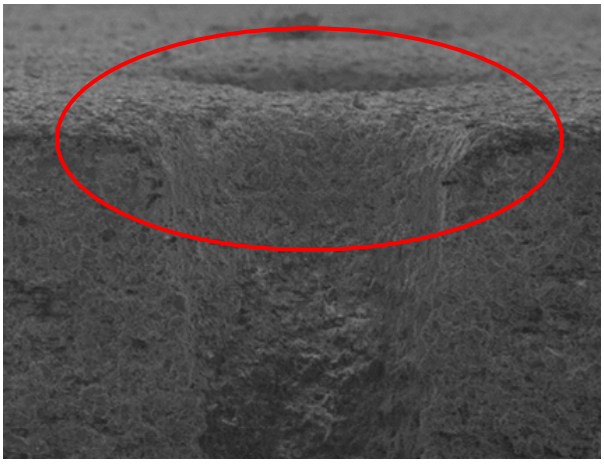

Figure 5.9: SEM picture of a cross section of a 200µm vias illustrating the smooth rounded edges on the structure edges (circled in red)

Under etching was simply measured by comparing the diameter of the powder blasted vias and the diameter of the apertures of the mask with which they have been fabricated. Figure 5.10 compiles the under etching obtained with the entry side of the vias (top surface) after 2, 3, 4 and 6 scans.

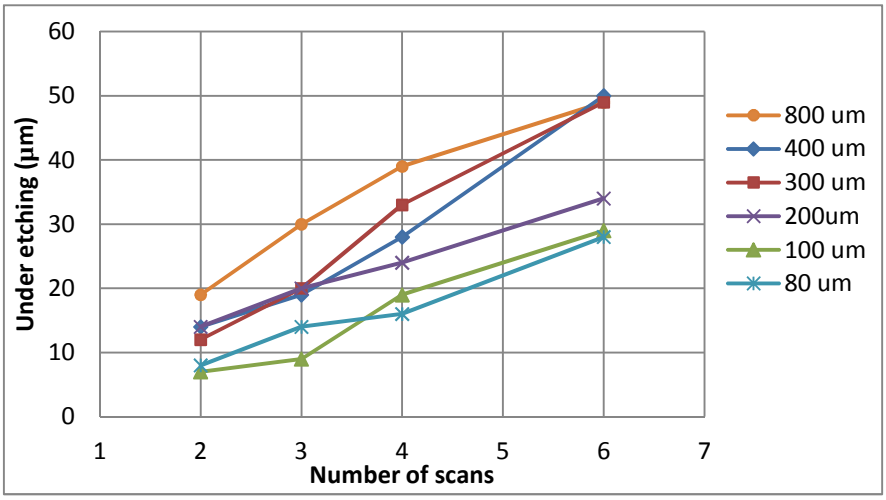

Figure 5.10: Under etching as a function of the number of passes and mask apertures

The under etching seems to increase linearly from two to six scans. Figure 5.10 also shows clearly that the under etching for small apertures is lower than for larger ones. After 4 scans, the under etching is around 40µm with 800µm apertures and decreases to

about 15µm with 80µm vias. This difference can be explained by a lower lift-off of the mask with smaller apertures. However, the ratio under etching/mask aperture diameter (which compares the size of the under etching to the size of the aperture) is higher for the small apertures: for 400µm apertures, the under etching (28µm) is about 7% of the mask aperture diameter. The under etching of an 80µm aperture (16µm) represents 20% of the apertures diameter.

Walls inclination: As mentioned in the first part of this chapter, the tapered shape of the wall of the structures can be reduced by increasing the number of scans. This increases the verticality of the walls and therefore increases the diameter of the exit side of the blasted vias. It is however difficult to measure precisely this inclination. The slope of the wall cannot be calculated with the diameter of the entry and the exit of the vias only because of the under etching affecting the structure's top edges. Cross section of vias, on the other hand, allows a better measurement of such slopes. Figure 5.11 shows a cross section of the vias in Table 5.1 after 4 scans with a 400, 200 and 100µm mask aperture diameters. It can clearly be seen that the walls are almost vertical after 4 scans with an inclination angle ranging from 85° to 90° with respect to the horizontal axis. It is important to note that precise cuts of vias are difficult because they are done manually with a scalpel: cuts performed off centred in the vias would result in slope seen more inclined than they really are. In particular, sub 100µm vias are extremely difficult to process.

400µm

200µm

100µm

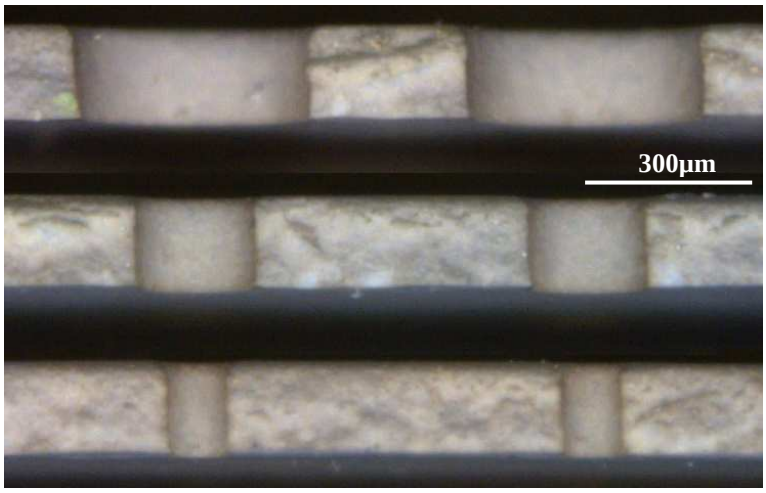

Figure 5.11: Cross section of vias showing the vertical walls obtained after 4 scans with a 400, 200 and 100µm apertures

Erosion at a distance of 50mm

The DuPont green tape was here powder blasted at a distance N-S of 50mm with the same pitch of 1mm. The particles have a longer distance to travel and lose their kinetic energy by friction with the surrounding air. This leads to a decrease in the erosion rate as shown in Chapter 3. At this distance, the density of particles is also reduced as the machinable area is increased from 15mm^2 at N-S=20mm to 78mm^2. Due to the lower erosion rate of the particles, the number of scans needed to pierce the layers increases. The results of the experiments are displayed in Table 5.2.

Table 5.2: Diameters of different vias powder blasted after 6, 8, 10 and 12 scans

	6 scans		8 scans		10 scans		12 scans	
	Entry	Exit	Entry	Exit	Entry	Exit	Entry	Exit
800	805	--	807	777	810	788	820	811
400	403	--	406	376	412	384	420	400
300	307	240	307	280	310	290	316	300
200	201	145	201	171	210	178	220	197
100	99	--	102	40	107	55	116	88
80	81	--	87		90		95	68

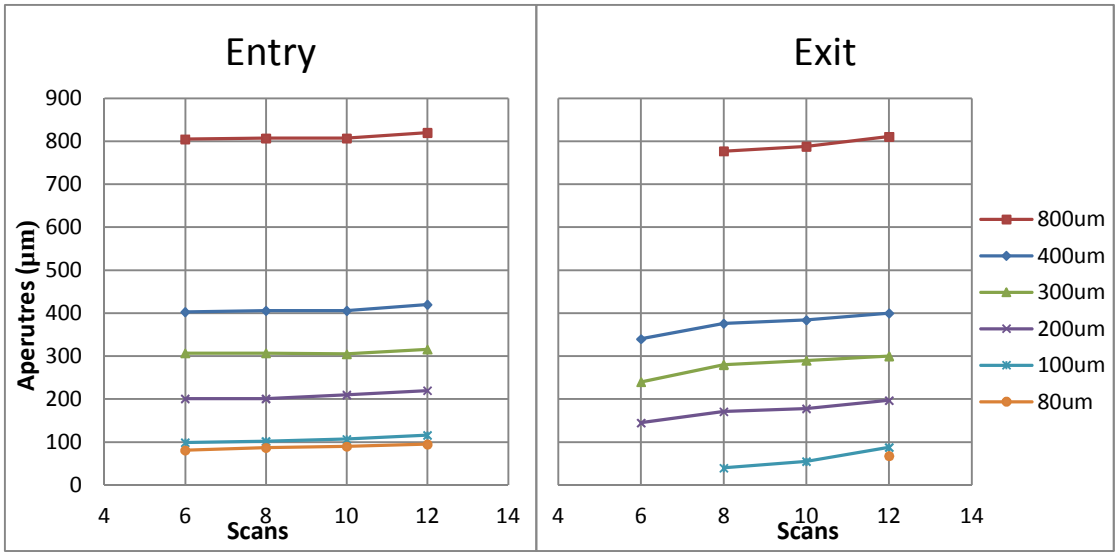

Two cases can be clearly distinguished:

- For large apertures diameter down to 200µm, 8 scans are enough to pierce the tape and obtain good vias with difference entry side/exit side of only 30µm. At this stage, the vias entry diameters are very close to the diameter of the apertures of the mask. On the other hand, the exit dimensions are smaller compare to the mask aperture by around 25-30µm. Walls are mostly vertical except at the bottom where a sharp curve indicates that they have just been pierced through. Increasing the number of scans to 12 brings the exit diameter of the vias to the same dimension than the aperture, but also increases the under etching on the entry side to 10 to 15µm. The difference entry side/exit side is then only about 15-20µm
- For sub 200µm apertures, 12 scans are needed to pierce the vias. With circular mask apertures of 100µm, 8 scans result in vias having an extremely small exit hole (40µm in diameter). With 80µm apertures, 12 scans are necessary.

Erosion rate and apertures size: The dependence of the erosion rate on the diameter of the aperture is similar to the one observed at N-S 20mm. Thanks to the lower erosion rate, a more precise mapping using the erosion recorded after 2, 4 and 6 scans can be done and has been reported in Figure 5.12. A similar erosion peak with apertures having diameter of around 200µm can be identified, but is less pronounced. Once again, with the largest 400 and 800µm aperture diameters, the erosion is lower than with 200 or 300µm aperture diameters. The tape was pierced after 6 scans only with vias powder blasted with the 200 and 300µm apertures.

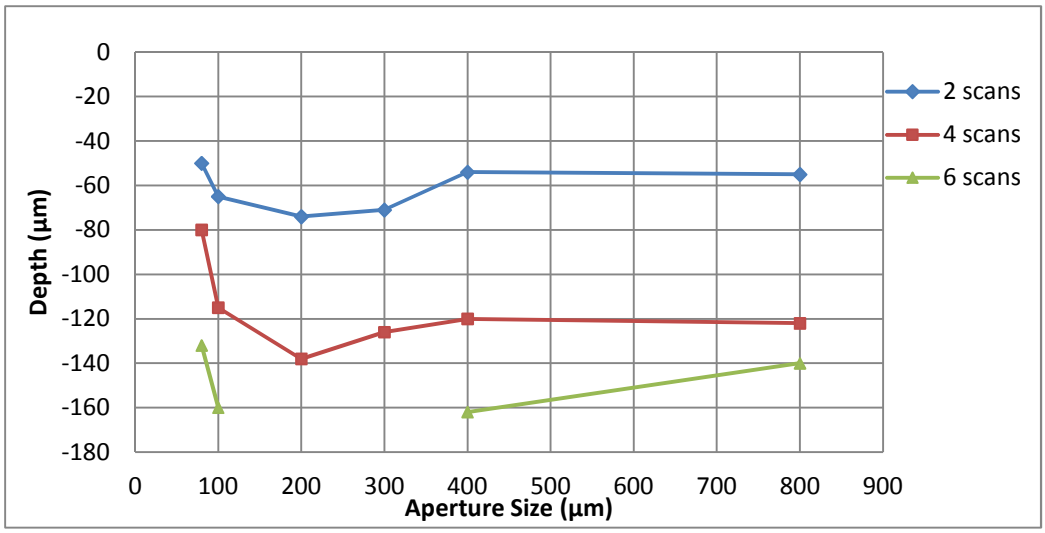

Figure 5.12: Depth of the openings measured after 2, 4 and 6 scans with different aperture diameters

Under etching: Table 5.2 clearly shows that under etching is lower compare to the distance N-S of 20mm, even after 12 scans. The results can be explained as follows:

- The lower power of the particles decreases the erosion power of the second impact of the particles (responsible for the under etching).
- The air pressure is weaker compared to the distance N-S=20mm and reduces the lift off of the mask.
- The higher number of scans needed to pierce the tape enables a better control of the piercing of the structure. The number of scans can be adjusted to coincide with the piercing of the tape, thus reducing unnecessary powder blasting process. On the contrary, at N-S =20mm, there is no such control and the process can only be stopped either after 2 scans (not enough) or 3 scans (slightly too much for certain apertures).

Comparison between N-S=20mm and N-S=50mm

Apart from the obvious slower erosion rate, a comparison is needed to analyse the benefits of one distance compared to the other on the dimensional characteristics of the structure. A fair comparison is done by selecting vias with similar exit dimensions for both distances, regardless of the number of scans needed to fabricate them. The under etching is shown in Figure 5.13.

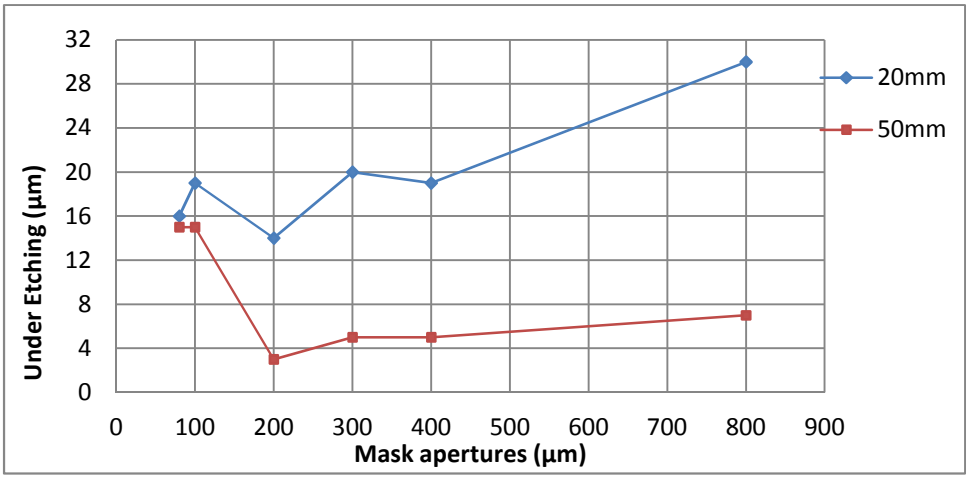

Figure 5.13: Under etching at N-S=20mm and N-S=50mm shows a clear advantage for the distance N-S=50mm

There is clearly less under etching at N-S=50mm than N-S=20mm. Two distinct

behaviours can be seen in Figure 5.13: for small apertures, there is not much difference in the under etching which is at around 16-20µm. For 200µm apertures and above, the under etching remains at around 4 to 8µm for N-S = 50mm but steadily increases from 14µm to 32µm for N-S=20mm.

The under etching is here only observed at the top of the structure. Despite the higher under etching at N-S=20mm, cross section of the vias for both N-S=20 and N-S=50mm distances shows that their walls have similar vertical slopes. However, the entry/exit side comparison between Table 5.1 and Table 5.2 can suggest otherwise with a larger difference (thus lower slope angle) obtained at N-S=20mm. This is due to the sharper edges of the structures (entry side only) at N-S=50mm. Thus both distances can be said to fabricate similar structure walls except that rounded edges are more important for N-S=20mm.

Clamping strength effect

The adhesion of the mask onto the ceramic green tape can influence the final diameter and shape of the via as shown previously with the mask lift off. To further investigate this effect, the clamping force of the masks onto the green tape was increased with additional metallic clamps positioned onto the mask. The mask was powder blasted at N-S=20mm and only the diameters of the vias obtained after 4 scans were measured. Table 5.3 compares the diameters of the vias with and without the extra metal clamp.

Although some of the entry side of the vias are larger with the additional clamping tools (partially because of the variations in the flow rate between the two experiments), table 5.3 clearly shows an improvement in the difference between the entry and the exit diameters. This difference is smaller and is reduced to about 10 to 15µm with vias powder blasted with apertures ranging from 800µm to 300µm. Without extra clamping tools, this difference is around 20 to 30µm. The extra metallic clamp did help to reduce the under etching by limiting the mask lift off (despite the under etching still being at around 30µm). The improvement is however limited to the apertures larger than 200µm. Without additional clamping tools, smaller apertures suffer less from lift off thanks to their sizes as previously discussed in this chapter and in Chapter 4. The clamping tools thus do little to change the under etching. However, this behaviour would change with a higher density of such apertures.

Table 5.3: Comparison between vias powder blasted after four scans with and without additional clamps

	4 scans		4 scans + metallic pieces	
Apertures	Entry	Exit	Entry	Exit
800µm	840	804	826	811
400µm	429	403	434	423
300µm	333	311	320	310
200µm	222	207	230	217
100µm	120	93	116	100
80µm	96	73	100	70

A look at the mask apertures back side helps to image the intensity of the under etching at the structures top edges. Figure 5.14 displays two pictures of two nickel masks back side powder blasted at a distance N-S of 20mm and 50mm. The halos surrounding the apertures results from particles hitting the substrate on their way out from the powder blasted vias. They are mainly due to the mask lift off. These halos are less pronounced with smaller apertures and at 50mm than at 20mm which confirms the lower under etching in the apertures vicinity.

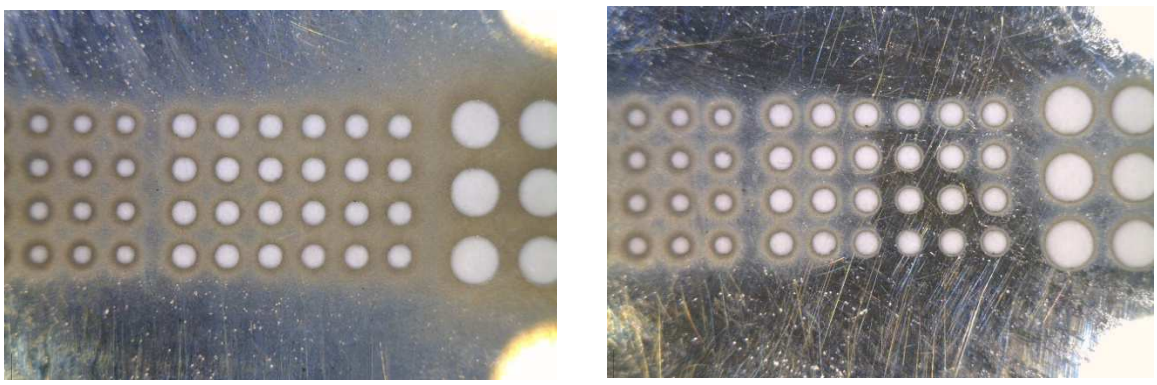

(a) (b)

Figure 5.14: Back side of nickel masks powder blasted at a distance of (a) 20mm and (b) 50mm

The non uniformity of the forces applied on the mask can clearly be seen in Figure 5.14 at N-S=50mm. The non etched part was strongly clamped down by the field while the rest of the mask was looser.

Smallest vias

The smallest vias were fabricated with a thin 35µm mask (from Microstencil Ltd) and 100, 80, 60 and 40µm aperture diameters. Such thickness is better suited to be used for 60 and 40µm diameters. The wide distribution of particles size increases the chances of oversized particles colliding with other particles inside the small apertures. In order to bring the under etching to a minimum (due to the lower clamping strength), the distance N-S selected was 50mm and additional clamps were used.

The smallest opened vias that this process could produce was obtained after 10-12 passes and apertures of 60µm. The vias have the following dimensions: 60-65µm for the top entry and 20µm for the exit side. The 40µm apertures did not produce any opened vias: the erosion is strongly reduced due to particles collisions clogging the mask apertures as well as the green tape vias. The entry of the unfinished vias had a diameter of around 50µm. Table 5.4 below resumes the results and Figure 5.15 shows a cross section of a 90µm entry/60µm exit vias.

Table 5.4: Dimensions of the smallest vias achievable with powder blasting in LTCC. The structures were obtained at a distance N-S of 50mm

	Vias dimensions			
Mask apertures	100	80	60	40
Entry diameter (µm)	112	93	62	51
Exit diameter (µm)	80	60	20	__

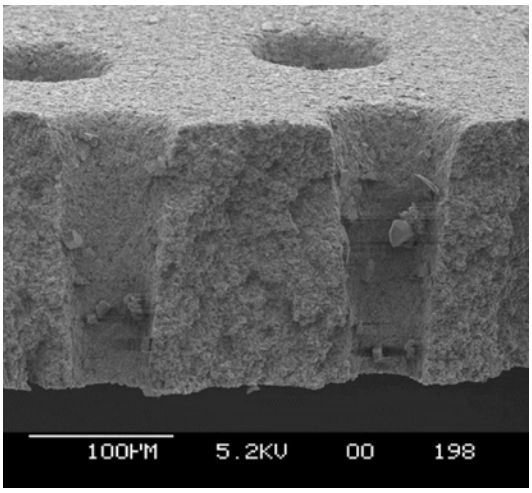

Figure 5.15: SEM cross section of a vias with 90µm entry and 60µm exit

5.3.3 Beams

The powder blasting of flat straight structures was also investigated. To do so, Mask B shown in Figure 5.16 was used. Its dimensions are 60x40mm. It is composed of 8 sets of rectangular apertures. Five groups can be distinguished and characterised by the width of the apertures: 300, 200, 100, 90 and 80µm. In each groups, the apertures are spaced by thin metal sheet which can be referred to as “beams” with width ranging from 500 to 80µm. The resulting powder blasted structures in the green tape resemble the beams of the mask. The shapes of these beams were characterised in this part.

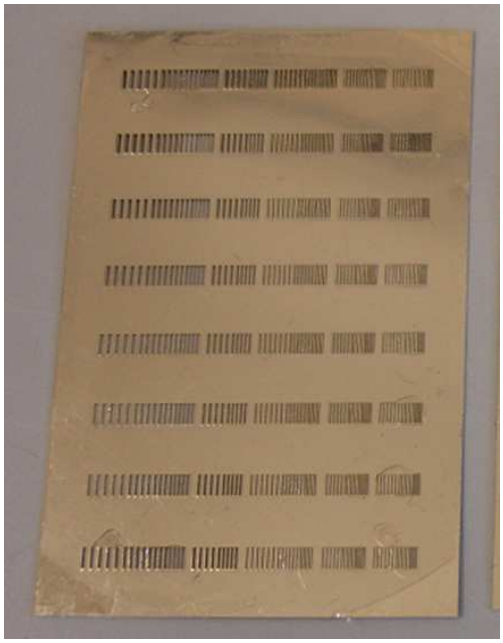

Figure 5.16: Nickel mask B featuring rectangular apertures

Erosion at a distance nozzle-substrate of 20mm

Similarly to the experiments realized on circular apertures, the characterisation of the structures was first started at a distance Nozzle-Substrate of 20mm. The masks were placed on the green tape without any extra metallic clamps. The pitch was set at 1mm.

Erosion rate vs aperture size: The dependence of the erosion rate on the aperture width was obtained by measuring the depth of the powder blasted structures after 1 and 2 scans. The depth was recorded from the photos of the cross sectioned beam. Four mask apertures were used: 80, 90, 200 and 300µm. The results displayed in Table 5.5 show a higher erosion rate for smaller apertures (80 and 90µm) than for the large apertures (200 and 300µm). In contrast with the circular apertures, the erosion rate peak was not found with the 200µm apertures but closer to the 90-100µm aperture. Three scans were needed to pierce the tape, regardless of the aperture diameter.

Table 5.5: Measured depth etched as a function of the aperture width after 1 and 2 scans

	Depth (µm)	
Aperture width	1 scan	2 scans
80 (µm)	80	163
90 (µm)	90	162
200 (µm)	65	145
300 (µm)	68	140

Erosion behaviour: as the number of scans increases, the manufacturing of the beam is monitored by measuring the beam at its top surface and halfway through the tape thickness. The mask design used in this experiment has a beam width of 100, 200, 300 and 500µm. Each beam is separated by a fixed apertures width of 300µm, so that the space between beams affects the erosion behaviour in a similar way. Measurements were done with a digital microscope and results are shown in Figure 5.17 and Figure 5.18.

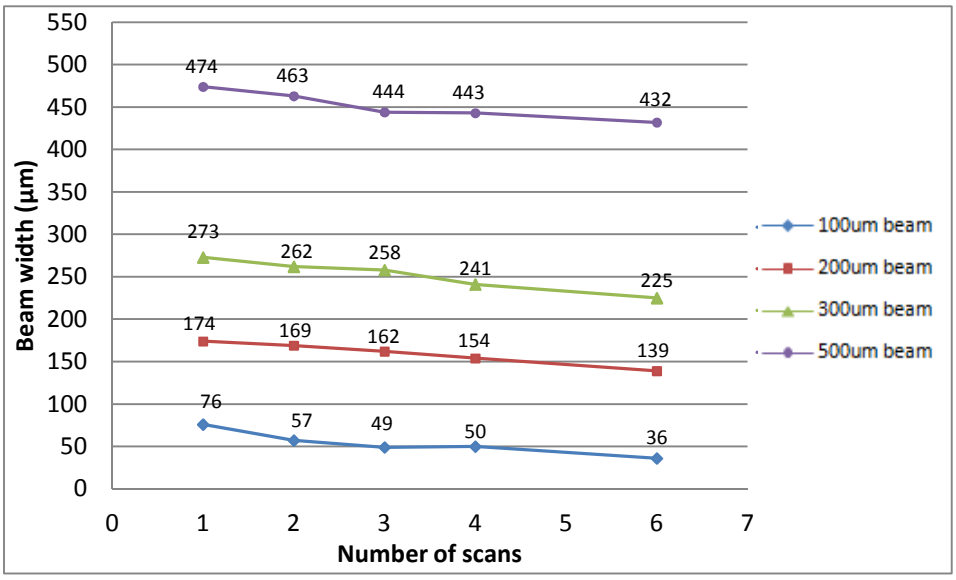

Figure 5.17: Width at the top surface of the beam depending on the number of scans

As expected, the walls of the powder blasted structures are gradually etched resulting in the width of the beam gradually decreasing as the number of scans increases. After the first scan, the beam has lost 25µm in width at its top surface. After 4 scans, about 45 to 55µm have been eroded.

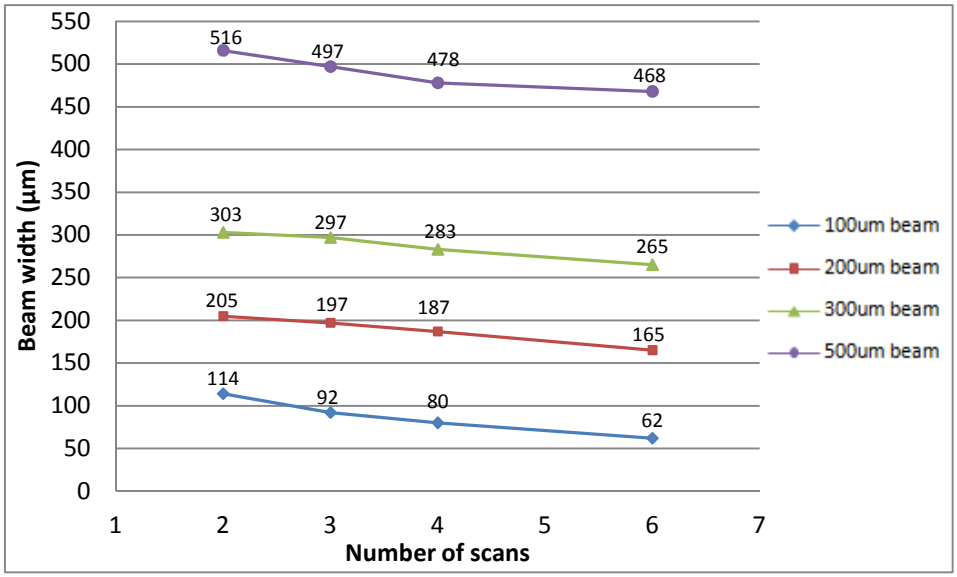

Figure 5.18: Width at the beam half thickness depending on the number of scans

On the other hand, at the half way section (Figure 5.18), the width of the beam only becomes smaller than the mask width after 3 scans. At this point, cross sections of the beams show that the walls are vertical enough and the process can be stopped. The four curves, which are parallel, show the good repeatability of the process regardless of the

beam size. Once the tape is pierced, the difference between the top and half way measurements is relatively steady and remains between 30 to 50µm.

The beam profile is obtained with a different mask featuring beam width/space of 200/200µm and 80/80µm. The mask was blasted with 3 and 4 scans with the resulting cross sections displayed in Figure 5.19. The beams have round top edges with nearly vertical walls. This round shape is accentuated in Figure 5.19 with the 80µm mask beam: the two sides of the beams almost joined together on the entry side.

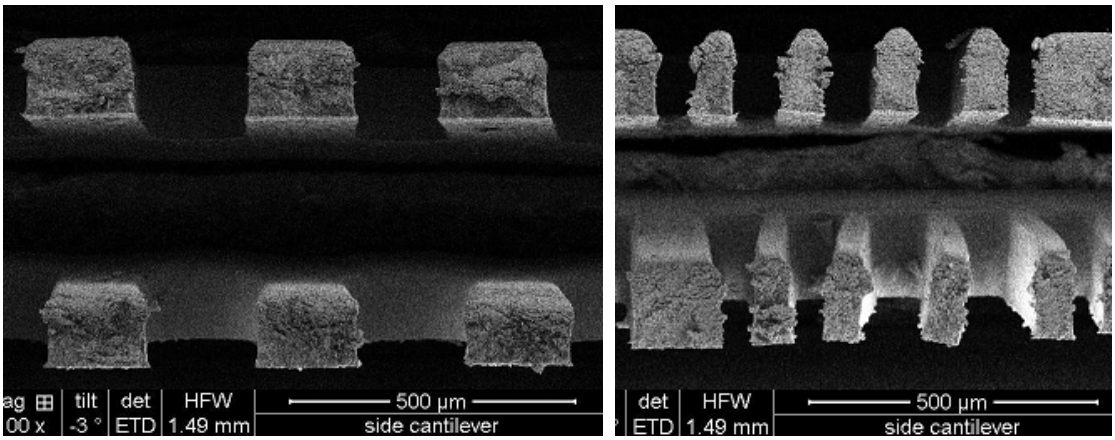

Figure 5.19: SEM cross section of powder blasted beams with 200µm and 80µm mask beam respectively spaced by 200µm and 80µm after 3 scans (top line) and 4 scans (bottom line)

Erosion at a distance nozzle-substrate of 50mm

Erosion rate vs aperture size: Table 5.6 summarises the depth measurement recorded after 2, 4 and 6 scans of powder blasted channels. The gradual erosion with a 200µm aperture/200µm pitch is shown in Figure 5.20.

Table 5.6: Depth etched in function of the apertures diameter after 1 and 2 scans

	Depth (µm)		
Aperture width	2 scans	4 scans	6 scans
80 (µm)	33	80	125
90 (µm)	45	100	150
200 (µm)	40	94	145
300 (µm)	40	96	151

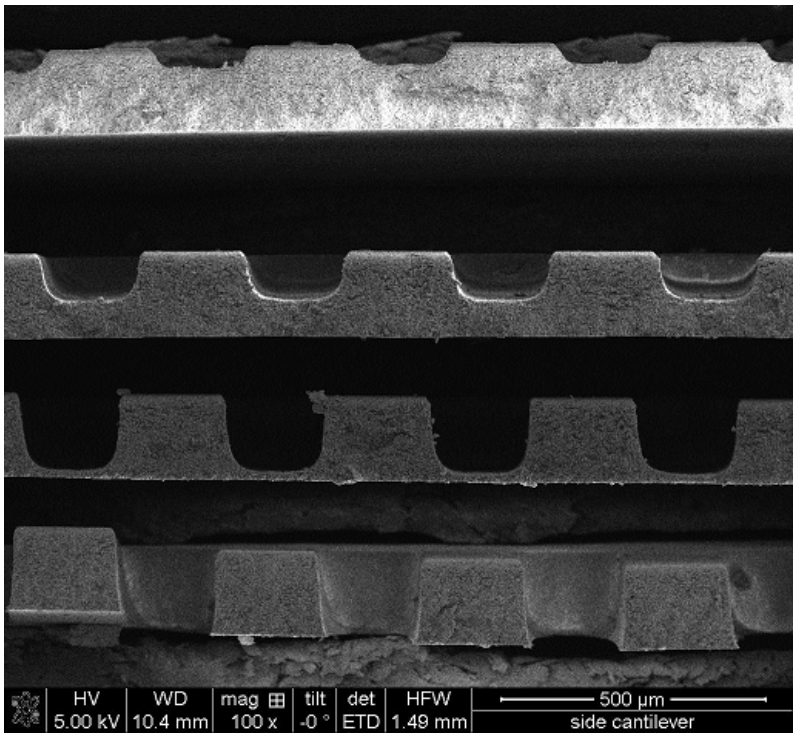

Figure 5.20: Set of cross sectioned 200µm beam powder blasted after 2, 4, 6 and 8 scans

This time, the erosion rate was found to be in agreement with the theory and showed that larger apertures enable the green tape to be submitted to a higher erosion than the smallest apertures. The threshold for which the erosion pattern is independent of the apertures is located around 90µm apertures.

Erosion behaviour: In general, the tape was pierced after 8 scans. Walls of the beams are almost vertical with a slight curved bottom end. However, for the smallest apertures,

12 scans are an absolute necessity to obtain vertical walls. The measurements of the beam top surface and half way thickness are presented in Figure 5.21 and 5.22. After 8 scans, the beam width stays within +10µm (for the top side) and -10 µm (half width) of the mask dimensions. Even after 14 scans, the top surface beam width is 30µm shorter than the mask beam while the half way measurements show similar dimensions compared with the mask. The dimensions at the top and half thickness of the beam evolve similarly with a difference between them of 20µm approximately.

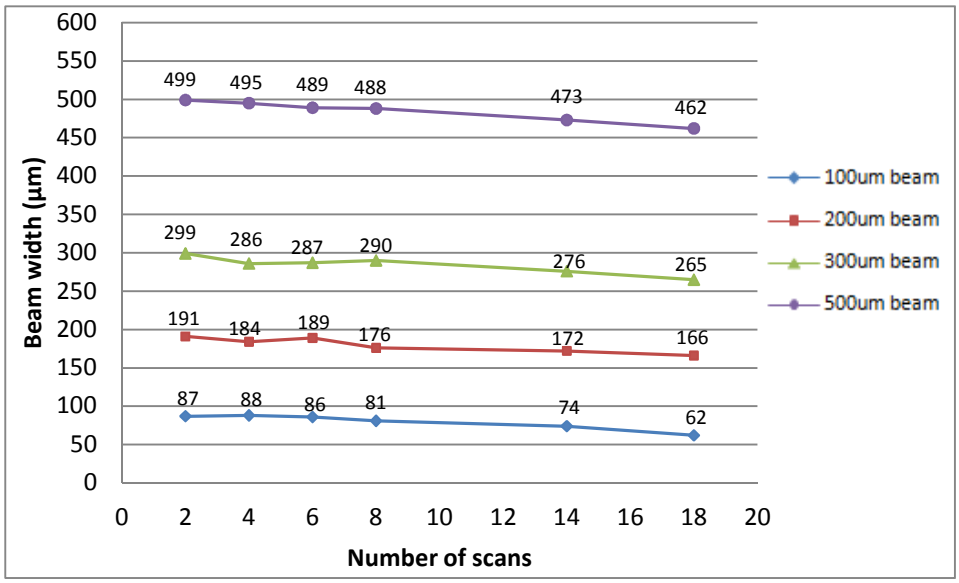

Figure 5.21: Variation of the width at the top surface of the beam depending on the number of scans

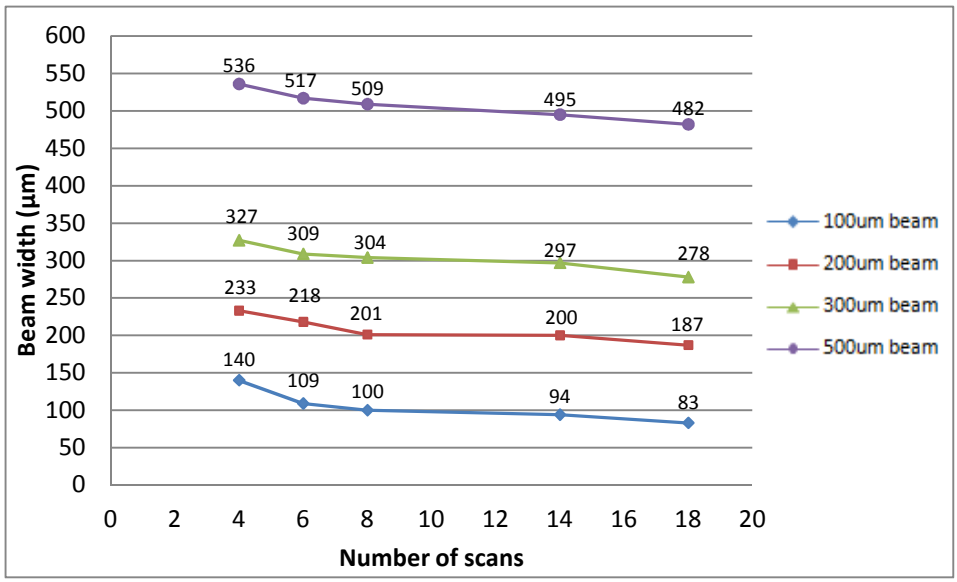

Figure 5.22: Variation of the width at the half thickness of the beam depending on the number of scans

Comparison between N-S=20mm and N-S=50mm

As mentioned for the circular apertures, the under etching at a distance N-S=50mm is smaller and results in sharper structures. Here the situation is similar, but thanks to the cross section of the beam, a more accurate analysis of the structures can be done. To better illustrate this, a direct comparison between cross sectioned beams powder blasted at N-S =20 and 50mm was carried out in Figure 5.23. These beams have been powder blasted with a similar mask and chosen so that they have the same width at the half way mark (197-187µm for N-S=20mm and 200µm for N-S=50mm). It can clearly be seen that the beam powder blasted at 20mm has a more pronounced rounded edge at the top surface than at 50mm. Measurements of the round edges show a radius of about 15 to 20µm at N-S=20mm while at 50mm, it is lower than 10µm.

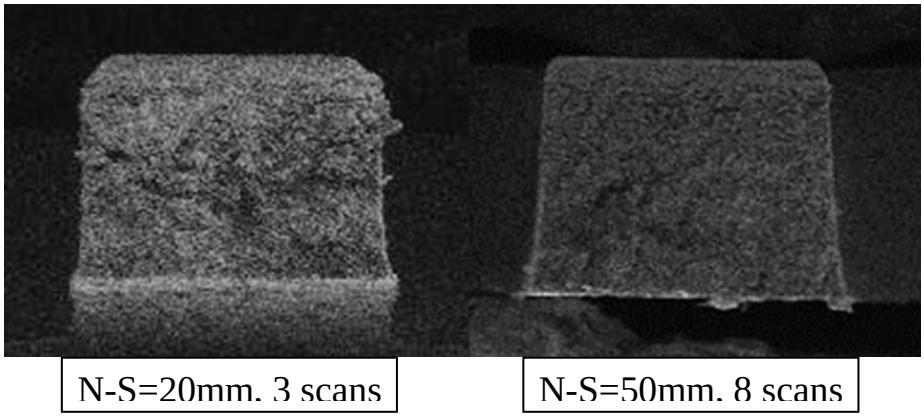

Figure 5.23: Cross section of two 200µm beam at N-S =20mm and 50mm after 3 and 8 scans, respectively

Smallest structures

The smallest beam size were achieved at a distance N-S=50mm and a thin 35µm mask (fabricated by Microstencil Ltd). Extra metallic clamps were used to maintain a very good contact onto the green tape. The mask had beam widths of 100, 80, 60 and 40µm spaced by 100µm. 10 scans were necessary to produce the beams shown in Figure 5.24. The 60µm mask beam produced beams with a top width of 23µm and bottom width of 54µm. Under etching is here in the similar range than the one found previously at N-S=50mm. A measure of the beam thicknesses also showed that the beams kept their original thickness and were not etched from the top. The beams produced in the green tape powder blasted with the 40µm beams were destroyed because of the under etching

which eroded the beam from top to bottom.

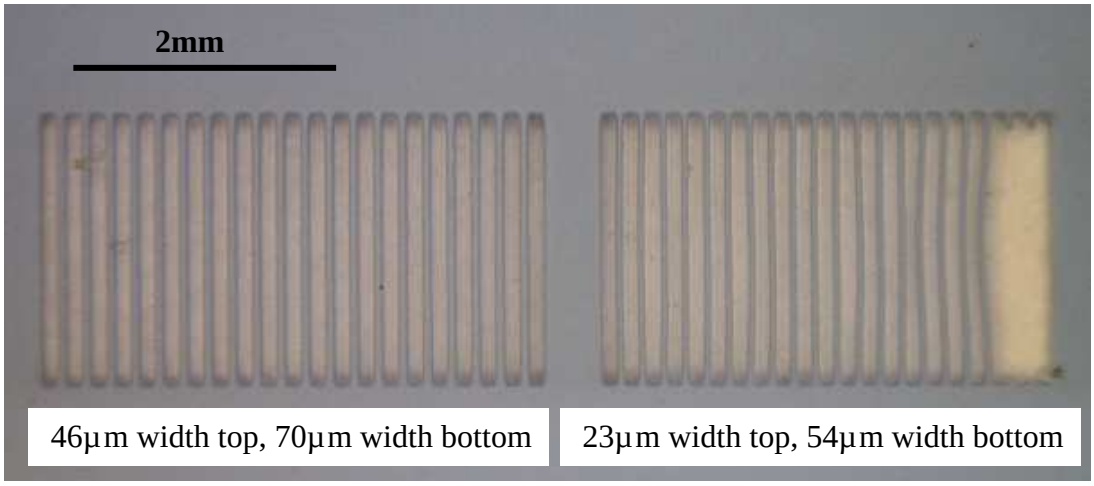

Figure 5.24: Top view of green tape beams powder blasted with 80 and 60µm beams at a distance nozzle-substrate of 50mm

5.3.4 Complex geometry

Powder blasting technique has been used to pattern more complex geometries in green tape ceramic. This was demonstrated with the successful patterning of sharp triangles or crosses. To achieve such structures, a nickel mask with cross and triangle shapes were used. Mask C has a total dimension of 55x35mm and has seven sets of crosses and triangles with different dimensions (Figure 5.25).

Figure 5.25: Nickel mask C featuring crosse and triangle shape

Sharp isosceles triangle 950µm height and a base of 300µm were successfully powder blasted at both N-S=20 and 4 scans (Figure 5.26b) and N-S=50mm and 12 scans (Figure 5.26c). Metallic clamps were used. The sharper shapes obtained at N-S=50mm are clearly visible: there is less under etching on the top edges, and corners are less round than at N-S=20mm. There is a lower erosion rate at the corners of the triangles, which result in the wall having a less vertical slope angle as emphasized by the darker shaded area. This is caused by an increase in the particle collisions inside the tighter space in the corner. Not surprisingly, the smaller angle of the triangle (17°) has the lowest erosion rate.

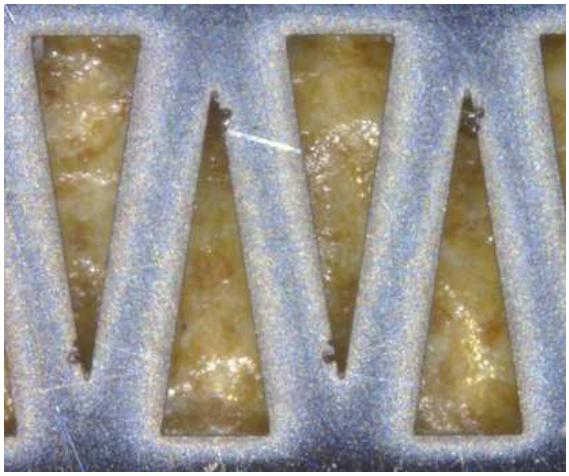

(a)

(b) (c)

Figure 5.26: (a) photograph of the mask back side featuring isosceles triangle with a height of ~960µm and a base of 300µm powder blasted at N-S=50mm. Resulting green tape at (b) N-S=20mm and (c) N-S=50mm.

Complex cross shapes also can easily be powder blasted. Figure 5.27 shows the result of powder blasted crosses in LTCC. The entire structure length is 900µm across and is composed of two central beams of 100µm width with four 200x200µm squares attached at each end. Once again, a better and shaper definition of the structures can be seen at N-S=50mm.

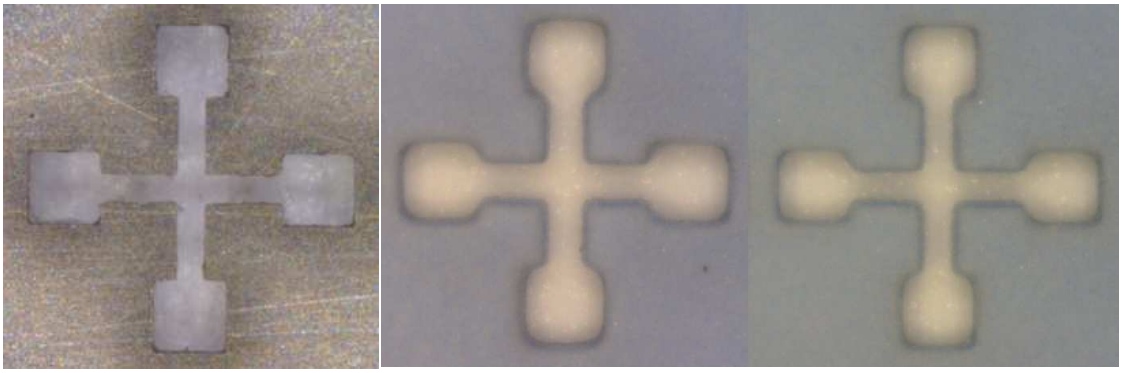

(a) (b) (c)

Figure 5.27: Assemblage of photo of (a) back side mask powder blasted at N-S=20mm of 900µm tall cross and the resulting pattern in LTCC at N-S=20mm (b) and N-S=50mm (c)

Stand alone structures: Standalone structures are relatively easy to fabricate. Nickel foil can be electroplated or laser cut to form independent complex shapes that can be used as a mask. No additional clamping force other than the magnetic field of the magnet can be used. Thus, a mask with a thickness of at least 100µm can only be used safely at a distance N-S of 50mm. Such masks shaped as simple wheels or as a cog wheel were easily fabricated and powder blasted. In addition, no protective coating was needed as the metallic surface under stress was small and compact enough to counter the peening effect. Figure 5.28 shows the powder blasted nickel masks and the powder blasted results in LTCC. Both simple wheel and cog wheel were imaged by an SEM microscope. The simple wheel was rastered at a speed of 5mm/s and pitch of 1mm. The small cog wheel, on the other end, had a diameter of 4mm, so it was machined in static mode (diameter of the machinable area at N-S=50mm: ~6mm).

Nickel mask

LTCC

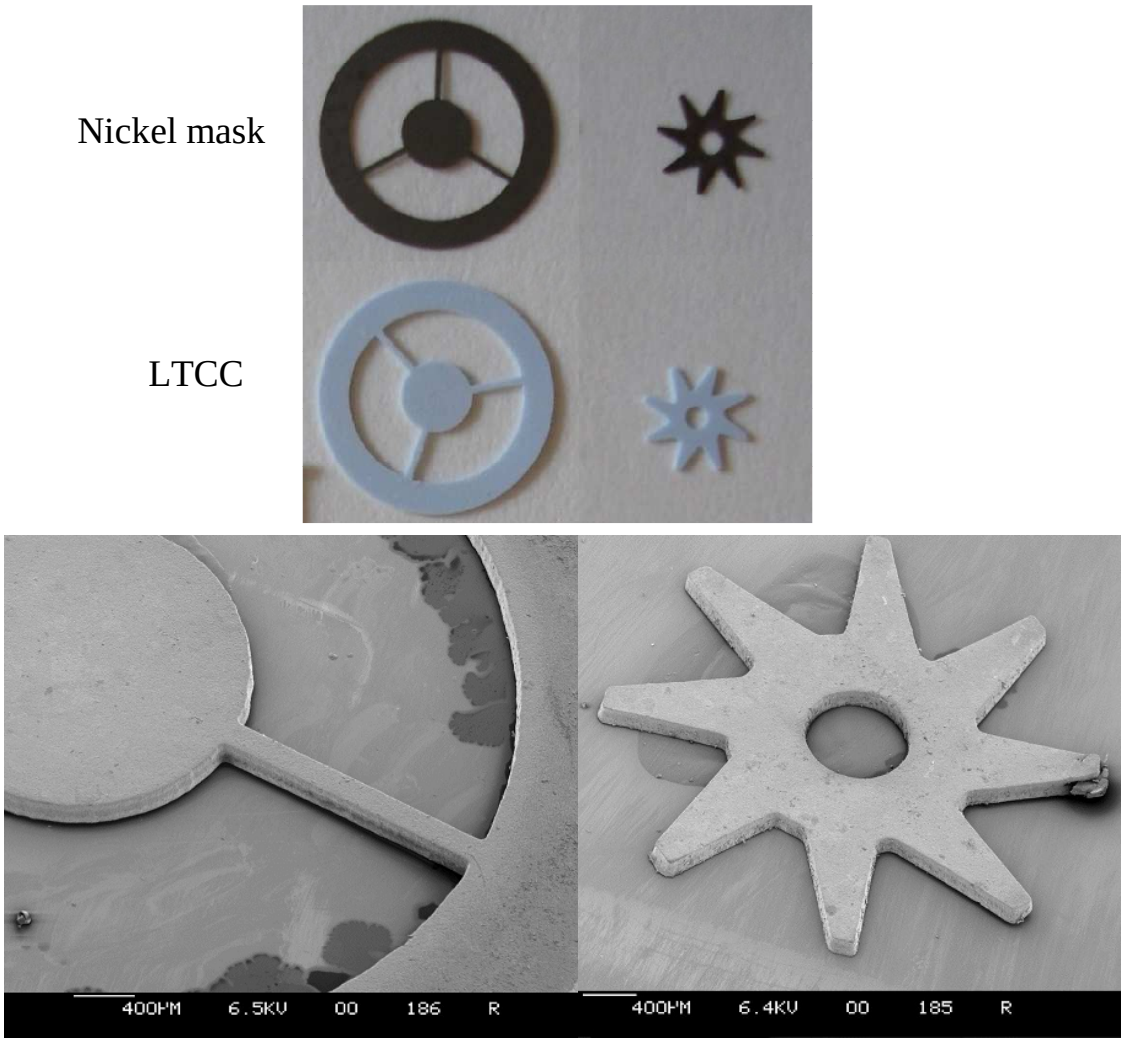

Figure 5.28: Cog wheel and simple wheel machined at 60 psi and 50mm N-S

Pattern arrays: Powder blasting is a very efficient process to pattern large arrays at once thanks to the large machinable area (15mm^2 at N-S=20mm and 78mm^2 at N-S=50mm). However, cautions should be taken due to the energy distribution of the particle and pitches of 1mm should be used in order to have uniform erosion over the entire mask. This uniform erosion is evidenced in Figure 5.29a&b which shows SEM photos of arrays of vias 200µm diameter and 100µm diameter both spaced by 100µm. The blasting was done at N-S=50mm. The erosion profile of the structures is similar to the ones described in 5.3.2 with similar under etching and dimensions obtained. As clearly shown, the shape uniformity is very good.

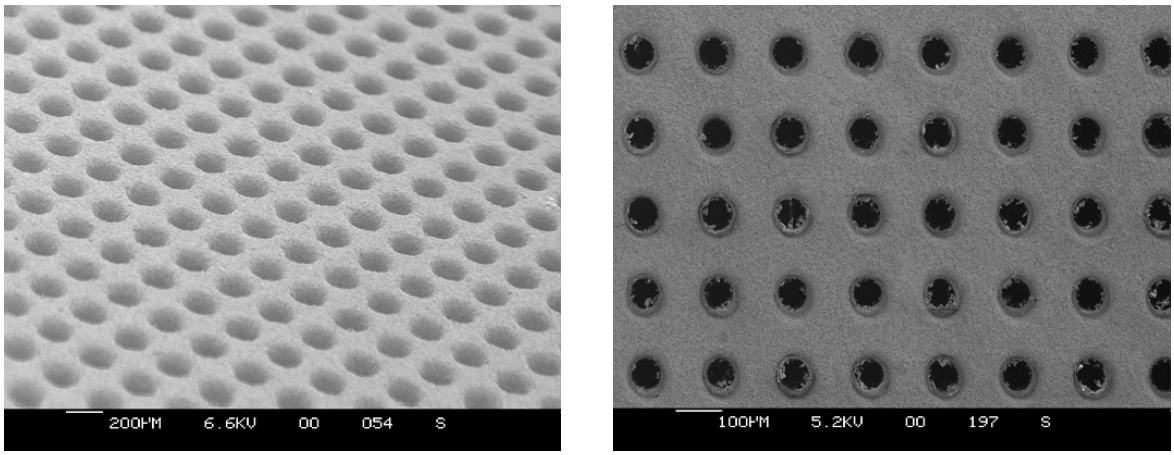

(a) (b)

Figure 5.29: Array of vias (a) 200µm in diameter and (b) 100µm in diameter powder blasted at 50psi and 50mm N-S. Also in (b),debris seen in the vias are alumina particles hanging on the back side of the tape

5.3.5 3D patterning

One of the advantages of powder blasting is the ability of the process to blast the substrate at a certain angle to create 3D structures. The nozzles can be inclined to force the particles to impact the green tape ceramic with a defined angle. Detailed investigations on this process on glass can be found here [125, 126] and fabrication of specific structures such as free standing cantilevers can be found here [10, 11]. These materials were thick enough and structures such as cantilevers could be created. The thin thickness of the ceramic tape would, however, limit the interest of this technology for such structures.

Vias

In this thesis, the study of the erosion on the green tape structures at different angles of impact was studied and restricted between 20º and 50º. This range limitation comes from two reasons. At an incidence closer to the normal (60º to 90°), the low inclination achieves limited structural changes in the slope of the walls. This is emphasized by the thin thickness of the tape. Conversely, at angles lower than 20°, the area machined is extremely large, rendering difficult the powder blasting of single structures. Moreover, perspectives of the aperture dimension at such low angle changes considerably. Indeed, with a 50µm thick mask, 200µm circular apertures resemble an oval 60x200µm aperture

at 20º. At 10º, 300µm apertures look barely opened.

The process was carried out at N-S=20mm with the pitch set according to the angle of inclination. This enables to reduce the erosion rate depending on the angle (the lower the inclination is, the larger the area as illustrated in Figure 5.30) and approaches it to the erosion rate obtained at normal incidence. In practice, however, the shape of the jet combined with the decreasing apertures opening dimension (different perspectives at lower angle) make this task difficult. In addition, as mentioned in Chapter 3, the erosion rate of the green tape increases when the angle of erosion of the particles decreases. In a general approximation, the pitch will be set at 1mm at 50º and 40º, 2mm at 30º and 3mm for 20º.

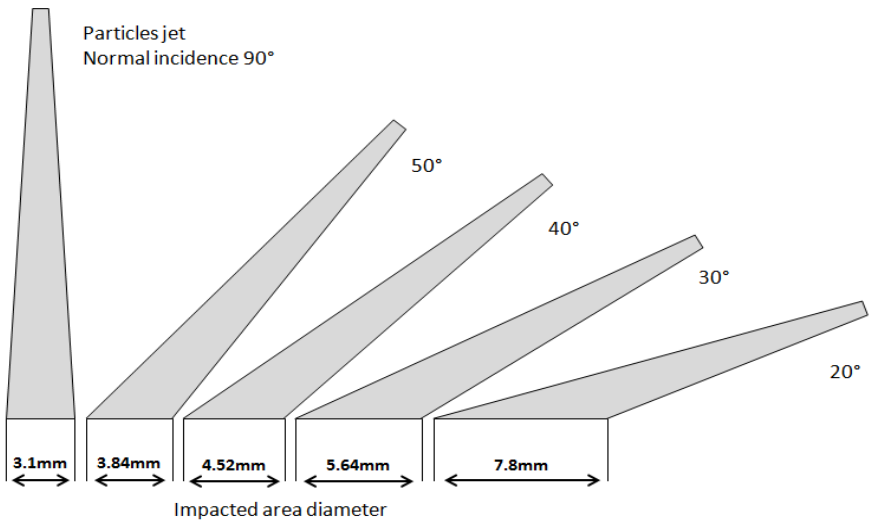

Figure 5.30: Diagram describing the evolution of the surface of the area submitted to the particle's jet according to the jet inclination. The distance N-S is 20mm

Typical erosion shape: The typical erosion behaviour by angled particles on the green tape is first described at a nozzle incident angle of 30º. The apertures used were circular with a diameter of 300µm. The numbers of scans per series were set as follows: 1, 2, 3, 4 and 5 scans. The masks were electroplated to a thickness of 40µm and knife coating technique was used to lay a protective layer of LF55gn 30 to 40µm thick. Additional metallic clamps were placed on the mask. The transverse vias fabricated in the tape were measured with an optical microscope.

Typical via entry and exit shapes are shown in Figure 5.31a. The graph in Figure 5.31b plots the evolution of the entry and exit diameters powder blasted with the 300µm aperture in function of the number of scans. The diameters of the vias on two directions were measured: parallel to the particles direction (labelled x) and perpendicularly to the particles direction (labelled y).

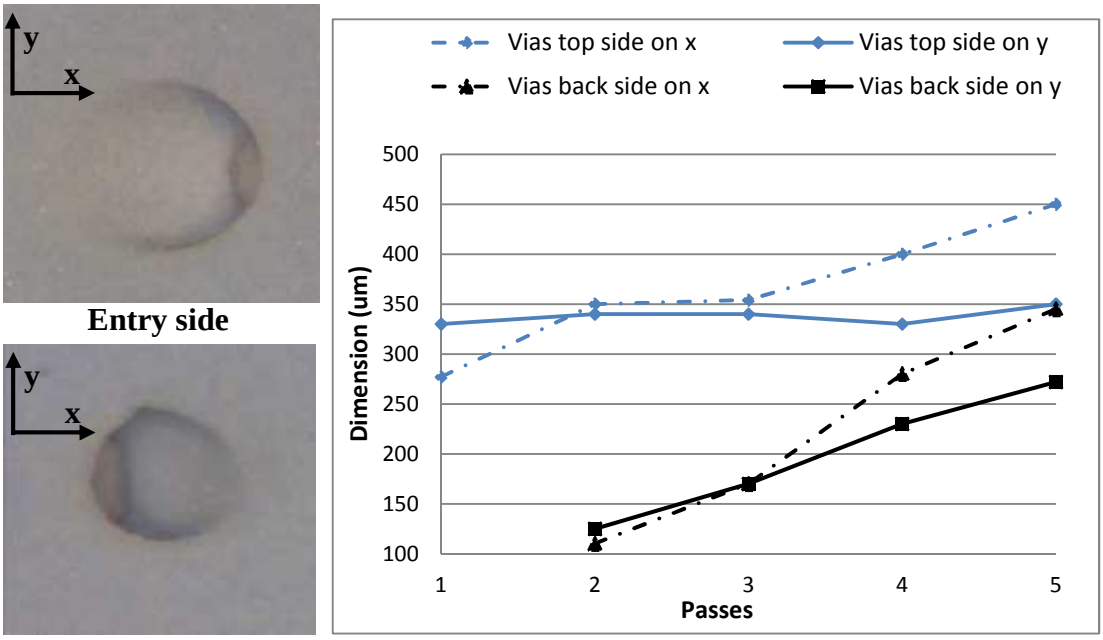

(a) (b)

Figure 5.31: (a) Typical entry and exit side of transverse vias fabricated after 4 passes with a 300µm aperture. (b) Graph of the entry and exit dimension of powder blasted vias with the same mask after 1, 2, 3, 4 and 5 scans

The tape was pierced after only two scans but the exit sides are small (~100µm). Four scans are needed to pierce the tape and obtain exit side dimension equivalent to the mask apertures (~250µm). However, the entry side also increased with the diameter parallel to the particles direction reaching ~400µm. On the other hand, the diameter along the y axis stayed steady at around 330µm, which transformed the entry into an oval shape. Although powder blasted with a circular aperture, this oval shape is due to the perspective at 30º and the under etching occurring under the aperture side facing or opposing the particles. Under etching was also enhanced by the mask lift off as air can penetrate more easily under the mask. Conversely, the diameter measured along the y-direction is not submitted to this type of under etching as it would require the particles to turn 90º, but is rather submitted to the under etching described in section 5.3.2. The

oval shape is gradually reached by the exit side as the entry side changes.

Cross sections of the transverse vias powder blasted in Figure 5.31 are showed in Figure 5.32. The transverse vias walls, or channel walls, become parallel after 3 to 4 scans. The channels are gradually etched as it was the case for the vias at the normal incidence. Due to the variation of perspective of the apertures compares to the normal incidence, 300µm circular apertures produce a channel width of 110µm after 3 scans and 150µm after 4 scans on x and about 330-340µm on y.

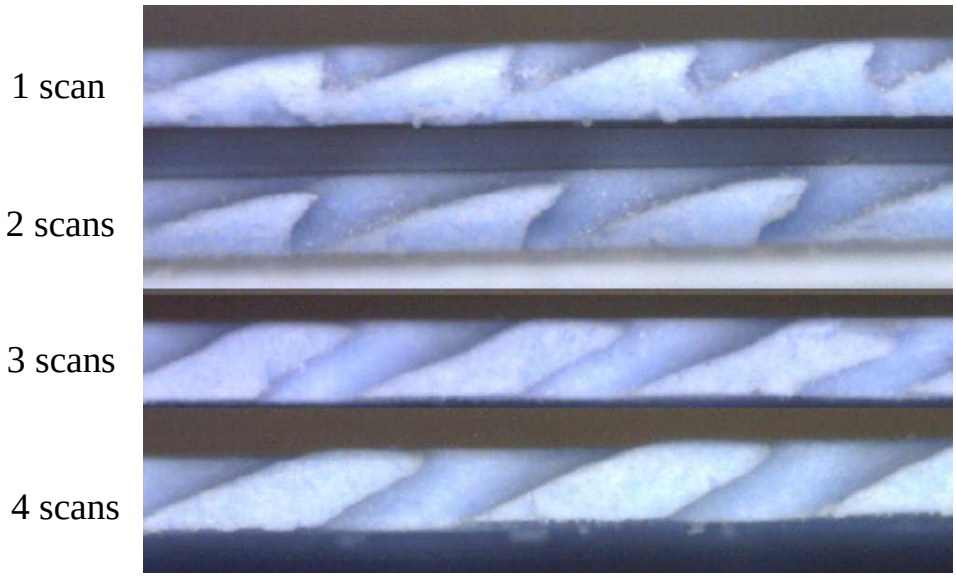

Figure 5.32: Cross section of vias powder blasted with an incident angle of 30° after 1, 2, 3 and 4 scans. Different mask were used with similar apertures diameter (300µm) but different spacing

Aperture size limit: The process was repeated for circular aperture size ranging from 500µm to 200µm at incident angle varying between 20° and 50°. The mask employed has a thickness of 75µm and had additional clamps. Channel widths obtained after 4 scans were measured and displayed in Figure 5.33. Channels were all pierced successfully with inclination ranging from 50° to 30° except at 30° and the 200µm aperture. As mentioned earlier in this section, the change in perspective introduced by the particle inclination reduces the openings of the apertures. Thus, at 20°, no apertures were pierced. As expected, the channel width decreases as the incidence angle decreases. The smallest channels were fabricated with a 200µm aperture at an incident angle of 40°. They had a width of around 125µm.

The measurement of the entry of these channels showed that the oval shape found at 30º on was lower for the angle of impact 50º and 40º. The difference between the diameter measured in x and y was only about 10 to 20µm. At 30°, the difference reached 50 to 60µm. This is mainly due to the higher under etching and the mask lift off at lower angle.

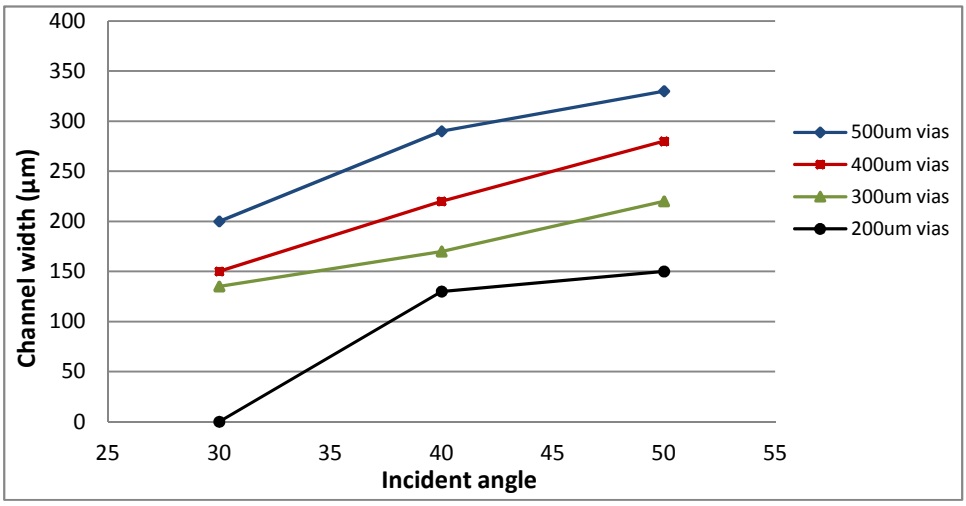

Figure 5.33: Channel width powder blasted at different incident angles and different apertures size

Channels

Channels can also be fabricated at an incident angle using rectangular beams, or blades. Such structures were powder blasted at 45º and 30º using a thin nickel mask (20µm thick + additional metallic clamps). The distance N-S was set at 50mm to limit the impact of the air flow on the mask, as those tests were done at ~80psi. Figure 5.34 illustrates some examples of 3D structures fabricated with different mask apertures in a single layer of green tape ceramic. Successful blades powder blasted with 100µm and 150µm mask beams were achieved with the following respective beam width dimensions: 70µm top/160µm bottom (a) and 110µm top/250µm bottom (b). However, beams smaller than 50µm could not produce structures with good quality. Blades fabricated with these masks had their top surface highly under etched (c). Similar under etching also happens when the incident angles is very low. Interesting results are shown in (d) of very thin blades over exposed at an incident angle of 30° with 100µm mask beam. However, low incident angle can be used in combination with larger apertures to create a single sloped wall as shown in (e).

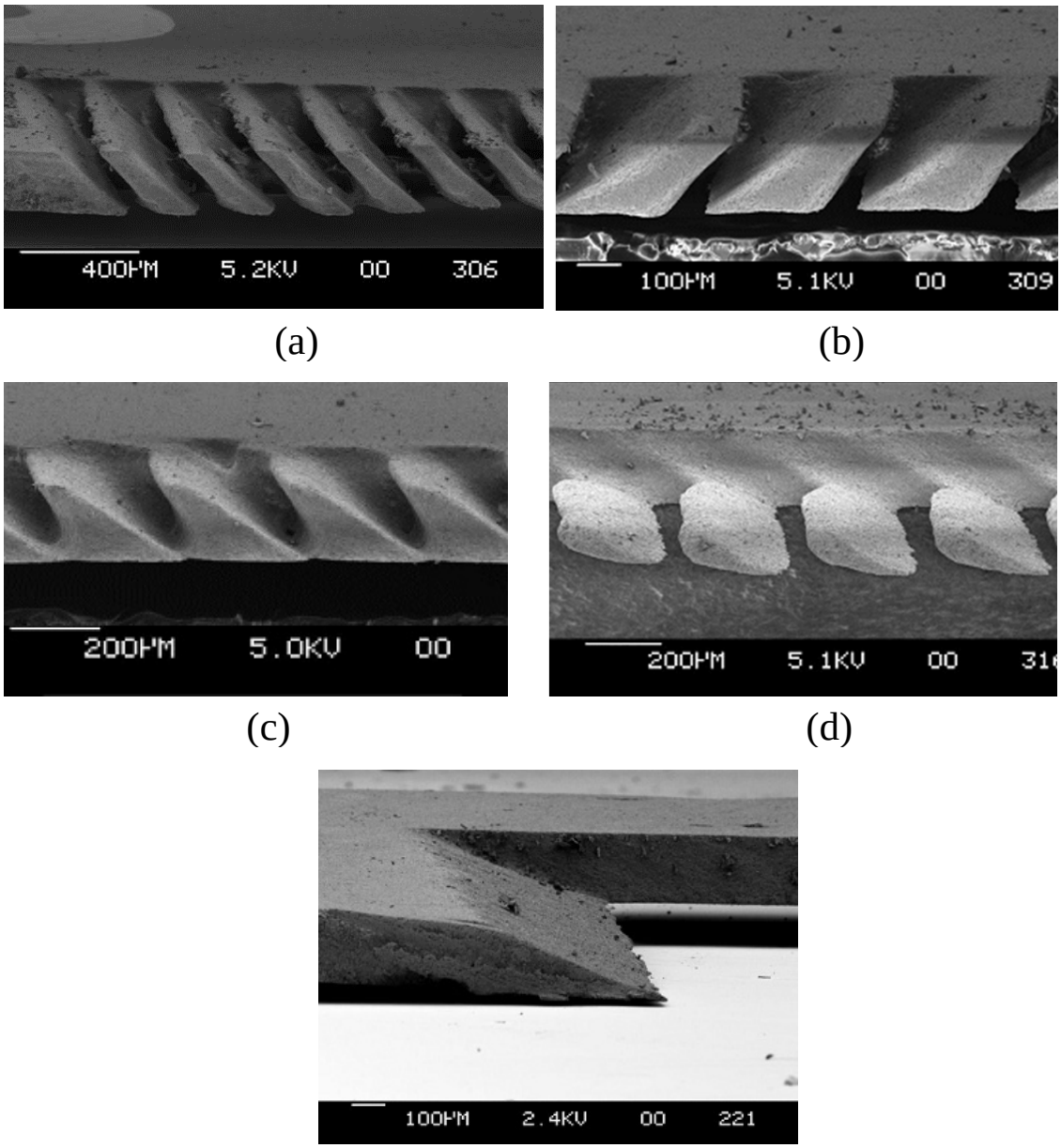

Figure 5.34: Beam cross section powder blasted at: (a) 45º with 100µm mask beam/200µm openings; (b) 45º with 150µm beam/200µmopening; (c) 45º, with 50µm mask beam/200µm opening; (d) 30º, 100µm beam and 300µm opening; (e) Single slope blasted at 30º

As confirmed by these SEM photos, the substrate erosion is limited to the direction parallel to the particles direction. The side walls of the structures adjacent to the slopes are flat and sharp as they would be if powder blasted at a normal angle. In addition, it is clear that the slopes fabricated have the same inclination as the particles with which

they have been powder blasted. Due to the higher force of the jet of particles, metallic clamps had to be used. However, this could not prevent the lift-off in the vicinity of the mask apertures. Furthermore, because of the jet angle, it is difficult to place these clamp closer as their thickness can obstruct the particles path.

5.4 Conclusion

A characterisation of the fabrication of microstructures using powder blasting process on green tape ceramic has successfully been done. The DuPont P2 tape 165µm thick was easily pierced at distance nozzle-substrate of 20mm and 50mm. Vias, channels and complex structures such as crosses and wheels can be realised. The typical U shape is present and can be suppressed by increasing the exposure of the substrate to the particles. The resulting structures are smooth with no melted edges. Debris such as particles can be easily cleaned and no PET foil residues were found in the apertures.

Powder blasting enables high fidelity between the pattern of the mask and the structures. Almost vertical walls can be achieved, conferring the structure uniform dimensions between the entry side and the exit side. This can be obtained with this setup after 3 to 4 scans at N-S=20mm and 8 to 12 scans at N-S=50mm. However, because of the under etching, the structures are larger than the patterns with which they have been fabricated. Under etching is larger at N-S=20mm because of the higher power of the particles and is around 30-40µm. But it can be reduced by increasing the distance N-S to 50mm at which its value diminishes to 10-20µm. Under etching is constant, allowing patterns reverse engineering to compensate for its effects.

It has been shown that this technique can produce small patterns. The smallest vias achievable with this technique had a diameter of 62µm for the entry side and 20µm for the exit side. Similarly, the smallest beam had a diameter of 23µm for the entry side and 54µm for the exit side. The process excels in the fabrication of large area where hundreds of structures can be fabricated at once thanks to the large jet of powder. However, the fabrication of fewer structures spread over a large area can considerably increase the processing time and also waste more powder material.

Chapter 6 Fabrication of a LTCC package for an opto-electronic device using powder blasting

6.1 Introduction

The optical encoder to be packaged using LTCC technology belongs to Renishaw Plc. Following a design created by Dr John P. Carr [127], the prototype is an improved version of the commercial encoder illustrated in Figure 6.1. In this sample, the photo detector chip of overall dimension of 4 x 3.5 x 0.5mm is placed underneath the analyser grating and wire bonded onto a PCB board. A LED, not seen in the picture and serving as a light source, lies behind the reference and index gratings. The circuit is then packaged with the rest of the electronics inside a metallic case.

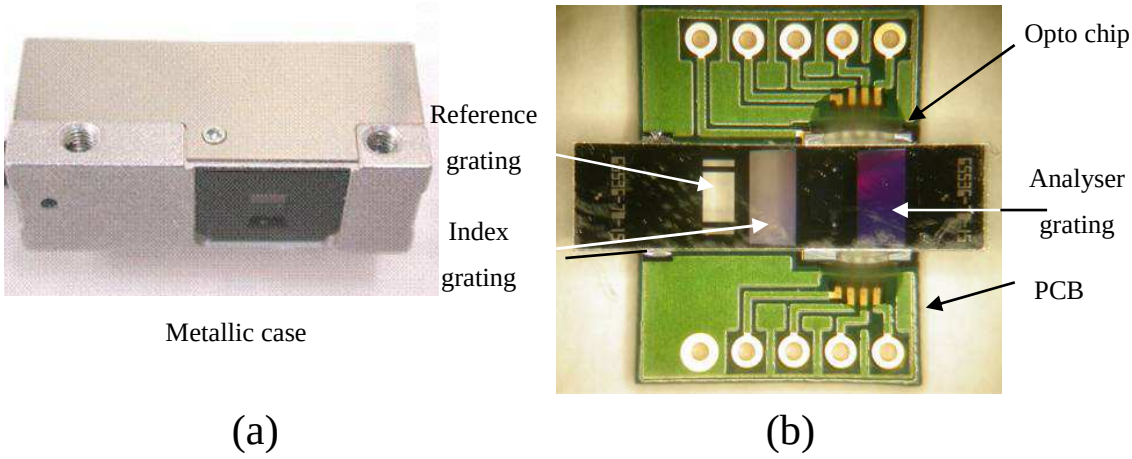

Figure 6.1: Photograph of the encoder with its package (courtesy of Renishaw)

The purpose of this chapter is to demonstrate that powder blasting can be used with LTCC as a packaging technology for the encoder. New process conditions such as longer exposure time, larger areas to pattern and extra tape handling, which were not encountered during the green tape characterisation described in Chapter 5, are addressed here.

In this Chapter, a quick overview of optical encoder technology is carried out alongside a description of the new encoder design. Secondly, the package features are detailed, which include the cavities and vias dimensions, the routing of the conductive tracks and number of layers needed. Finally the fabrication of the package and its testing are described.

6.2 Optical encoder characteristics

6.2.1 Overview

Principle

Optical encoders are transducers that convert a mechanical position into an electrical signal thanks to a linear scale (linear displacement) or a disc (angular displacement). If light interferometry is used, the encoder comprises a light source, a gratings system and a photodetector. The transduction principle is illustrated in Figure 6.2: a light source illuminates a scale grating fixed onto the system whose position is to be measured through a periodic patterned scale (index grating) made of transparent and opaque lines. The superposition of the index and the scale grating creates Moiré fringes patterns in the light. The variations of the light intensity are recorded by the photo-detectors placed opposite to the light source (transmission mode) or on the same side (reflection mode). The intensity variations are converted by electronics into readable/ square waveform.

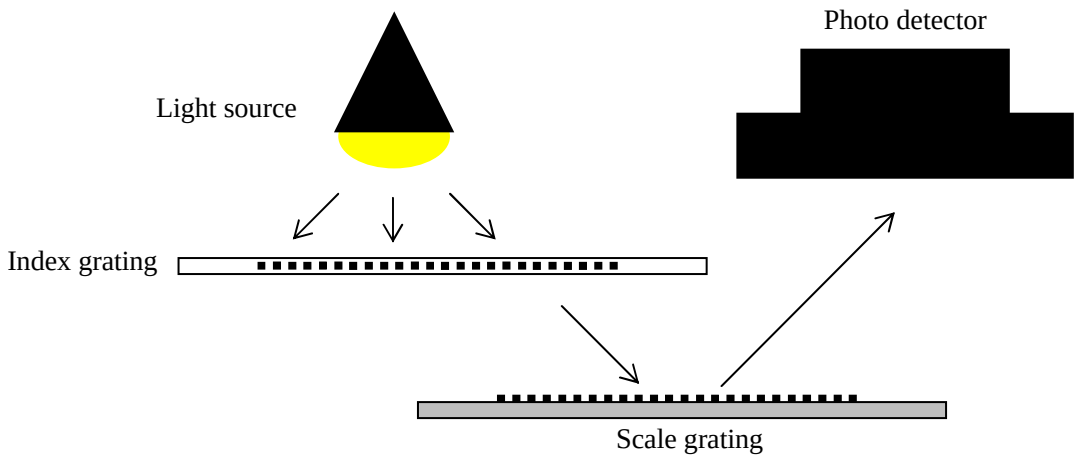

Figure 6.2: Optical encoder principle operating in reflection mode

Two different techniques can be used to measure displacement: incremental encoding and absolute encoding. The former measures the relative displacement from a single track of evenly spaced opaque and transmissive or reflective gradations. The displacement is known by counting the pulses generated by the photodetected light. These types of scale are simple and thus easy to fabricate. However, as the gradations on the scale grating are identical, there are no indications on the precise location the measurement started. A reference marker is needed to identify a starting point or known location. Absolute encoders provide such absolute positioning thanks to a complex

patterning of the scale. Several photo-detectors have to be used, each one designated to record a specific pattern on the scale at the cost of a more complicated system integration. Such encoders do not require however reference marker and do not lose position location during power failure or misreading.

Renishaw encoder

Renishaw optical encoder is an incremental encoder using reflective scales. It is based on a slightly more complex grating system than the one presented above in the sense that an additional grating (analyser grating) is placed in front of the photo detectors as showed in Figure 6.3. The index and scale gratings have the same gradation pattern. The analyser grating has a different pitch than the other two gratings. The analyser converts these fringes into light modulation and, coupled to a photo-detector with a specific array structure, generates four phase shifted cyclically electrical signals combined in quadrature fashion. These phase-shifted signals have the advantages of increasing the signal amplitude and cancelling out common mode noise.

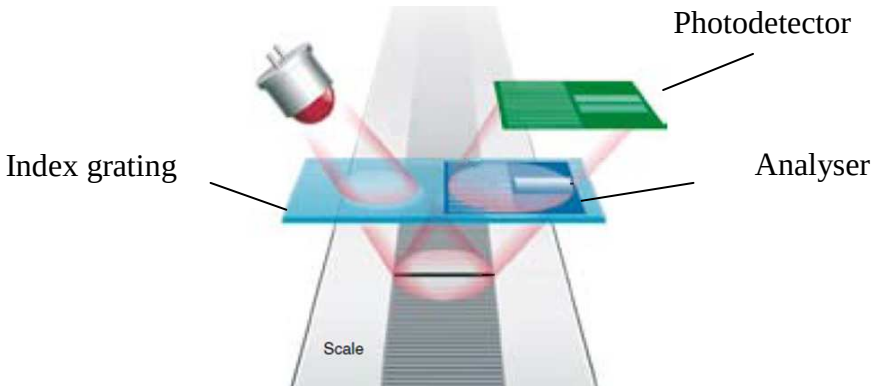

Figure 6.3: Three grating system used in the Renishaw optical encoder (courtesy of Renishaw)

The LED, photo-detector and gratings are assembled with some electronics processing on PCB boards mounted inside a rectangular metallic case. A window is inserted in the case to enable reading of the scale graduation. The overall assembly is called readhead.

6.2.2 Optical encoder prototype

Fabrication

The optical encoder chip replacing the original encoder is based on an InP substrate on which the LED, optical gratings and photo detectors are monolithically integrated. This method of fabrication reduces the cost and size of the device, and enables rapid and precise alignment of the grating with the LED and the photodiodes, a critical step for the detection of the fringes. The schematic of the surface emitting chip can be seen in Figure 6.4. The structure is deposited on the substrate using metal organic phase vapour epitaxy (MOPVE) technique. A more detailed fabrication process can be found in [127]. Index and analyser gratings are added later directly on the top of the LED and photo detector arrays by standard lithographic processes. The chip is fabricated at Compound Semiconductor Technologies Ltd (CST), Hamilton, Scotland.

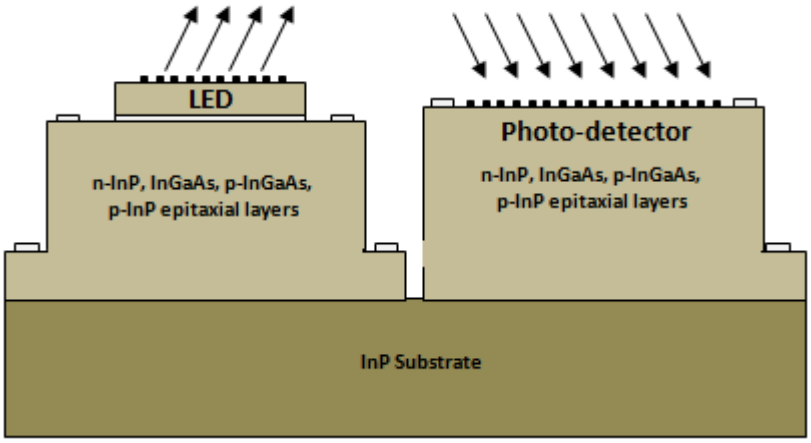

Figure 6.4: Monolithically integrated surface emitting chip (courtesy of Renishaw)

Chip layout

The chip layout, seen in Figure 6.5, is symmetrical. Five LEDs, lined up in the middle, split in half the chip layout. On each side lie two arrays of incremental photo-detectors. Each array is composed of diagonal photo-detectors lines, each one detecting one of the four phase shifted signals (0º, 90º, 180º and 270º). Reference markers are placed along two of the chip edges parallel to the LEDs while gold bond pads are located on the two remaining edges (perpendicular to the LEDs). The overall layout fits on a rectangular InP substrate of dimension 3.2x2.9x0.53mm. There are 16 chips outputs, but due to the chip layout symmetry, some contacts are doublets. These contacts are shown in Figure 6.5 and are labelled as follow: four doublets channels A, B, C and D corresponding to

the 4 phase shifted signals, one doublets ground Gnd, two doublets reference marker Ref I/O (input/output) and the LED power supply.

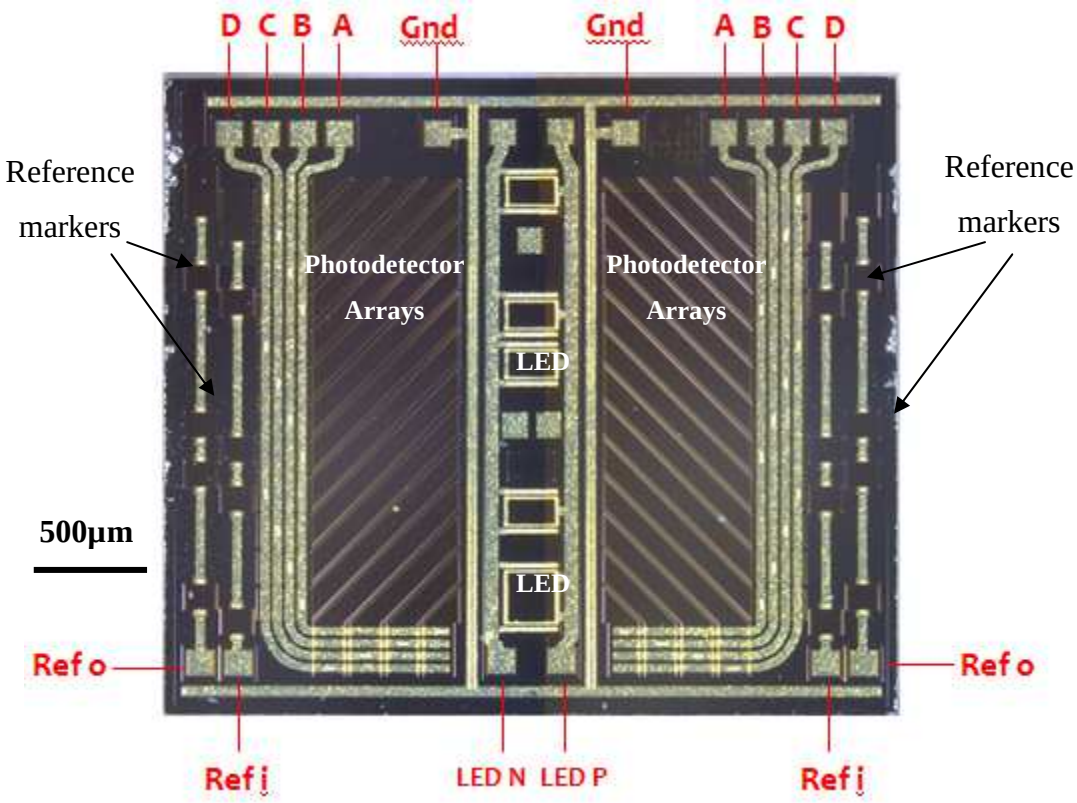

Figure 6.5: Top view photograph of the optical encoder layout

Glass window

The chip has been designed to be attached face down to a glass window: the bonding pads are on the same side as the encoder components. The window ensures the protection of the chip against the external environment. A bonded chip onto its glass substrate can be seen in Figure 6.6. The glass is a borosilicate glass with dimensions of 6.5x6x0.5mm. Ti/Au tacks were deposited by physical vapour deposition (PVD) to ensure the chip attachment and redistribution of the interconnects to the glass edges. Chip to glass bonding is done using is thermo-compression: heat and pressure are applied simultaneously to create atomic diffusions between two metallic surfaces. Twenty micron gold bumps electroplated on the glass side were utilised. The chips were bonded at Heriot-Watt University at 300ºC with a bonding force ranging from 35 to 45g per pad.

The glass is meant to be flip chip bonded onto the LTCC substrate. Flip chip bonding

reduces the circuit footprint, cost and improves reliability. Furthermore, it is the only viable option as the bonding pads of both glass and LTCC must face each other. The pads at the end of the gold tracks are large with a circular dimension of 500µm in diameter with a spacing of 1mm. Two extra pads with no connection to the chip are present to increase the strength and stability of the bond between the glass and the LTCC package.

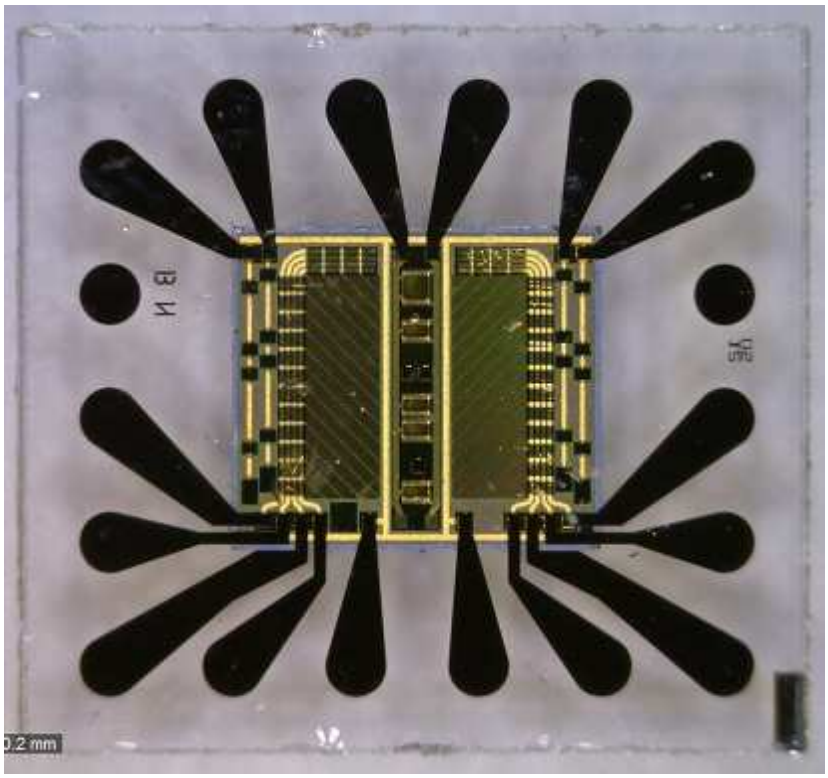

Figure 6.6: Photograph of an encoder chip flip chip bonded onto the glass window. The glass is on top, the encoder LED and photodiode are seen through the glass

6.3 LTCC Package

The package to be fabricated has to house the glass window on which the chip is bonded and a flexible connector which connects the chip to the external electronics. The connector is a 10-way connector FH19C-10S-0.5SH connector (Figure 6.7) fabricated by Hirose and has overall dimensions of 7 x 3.5 x 0.9mm. In order to reduce the circuit foot print and allow access to the 10-way connector while the LTCC package is attached to its metallic case, the connector and the glass window are placed on opposite side on the package. Thanks to the 3D circuitry capability of the LTCC, the electrical connection between the chip on the glass and the flexible connector takes place inside

the package. Furthermore, the doublets present on the chip will also be joined inside the package. This enables the reduction of the circuit footprint compare to PCB. LTCC also offers a better CTE match with the glass window. Therefore, dimensions of the LTCC package are directly dependant on the dimensions of these two components and the internal circuitry.

6.3.1 Package shape

The design retained for the package is illustrated in Figure 6.7a with a cross section of the package in Figure 6.7b.

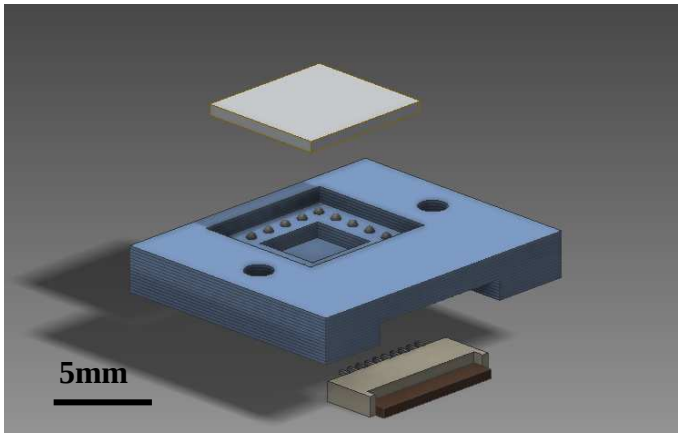

(a)

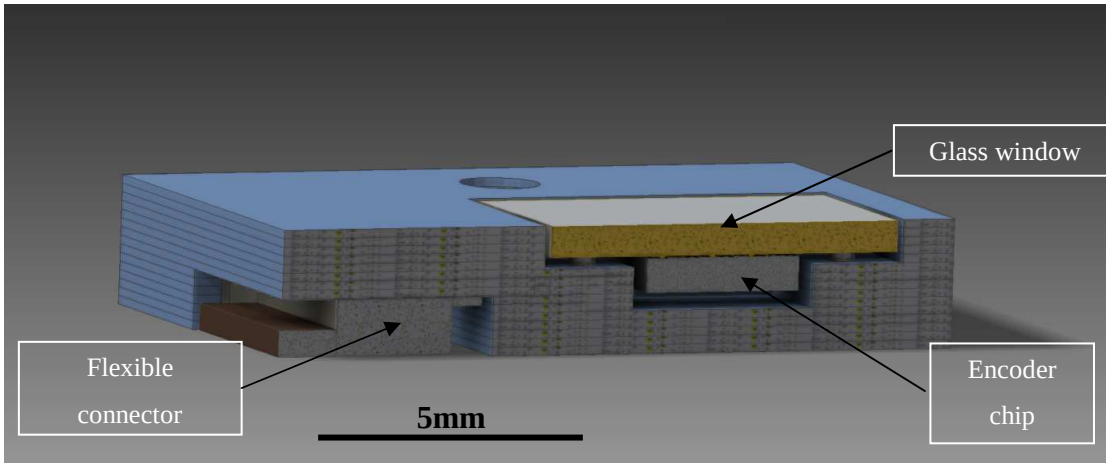

(b)

Figure 6.7: (a) Final fired package with glass and flexible connectors. (b) Package cross-section with the glass window, chip and the flexible connector mounted inside their respective cavity

The glass seats on top of the package surrounded by LTCC. Underneath, the chip is embedded into a smaller cavity. The flexible connector is placed at the back of the

package opened in the opposite side compared with the other two cavities. The flexible connector is mounted upside down with the contact pads facing the LTCC back side. The dimensions of the final package are 14 x 11.6mm and a thickness of 2.24mm. In addition to the insertion of the glass and flexible connector, two screw holes will be pierced on each side of the package to attach it to its metallic case

The package can be broken down into three separate parts. Dimensions of each cavity are given after shrinkage and with a 0.2mm margin aimed at ensuring the cavities are large enough to fit the components.

Glass cavity

This part simply consists of a cavity to house the glass window. The glass dimensions being 6.5x6mm, the cavity's dimensions are 6.7x6.2mm. The number of layer composing this cavity is dependent on the glass thickness (0.5mm) but also on the bump height that will be used to bond the glass to the package. The aim is to have the top surface of the glass levelled with the package. The solder bump height was set to 0.15mm, which brings the cavity depth to 0.65mm. With one single layer of green tape ceramic being 0.14mm after firing, five layers need to be used for a total cavity thickness is 700µm.

Chip cavity

This part is the most complex part of this package. It is composed by the chip cavity and the 3-D circuitry that connects the chip to the flexible connector. It is also on this part that both glass and flexible connector are attached. The tracks layout are organized around the chip cavity. The chip dimensions are 3.2x2.9mm, the cavity dimensions are 3.4x3.1mm. The chip thickness is 0.56mm. The addition of the thermocompressed gold bumps (20µm in height) brings the total thickness to 0.58mm. To facilitate the layers' design, the chip thickness will be considered to be 0.6mm. Therefore, the depth of the chip cavity should be at least 0.6mm. However, as it can be seen in Figure 6.7b, the glass window on which the chip is attached is not in contact with the chip cavity but is placed at about 0.15mm above it. In consequence, the chip does not need a cavity 0.6mm deep but only 0.45mm deep. The chip cavity will be made with 5 layers of green tape.

Flexible connector cavity

As seen in the diagram in Figure 6.7, the flexible cavity is off centred and has the following dimensions: 7.2x3.7mm. With a flexible connector thickness of 0.9mm, eight layers of green tape ceramic are used for an overall thickness of 1.12mm. Two of these layers are patterned with the chip cavity to increase the latter to 0.7mm to ensure that the chip fits into the cavity.

6.3.2 3D circuitry layout

The track layout is based on the pads of the glass window. Figure 6.8 illustrates the package with the mounted glass window. Seen in transparency is the track layout in grey which has been selected. As the package is seen from above, conductive tracks from different layers can be seen overlapping. The layout must ensure the connection from the chip to the 10-way connector and join the doublets. For this thesis, the foot print of the circuitry and the structures shape is bound to the guideline edited by VTT Technical Research Centre of Finland [128]. This guideline shows the recommended minimal features in LTCC that is achievable with production type LTCC equipment. The Table 6.1 compares the features size from the guideline and the ones fabricated for this package.

Table 6.1: Recommended and fabricated features dimensions in LTCC. The numbers highlighted in red are features smaller than the recommended dimension

Features	Recommended	Fabricated
Minimum Conductor Width	150µm	150µm
Minimum Conductor Spacing	150µm	250µm
Minimum Conductor Clearance with Edge	250µm	250µm
Catch pad size for sub 200µm Ø Vias	50µm larger	
Minimum Vias Pitch	2.5 x Via Ø	2 x Via Ø
Minimum Vias diameter vs Tape Thickness	1:1 Aspect Ratio	1:2 Aspect Ratio
Minimum distance between Vias and Edges	2 x Via Ø	3 x Via Ø

All tracks join at an intermediate zone (rectangle with red dot line) located between the chip and the flexible cavity. In this zone, the tracks are connected through filled vias to another set of tracks printed on the back of the last layer to the flexible connector. From

the chip's 16 inputs, there are only 9 outputs after doublets connections. The 10-way connector was chosen due to the extreme difficulty of obtaining 9-ways connectors.

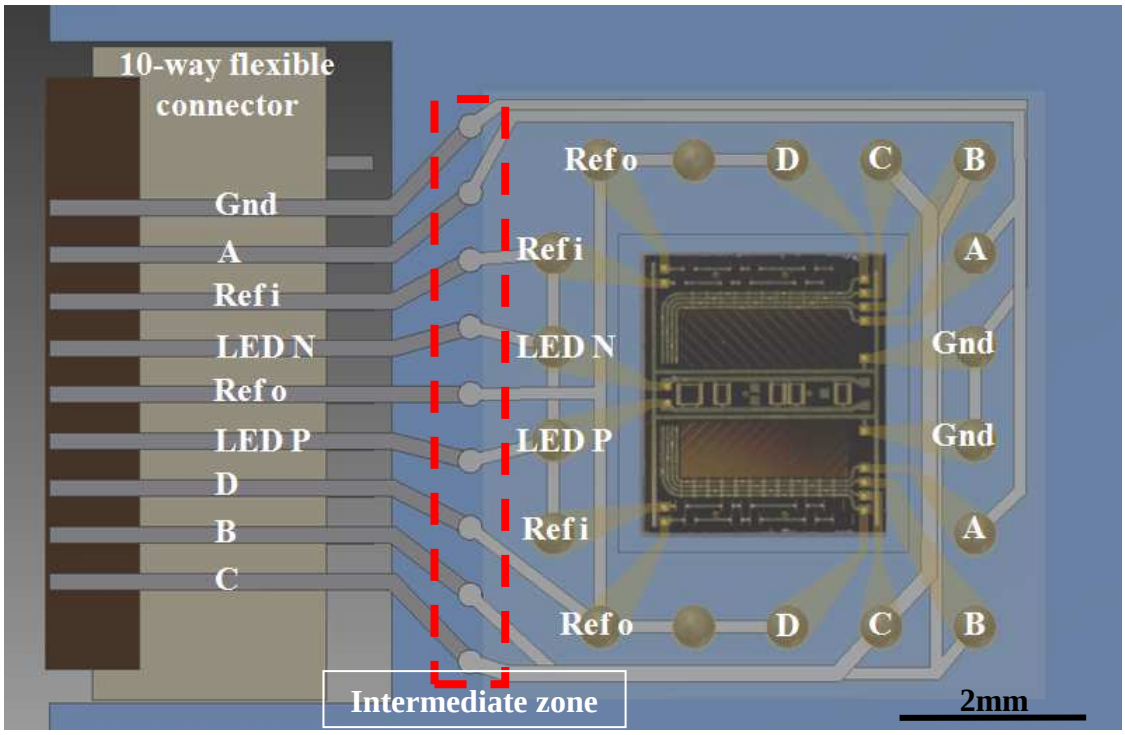

Figure 6.8: Top view of the tracks layout inside the LTCC package

The track layout is shown in more detail in Figure 6.9. The design fits into only three green tape layers. The design also features 300µm catch pads printed at every intersection between the tracks and vias to prevent misalignment. Layer 1 features the 520µm catch pads for the glass window and the vias underneath connecting to the second layer. Catch pads are printed, which ensures perfectly circular pad for the bonding. Layer 2 track layout connects the doublets A and C and Reference out and link them with the LED to the intermediate zone from which they are connected to layer 3. The other inputs are directly connected to layer 3. The last layer, layer 3, connects the doublets B and D, which join the Ground and Reference in the intermediary zone. All connections are present in the intermediate zone and are connected to the back of layer 3 through filled vias. From there, they are linked to the flexible connector.

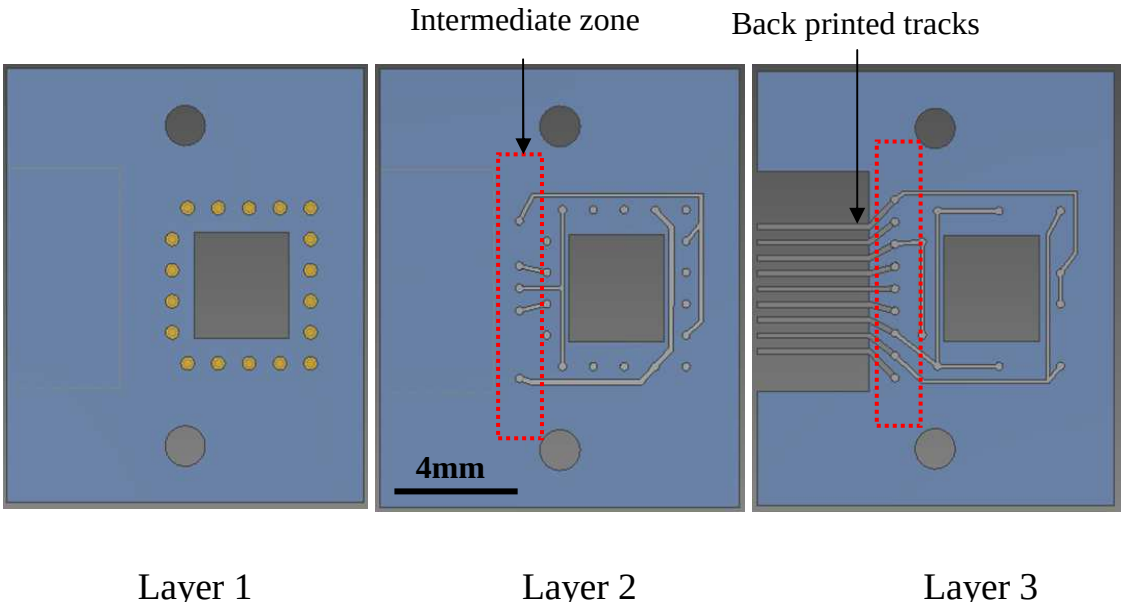

Figure 6.9: Diagram of the three printed layers

Table 6.2 summarizes the dimensions of the cavities to be created inside the package. In addition, the two holes for the screws needed to attach the overall system have a diameter of 1.3mm and a distance to the edges of 1.15mm.

Table 6.2: Cavity dimensions required to accommodate each component in the LTCC package

	Glass cavity	**Chip cavity**	**Flexible connector cavity**
Dimensions (mm)	**6.7 x 6.2 x 0.65**	**3.4 x 3.1 x 0.7**	**7.2 x 3.7 x 1.12**

6.4 Fabrication process

This part describes the different processes involved in the fabrication of the LTCC package. Here, dimensions have been scaled up to 12.7% to compensate for the shrinkage of the tape in X&Y. The 15% shrinkage in the Z-direction does not matter anymore as the number of layer was determined previously.

6.4.1 Layout design

The design of the layer layout is based on the dimension of the stacking device that was used for this experiment. The stacker has a total surface of 45x45mm but has only a maximum usable area of about 31x31mm. Four packages can thus be fitted in the green tape and use a combined space of 32x27mm. The typical layout for the package layers is illustrated in Figure 6.10 with, as an example, layer 3. Only the printed tracks and the cavity position and size would change according to the layer number. Not represented in this diagram are the cavities for the glass window. The four stacking pins and fiducials for track printing are present on each corner of the layer.

The fictitious dashed lines in orange delimit each package but are not used during the layer fabrication as the singulation of the packages will be implemented with a diamond saw. Not seen in the single package design, but illustrated here in black in Figure 6.10, are the additional connections from the 10-way connectors tracks to two large 5x2mm pads outside the packages area (hence the length of the tracks). These connections are temporary connection and will be cut off during the singulation process. Their sole purpose is to connect the catching pads to the cathode through the package to enable the electroplating of the glass window bonding pads through the package circuitry.

The four different packages present on one single layers all feature vias with different diameters. Starting from the top left and going clockwise, their diameter is 400, 300, 200 and 100µm. Although their purpose can be discussed for layer 1 due to the presence of large 500µm catching pad over the top, they enable a feasibility study for powder blasted packages with vias as small as 100µm, but also on the printing and alignment reliability.

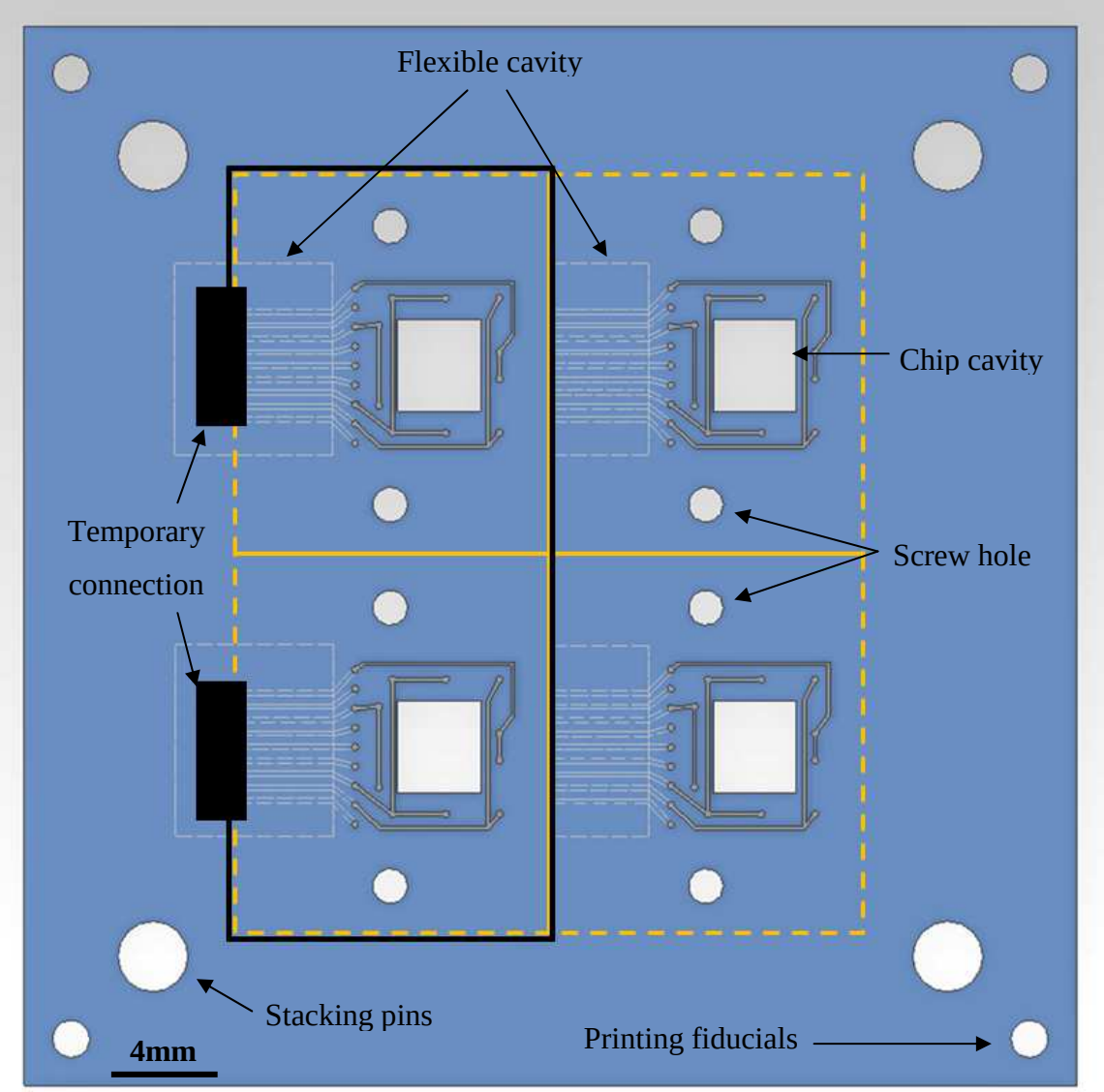

Figure 6.10: LTCC package with the integrated glass

6.4.2 Mask fabrication

Despite the issues encountered with the fabrication of the electroplated mask discussed in Chapter 4, the masks used for the powder blasting of the LTCC package were electroplated. This was possible thanks to the minimum features being only 100µm vias, a thinner plated thickness of 70-80µm and higher tolerances for dimensional variation of the mask features that wasn't possible during the green tape characterisation.

The number of layers to be fabricated for this package is 16 but there are only 6 different designs. The fabrication will require therefore 6 different masks for the powder blasting process as the same masks can be used several times, as described in Chapter 4. The mask layers are labelled as follows with their specificity. The number of layer to

produce is indicated in brackets:

- Layer 0: Cavity protecting glass window (5)
- Layer 1: Chip cavity + bonding pads for the glass window (1)
- Layer 2: Chip cavity + intermediate printed tracks (1)
- Layer 3: Chip cavity + printed tracks with connection to the flexible connector (1)
- Layer 4: Chip cavity + flexible connector (2)
- Layer 5: Flexible connector cavity (6)

The masks were fabricated following the process described in Chapter 4. Their dimension is 45x45mm, similar to the stacker dimensions. The usable area being about 90x120mm on the stainless steel plate, four masks can be plated at the same time at 10mA/cm^2 with timing depending on the thickness desired. Once plated, the masks are spin coated with flexopolymer LF55gn at 2500rpm, which gives a coating thickness of 60µm. The result of the electroplated nickel mask featuring Layer 2 and coated with LF55gn can be seen in Figure 6.11a with a close in on the apertures (Figure 6.11b).

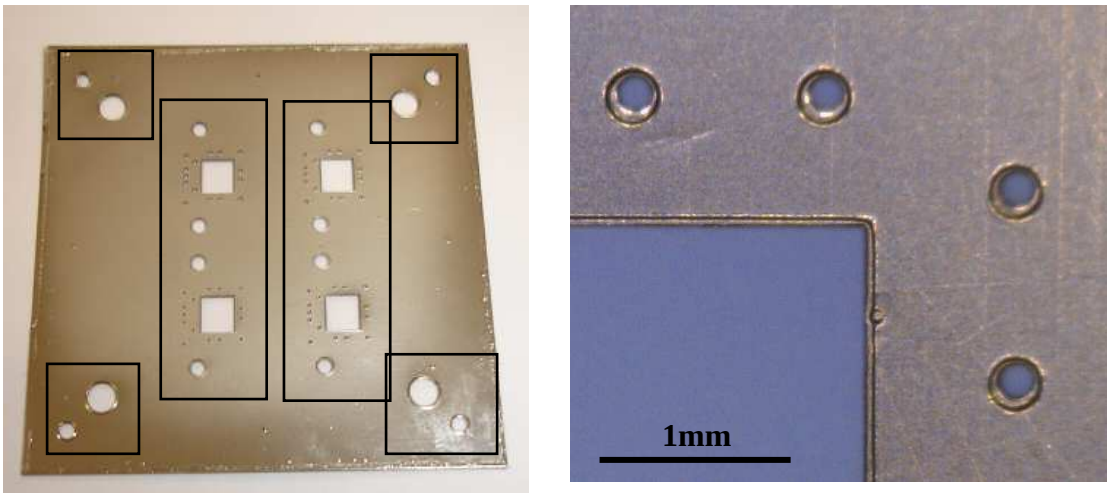

(a) (b)

Figure 6.11: (a) Nickel mask coated with its protective layer (Layer 2) with black rectangle representing the zones to powder blast and (b) close up on 200µm mask apertures

6.4.3 Powder blasting

The powder blasting of the masks is split into 6 zones marked by black rectangles as

shown in Figure 6.11a. These zones delimit the area which needs to be powder basted. Each zone is set manually with the computer interface presented in Chapter 3. The zones are blasted one after the other in order to minimize the time that the nozzle has to travel from one zone to the other. The process starts clockwise from the top left. This procedure is utilised for the 6 different Layer designs.

The masks are placed on the magnetic clamping system on the green tape layer and its backing PET foil. Extra metallic tools were placed on the top of the mask to strengthen the clamping force and compensate for the thinner metallic foil. There were placed in the centre of the mask and on each side. The parameters used for powder blasting are showed in Table 6.3.

Table 6.3: Powder blasting parameters

Pressure	50 psi
Particles	9µm average size
Flow rate	0.1g/s
Distance N-S	20mm
Scanning speed	5mm
Pitch	1mm
Scans number	4

The resulting LTCC layer can be seen in Figure 6.12. Every vias of the four in the package were pierced, even the ones machined with the 100µm circular apertures. The dimensions of the vias and the cavities manufactured correspond to the one reported in Chapter 5 with similar under etching. A faint darker coloration can be seen around the vias and cavities edges. In total, it took 14 minutes to powder blast the entire layer. For a single package which contains 16 layers, the fabrication time is close to 240 minutes, which does not take into account the time to set up each layer. After powder blasting, the layers are gently cleaned with the help of a brush and compressed air to remove alumina particles left on the top and back surface.

The PET foil underneath the green tape was not pierced. The fabrication of almost vertical walls only requires four scans, but a longer exposure to the particles would eventually pierce it. However, this would also increase significantly the under etching of the tape and the erosion of the mask.

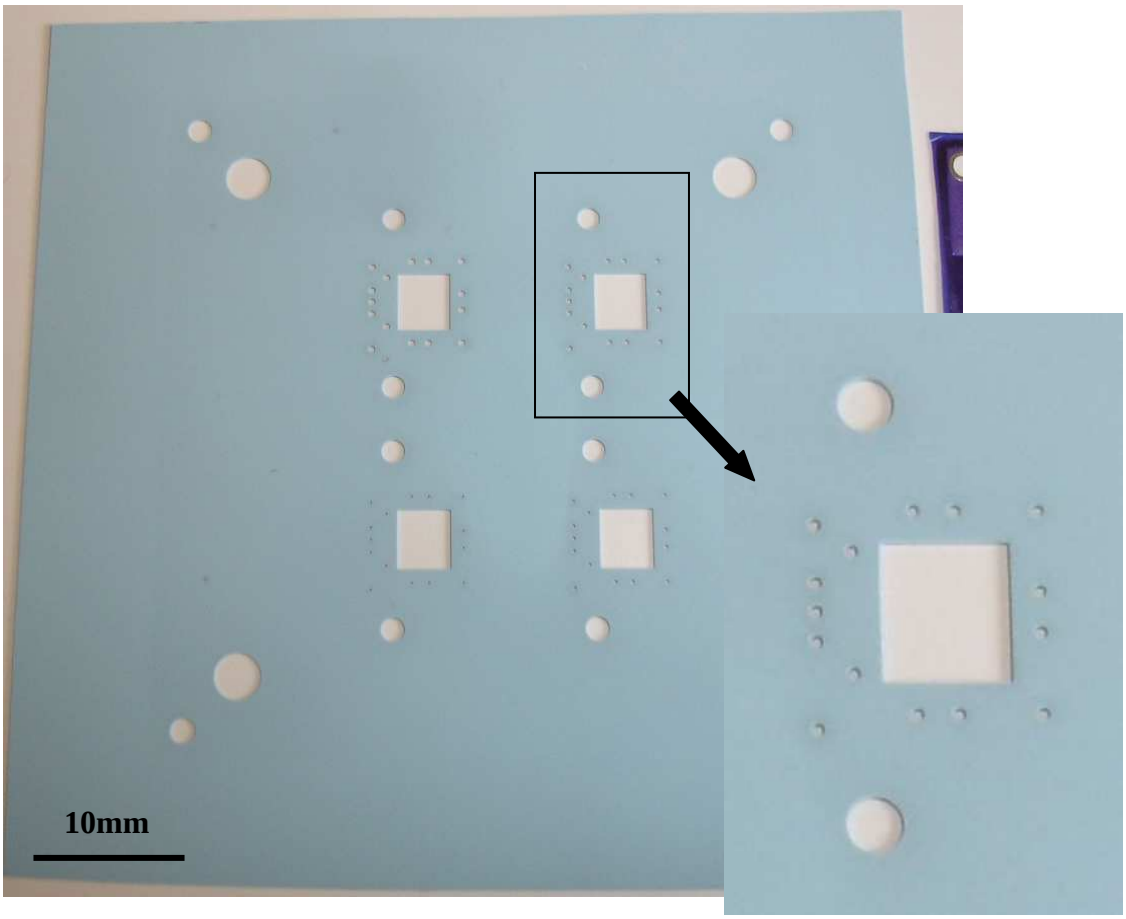

Figure 6.12: Green tape Layer 2 after powder blasting. The close up of the package with the 300µm vias shows the quality of the structures

6.4.4 Screen printing

Vias filling

Each layer is printed using a 50µm thick PET foil; the same type of backing foil provided with the green tape. The foil is patterned using a 30W CO_2 CNC laser cutter from the company Epilog. The mask is aligned on the powder blasted green tape on the same stacker that will be used for the stacking process. A flat blade is used as squeegee to squeeze the paste into the mask apertures. After the printing, the pins are carefully removed and the mask lifted. This process works very well but is limited by the

dimensions of the mask apertures: it was not possible to laser cut circular apertures smaller than ~280µm. Thus the apertures of the mask for filling 100 and 200µm vias have a diameter of ~280µm. Moreover, the laser cutting of the foil creates melted rims on the edge of the apertures that raise the mask thickness to around 110µm. This thicker deposit must therefore be removed. Fortunately, those excess can be easily scrapped with a sharp flat blade before the paste is dried at 120ºC for 5 minutes. The backing PET foil protecting the green tape is then removed to allow back side inspection.

Figure 6.13a&b show the 100µm filled vias from the top and back side. Only the top side needed to be scrapped. It can be seen in Figure 6.13a that thin remains of the paste still surround the vias. Short circuits were avoided thanks to the designs of the circuitry that ensured that potential tracks passes away from the paste remains. Two types of paste were used: DuPont Ag 6141 for internal vias filling and DuPont AgPd 6138 for the external vias (only for Layer 1). This latter paste is a transition paste for the printings of AgPd catching pads.

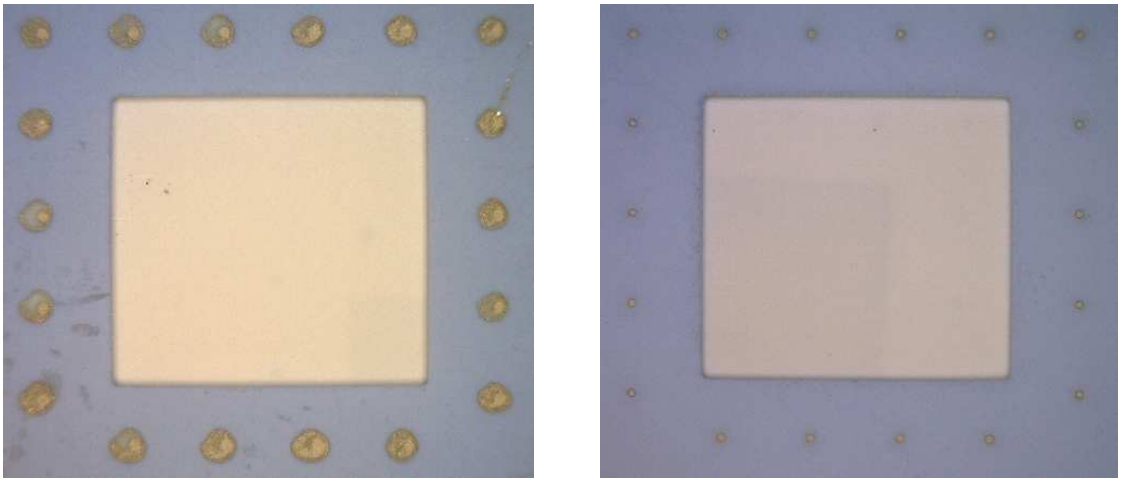

(a) (b)

Figure 6.13: 100µm filled vias of the layer 1 (glass window pads) viewed from (a) the top surface after the excess paste has been scrapped and (b) the back side

Conductor printing

The printing of the conductive tracks is done with conventional screen printing techniques. A Horizon 03i screen printing equipment manufactured by DEK was used in combination with an emulsion screen recommended by the paste manufacturer

DuPont (325 stainless steel mesh of 14µm emulsion thickness). The emulsion screen and the green tape are aligned thanks to a dual sight camera with shape recognition software, which recognizes the 1.6mm circular fiducials. The layers are printed with a rubber squeegee at a pressure of 4.4kg and a speed of 3mm/s. The gap between the emulsion screen and the layer is set at 1.5mm. Only one pass is necessary with an offset of +0.240mm in the X-direction, 0mm in the Y-direction and +100° for the angular angle is needed.

In order to successfully print and align the conductive tracks onto the powder blasted layer, the powder blasted fiducials marks must be correctly recognized by the printer recognition system. The system is set in automatic fiducials recognition mode, which lets the system decide the shape of the fiducial (square, triangle, and circle) depending on the image it sees. The printer recognizes the circular fiducials very easily with precision score of 989 out of 1000 thanks to the high precision of the fiducials machining.

Following the fiducials recognition, the tracks were printed and their integrity and alignment to the vias were checked. Internal tracks for Layers 2&3 were printed with DuPont silver paste Ag 6142 while the catching pads for Layer 1 and the tracks on the back of Layer 3 were printed with DuPont silver Palladium AgPd 6146. The AgPd paste is more suited for solder attachment than silver pastes. The tracks are also dried at 120ºC for 5 minutes.

Compared to conventional machining methods, dimensional changes can be enhanced by the different unavoidable steps during the powder blasting process such as the placement and removal of the mask onto the tape, the tape cleaning with brush and compressed air to remove particles inside the vias. As evidenced by Figure 6.14, which shows two printed packages (300 and 100µm vias) on the same layer, there was no particular problem in the alignment with similar results obtained with laser cut prototypes.

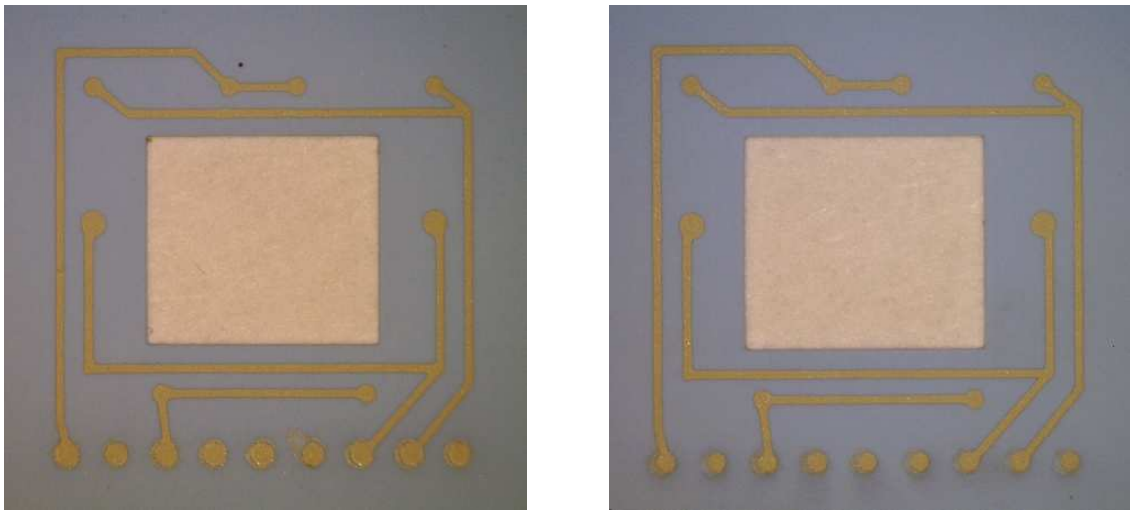

(a) (b)

Figure 6.14: Printed tracks aligned with (a) 300µm vias diameter and (b) 100µm vias diameter

6.4.5 Stacking

The stacker used consists of two thick aluminium plates which have a surface of 45x45mm. The layers are stacked on the four pins. A PET foil is placed on the top and bottom of the ceramic stack to prevent any contact between the metal and the tape. Care is taken to place the anti-sticky side of the foil on the ceramic side (this side has a thin release layer that is originally used to ease the tape separation from the foil). During the stacking, the cavities are filled with cut out silicone sheet 0.5mm thick (Figure 6.15a) to avoid their collapse during lamination. Silicone layers are cut to the right size and thinned down to the right thickness with the CO_2 laser. Silicone is a good material as it is easily machinable and does not stick to the cavities or to the metallic tracks. All cavities are opened cavities and the silicone is removed before firing.

The staking is done as follow: the design layers 5&4 are stacked first, and the flexible cavity is filled with the silicone. Then layers 3, 2&1 are placed and the chip cavity filled. The screw holes are also filled as they may also be crushed by the high pressure. Figure 6.15b shows the stack sandwiched between the two stacking plate. The glass cavity Layers 0 are stacked and fired independently using the same stacker and the same methods.

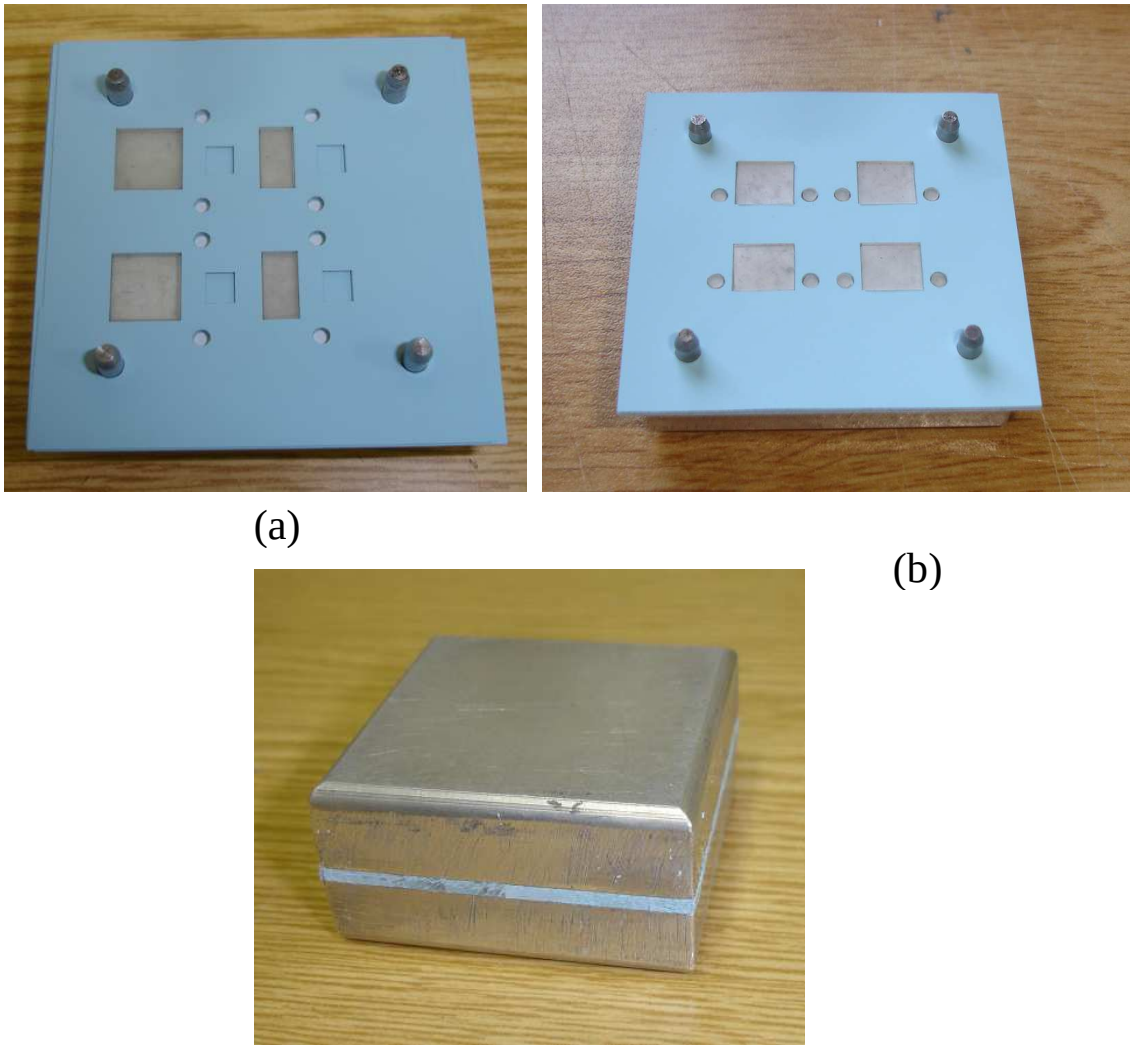

Figure 6.15: Photograph of (a) flexible connector cavity Layer 5&4 and (b) glass cavity Layer 0 stacked and cavities filled with silicon. (c): Package stacked and ready to be laminated

6.4.6 Lamination and firing

The stack was then placed into sealing bag and was vacuum sealed. Standard isostatic lamination process were done with an isostatic press from Keko equipment Ltd, model ILS-4, at a pressure of 15MPa and a temperature of 70ºC.

The firing profile used is also a standard profile, ramping up slowly to 850ºC in 150min. The fired stack is shown in Figure 6.16. The four packages can be seen with the chip cavities (front side) and the flexible connectors cavities (back side). There were no delaminations in the package after firing.

The view from the package front side clearly shows surface deformation of the flexible cavity despite the use of the silicon filler. This warpage is caused by the AgPd paste, behaviour which was studied by H.Birol et al [129]. The difference in shrinkage between the paste and the tape create this depression during firing. This is enhanced by either a large printed area or the thin thickness of the substrate, which are both characteristics of the flexible connector cavity. As such deformations impede the flexible connector attachment. The solution proposed in their study required to mix the paste with silica (SiO_2). This was not employed and the paste was simply replaced by the sliver paste Dupont Ag 6142 (the bonding method for the flexible connector, based ICA silver paste, does enable the use of the Ag6142 silver pastes [105]), which did not create any warpage post firing.

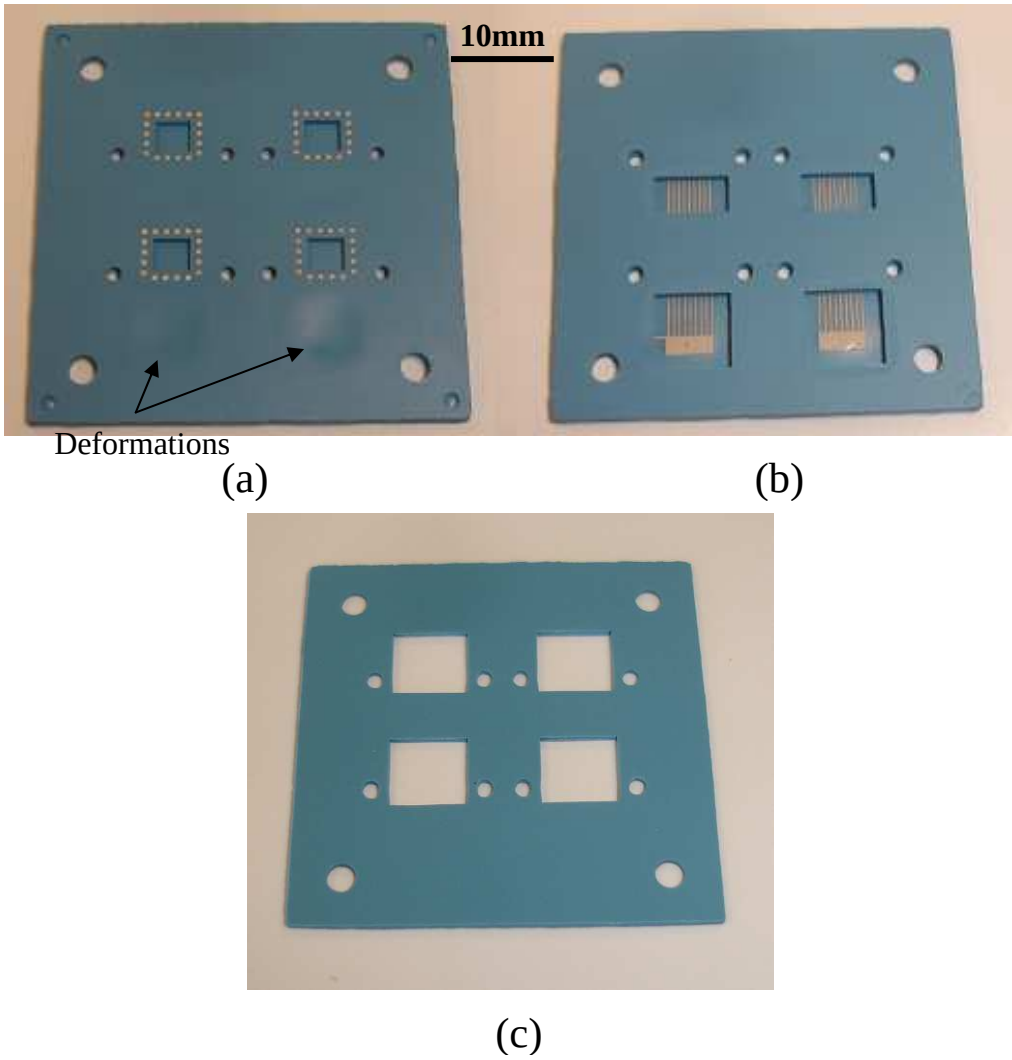

Figure 6.16: Sintered package (Layer 5 to 1) (a) front and (b) back side. (c) Sintered Layer 0 for the glass window

6.4.7 Post-processing

The post processing of the package relates to the bonding of the glass window and the bonding of the flexible connector.

Under Bump Metallisation (UBM)

As mentioned in this chapter, the glass window must be flip chip bonded onto the LTCC. The paste selected for the attachment was a lead free solder paste. It is the preferred attachment medium in the industry, with lead free SnAgCu solders becoming today the most favoured solder [130]. It has advantages compared to silver epoxy conductive paste, in particular it creates a stronger bond with the metalized surface and allows reflow processes (details later in this chapter).

However, lead free solders require an extra processing step called Under Bump Metallisation. Solder pastes have been utilised with the original metallisation Ag/Pt and Ag/Pd that LTCC offers [131] with relative success. However, higher failure rate were noticed with the Ag/Pd metallisation layer. This was attributed to the formation of excessive intermetallic compounds Ag_3Sn and $PdSn_4$ between the AgPd and Sn. The consequence is a hardening of the solder at this boundary region which facilitates the formation of cracks.

Under Bump metallisation consists in the successive deposition of metallic layers selected accordingly to the type of solder employed and on the type of pads it is deposited onto. Its main purpose is to enhance the adhesion of the solder on the metallic pads, to act as an effective diffusion barrier and to improve the pad's wettability. The most common UBM method for lead free solder is nickel gold metallisation used on aluminium and copper. This type of metallisation was also used for the UBM of the package. Electroless Nickel Immersion Gold (ENIG) is a widely used technique for the UBM process, but is not available at Heriot-Watt University. Thus the plating was done using DC plating bath.

The UBM is done on the silver-palladium catching pads. The connection to the cathode to the two large pads present at the back of the package (seen in Figure 6.10 and 6.16b) was done thanks to temporary attached conductive wires and silver epoxy paste. These

temporary wires are used for both nickel and gold plating processes. The plating thickness for each layer was done according to DT microcircuits corporation guideline [132]: a few microns of nickel (2 to 5µm) material are enough to prevent the silver migration while 0.05 to 0.1µm of gold prevents the oxidation of the nickel.

Nickel plating: the packages are placed on a holder (Figure 6.17a) and plated at 10mA/cm^2 in the plating bath showed in Chapter 4. Due to the small area formed by the catching pads (15 mm^2 for 72 catch pads), the current required would be 1.5mA, too low for the power supply. An additional 800mm^2 of platable area was added on the holder to raise the current to about 81mA. At this current density, the deposition rate is about 10µm per hour. Three to 6µm were plated onto the catching pads.

Gold plating: The gold plating bath was custom made in [127] and is shown in Figure 6.17b. The beaker contains 1.5 litres ECF60 gold plating solution from Metalor Technologies. The solution is brought to a temperature of 50ºC and stirred to about 250rpm. Gold deposition is very quick and only 30 seconds are needed to achieve tens of nanometers of gold. The UBM on the LTCC pads is shown in Figure 6.17c.

After the electroplating, the samples are singulated into four single packages and inspected for open circuits. Open circuits are easily recognizable as the lack of connection will prevent the pad from being plated. The packages with at least one non plated pad are discarded.

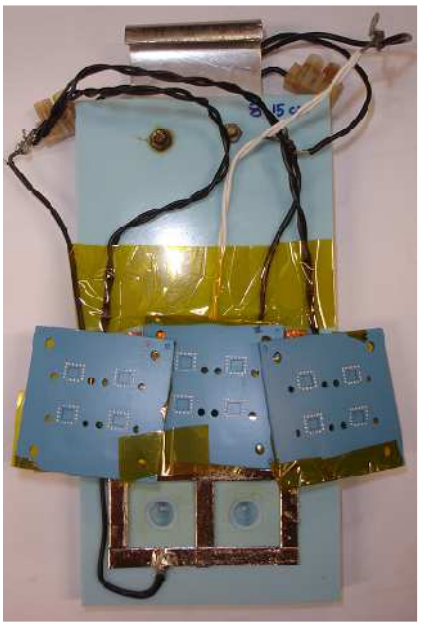

(a)

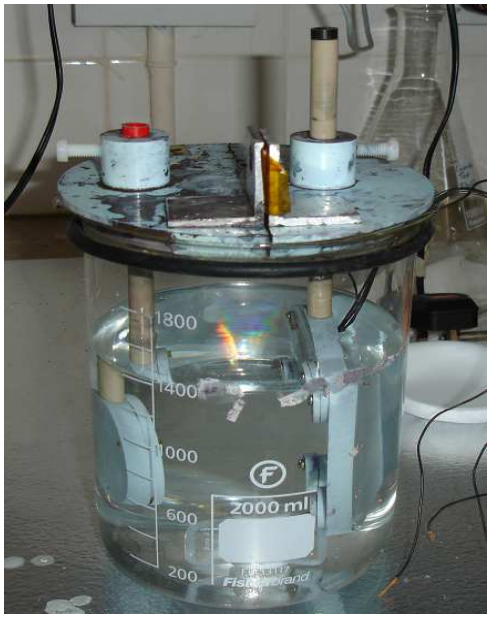

(b)

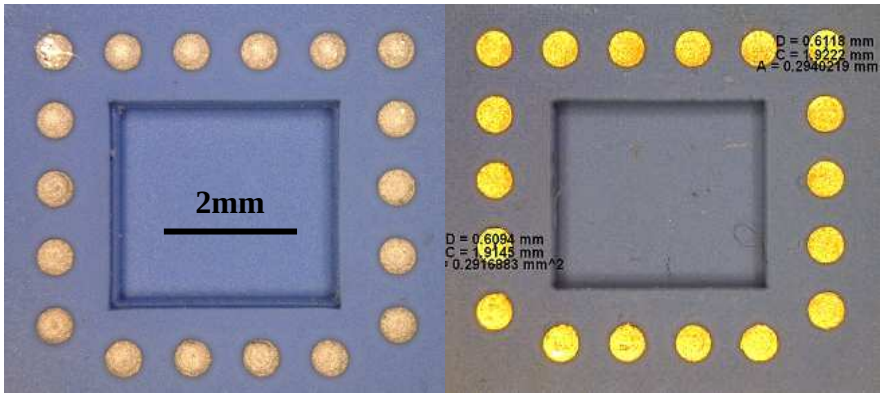

Before plating After plating

(c)

Figure 6.17: (a) LTCC package placed on the holder ready for nickel plating. (b) Custom DC gold electroplating bath. (c) Catching pads for the glass window before and after electroplating with the gold finish

Flexible connector attachment

The flexible connector is bonded using a pick and place method. The attachment medium is the silver epoxy paste: the paste can be cured at different range of temperatures from 80ºC in three hours to 175ºC in five minutes. Most importantly, once cured, the paste does not “reflow” when brought back to high temperature. It then prevents the connector to unbound from the package during the reflowing of the solder

(240°C) used for the flip chip bonding. The flexible connector contact pads are dipped in the ICA paste and aligned to the LTCC contact pads. This is done manually and, fortunately, the alignment is facilitated by the cavity walls which guide the connector into the right position. The ICA paste is then cured at 150°C for 5mins.

The resulting bond is very fragile due to the small volume of the paste used. To strengthen the bond, an encapsulant (HYSOL® EO1080) is poured in the interstice between the connector and the cavity and cured for 20mins at 150ºC. With it, the flexible cable can be inserted and removed without breaking the connections. An attached flexible connector with its cable and the encapsulant is shown in Figure 6.18. The pads of the flexible cable are probed to reveal potential short circuit: only the packages without short circuits are kept for the flip chip bonding.

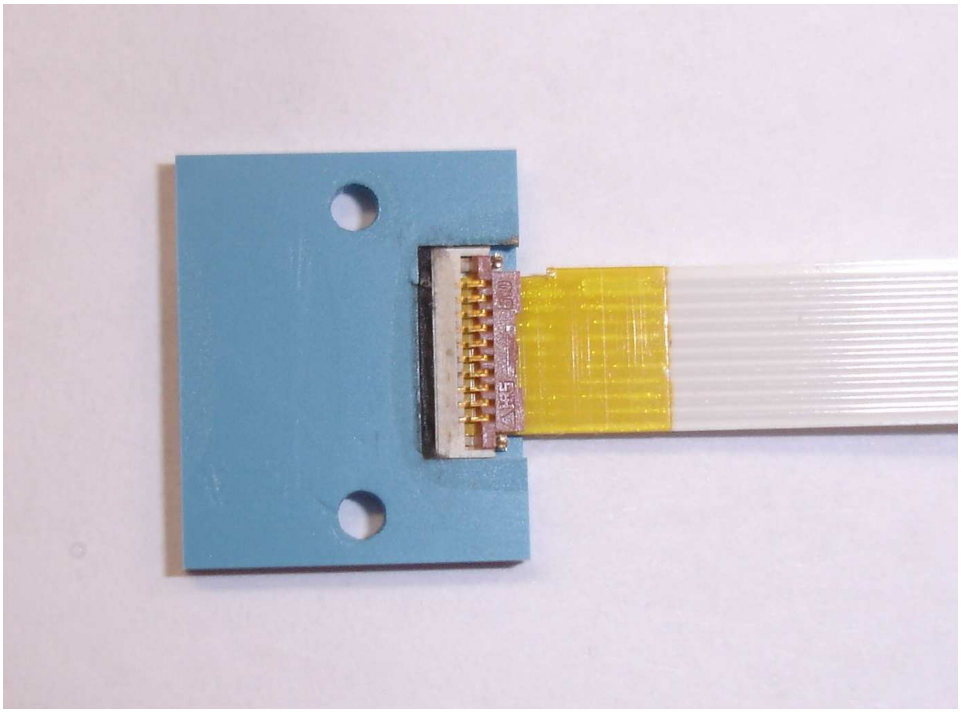

Figure 6.18: 10-way connector fixed on the LTCC package with the encapsulant (black) and the flexible cable

Glass flip-chip bonding

The solder paste used is to attach the glass onto the LTCC package is the Pb-Free solder paste Indium8.9HF composed by 96.5Sn/3Ag/0.5Cu. The solder melting point temperature is 217ºC, but a temperature of 240ºC is required to ensure good wetting.

The process for flip chip bonding was done as follows:

The solder paste was printed directly onto the LTCC catch pads using the laser cut 110µm thick PET foil as mask with apertures 650µm in diameter. After printing, the paste was melted at 240°C to form spherical bumps which wet on the pads' surface. The height of the bump obtained was around 150µm can be calculated thanks to the quantity of paste deposited and the dimensions of the catch pads (Appendix A). The flux which has surrounded the bumps was then cleaned by immersing the LTCC packages in DI water with cleaning agent (Vigon A250) and put in an ultrasonic bath at 50ºC for 10-20mins. Flux aims to remove oxides and prevents further oxidation of the solder [133]. Oxides have a poor thermal conduction and prevent the heat transfer, delaying the fusion of the latter with the metal pads. The flux is then an important component. However, it outgases during the reflow process and leaves unwanted residues; gases which can be potentially damaging for the encoder chip. The transition of the printed solder before and after reflow on the LTCC catch pads can be seen in Figure 6.19 a&b.

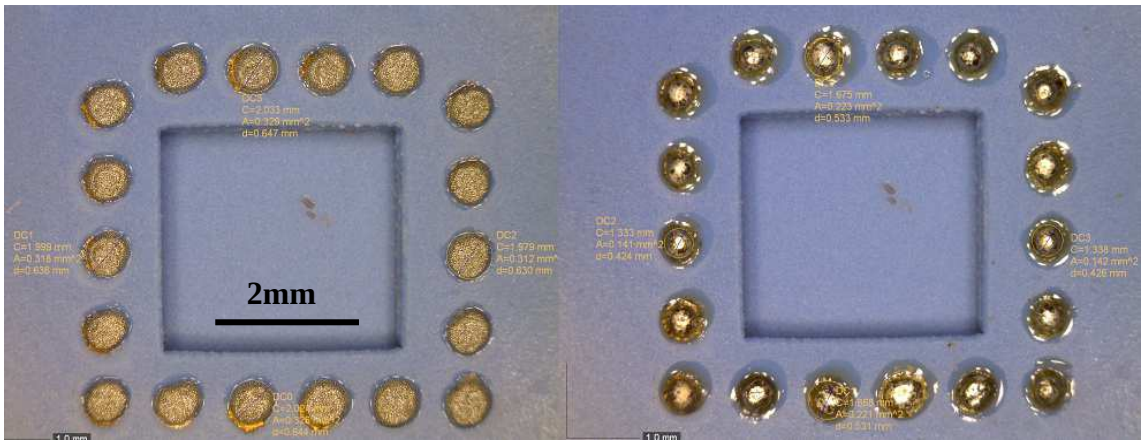

(a) (b)

Figure 6.19: (a) Printed solder on metalized pads. (b) Reflowed solder before the flux cleaning

The flip chip bonding was carried out using the Karl Suss machine model FC-6. It has an X&Y stage resolution of 0.5µm and a camera magnification of 400. The mode used is the reflow mode and the basic process parameters are detailed in Figure 6.20. During the process, the glass window is first put in contact with the package solder bumps thanks to the automated arms to define the zero position between the two parts. The glass part is then separated and stationned 40µm away from the bumps. The latter are then heated to 240ºC to be reflowed. At this point, the glass window is brought to a

distance of -80µm in order to fully wet the metallic pads of the glass. After 10 seconds, the window is moved back up to 0 and kept at that position until the solder is solidified once again has after cooling down to ambient temperature. The finished package can be seen in Figure 6.21.

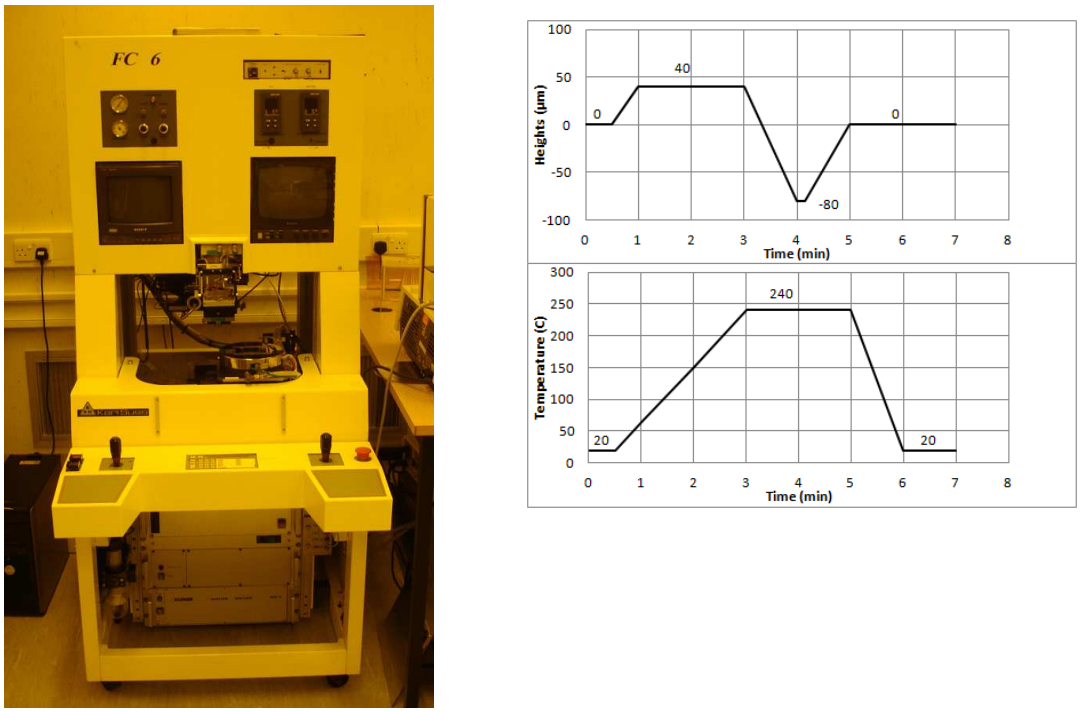

Figure 6.20: Photograph of the FC6 flip chip bonder and temperature and distance profile utilised during the flip chip bonding

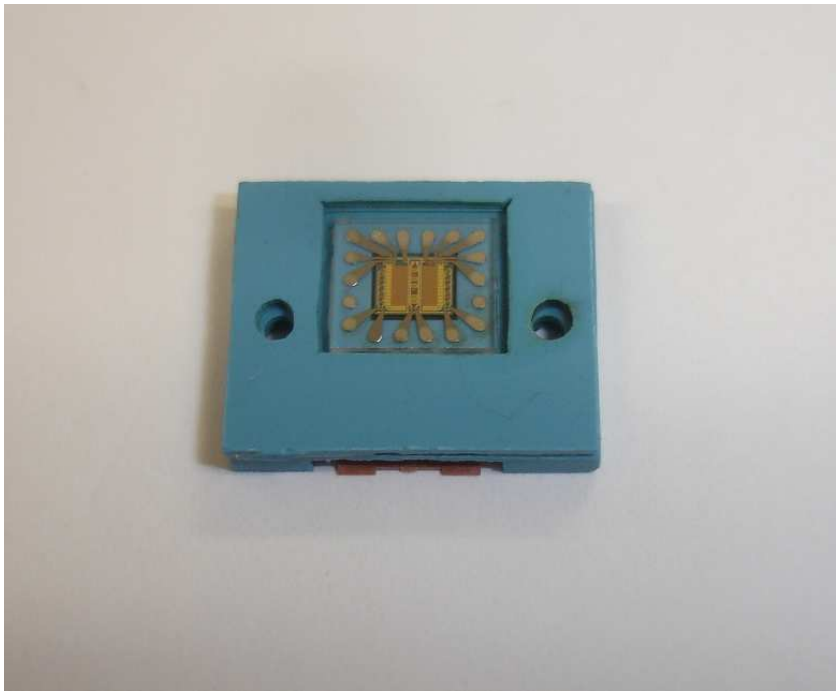

Figure 6.21: Final package with glass window bonded and the chip encoder

6.5 Package characterisation and limitations

6.5.1 Package integrity

Open circuits

In order to respond rapidly to the growing interest showed by Renishaw for this new technology, the fabrication of the optical encoder packages was first executed with the CO_2 laser mentioned previously in this thesis. A certain number of packages were made and the printing and stacking technique finely tuned with this process. Via filling was done manually with and without the PET foil on. When the latter was removed, the LTCC layer was supported by a plain PET layer. The test conducted clearly showed that leaving the backing foil during the filling process of the vias reduces the chances of open circuits. The package yield went from 40% to 90% by leaving the foil attached to the tape until the stacking steps.

It is not very clear why such a high success rate was obtained with the foil on. One hypothesis can be made on the filling of the PET foil vias. Indeed, one of the possibilities offered by conventional machining such as laser cutting or punching machining is to pierce both ceramic and PET foil at the same time. Thus, during vias filling, the conductive paste is squeezed both in the tape vias and in backing foil vias. On the contrary, if the PET foil is not pierced, the paste is squeezed in the green tape vias but is stopped against a flat surface at the bottom of the tape vias. This must promote the formation of voids or air bubbles which can then create open circuits (despite the visual checking of each layers after backing foil removal and the high lamination pressure that should crush the air gap).

As the yield of LTCC package produced with powder blasting came close to 50%, it was assumed that similar problems occurred. Due to the non piercing of the backing foil by the particles, the paste is blocked by the PET flat surface and creates open circuits. Furthermore, in these conditions, the visual checking of the filled vias through the PET foil cannot be done and has to wait after the tracks printing and the removal of the foil. This non piercing of the PET foil by the powder blasting process is here certainly a problem.

Mask clamping and duration of the process

As mentioned previously, the clamping force was increased by adding pieces of metal onto the mask. This ensured a very good contact between the tape and the mask, reducing the under etching. However, due to the magnetic field and the large area to powder blast, these pieces cannot always be placed where desired to prevent the mask from lifting up. Furthermore, once placed, they can slide due to the vibrations of the stage and the pressurized air, despite the stickiness of the polymer. Their movement can damage the coating as illustrated in Figure 6.22 and impede the machining process.

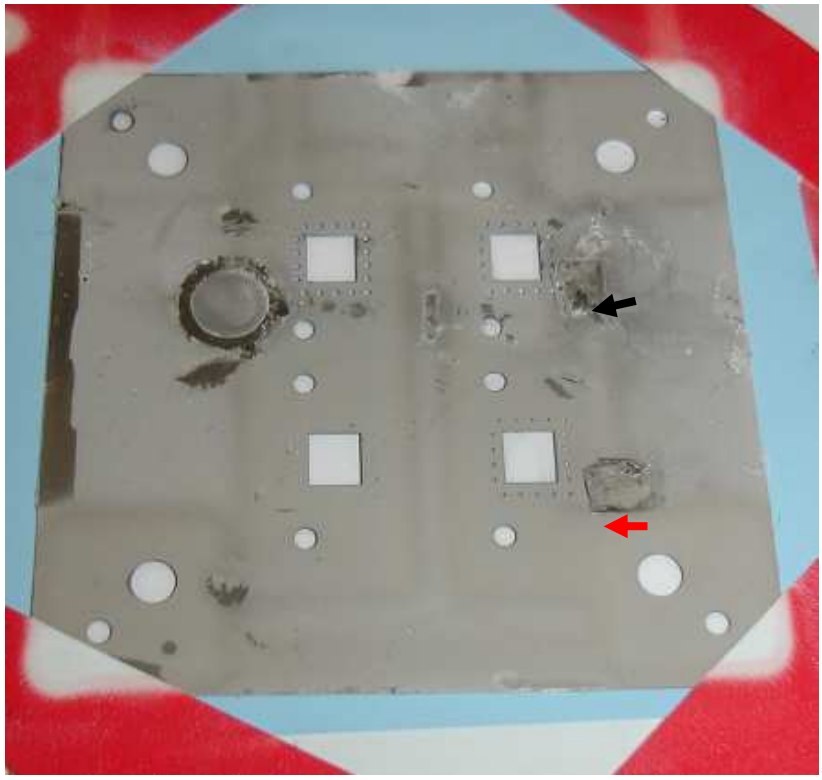

Figure 6.22: Photograph of the nickel mask clamped down with additional tool after powder blasting. The tools movement during the process (red arrows) damaged the protective coating and also impede the machining (black arrow)

The duration of the process can be also questioned. 240mins to powder blast 16 layers is a very long time, especially considering that the CO_2 laser cutting duration for similar design would be approximately ten times shorter. This is without taking into account the extra steps for the mask fabrication. The quality is however on the powder blasting side as 100µm vias are achievable while the minimum feasible via diameter is 250µm with poor circular edges. Bringing this down to the fabrication of 1 single package (taking

into account that each layer needs four stacking pins and 2 printing fiducials, so 5 minutes), it will still require 114mins.

6.5.2 Glass – LTCC Package conductivity tests

The packages were connected with a flexible cable to a specifically designed PCB board which can be plugged onto the testing rig. This rig houses an ASIC and electronics to power up the LED and produce the phase and quadrature from the four channel signals. The setup can be seen in Figure 6.23. The metallic scale used is placed underneath the package on a set of stages allowing translation (x, y and z axis) and rotational (pitch, roll and yaw) movements. Test of the encoder chips is not the purpose of this work and only the functioning of the chip on the package will be tested here.

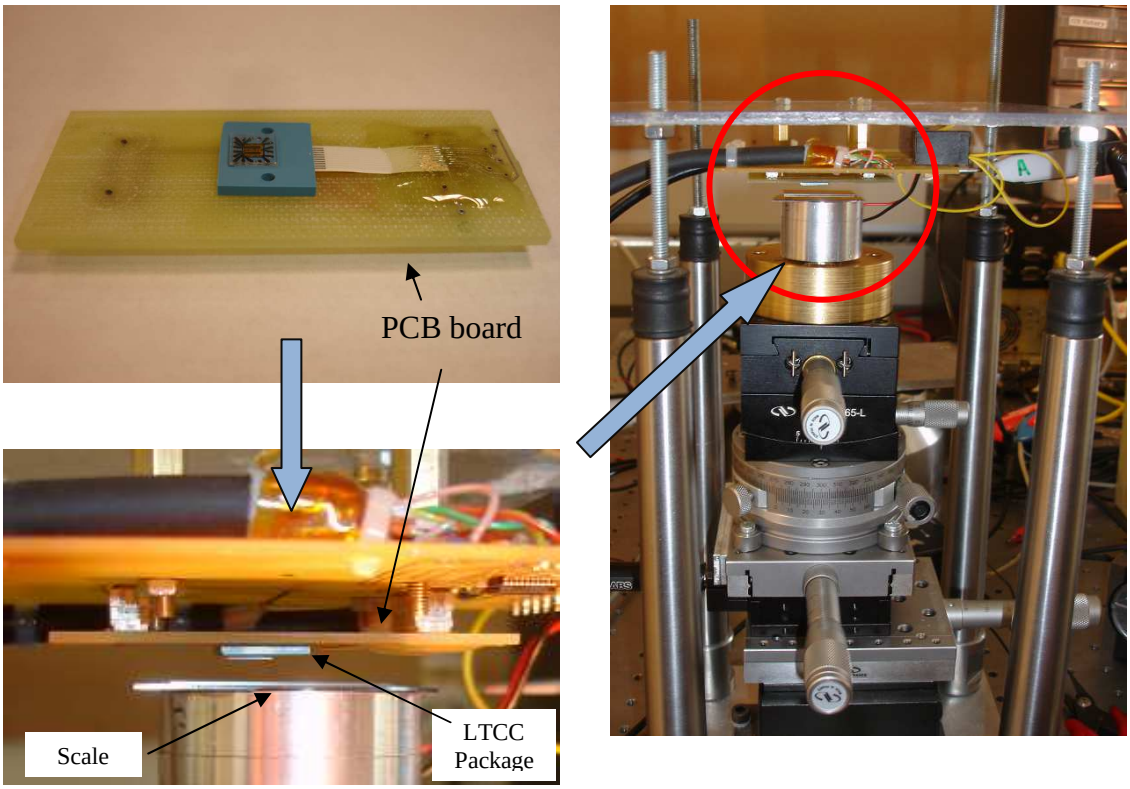

Figure 6.23: From top left anticlockwise: LTCC package attached onto the PCB board; PCB board connected to the rig and flipped to face the scale; Translation and rotational stages on which the scale faces the encoder chip

The packages were tested with a linear scale with 8µm pitch. The LED was successfully powered up with a drive current of about 25mA. The signals recorded showed that the chip performed according to its specification. Incremental graduation and reference

marker could be recorded adequately meaning that the all the channels performed well. Figure 6.24 shows the signal oscillation of the incremental (bottom row) matching perfectly the scale graduations. Similarly, the reference marker could be easily identified thanks to large amplitude of the signal received.

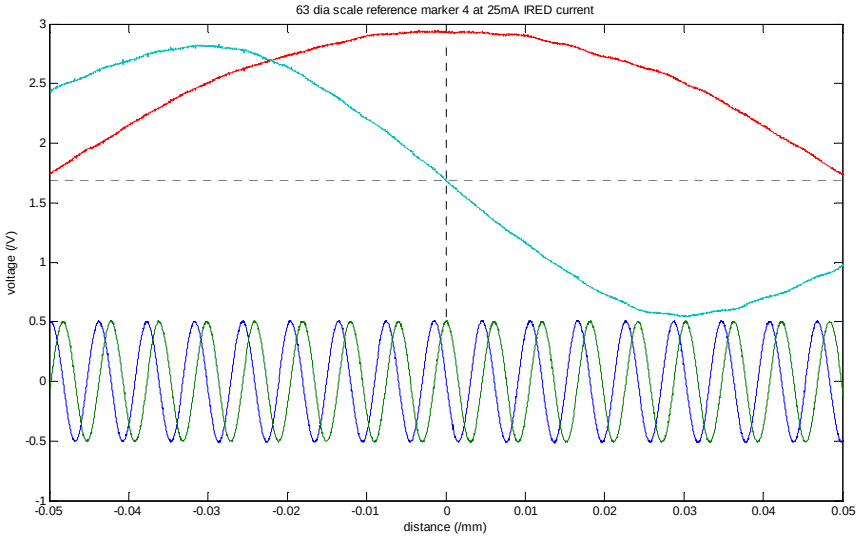

Figure 6.24: Incremental (bottom) and the reference marker (top) signal recorded on the oscilloscope. The reference signal is clearly visible for a 1Volt peak to peak of the incremental signal

6.6 Conclusions

The fabrication of a package in LTCC for an optical encoder using powder blasting was demonstrated. Each layer of the package was accurately machined thanks to the nickel mask being magnetically clamped. The powder blasted structures dimensions and shape matched similar features fabricated during the green tape characterisation in Chapter 5 with similar parameters. The full package took 240 minutes to produce with nickel masks being re-used for certain layers. After patterning of the layers, the fabrication steps for LTCC package could be followed normally. Via filling of apertures as small as 100µm was successful and fiducials detection to print the tracks was better than the one obtained with Epilog CO_2 laser cutting. No delamination of the layer could be seen after firing. However, the package yield was only around 50%, probably due to the via filling and the lack of apertures in the PET foil.

The glass and the flexible connector were bonded onto the package and every bonded

package passed successfully the connectivity tests proving that both solder and epoxy pastes were a good choice. The LTCC package enabled the chip to perform as expected: the LED was powdered and the incrementals and reference marker were recorded from the different photodiode channels signals.

Chapter 7 Conclusion and future work

7.1 Conclusion

An overview of the LTCC process was presented in thesis. The interest that such technology can confer for packaging devices resides in the low CTE of the material, 3-D circuit capability, low tangent loss and high relative permittivity. The conventional techniques utilised to machine the green tape ceramic were described and their limitations highlighted. Notably, the burrs and debris frequent in punching machining, the melted edges and lack of uniformity for small structures for the laser cutting and the lack of movement freedom and expensive price for both of them were emphasized.

The adaptation of the powder blasting process to LTCC machining was demonstrated through the preparation and improvement of the powder blasting setup owned by Heriot-Watt University. Flow variations and clogging were reduced thanks to the addition of a smaller reservoir and a heater which keeps the temperature at around 50°C. The characterisation of the erosion rate of the green tape has allowed the optimisation of process parameters such as pressure, and flow rate, to enable the efficient use of the machine. According to these results, the optimized pressure was 50 psi for a flow rate of ~0.1g/s. The distance N-S should not be lower than 20mm as the erosion rate becomes too strong below that distance.

The novel stencil mask introduced in this work is based on a metallic foil fabricated using UV-LIGA process or laser cutting on which a coating made of a photoimageable polymer was laid down. The mask is magnetically clamped down. The two materials have different purposes: the metallic layer ensures the high transfer accuracy of the pattern of the mask to the green tape ceramic and the polymer protects the metallic layer from deformations. It was demonstrated that this type of mask combined with magnetic clamping was the only masking method usable as glue or standard polymer mask destroy the LTCC tape. Nickel was selected as the material of choice for the work as it has very good feature size resolution and generates a higher magnetic clamping force than other metals such as stainless steel. At 50 psi and a minimal distance N-S of 20mm, a thickness of 100µm is sufficient to hold the mask in place with the magnetic setup. Additional clamping tools can be added to strengthen the clamping force and enable the use of thinner mask. The erosion rate at a nozzle speed of 5mm/s and pitch of

1mm is around 1.8µm vertically and 0.7µm laterally per scan. The mask can then be re-used several times. Two coatings were investigated to prevent deformation: dry film resist and flexopolymer LF55gn. The results showed that dry film is easier to use but suffers a higher erosion rate than the LF55gn which was recommended as the coating of choice for such a purpose. A thin layer of 100µm can protect the metal foil until lateral erosion of the later induces a loss in the patterning accuracy.

A characterisation of the erosion process on the green tape was conducted using the novel stencil mask. Micro patterned structures such as vias and channels were successfully blasted at 50 psi, proving that the technology works. Structured walls bear the typical U shape found in brittle material; this shape can be minimised by over exposing the substrate to the powder. Powder blasted structures have smooth edges and do not have the melted glass encountered with laser cutting. There is also a lack of burrs seen with other techniques. Almost vertical walls can be achieved repeatedly for any type of structures. This can be obtained after four scans at a distance N-S 20mm and or ten scans at N-S 50mm. Due to the higher energy, under etching is stronger at N-S 20mm and is about 30-40µm after 4 scans. At N-S 50mm, it is only 10-20µm after 10 scans.
Vias as small as 62µm in diameter for the entry side and 20µm for the exit side were successfully fabricated with a mask aperture of 60µm. However, to achieve repeatable vias shape, mask apertures for vias should not be smaller than 80-100µm. Similarly, the smallest beam had a width of 23µm for the entry side and 54µm for the exit side with mask beam 60µm in width. But for repeatable results, the mask should not be smaller than 80µm.

Following the green tape characterisation, a LTCC package for an optical encoder was successfully fabricated. It featured sixteen layers with six different designs. 45x45mm nickel masks coated with LF55gn flexopolymer were produced featuring 3mm stacking pins, 1.5mm fiducials mark, cavities and circular apertures ranging from 100µm to 400µm diameters for interconnections. Each mask was powder blasted at 50 psi with a flow rate of about 0.1g/s, a distance N-S of 20mm and a speed of 5mm/s. The optical encoder was attached on the package by flip chip bonding and successfully tested electrically.

A low device yield of around 50% was obtained as some packages had at least one or two open circuits. This was be attributed to the non-piercing of the PET foil by the powder blasting which impeded the filling of the vias, especially for the smallest 100µm and 200µm vias. The duration of the process was also long (240 minutes) where conventional techniques would only require around 20 minutes.

7.2 Future work

The successful powder blasting of green tape ceramic layers showed the viability of the project. However, improvements can be made to increase its usability.

First, investigation on another type of mask could be carried out. They could be made, for instance, out of solid plastic such as PMMA. Laser cut PMMA can have pretty good resolution and is inexpensive. Thin sheets of a few hundred microns could resist the blast enough to pattern the ceramic layers. The mask would be clamp magnetically with magnetic tools attached to the PMMA sheet thanks to half way through recessed cavity laser cut in the mask.

Improvement on the magnetic field could be done to increase its strength or reduce the non uniformity of the forces applied the metal sheet. Typically, an assembly of hundreds of smaller magnets could have a better clamping filled than the two large ones that have been used in this work. Electromagnets could be used so mask, and the additional tooling clamps, can be placed and removed easily from the green tape.

An investigation should also be done on the coating of LF55gn. The dimensions of the apertures of the coating could be patterned to match the ones of the nickel mask. With a thickness to about 50µm, this should reduce their impact on the erosion for apertures smaller than 200µm. Such thin coatings would have to be changed more frequently. The lateral erosion of the nickel mask should also be investigated.

Research could also be orientated toward the use of a positive dry film resist. Such a resist does not exist anymore and therefore could not be found during the time length of this project. The impact of such a resist for this process could be enormous. Indeed, here, the metal mask on which dry film would be laminated onto would also serve as the

photomask for the positive dry film. Placed metal sheet face up, the UV light would enter the metal mask apertures and expose the film. It would provide a perfect alignment, therefore would not require buying an additional photo mask, and will ease the process. However, unless a stronger film is fabricated, the resist would be etched quickly and would need to be changed frequently.

Further study on the package reliability, not achieved during the time scale of this project, should be done. X-ray analysis and cross sections of interconnection should confirm the reasons for the low yield with the open circuit locations. Thus improvements on the via filling could be implemented. The duration of the process could also be improved. Modification of the blasting setup to allow vectorisation of the nozzle instead of rasterisation would reduce considerably the machining time. Parallel processing can be thought as one option to decrease the fabrication time, but it would require a stronger clamping system capable of countering the lifting forces generated by several nozzles.

There is a niche of application that can benefit from the powder blasting machining which would require small vias with perfect circular shape and not melted edges. In addition, complex design such as large arrays of tightly spaced vias can be quickly machined thanks to the large machining area. However, this niche could be broadened using the machining characteristics of the structures in microfluidics or optical applications. The typical U shape of vias could be used in electronics to reach thin tracks underneath the vias or as thin ball valve such as the one introduced in [8]. Similarly, round bottom channels can be used for fibre alignment for example. Tapered vias can also be more easily coated or electroplated. Finally, the possibility of machining the tape with an angle can also open the angled sidewall reflectors in LTCC demonstrated with embossing technique in [78].

Appendix A:

Paste volume calculation

The height and diameter expected of the solder ball can be predicted using the truncated sphere theory based on the volume of paste deposited [134]. With the final bump height of the reflowed solder and catch pads area determined, the volume of paste needed can be calculated and modified thanks to the mask apertures and thickness. However, care should be taken when the mask apertures dimensions are changed. Indeed, during reflow, the solder ball only wet on the catch pads, which means that print deposit can exceed the catch pad area. This characteristic is used as an advantage to deposit a volume of solder larger than what would be allowed with the pad area. But as the solder collapses slightly after printing, enough space should be left between two deposits to prevent bridging.

Before printing, a few rules have to be considered:

- The aperture should not be smaller than 5 times the size of the solder beads. With Indium 9.8 HF, the beads are 20-25µm, so the minimum aperture size to 125µm.
- The solder paste undergoes high volume variation during reflow as the flux which it contains disappeared. This Pb-free solder contains 45% in volume of flux, meaning that the reflowed solder bumps are only 55% of the initial volume of printed solder. To calculate the initial volume of the paste, V_i, the reflowed volume is simply divided by 0.55.
- 10-20% of the paste is assumed lost during printing as the solder adheres to the screen during the printing process. It is assumed here 10% losses in the PET mask.

Two coefficients can be calculated to ensure the right printing conditions:

- *Area ratio* A_r. This is the ratio between the surface of the aperture and the surface of the aperture walls in the stencil and is given by r/2h where r is the radius of the via and h is its thickness. This ratio provides an empirical value of how much the paste sticks to the aperture. A commonly accepted value should be over 0.66.
- *Aspect ratio*. This is the ratio of the aperture diameter to the stencil thickness. For chemically etched stencils, this value should be greater than 1.5, for laser cut stencils it should be greater than 1.2 and for electroformed stencils which has the best solder paste release characteristics this should be greater than 1.1.

The volume of a truncated sphere is known by the following equation:

$$V = \frac{\pi}{6} * (h^3 + 3ha^2) \qquad \text{A.1}$$

Where h is the height of the solder ball, and a is the pad radius. Assuming a given volume, the height h can be determined by equation A.2:

$$h = \sqrt[3]{(\frac{(-V + \sqrt{\Delta})}{2})} \qquad \text{A.2}$$

However h is predetermined; there is no need to calculate it.

The catch pads of Layer 1 have a diameter of 520µm. For a final ball height of 150µm, the volume of reflowed solder is 0.017mm^3 following equation A.1. Therefore, after a 45% volume loss from the flux and a 10% volume loss during printing, the volume of solder needed to be deposited is 0.035mm^3. This volume can be obtained with a mask thickness of 110µm (50µm PET foil plus melted edges) and an aperture diameter of 643µm. The aspect ratio and area ratio are 5.85 and 1.46, respectively, well above the threshold (although thresholds are not specified for mask apertures made in PET foil).

References

1. Kulke, R., et al., *LTCC- Multilayer Ceramic for Sensor and Wireless Applications*. 2001, Eugen G Leuze Verlag. p. 2131-2136.

2. Enviro-Management & Research, I., *Abrasive Blasting Operations: Engineering Control and Work Practices Manual*. 1976, Enviro-Management & Research, Inc.: Washington, D.C. 2001.

3. *Guyson white saftigrit*, Guyson.

4. Slikkerveer, P.J., et al., *Erosion and damage by sharp particles.* Wear, 1998. **217**(2): p. 237-250.

5. Finnie, I., *Some reflections on the past and future of erosion.* Wear, 1995. **186–187, Part 1**(0): p. 1-10.

6. Wensink, H., et al., *Mask materials for powder blasting* Journal of Micromechanics and Microengineering 2000. **10**(2): p. 175-181.

7. Liebhard, M. and A. Levy, *The effect of erodent particle characteristics on the erosion of metals.* Wear, 1991. **151**(2): p. 381-390.

8. Yamahata, C., et al., *A ball valve micropump in glass fabricated by powder blasting.* Sensors and Actuators B: Chemical, 2005. **110**(1): p. 1-7.

9. Sayah, A., et al., *Fabrication of microfluidic mixers with varying topography in glass using the powder blasting process.* Journal of Micromechanics and Microengineering, 2009. **19**(8): p. 085024.

10. Pawlowski, A.-G., Belloy, E, Sayah, A, Gijs, M.A.M., *Powder blasting patterning technology for microfabrication of complex suspended structures in glass.* Microelectronic Engineering, 2003. **67-68**: p. 9.

11. Belloy, E., A. Sayah, and M.A.M. Gijs, *Micromachining of glass inertial sensors.* Microelectromechanical Systems, Journal of, 2002. **11**(1): p. 85-90.

12. Ligthart, H.J., et al., *Glass and glass machining in Zeus panels.* Philips Journal of Research, 1996. **50**(3–4): p. 475-499.

13. Ghobeity, A., et al., *Process repeatability in abrasive jet micro-machining.* Journal of Materials Processing Technology, 2007. **190**(1–3): p. 51-60.

14. Barnum, J.K.P.a.R.A., *Powder flowability*. 2000, Pharmaceutical technology. p. 60-85.

15. Gyurk, W.J., *Methods for manufacturing multilayered monolithic ceramic bodies* 1965, RCA CORP: United States.

16. Stetson, H.W., *Method of making multilayer circuits*. 1965, RCA CORP: United States

17. Tummala, R.R., E.J. Rymaszewski, and K. G., *Microelectronics Packaging Handbook: Semiconductor Packaging*. 1997, Springer. p. 285.

18. Davis, E.M., et al., *Solid Logic Technology: Versatile, High-Performance Microelectronics.* IBM Journal of Research and Development, 1964. **8**(2): p. 102-114.

19. Tummala, R.R., E.J. Rymaszewski, and A.G. Klopfenstein, *Microelectronics Packaging Handbook: Semiconductor Packaging*. 1997, Springer. p. 294.

20. Seraphim, D.P. and I. Feinberg, *Electronic Packaging Evolution in IBM.* IBM Journal of Research and Development, 1981. **25**(5): p. 617-630.

21. Rinne, R.A. and D.R. Barbour, *Multi-Chip Module Technology.* Electrocomponent Science and Technology, 1982. **10**: p. 31-49.

22. Rabe, T., et al., *Hot Embossing: An Alternative Method to Produce Cavities in Ceramic Multilayer.* International Journal of Applied Ceramic Technology, 2007. **4**(1): p. 38-46.

23. Fournier, Y., *3D Structuration Techniques of LTCC for Microsystems Applications*. 2010, EPFL.

24. Fournier, Y., et al., *Influence of lamination parameters on LTCC shrinkage under unconstrained sintering*, in *4th European Microelectronics and Packaging Symposium - IMAPS*. 2006: Terme Catež (SI). p. 165-170.

25. Mohanram, A., et al., *Constrained Sintering of Low-Temperature Co-Fired Ceramics*. Journal of the American Ceramic Society, 2006. **89**(6): p. 1923-1929.

26. Mikeska, H.R., D.T. Schaefer, and R.H. Jensen, *Method for reducing shrinkage during firing of the green ceramic bodies*. 1992, E. I. Du Pont de Nemours and Company: United States.

27. Lautzenhiser, F. and E. Amaya *HeraLockTM 2000 Self-constrained LTCC Tape*.

28. Seigneur, F., et al., *Hermetic package for optical MEMS*, in *Ceramic Interconnect and Ceramic Microsystems Technologies (CICMT)*. 2008: Munich, DE. p. 627-633.

29. Birol, H., T. Maeder, and P. Ryser, *Application of graphite-based sacrificial layers for fabrication of LTCC (low temperature co-fired ceramic) membranes and micro-channels*. Journal of Micromechanics and Microengineering, 2007. **17**: p. 50-60.

30. *Duraver -E-Cu quality 104 KF*, Isola.

31. *TLX PTFE*, Taconic.

32. *DuPont Green tape 9k7*.

33. *High and Low Temperature Cofired Multilayer Ceramics (HTCC and LTCC)*, Schott.

34. *DuPont Green Tape 951*, DuPont.

35. Lin, J.C., et al., *The optimal clearance design of micro-punching die.* Journal of Achievements in Materials and Manufacturing Engineering, 2008. **29**(1): p. 4.

36. Sang Min Yi, et al., *Mechanical punching of 15 μm size hole.* Microsystem Technologies 2006. **12**(9): p. 6.

37. Breitling, J., et al., *Process control in blanking.* Journal of Materials Processing Technology, 1997. **71**(1): p. 187-192.

38. Tekiner, Z., M. Nalbant, and H. Gürün, *An experimental study for the effect of different clearances on burr, smooth-sheared and blanking force on aluminium sheet metal.* Materials & Design, 2006. **27**(10): p. 1134-1138.

39. Joo, B.-Y., S.-H. Rhim, and S.-I. Oh, *Micro-hole fabrication by mechanical punching process.* Journal of Materials Processing Technology, 2005. **170**(3): p. 593-601.

40. Heilala, J., et al., *LTCC technology for cost-effective packaging of photonic modules.* Assembly Automation, 2005. **25**(1): p. 8.

41. Sadler, D.J., et al., *Thermal management of BioMEMS: temperature control for ceramic-based PCR and DNA detection devices.* Components and Packaging Technologies, IEEE Transactions on, 2003. **26**(2): p. 309-316.

42. Goldberg, A., et al. *Multilayer technology as an integration system for ceramic micro fuel cells*. in *Microelectronics and Packaging Conference (EMPC), 2011 18th European*. 2011.

43. Karthikeyan, K., et al., *Low temperature co-fired ceramic vaporizing liquid microthruster for microspacecraft applications.* Applied Energy, 2012. **97**(0): p. 577-583.

44. Natarajan, G. and J.N. Humenik, *3D Ceramic Microfluidic Device Manufacturing.* Journal of Physics: Conference Series, 2006. **34**(1): p. 533.

45. Goldberg, A. *Micro Proton-Exchange-Membrane Fuel Cell System in LTCC (Low Temperature Cofired Ceramics)*. in *Electronics Technology, 2006. ISSE '06. 29th International Spring Seminar on*. 2006.

46. Gangqiang, W., et al., *Fabrication of microvias for multilayer LTCC substrates.* Electronics Packaging Manufacturing, IEEE Transactions on, 2006. **29**(1): p. 32-41.

47. Aguirre, J., et al. *An LTCC 94 GHz antenna array*. in *Antennas and Propagation Society International Symposium, 2008. AP-S 2008. IEEE*. 2008.

48. Wolter, K.-J. and L. Rebenklau. *Via Formation in LTCC Tape: A Comparison of Technologies* in *IMAPS CICMT*. 2005. Baltimore, Maryland USA.

49. Rhim, S.H., et al., *Burr formation during micro via-hole punching process of ceramic and PET double layer sheet.* The International Journal of Advanced Manufacturing Technology, 2006. **30**(3-4): p. 227-232.

50. Hagen, G. and L. Rebenklau. *Fabrication of Smallest Vias in LTCC Tape*. in *Electronics Systemintegration Technology Conference, 2006. 1st*. 2006.

51. Rebenklau, L., K.J. Wolter, and G. Hagen. *Realization of um-Vias in LTCC Tape*. Electronics Technology, 2006. ISSE '06. 29th International Spring Seminar on 2006 10-14 May 2006; 55-63].

52. Peterson, K.A., et al. *Microsystem Integration with New Techniques in LTCC*. in *IMAPS CICMT*. 2004. Denver, Colorado.

53. Sunappan, V., et al. *Process issues and characterization of LTCC substrates*. in *Electronic Components and Technology Conference, 2004. Proceedings. 54th*. 2004.

54. Fujimoto, M., et al., *Laser Drilling Technique for Multilayer Ceramic Chip Component and Module.* Journal of the Ceramic Society of Japan 2000. **108**(9): p. 6.

55. Jurków, D., et al., *Laser patterning of green ceramic tapes for 3D structures*, in *XXXIII International Conference of IMAPS - CPMT IEEE* 2009: Pszczyna, Poland.

56. Migliore, L., *Laser Drilling of PET-backed Unfired Ceramic*. 2006, Coherent Laser Group Santa Clara CA USA.

57. ; Available from: http://www.epiloglaser.com.

58. Nowak, K.M., H.J. Baker, and D.R. Hall, *Cold processing of green state LTCC with a CO2 laser.* Applied Physics A, 2006. **84**(3): p. 267-270.

59. Imen, K. and S.D. Allen, *Pulse CO2 Laser Drilling of Green Alumina Ceramic.* Advanced Packaging, IEEE Transactions on, 1999. **22**(4): p. 620-623.

60. Nowak, K.M., H.J. Baker, and D.R. Hall, *A model for "cold" laser ablation of green state ceramic materials.* Applied Physics A, 2008. **91**(2): p. 341-348.

61. Fields, R.A., M. Birnbaum, and F. C.L., *Highly efficient Nd:YVO4 diode-laser end-pumped laser.* Applied Physics Letters, 1987. **51**(23): p. 2.

62. Kita, J., et al., *Laser treatment of LTCC for 3D structures and elements fabrication.* Microelectronics International, 2002. **19**(3): p. 14-18.

63. Zhu, J. and W. Yung, *Studies on laser ablation of low temperature co-fired ceramics (LTCC).* The International Journal of Advanced Manufacturing Technology, 2009. **42**(7-8): p. 696-702.

64. Albertsen, A., et al., *Combined Manufacture Methods for High Density LTCC Substrates: Thick Film Screen Printing, Ink Jet, Postfiring Thin Film Processes, and Laser-Drilled Fine Vias.* Journal of Microelectonics and Electronic Packaging, 2009. **6**(1): p. 7.

65. Kita, J., et al., *Laser forming of LTCC Ceramics for Hot-Plate Gas Sensors.* Journal of Microelectronics and Electronic Packaging, 2005. **2**(1): p. 14-18.

66. Worgull, M., *Hot Embossing: Theory and Technology of Microreplication*. 2009, William Andrew. p. 368.

67. Heckele, M. and W.K. Schomburg, *Review on micro molding of thermoplastic polymers.* Journal of Micromechanics and Microengineering, 2004. **14**(3): p. R1.

68. Andrijasevic, D., et al., *An Investigation on Development of MEMS in LTCC by Embossing Technique*, in *third international conference on multi-material micro manufacture*. 2007: Borovets, Bulgaria. p. 4.

69. Xuechuan, S., et al. *Large area roller embossing of multilayered ceramic green composites*. in *Design, Test, Integration and Packaging of MEMS/MOEMS, 2008. MEMS/MOEMS 2008. Symposium on*. 2008.

70. Maw, H.P., et al. *Micro Embossing of LTCC (Low Temperature Co-fired Ceramic) Green Substrates*. in *Electronics Packaging Technology Conference, 2007. EPTC 2007. 9th*. 2007.

71. Shan, X.C., et al., *Micro Embossing of Ceramic Green Substrates for Micro Devices*, in *Symposium on Design, Test, Integration and Packaging of MEMS/MOEMS, DTIP*. 2008: Nice, France.

72. Bredeau, S. and J. Bancillon, *Opportunities and Challenges in Room Temperature Embossing/Punching for Ceramic Green Tapes*, in *8th International Conference on Multi-Material Micro Manufacture*. 2011: Suttgart, Germany.

73. Haertel, A., H.-J. Richter, and T. Moritz, *Cold embossing of ceramic green tapes.* Journal of microelectronics and electronic packaging 2012(9): p. 6.

74. Shan, X., et al., *Microstructure formation on low temperature co-fired ceramic green substrates using micro embossing.* Microsystem Technologies, 2008. **14**(9-11): p. 1405-1409.

75. Perrone, R., et al., *Miniaturized Embossed Low Resistance Fine Line Coils in*

LTCC. Journal of Microelectronics and Electronic Packaging, 2009. **6**(1): p. 7.

76. Perrone, R., et al. *Filling methods for embossed low resistance fine line coils in LTCC*. in *CICMT 2008*. 2008. Munich, Germany.

77. Buss, W., et al., *LTCC-Based Optical Elements for Opto-Electronic Applications*, in *EMPC*. 2005: Brugge, Belgium. p. 4.

78. Buss, W., et al. *Embossed ceramic reflectors with nano dispersive coatings for compact optoelectronic systems*. in *Microelectronics and Packaging Conference (EMPC), 2011 18th European*. 2011.

79. Wilhelm, S., et al., *Lamination based embossing technique for LTCC*. Microsystem Technologies, 2012: p. 1-7.

80. TexasAirsonics. Available from: http://texasairsonics.com.

81. Powell, R.C., A.K. Gray, and T.A. Coleman, *Material Supply System and Method*. 2007, First Solar, LLC., Perrysburg, OH, (US): United States.

82. Pawlowski, A.-G., *Développement et étude d'une technique de microsablage à haute résolution*, in *Faculté des sciences et techniques de l'ingénieur STI*. 2006, Ecole polytechnique fédérale de Lausanne EPFL: Laussane. p. 158.

83. Wensink, H., et al., *High resolution powder blast micromachining*, in *Micro Electro Mechanical Systems, 2000. The Thirteenth Annual International Conference on*. 2000. p. 769-774.

84. Wensink, H., *Fabrication of microstructures by powder blasting*. 2002, University of Twente: Enschede. p. 144.

85. Achtsnick, M., et al., *Modelling and evaluation of the micro abrasive blasting process*. Wear, 2005. **259**(1–6): p. 84-94.

86. Karpuschewski, B., A.M. Hoogstrate, and M. Achtsnick, *Simulation and*

Improvement of the Micro Abrasive Blasting Process. CIRP Annals - Manufacturing Technology, 2004. **53**(1): p. 251-254.

87. Burzynski, T. and M. Papini, *Measurement of the particle spatial and velocity distributions in micro-abrasive jets.* Measurement Science and Technology, 2011. **22**(2): p. 025104.

88. Fan, J.M., et al., *A study of the flow characteristics in micro-abrasive jets.* Experimental Thermal and Fluid Science, 2011. **35**(6): p. 1097-1106.

89. Ghobeity, A., J.K. Spelt, and M. Papini, *Abrasive jet micro-machining of planar areas and transitional slopes.* Journal of Micromechanics and Microengineering, 2008. **18**(5): p. 055014.

90. Anand, K., et al., *Flux effects in solid particle erosion.* Wear, 1987. **118**(2): p. 243-257.

91. Krishnamoorthy, P.R., S. Seetharamu, and P. Sampathkumaran, *Influence of the mass flux and impact angle of the abrasive on the erosion resistance of materials used in pulverized fuel bends and other components in thermal power stations.* Wear, 1993. **165**(2): p. 151-157.

92. D. R. Andrews, N.H., *Particle collisions in the vicinity of an eroding surface.* J. Phys. D: Appl. Phys., 1983. **16**.

93. Shipway, P.H. and I.M. Hutchings, *A method for optimizing the particle flux in erosion testing with a gas-blast apparatus.* Wear, 1994. **174**(1–2): p. 169-175.

94. Oka, Y.I., et al., *Control and evaluation of particle impact conditions in a sand erosion test facility.* Wear, 2001. **250**(1–12): p. 736-743.

95. Verma, A.P. and G.K. Lal, *An experimental study of abrasive jet machining.* International Journal of Machine Tool Design and Research, 1984. **24**(1): p. 19-29.

96. Belloy, E., Sayah, A., Gijs, M. A. M., *Powder blasting for three-dimensional microstructuring of glass.* Sensors & Actuators, 2000. **86**: p. 7.

97. Sheldon, G.L., I. Finnie, and A.S.o.M. Engineers, *On the ductile behavior of nominally brittle materials during erosive cutting*. 1965: ASME.

98. Ritter, J.E., *Erosion of Ceramic Materials.* Key Engineering Materials, 1992. **71**.

99. Slikkerveer, P.J., P.C.P. Bouten, and F.C.M. de Haas, *High quality mechanical etching of brittle materials by powder blasting.* Sensors and Actuators A: Physical, 2000. **85**(1–3): p. 296-303.

100. Kay, R. and M.P.Y. Desmulliez, *A review of stencil printing for microelectronic packaging.* Soldering & Surface Mount Technology, 2012. **24**(1): p. 22.

101. Getu, H., et al., *Abrasive jet micromachining of polymethylmethacrylate.* Wear, 2007. **263**(7–12): p. 1008-1015.

102. Getu, H., et al., *Abrasive jet micromachining of acrylic and polycarbonate polymers at oblique angles of attack.* Wear, 2008. **265**(5–6): p. 888-901.

103. Misri, I., et al., *Microfabrication of bulk PZT transducers by dry film photolithography and micro powder blasting.* Journal of Micromechanics and Microengineering, 2012. **22**(8): p. 085017.

104. Park, D.-S., et al., *Micro-grooving of glass using micro-abrasive jet machining.* Journal of Materials Processing Technology, 2004. **146**(2): p. 234-240.

105. Kim, K.-I., et al., *Packaging for RF MEMS devices using LTCC substrate and BCB adhesive layer.* Journal of Micromechanics and Microengineering, 2006. **16**(1): p. 150.

106. Saragih, A. and T. Ko, *A thick SU-8 mask for microabrasive jet machining on glass.* The International Journal of Advanced Manufacturing Technology, 2009. **41**(7-8): p. 734-740.

107. Sayah, A., V.K. Parashar, and M.A.M. Gijs. *LF55GN photosensitive flexopolymer as a new material for ultra-thick and high aspect-ratio MEMS fabrication*. in *Micro Electro Mechanical Systems, 2007. MEMS. IEEE 20th International Conference on*. 2007.

108. Sayah, A., et al., *Elastomer mask for powder blasting microfabrication.* Sensors and Actuators A Physical, 2005. **125**(1): p. 84-90.

109. Lomas, T., et al., *A precision hot embossing mold fabricated by high-resolution powder blasting with polydimethylsiloxane and SU-8 masking technology.* Journal of Micromechanics and Microengineering, 2009. **19**(3): p. 035002.

110. Wiederkehr, R.S., et al., *The gas flow rate increase obtained by an oscillating piezoelectric actuator on a micronozzle.* Sensors and Actuators A, 2008. **144**: p. 154-160.

111. Shan, X., H. Maw, and C. Lu, *Solvent-assisted low pressure room temperature lamination of low temperature cofirable ceramic green tapes for formation of embedded micro channels.* Microsystem Technologies, 2010. **16**(8): p. 1501-1506.

112. Jurkow, D., H. Roguszczak, and L. Golonka, *Cold chemical lamination of ceramic green tapes.* Journal of the European Ceramic Society, 2009. **29**(4): p. 703-709.

113. J. J. Santiago-aviles , P.E., *Photolithographic Processes for Creating a Proximity Sensor in Low Temperature Co-Fired Ceramic Tapes* NSF Summer Undergraduate Fellowships in Sensor Technology (SUNFEST)

114. ESPINOZA-VALLEJOS, et al., *Lithographic processing of LTCC tapes*. Vol. 3906. 1999, Bellingham, WA, INTERNATIONAL: Society of Photo-Optical Instrumentation Engineers. XIX, 806 p.

115. Belloy, E., et al., *The introduction of powder blasting for sensor and*

microsystem applications. Sensors & Actuators A, 2000. **84**(3): p. 330-337.

116. Sayah, A., V.K. Parashar, and M.A.M. Gijs, *LF55GN Photosensitive Flexopolymer: A New Material for Ultrathick and High-Aspect-Ratio MEMS Fabrication.* Microelectromechanical Systems, Journal of, 2007. **16**(3): p. 564-570.

117. Sayah, A., V.K. Parashar, and M.A.M. Gijs, *Ultra-Thick Optical Components Using LF55GN Photosensitive Flexopolymer*, in *IEEE Transducers 2007*. 2007: Lyon, France. p. 303-306.

118. *LF 55 GN (TRO55) Liquid Photopolymer*, MacDermid.

119. Slikkerveer, P.J., M.H.A. van Dongen, and F.J. Touwslager, *Erosion of elastomeric protective coatings.* Wear, 1999. **236**(1-2): p. 189-198.

120. Ghobeity, A., M. Papini, and J.K. Spelt, *Computer simulation of particle interference in abrasive jet micromachining.* Wear, 2007. **263**(1–6): p. 265-269.

121. Ghobeity, A., et al., *Surface evolution models in abrasive jet micromachining.* Wear, 2008. **264**(3–4): p. 185-198.

122. Pawlowski, A.G., A. Sayah, and M.A.M. Gijs, *Precision poly-(dimethyl siloxane) masking technology for high-resolution powder blasting.* Microelectromechanical Systems, Journal of, 2005. **14**(3): p. 619-624.

123. Slikkerveer, P.J. and F.H.i.t. Veld, *Model for patterned erosion.* Wear, 1999. **233–235**(0): p. 377-386.

124. Ghobeity, A., M. Papini, and J.K. Spelt, *Abrasive jet micro-machining of planar areas and transitional slopes in glass using target oscillation.* Journal of Materials Processing Technology, 2009. **209**(11): p. 5123-5132.

125. Park, D., M.-W. Cho, and H. Lee, *Effects of the impact angle variations on the erosion rate of glass in powder blasting process.* The International Journal of

Advanced Manufacturing Technology, 2004. **23**(5-6): p. 444-450.

126. Belloy, E., A. Sayah, and M.A.M. Gijs, *Oblique powder blasting for 3-D micromachining of brittle materials.* Sensors and Actuators A 2001. **92**: p. 6.

127. Carr, J.P., *Integrated Optical Encoder*, in *School of engineering and Physical Sciences*. 2010, Heriot-Watt University: Edinburgh.

128. Finland, V.T.r.C.o. *Design Guidelines Low Temperature Co-Fired Ceramic Modules*. [Guideline] 2008; 2008:[12]. Available from: www.vtt.fi/files/research/mel/ltcc_design_rules.pdf.

129. Hansu Birol, T.M., Peter Ryser, *odification of Thick-Film Conductors Used in IP Technology for Reduction of Warpage during Co-Firing of LTCC (Low Temperature Co-Fired Ceramic) Modules.* Key Engineering Materials 2007. **336 - 338**: p. 4.

130. Greig, W.J., *Integrated Circuit Packaging, Assembly and Interconnections*. 1 ed, ed. A. Microelectronics. 2007: Springer 328.

131. Olli Nousiaianen, R.R., Kari Kautio, Jussi Jääskeläinen, Seppo Leppävuori, *Solder joint reliability in AgPt-metallized LTCC modules.* Soldering & Surface Mount Technology, 2005. **17**(3): p. 10.

132. Corporation, D.m., *LTCC DESIGN GUIDELINES Chapitre 2 - Technologies*. 2002, DT microcircuits Corporation

133. Giles Humpston, D.M.J., *Principles of Soldering*. Vol. 1. 2004, Ohio: ASM international. 271.

134. Kuo-Ning, C. and Y. Chang-An, *An overview of solder bump shape prediction algorithms with validations.* Advanced Packaging, IEEE Transactions on, 2001. **24**(2): p. 158-162.